Alma Mater Studiorum – Università di Bologna

DOTTORATO DI RICERCA IN

CHIMICA

Ciclo XXVII

Settore Concorsuale di afferenza: **03/B1**

Settore Scientifico disciplinare: **CHIM/03**

# DESIGN AND CHARACTERIZATION OF LUMINESCENT SILICA NANOPARTICLES

**Presentata da: Luca Petrizza**

**Coordinatore Dottorato** **Relatore**

**Prof. Aldo Roda** **Prof. Luca Prodi**

***Esame finale anno 2015***

# Contents

# Chapter 1

# Introduction

## 1.1 Nanotechnology for bioanalytical applications

Nanotechnology is a well-established and fast growing discipline that has generalized applications in health, environmental and social field. In the last decade, nanotechnology has become extraordinarily important because manages to combine materials, properties and purposes to develop multimaterial, multimodal and multitarget nanoplatforms to overcome present unresolved problems.[1]

In particular, the advent of nanotechnology enables modern medicine to have great improvements in strategies that merge both diagnosis and therapeutics,[2,3] referred to as *theranostics*.[4,5] In this context, the design of devices suitable for *in vivo* applications must carefully consider some requirements, such as stability, toxicity,[6] time of clearance and output signal reliability.[7] It is possible to achieve these last parameters by using exogenous chemical contrast agents (CA), allowing non-invasive imaging approaches that are valuable in diagnostics and in medical treatments such as drug delivery and therapy monitoring;[8] consequently, the development of new contrast agents with increased sensitivity and specificity is a crucial issue for *in vivo* imaging.[9]

Nanoprobes that are suitable for targeting and compatible with different imaging techniques have emerged as promising tools in recent research.[10-13] Modern medical imaging techniques - such as magnetic resonance imaging (MRI),[14] computed X-ray tomography (CT),[15] positron emission tomography (PET),[16] single-photon emission computed tomography (SPECT)[17] and ultrasound imaging (US)[18] - have already a large clinical application and differ in basic peculiarities such as costs, time of analysis and resolution (Table 1.1). Synergy between the various techniques (by using *multimodal* approaches) appears to be the best solution to overcome limitations in getting comprehensive imaging, since each individual method has its pros and cons.[19]

Among the various techniques listed above, we will focus particularly on Optical (OI)[13] and photoacoustic imaging (PAI)[20], which have limited clinical applications nowadays but are of considerable scientific interest[21,22] because of their high sensitivities and short time of measurements, accompanied by low operating costs. In addition, compared to other imaging techniques, OI displays a reduced resolution, but it has the advantage of being suitable not only for diagnostic purposes but also for therapeutic treatments, such as the Photodynamic (PDT) and Photothermal (PTT) therapy.[23-27]

OI and PAI show low investigation depth (< 20 mm for OI and ~ 60 mm for PAI), which is their main limitation for *in vivo* applications in the Ultraviolet-Visible (UV-Vis) spectral range; indeed, in such a range absorption, autofluorescence and scattering of tissues limit the propagation of the excitation and, when relevant, emission radiation. It is possible to

partially overcome these problems using probes that exploit near-infrared (NIR) light, especially in the spectral range between 700 and 1000 nm.[28,29] To better analyze this concept, it is useful to know that hemoglobin and water are the major photon absorbers in living tissues. The highest absorption coefficient for hemoglobin is present within Vis wavelengths, while for water is present within UV and infrared wavelengths. In contrast, hemoglobin, water, lipids and other endogenous chromophores, such as melanin, have their lowest absorption coefficient within the NIR spectrum which allows increased photon depth penetration into tissues.[28-30]

**Table 1.1** *Main imaging techniques and their fundamental features, as in reference 19.*

| IT[a] | Energy Used | CA used | Sensitivity (mol/L) | Resolution (mm)[b] | Depth (mol/L) | Time of analysis | Additional advantages | Additional disadvantages | Costs[c] |
|---|---|---|---|---|---|---|---|---|---|
| ***MRI*** | Radio Waves | 1) Gd chelates 2) Gd-cont.NPs 3) IO-NPs[d] | $10^{-3}$-$10^{-5}$ | 0.01-0.1 (small animal) 0.5-1.5 (clinical) | No limit. | min-hrs | | 1) High soft tissue discrimination 2) No imaging probes for functional imaging | H |
| ***CT*** | X-rays | 1) Iodinated molecules 2) X-ray abs NPs | $10^{-1}$ | 0.03-0.4 | No limit. | sec-min | 1) Limited soft tissue discrimination 2) Radiation concerns | | M/L |
| ***US*** | Sound waves (high frequency) | 1) μ-bubbles 2)NPs | $10^{-9}$-$10^{-11}$ | 1) 0.04-0.1 (small animal) 2) 0.1-1 (clinical) | 1-200 | sec-min | 1) No whole body imaging 2) Seldom target specific imaging | 1) High sensitivity 2) Portable | M/L |
| ***PET*** | Annihilation (γ) photons | Radio-nuclides | $10^{-10}$-$10^{-12}$ | 1) 1-2 (μ PET) 2) 6-10 (clinical PET) | No limit. | min | 1) Radiation concerns 2) Seldom target specific imaging | 1) High soft tissue discrimination 2) Tracer amounts of probes and high contrast | H |
| ***SPECT*** | γ-rays | Radio-nuclides | $10^{-10}$-$10^{-12}$ | 0.5-2 (μ SPECT) 7-15 (clinical SPECT) | No limit. | min | | 1) High soft tissue discrimination 2) Tracer amounts of probes | M |
| ***PA*** | VIS-IR light | NIR-abs dyes and NPs | $10^{-9}$ | 0.03-0.05 | 1-60 | min | | | L |
| ***OI*** | UV-VIS and IR light | Lumin. Dyes and NPs | $10^{-9}$-$10^{-12}$ | 1-3 | 1-20 | sec-min | | 1) Multiplexing imaging 2) Targeted and activable probes | L |

*[1]IT=imaging techniques. Colors were used to indicate the clinical translation of main imaging techniques. Green=yes; yellow=no; red=partial. [2]Spatial resolution in experiments with small anaimals. In the case of clinical applications a resolution decrease of a factor varying from 2 to about 10 usually takes place. [3]IO=Iron Oxide; [4]H=High; M=Medium; L=Low.*

Between the huge variety of new materials that nanotechnology has suggested in recent decades, nanoparticles are, without doubt, those that are most used and versatile. Moreover, self-organizing synthetic strategies managing to implement these nanoplatforms, produce materials suitable for complex functions.[31-36] For these reasons, nanoparticles will have a key role in the course of this thesis, as will be explained in the next section.

## 1.2 Aim of the work

The aim of this thesis is to design, synthesize and characterize systems based on luminescent nanoparticles to be exploited as chemosensors or as labels for bioapplications.

A chemosensor is a device that combines three different components: (i) a recognition site (or receptor), able to molecular recognize the analyte; (ii) a signaling unit, apt to transform the molecular recognition into a detectable signal[37-39] and, in most cases, (iii) a linker to separate spatially the receptor and the analyte. A label is a device that provides a detectable signal, leading to the spatial and temporal collocation of an analyte.[40-42] Unlike the previous case, the signaling unit does not depend on the recognition event (Figure 1.1).

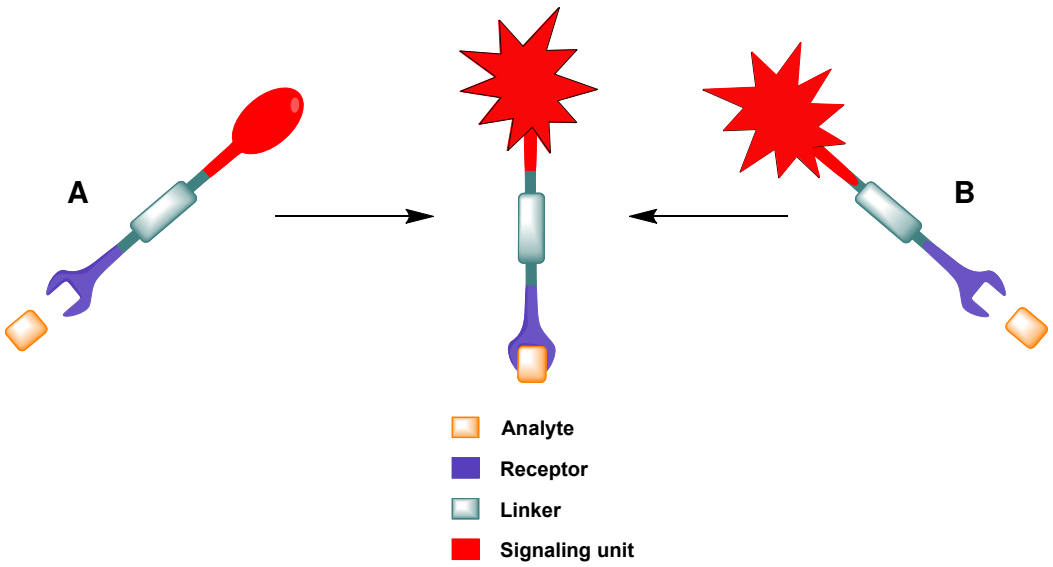


**Figure 1.1** *Schematic representation of a luminescent chemosensor (A) and label (B).*

Between the different imaging approaches suitable for bioanalytical applications, luminescence - and, especially, fluorescence - based techniques are particularly of interest to collect molecular level information about biologically relevant processes, because of their versatility, capacity to allow spatial and temporal resolution and low costs.[37,43-45] In the next section the basics of fluorescence will be introduced, focusing on the essential parameters to be considered for the design of fluorescent nanoprobes.

## 1.3 Fluorescence

### 1.3.1 Photophysical processes

Light excitation with a photon (hν) of suitable energy leads to the promotion of a molecule from its ground state (A) to an electronically excited state (A*) (Figure 1.2).

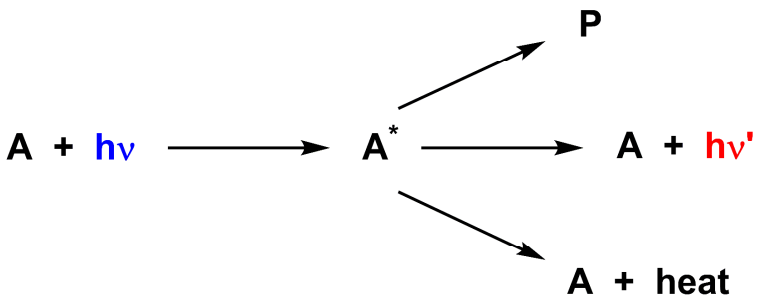


**Figure 1.2** *Schematic representation of essential steps of the light-molecule interaction.*

Due to their high-energy content, electronically excited states are metastable and in a short period of time are subjected to deactivation; this process takes place following three main pathways:

1) Photochemical reaction: it is a reaction induced by the light that leads to the formation of other species (P).

2) Nonradiative deactivation: the excess energy is dissipated as heat due to collision with other surrounding molecules, especially those of the solvent.

3) Radiative deactivation: the return of the molecule to its ground state is accompanied by the emission of a photon.

An energy diagram, commonly known as Jablonski diagram, is used to represent the photophysical processes which affect the ground and the excited states of a molecule (Figure 1.3).

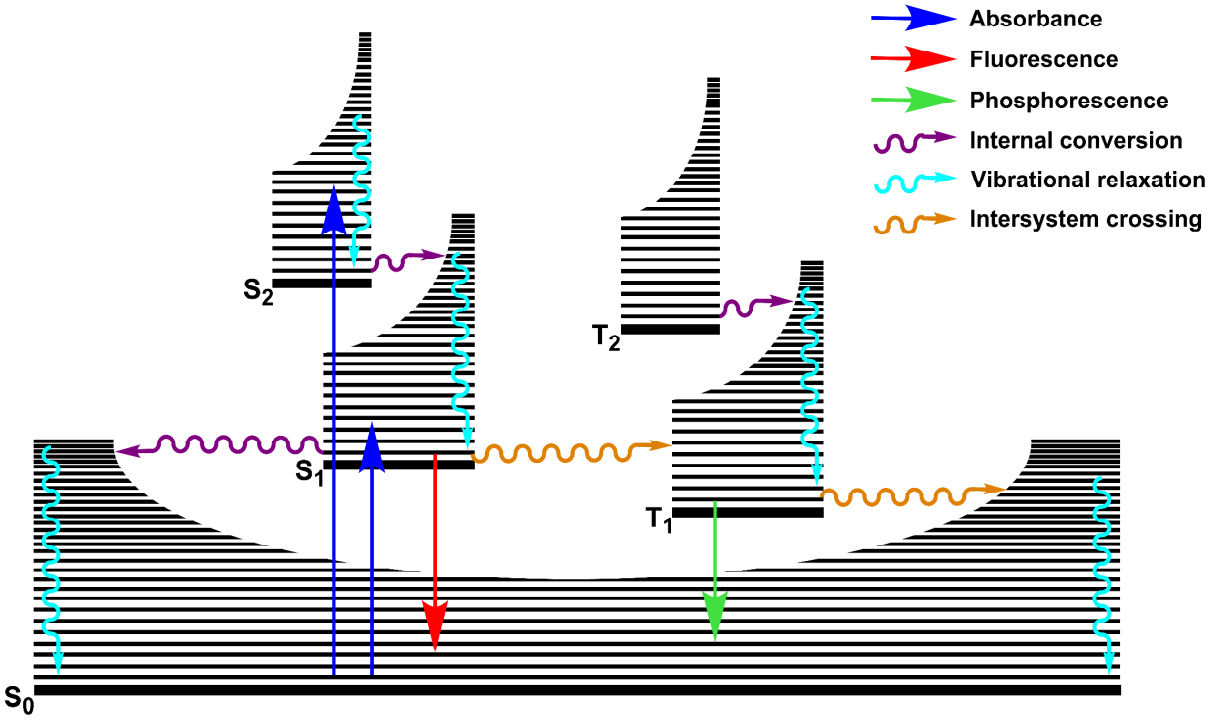


**Figure 1.3** *Schematic representation of simplified Jablonski diagram for a generic organic fluorophore.*

In such a diagram, the electronic states are depicted as thick horizontal lines and their relative energies are positioned in vertical order. The transitions between states are depicted as vertical lines and occur in a time (about $10^{-15}$ s) too short for noticeable displacement of nuclei, as inferred from the Franck-Condon principle. Vibrational levels are shown by thin lines while, for clarity, rotational levels are not indicated. Radiative transitions, relative to the absorption or emission of a photon, are shown by straight arrows, while radiationless transitions are represented by wavy arrows.

The ground state is assumed to be a singlet and depicted as $S_0$, as for many organic fluorophores, while $S_1$ and $S_2$ are the excited states with its same spin multiplicity. For clarity, only the first tripled excited state, $T_1$, is shown.

Light absorption commonly generates the excited state in a high vibrational level. The molecules tend to dissipate their excess vibrational energy by collisions with surrounding molecules in a very fast process (about $10^{-12}$ s) called *vibrational relaxation*. Radiationless transitions among states of equal spin multiplicity ($S_2$ and $S_1$, for example) are called *internal conversion,* that generally occur within $10^{-12}$ s or less and are immediately followed by vibrational relaxation.

The excited molecule can return to the ground state following the internal conversion/vibrational relaxation pathway, or through a radiative transition associated with the emission of a photon, known as *fluorescence*. Given that fluorescence is a slower process ($10^{-9}$-$10^{-6}$ s) than those previously cited, it can generally be observed only from the lowest vibrational level of $S_1$ (Kasha's rule):[46] it follows that fluorescence spectrum is typically the mirror image of the of the $S_0$ $S_1$ transition. Because of the loss of energy due to vibrational relaxation, the energy of the emission is less than that of absorption: consequently, fluorescence typically occurs at lower energies (or longer wavelengths).

Molecules in the S1 state can also be subjected to a spin conversion to the first triplet state $T_1$, through *intersystem crossing*, i.e., a non-radiative transition between states of different spin multiplicity; this transition is theoretically forbidden by the spin electron rule but can be promoted, through the spin-orbit coupling, in molecules containing halogens[47-49] or in transition metal complexes.[50-52] Emission from $T_1$ is termed *phosphorescence* ($10^{-2}$-$10^{2}$ s) and is commonly shifted to longer wavelength compared to fluorescence; however, it is rare to observe phosphorescence at room temperature due to the predominance of accessible non-radiative pathways.

### 1.3.2 Fluorescent nanoparticles

Luminescence is a very sensitive technique that allows the detection down to single molecule detection and offers submicron visualization and sub millisecond temporal resolution. Systems that used luminescence-related techniques[13,53-55] to collect molecular level information about biologically relevant processes could overcome many of the typical limitations of conventional luminophores - organic dyes (Figure 1.4) - such as poor photostability and water solubility, low quantum yield and aggregation under physiological conditions.

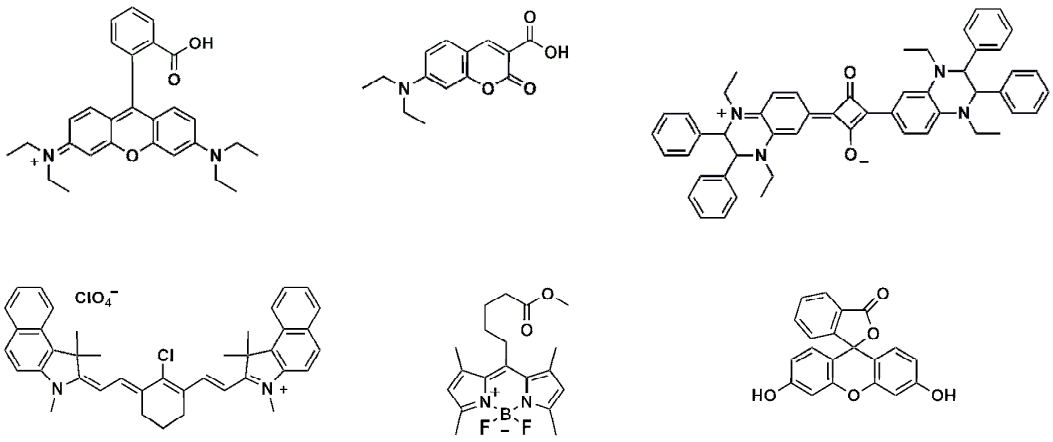


**C** **D** **E**

**Figure 1.4** *Chemical structures of (A) rhodamine-B, (B) cumarine, (C) squaraine, (D) cyanine, (E) BODIPY and (F) fluorescein derivatives.*

In this context, nanotechnology leaded to the design of platforms taking advantage of many classes of nanoparticles - organic, inorganic and metallic - which are currently used as fluorescent emitters, each presenting its own pros and cons. Luminescent dye-doped latex nanoparticles[56,57] or intrinsically luminescent nanomaterials,[12] like quantum dots (QDs) are broadly studied.[58-67]

In particular, dye-doped silica nanoparticles are a very successful example, and in the next paragraph we will describe their principal features and bioanalytical applications.

## 1.4 Dye-doped silica nanoparticles

Dye-doped silica nanoparticles (DSNPs) offers all the necessary features to develop impactful tools for diagnostic and theranostic applications;[13,32,37,42,68-72] indeed, their synthetic versatility leads to the achievement of multifunctional targeted nanosystems (Figure 1.5). A fine control of functionalization can produce important consequences: (i) the improvement of specific binding by the target sites;[73,74] (ii) the decrease in nonspecific interactions;[9,75] (iii) the enhancement of internalization by cells that overexpress the target receptor;[76] (iv) the limitation of capture by macrophages of the reticuloendothelial system (RES),[77] increasing the blood circulation times.[78]

The advantages of DSNPs are due to their convenient use as fluorescent probes for applications ranging from biosensors[38,79] to interfacial interaction studies such as immunoassays,[80] multiplexed nucleic acid analysis[81,82] and drug delivery.[83]

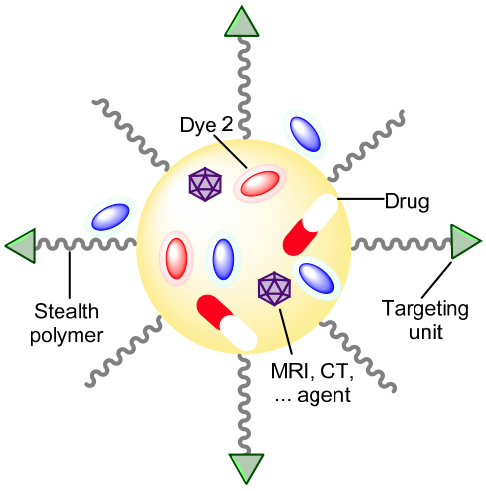


**Figure 1.5** *Schematic representation of DSNPs as multifunctional system for nanomedicine as in reference 59.*

The methods to synthesize DSNPs are very versatile - allowing the control over the architecture of the resulting materials - and share fundamental features such as simplicity, low costs and trouble-free disposal; a more detailed description of the synthetic methods will be performed in Chapter 2.

Materials suited to bioanalysis must be non-toxic, (photo)chemically stable and biocompatible. For the reasons expressed above, the toxicity of SNPs is a key topic that is inserted into the more general issue of the potential risks, for both humans and the environment, associated with nanomaterials. The uptake, persistence, transformation and excretion of silica-based nanoparticles are under investigation nowadays.[84] The lack of complete understanding of their *in vivo* toxicity and distribution makes human clinical trials not very common, despite the fact that these nanomaterials are of increasing interest in bioapplications. To confirm this trend, most SNPs-based systems for drug-dye delivery are still in the preclinical development stage. Appropriate answers to these problems require a thorough analysis of several parameters - such as different design, dimensions and charges[70,85,86] - which can result in a different toxicity; for this reason the accurate characterization of SNPs is a prerequisite for the toxicity assessment.[87] *In vitro* assays are widely used to assess the toxicity, as they are inexpensive, easy and reliable;[88,89] on the contrary, *in vivo* tests[90-93] are much less frequently reported, making the study of long-term effects, retention and excretion incomplete.[40,54,70,94,95] However, in this complicated scenario we can say that the evidence obtained so far demonstrated that (i) silica does not show intrinsic toxicity and is not subjected to microbial attack and (ii) DSNPs does not exhibit appreciable toxicity in different relevant cell models.[40] These data support the safe use of these nanoplatforms for diagnostic and therapeutic applications.

To be more specific regarding the features possessed by luminescent silica nanoparticles, we should start from the intrinsic properties of silica, which is photophysically inert; therefore, the photophysical properties of the final platforms are given by the doping and/or the capping agents. Each DSNP may contain many dyes and consequently shows extremely high extinction coefficient, since its total value is equal to the sum of those of the individual chromophore.[31,32,37] In addition to that, the inclusion in the silica matrix supplies a constant chemical environment to active species and protects from external chemicals, leading to (i) the decrease in the probability of unwanted photoreactions and (ii) the increase in the photostability of the system.[96] Doping species are responsible for the emission properties of DSNPs, with effects due not only to their own features, but also to their potential cross-interactions. By means of classic photophysical techniques - such as fluorescence anisotropy and steady-state and time-resolved fluorescence - it is possible to obtain information on the distance and communication among the active species, on their rotational mobility and on the effect of signal amplification. These data, for example, are of interest to the evaluation of homo-energy transfer processes, as they can cause unwanted self-quenching phenomena; nevertheless, Genovese *et al.* showed that they can be exploited to make the excitation energy available for the final processes of interest, thus increasing the signal amplification effect.[97] Otherwise, if DSNPs are loaded with different dyes, the possible hetero-energy transfer processes can be promoted to obtain nanoparticles suitable for multiplex Förster resonance energy transfer (FRET) bioassays,

because of a high fluorescence intensity, wide absorption and large Stokes shift,[45,98] i.e., the difference among the first absorption band and the maximum of the fluorescence spectrum. On the other hand, with a convenient design, hetero-energy transfer processes can also be intentionally avoided, leading to ratiometric systems.[99,100]

At the beginning of this section, we have presented the versatility of DSNPs as the starting point for exploring their promising developments. At this point, it is important to underline that versatility is intrinsic to luminescence spectroscopy; indeed, in addition to the luminescent parameters exploited for monitoring the target species[43] - such as intensity, anisotropy, emission and excitation spectra and excited state lifetime - the different origins of the luminescent process can introduce another element of versatility. In particular, the generation of luminescence without photo-excitation leads to higher sensitivity due to the increased signal-to-noise ratio; the most commonly exploited techniques are those that are able to generate luminescence from electrogenerated species in solution, namely chemiluminescence (CL)[101-103] and electrochemiluminescence (ECL).[104,105] In this regard, it is important to note that ECL is regularly used for the quantification of biomolecules and ECL nanoprobes are quickly increasing in number and complexity.[35,36,106] We also want to emphasize the promising prospects offered by thermochemiluminescence (TL), where the excited state is generated by the thermolysis of suitable molecules; it is a technique that, for the first time, has recently been used in combination with nanoparticles, providing encouraging results.[34]

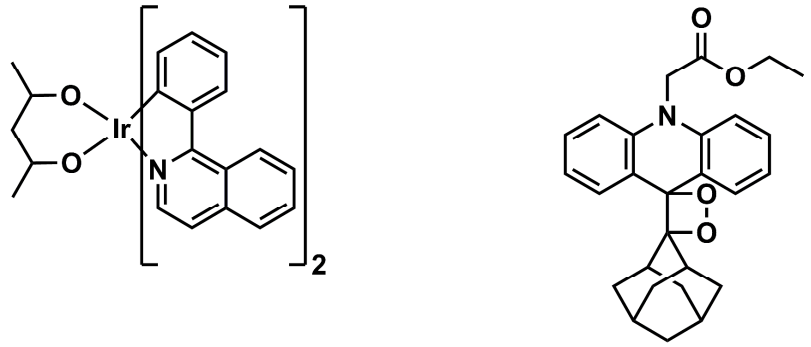


**Figure 1.6** *Schematic representation of derivatives used for: A) ECL, as in reference 106; B) TCL, as in reference 34.*

A more complete description of DSNPs will be discussed in the next chapter, concerning the common synthetic approaches to these materials.

## 1.5 Notes and references

(1) Prasad, P. N. *Introduction to Nanomedicine and Nanobioengineering*; John Wiley & Sons, 2012; Vol. 1.

(2) Pene, F.; Courtine, E.; Cariou, A.; Mira, J. P. *Critical Care Medicine* **2009**, *37*, S50.
(3) Xiao, Q. F.; Zheng, X. P.; Bu, W. B.; Ge, W. Q.; Zhang, S. J.; Chen, F.; Xing, H. Y.; Ren, Q. G.; Fan, W. P.; Zhao, K. L.; Hua, Y. Q.; Shi, J. L. *J. Am. Chem. Soc.* **2013**, *135*, 13041.
(4) Hecht, M.; Climent, E.; Biyikal, M.; Sancenón, F.; Martínez-Máñez, R.; Rurack, K. *Coordin Chem Rev* **2013**, *257*, 2589.
(5) Kim, J.; Piao, Y.; Hyeon, T. *Chem Soc Rev* **2009**, *38*, 372.
(6) Chen, C. Y.; Li, Y. F.; Qu, Y.; Chai, Z. F.; Zhao, Y. L. *Chem Soc Rev* **2013**, *42*, 8266.
(7) Weissleder, R.; Nahrendorf, M.; Pittet, M. J. *Nat Mater* **2014**, *13*, 125.
(8) Hussain, T.; Nguyen, Q. T. *Adv Drug Deliver Rev* **2014**, *66*, 90.
(9) Kaur, S.; Venktaraman, G.; Jain, M.; Senapati, S.; Garg, P. K.; Batra, S. K. *Cancer Letters* **2012**, *315*, 97.
(10) Biju, V. *Chem Soc Rev* **2014**, *43*, 744.
(11) Gong, H.; Peng, R.; Liu, Z. *Adv Drug Deliver Rev* **2013**, *65*, 1951.
(12) Novio, F.; Simmchen, J.; Vazquez-Mera, N.; Amorin-Ferre, L.; Ruiz-Molina, D. *Coordin Chem Rev* **2013**, *257*, 2839.
(13) Arap, W.; Pasqualini, R.; Montalti, M.; Petrizza, L.; Prodi, L.; Rampazzo, E.; Zaccheroni, N.; Marchio, S. *Current Medicinal Chemistry* **2013**, *20*, 2195.
(14) Gallo, J.; Long, N. J.; Aboagye, E. O. *Chem Soc Rev* **2013**, *42*, 7816.
(15) Lee, N.; Choi, S. H.; Hyeon, T. *Adv Mater* **2013**, *25*, 2641.
(16) Mitchell, N.; Kalber, T. L.; Cooper, M. S.; Sunassee, K.; Chalker, S. L.; Shaw, K. P.; Ordidge, K. L.; Badar, A.; Janes, S. M.; Blower, P. J.; Lythgoe, M. F.; Hailes, H. C.; Tabor, A. B. *Biomaterials* **2013**, *34*, 1179.
(17) Khalil, M. M.; Tremoleda, J. L.; Bayomy, T. B.; Gsell, W. *International Journal of Molecular Imaging* **2011**, *2011*.
(18) Kiessling, F.; Fokong, S.; Bzyl, J.; Lederle, W.; Palmowski, M.; Lammers, T. *Adv Drug Deliver Rev* **2014**, *72*, 15.
(19) Xing, Y.; Zhao, J.; Conti, P. S.; Chen, K. *Theranostics* **2014**, *4*, 290.
(20) Zackrisson, S.; van de Ven, S. M.; Gambhir, S. S. *Cancer Research* **2014**, *74*, 979.
(21) Liu, Q.; Feng, W.; Li, F. Y. *Coordin Chem Rev* **2014**, *273*, 100.
(22) Hemmer, E.; Venkatachalam, N.; Hyodo, H.; Hattori, A.; Ebina, Y.; Kishimoto, H.; Soga, K. *Nanoscale* **2013**, *5*, 11339.
(23) Li, Y. P.; Lin, T. Y.; Luo, Y.; Liu, Q. Q.; Xiao, W. W.; Guo, W. C.; Lac, D.; Zhang, H. Y.; Feng, C. H.; Wachsmann-Hogiu, S.; Walton, J. H.; Cherry, S. R.; Rowland, D. J.; Kukis, D.; Pan, C. X.; Lam, K. S. *Nat Commun* **2014**, *5*.
(24) Vankayala, R.; Huang, Y. K.; Kalluru, P.; Chiang, C. S.; Hwang, K. C. *Small* **2014**, *10*, 1612.
(25) Guo, M.; Mao, H. J.; Li, Y. L.; Zhu, A. J.; He, H.; Yang, H.; Wang, Y. Y.; Tian, X.; Ge, C. C.; Peng, Q. L.; Wang, X. Y.; Yang, X. L.; Chen, X. Y.; Liu, G.; Chen, H. B. *Biomaterials* **2014**, *35*, 4656.
(26) Wang, B. K.; Wang, J. H.; Liu, Q.; Huang, H.; Chen, M.; Li, K. Y.; Li, C. Z.; Yu, X. F.; Chu, P. K. *Biomaterials* **2014**, *35*, 1954.
(27) Terentyuk, G.; Panfilova, E.; Khanadeev, V.; Chumakov, D.; Genina, E.; Bashkatov, A.; Tuchin, V.; Bucharskaya, A.; Maslyakova, G.; Khlebtsov, N.; Khlebtsov, B. *Nano Res* **2014**, *7*, 325.
(28) Sato, Y.; Kanazawa, S.; Saiki, T. *Microscopy* **2014**, *63*, i10.
(29) Biffi, S.; Petrizza, L.; Rampazzo, E.; Voltan, R.; Sgarzi, M.; Garrovo, C.; Prodi, L.; Andolfi, L.; Agnoletto, C.; Zauli, G.; Secchiero, P. *RSC Advances* **2014**, *4*, 18278.
(30) Golmohammadi, S.; Khalilou, Y.; Ahmadivand, A. *Optics Communications* **2014**, *321*, 56.
(31) Rampazzo, E.; Bonacchi, S.; Juris, R.; Montalti, M.; Genovese, D.; Zaccheroni, N.; Prodi, L.; Rambaldi, D. C.; Zattoni, A.; Reschiglian, P. *The journal of physical chemistry. B* **2010**, *114*, 14605.
(32) Genovese, D.; Bonacchi, S.; Juris, R.; Montalti, M.; Prodi, L.; Rampazzo, E.; Zaccheroni, N. *Angew. Chem.-Int. Edit.* **2013**, *52*, 5965.
(33) Dolci, L. S.; Zanarini, S.; Ciana, L. D.; Paolucci, F.; Roda, A. *Analytical Chemistry* **2009**, *81*, 6234.
(34) Roda, A.; Di Fusco, M.; Quintavalla, A.; Guardigli, M.; Mirasoli, M.; Lombardo, M.; Trombini, C. *Analytical Chemistry* **2012**, *84*, 9913.
(35) Valenti, G.; Rampazzo, E.; Bonacchi, S.; Khajvand, T.; Juris, R.; Montalti, M.; Marcaccio, M.; Paolucci, F.; Prodi, L. *Chemical Communications* **2012**, *48*, 4187.
(36) Rampazzo, E.; Bonacchi, S.; Genovese, D.; Juris, R.; Marcaccio, M.; Montalti, M.; Paolucci, F.; Sgarzi, M.; Valenti, G.; Zaccheroni, N.; Prodi, L. *Coordin Chem Rev* **2012**, *256*, 1664.
(37) Bonacchi, S.; Genovese, D.; Juris, R.; Montalti, M.; Prodi, L.; Rampazzo, E.; Zaccheroni, N. *Angew. Chem.-Int. Edit.* **2011**, *50*, 4056.
(38) Bonacchi, S.; Genovese, D.; Juris, R.; Montalti, M.; Prodi, L.; Rampazzo, E.; Sgarzi, M.; Zaccheroni, N. *Topics in Current Chemistry* **2011**, *300*, 93.

(39) Rampazzo, E.; Bonacchi, S.; Genovese, D.; Juris, R.; Sgarzi, M.; Montalti, M.; Prodi, L.; Zaccheroni, N.; Tomaselli, G.; Gentile, S.; Satriano, C.; Rizzarelli, E. *Chemistry – A European Journal* **2011**, *17*, 13429.
(40) Rampazzo, E.; Voltan, R.; Petrizza, L.; Zaccheroni, N.; Prodi, L.; Casciano, F.; Zauli, G.; Secchiero, P. *Nanoscale* **2013**, *5*, 7897.
(41) Rampazzo, E.; Boschi, F.; Bonacchi, S.; Juris, R.; Montalti, M.; Zaccheroni, N.; Prodi, L.; Calderan, L.; Rossi, B.; Becchi, S.; Sbarbati, A. *Nanoscale* **2012**, *4*, 824.
(42) Montalti, M.; Prodi, L.; Rampazzo, E.; Zaccheroni, N. *Chem Soc Rev* **2014**, *43*, 4243.
(43) Bonacchi, S.; Genovese, D.; Juris, R.; Montalti, M.; Prodi, L.; Rampazzo, E.; Sgarzi, M.; Zaccheroni, N. In *Luminescence Applied in Sensor Science*; Prodi, L., Montalti, M., Zaccheroni, N., Eds.; Springer Berlin Heidelberg: 2011; Vol. 300, p 93.
(44) Puntoriero, F.; Nastasi, F.; Cavazzini, M.; Quici, S.; Campagna, S. *Coordin Chem Rev* **2007**, *251*, 536.
(45) Bonacchi, S.; Genovese, D.; Juris, R.; Marzocchi, E.; Montalti, M.; Prodi, L.; Rampazzo, E.; Zaccheroni, N. In *Reviews in Fluorescence 2008*; Geddes, C., Ed.; Springer New York: 2010; Vol. 2008, p 119.
(46) Demchenko, A. P.; Heldt, J.; Waluk, J.; Chou, P.-T.; Sengupta, P. K.; Brizhik, L.; del Valle, J. C. *Angew. Chem.-Int. Edit.* **2014**, *53*, 14316.
(47) Bolton, O.; Lee, K.; Kim, H.-J.; Lin, K. Y.; Kim, J. *Nat Chem* **2011**, *3*, 205.
(48) Gao, H. Y.; Zhao, X. R.; Wang, H.; Pang, X.; Jin, W. J. *Cryst Growth Des* **2012**, *12*, 4377.
(49) Vestfrid, J.; Botoshansky, M.; Palmer, J. H.; Durrell, A. C.; Gray, H. B.; Gross, Z. *J. Am. Chem. Soc.* **2011**, *133*, 12899.
(50) Zhao, Q.; Huang, C.; Li, F. *Chem Soc Rev* **2011**, *40*, 2508.
(51) Jia, W.-L.; Liu, Q.-D.; Wang, R.; Wang, S. *Organometallics* **2003**, *22*, 4070.
(52) Fernandez-Moreira, V.; Thorp-Greenwood, F. L.; Coogan, M. P. *Chemical Communications* **2010**, *46*, 186.
(53) Bae, S. W.; Tan, W.; Hong, J.-I. *Chemical Communications* **2012**, *48*, 2270.
(54) Bradbury, M. S.; Phillips, E.; Montero, P. H.; Cheal, S. M.; Stambuk, H.; Durack, J. C.; Sofocleous, C. T.; Meester, R. J. C.; Wiesner, U.; Patel, S. *Integrative Biology* **2013**, *5*, 74.
(55) Ray, P. C.; Khan, S. A.; Singh, A. K.; Senapati, D.; Fan, Z. *Chem Soc Rev* **2012**, *41*, 3193.
(56) Miragoli, M.; Novak, P.; Ruenraroengsak, P.; Shevchuk, A. I.; Korchev, Y. E.; Lab, M. J.; Tetley, T. D.; Gorelik, J. *Nanomedicine* **2012**, *8*, 725.
(57) Prilloff, S.; Fan, J.; Henrich-Noack, P.; Sabel, B. A. *European Journal of Neuroscience* **2010**, *31*, 521.
(58) Wu, P.; Yan, X.-P. *Chem Soc Rev* **2013**, *42*, 5489.
(59) Lesnyak, V.; Gaponik, N.; Eychmuller, A. *Chem Soc Rev* **2013**, *42*, 2905.
(60) Taylor, A.; Wilson, K. M.; Murray, P.; Fernig, D. G.; Levy, R. *Chem Soc Rev* **2012**, *41*, 2707.
(61) Freeman, R.; Girsh, J.; Willner, I. *ACS Applied Materials & Interfaces* **2013**, *5*, 2815.
(62) Freeman, R.; Willner, B.; Willner, I. *The Journal of Physical Chemistry Letters* **2011**, *2*, 2667.
(63) Willner, I.; Willner, B. *Nano Letters* **2010**, *10*, 3805.
(64) Amelia, M.; Lincheneau, C.; Silvi, S.; Credi, A. *Chem Soc Rev* **2012**, *41*, 5728.
(65) Margapoti, E.; Gentili, D.; Amelia, M.; Credi, A.; Morandi, V.; Cavallini, M. *Nanoscale* **2013**.
(66) Credi, A. *New Journal of Chemistry* **2012**, *36*, 1925.
(67) Wang, Y.; Hu, R.; Lin, G.; Roy, I.; Yong, K.-T. *ACS Applied Materials & Interfaces* **2013**, *5*, 2786.
(68) Piao, Y.; Burns, A.; Kim, J.; Wiesner, U.; Hyeon, T. *Adv. Funct. Mater.* **2008**, *18*, 3745.
(69) Montalti, M.; Rampazzo, E.; Zaccheroni, N.; Prodi, L. *New Journal of Chemistry* **2013**, *37*, 28.
(70) Helle, M.; Rampazzo, E.; Monchanin, M.; Marchal, F.; Guillemin, F.; Bonacchi, S.; Salis, F.; Prodi, L.; Bezdetnaya, L. *ACS Nano* **2013**, *7*, 8645.
(71) Kumar, R.; Roy, I.; Ohulchanskyy, T. Y.; Goswami, L. N.; Bonoiu, A. C.; Bergey, E. J.; Tramposch, K. M.; Maitra, A.; Prasad, P. N. *ACS Nano* **2008**, *2*, 449.
(72) Vivero-Escoto, J. L.; Huxford-Phillips, R. C.; Lin, W. *Chem Soc Rev* **2012**, *41*, 2673.
(73) Rocco, M. A.; Kim, J.-Y.; Burns, A.; Kostecki, J.; Doody, A.; Wiesner, U.; DeLisa, M. P. *Bioconjugate Chemistry* **2009**, *20*, 1482.
(74) Soster, M.; Juris, R.; Bonacchi, S.; Genovese, D.; Montalti, M.; Rampazzo, E.; Zaccheroni, N.; Garagnani, P.; Bussolino, F.; Prodi, L.; Marchio, S. *International Journal of Nanomedicine* **2012**, *7*, 4797.
(75) Dufort, S.; Sancey, L.; Coll, J.-L. *Adv Drug Deliver Rev* **2012**, *64*, 179.
(76) Ryu, J. H.; Koo, H.; Sun, I.-C.; Yuk, S. H.; Choi, K.; Kim, K.; Kwon, I. C. *Adv Drug Deliver Rev* **2012**, *64*, 1447.
(77) Dobrovolskaia, M. A.; Aggarwal, P.; Hall, J. B.; McNeil, S. E. *Molecular pharmaceutics* **2008**, *5*, 487.
(78) van Schooneveld, M. M.; Vucic, E.; Koole, R.; Zhou, Y.; Stocks, J.; Cormode, D. P.; Tang, C. Y.; Gordon, R. E.; Nicolay, K.; Meijerink, A.; Fayad, Z. A.; Mulder, W. J. M. *Nano Letters* **2008**, *8*, 2517.
(79) Burns, A.; Sengupta, P.; Zedayko, T.; Baird, B.; Wiesner, U. *Small* **2006**, *2*, 723.

(80) Nooney, R. I.; McCormack, E.; McDonagh, C. *Analytical and Bioanalytical Chemistry* **2012**, *404*, 2807.
(81) Wang, L.; Tan, W. *Nano Letters* **2005**, *6*, 84.
(82) Yan, J.; Estévez, M. C.; Smith, J. E.; Wang, K.; He, X.; Wang, L.; Tan, W. *Nano Today* **2007**, *2*, 44.
(83) Zhang, P.; Kong, J. *Talanta* **2015**, *134*, 501.
(84) Sharifi, S.; Behzadi, S.; Laurent, S.; Laird Forrest, M.; Stroeve, P.; Mahmoudi, M. *Chem Soc Rev* **2012**, *41*, 2323.
(85) Kim, J.-H.; Kim, C.-S.; Ignacio, R. M. C.; Kim, D.-H.; Sajo, M. E. J.; Maeng, E. H.; Qi, X.-F.; Park, S.-E.; Kim, Y.-R.; Kim, M.-K.; Lee, K.-J.; Kim, S.-K. *International Journal of Nanomedicine* **2014**, *9*, 183.
(86) Bhattacharjee, S.; de Haan, L.; Evers, N.; Jiang, X.; Marcelis, A.; Zuilhof, H.; Rietjens, I.; Alink, G. *Particle and Fibre Toxicology* **2010**, *7*, 25.
(87) Sapsford, K. E.; Algar, W. R.; Berti, L.; Gemmill, K. B.; Casey, B. J.; Oh, E.; Stewart, M. H.; Medintz, I. L. *Chem Rev* **2013**, *113*, 1904.
(88) Lewinski, N.; Colvin, V.; Drezek, R. *Small* **2008**, *4*, 26.
(89) Halamoda Kenzaoui, B.; Chapuis Bernasconi, C.; Guney-Ayra, S.; Juillerat-Jeanneret, L. *Biochemical Journal* **2012**, *441*, 813.
(90) Fischer, H. C.; Chan, W. C. W. *Current Opinion in Biotechnology* **2007**, *18*, 565.
(91) Khlebtsov, N.; Dykman, L. *Chem Soc Rev* **2011**, *40*, 1647.
(92) Mahmoudi, M.; Hofmann, H.; Rothen-Rutishauser, B.; Petri-Fink, A. *Chem Rev* **2012**, *112*, 2323.
(93) Cho, M.; Cho, W.-S.; Choi, M.; Kim, S. J.; Han, B. S.; Kim, S. H.; Kim, H. O.; Sheen, Y. Y.; Jeong, J. *Toxicology Letters* **2009**, *189*, 177.
(94) He, X.; Nie, H.; Wang, K.; Tan, W.; Wu, X.; Zhang, P. *Analytical Chemistry* **2008**, *80*, 9597.
(95) Burns, A. A.; Vider, J.; Ow, H.; Herz, E.; Penate-Medina, O.; Baumgart, M.; Larson, S. M.; Wiesner, U.; Bradbury, M. *Nano Letters* **2008**, *9*, 442.
(96) Rampazzo, E.; Bonacchi, S.; Genovese, D.; Juris, R.; Montalti, M.; Paterlini, V.; Zaccheroni, N.; Dumas-Verdes, C.; Clavier, G.; Meallet-Renault, R.; Prodi, L. *J Phys Chem C* **2014**, *118*, 9261.
(97) Genovese, D.; Rampazzo, E.; Bonacchi, S.; Montalti, M.; Zaccheroni, N.; Prodi, L. *Nanoscale* **2014**, *6*, 3022.
(98) Wang, L.; O'Donoghue, M. B.; Tan, W. *Nanomedicine (Lond)* **2006**, *1*, 413.
(99) Doussineau, T.; Schulz, A.; Lapresta-Fernandez, A.; Moro, A.; Korsten, S.; Trupp, S.; Mohr, G. J. *Chemistry- A European Journal* **2010**, *16*, 10290.
(100) Arduini, M.; Mancin, F.; Tecilla, P.; Tonellato, U. *Langmuir* **2007**, *23*, 8632.
(101) Su, Y.; Xie, Y.; Hou, X.; Lv, Y. *Applied Spectroscopy Reviews* **2013**, *49*, 201.
(102) Iranifam, M. *TRAC Trends in Analytical Chemistry* **2014**, *59*, 156.
(103) Iranifam, M. *TRAC Trends in Analytical Chemistry* **2013**, *51*, 51.
(104) Deng, S.; Ju, H. *Analyst* **2013**, *138*, 43.
(105) Li, J.; Guo, S.; Wang, E. *RSC Advances* **2012**, *2*, 3579.
(106) Zanarini, S.; Rampazzo, E.; Bonacchi, S.; Juris, R.; Marcaccio, M.; Montalti, M.; Paolucci, F.; Prodi, L. *J. Am. Chem. Soc.* **2009**, *131*, 14208.

# Chapter 2

# Synthesis of luminescent silica nanoparticles

## 2.1 Introduction

The synthetic approaches in solution to perform silica nanoparticles (SNPs) are based on sol-gel processes, by using tetrahethoxysilane (TEOS) as their silica precursor.[1] These methods share important features such as high versatility and reproducibility, low costs, mild synthetic conditions, control over the dimensional range of the resulting nanoparticles, and the possibility of choosing parameters such as catalytic conditions and the nanoparticle nucleation-growth confinement.

These main synthetic methods are known as Stöber-Van Blaaderen, reverse microemulsion (also called "water in oil")[2-5] and direct micelles assisted methods[2,6-8] and allow a great versatility in the design of SNPs. However, it is important to take into account the qualities and weaknesses of each synthetic strategy, since these features are transferred to the resulting nanostructures (Table 2.1).

**Table 2.1** *Main fluorescent Silica nanoparticles synthetic methods: versatility ( ☆= poor; ☆☆☆ = very good).*

| SNPs synthetic method | Dimensional range | Colloidal stability | Dyes incorporation | Surface modification | Accessibility to hybrid systems | Overall efficiency |
|---|---|---|---|---|---|---|
| *Stöber* | ☆☆☆ | ☆☆☆ | ☆☆ | ☆ | ☆☆ | ☆ |
| *Reverse microemulsion* | ☆☆ | ☆☆ | ☆ | ☆☆☆ | ☆☆☆ | ☆☆ |
| *Direct micelles* | ☆ | ☆☆☆ | ☆☆☆ | ☆☆☆ | ☆☆ | ☆☆☆ |

In most cases the synthesis of luminescent SNPs relies on trialkoxysilane derivatized dyes which are covalently linked to the silica matrix, to avoid dye leaching in the external environment, to prevent dye toxicity and therefore to securely fix fluorescent emission due to SNPs in biological media.[9,10]

The number of dyes which can be incorporated within a nanoparticle is a very important parameter: potential problems can be due to the dye solubility in the reaction medium, and to the difficulty of synthesis and purification of the trialkoxysilane derivatives. As a general indication, electrostatic interactions among the dyes and the silica core of SNPs promote the incorporation of positively charged molecules and inhibit the inclusion of negatively charged species.

In the case of biomedical applications, the overall synthesis efficiency is an average of a large number of parameters such as the brightness of the system (concerning the dye incorporation), the surface derivatization (concerning the targeting, colloidal stability and behavior in biological environments), and the dimensional range. The spatial control over

nanoparticles components is often a priority to carry specific functions, especially in complex architectures.

## 2.2 Stöber method

This method exploits TEOS hydrolysis for the nanoparticle formation using ammonia as catalyst in an ethanol/water mixture. This synthetic procedure to obtain colloidal silica originates from a study of Kolbe and Stöber,[11] then improved by Van Blaaderen using triethoxysilane (-Si) modified dyes, such as fluorescein isothiocyanate-Si[9] and rhodamine B isothiocyanate-Si (Figure 2.1).[10]

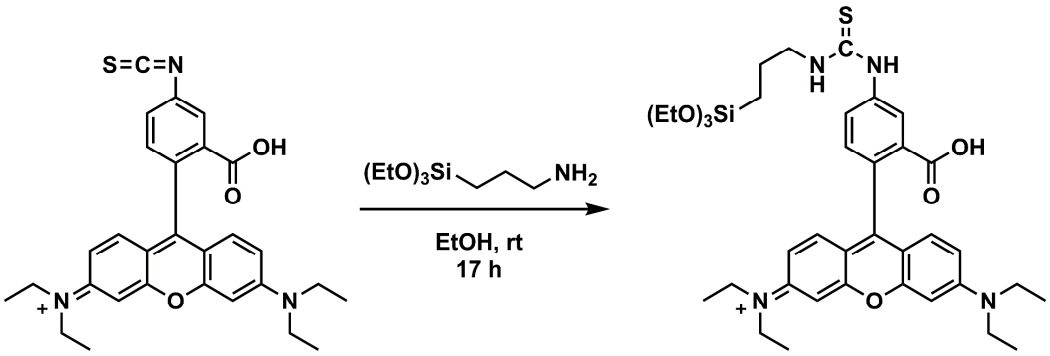


**Figure 2.1** *Synthesis of rhodamine B isothiocyanate-Si as in reference 10.*

With the Stöber-Van Blaaderen method, the achievable dimensional range - with one pot procedures - is quite large, spanning from 10 to several hundreds of nm. This approach requires mild conditions (Figure 2.2) and allows the control of dimensional range by varying concentrations and ratios of the components in the reactions mixture (TEOS, water and ammonia).[12]

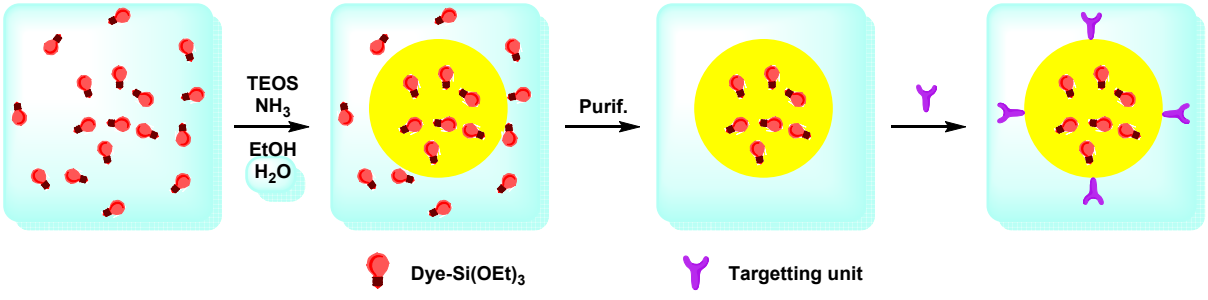


**Figure 2.2** Schematization of the *Stöber-Van Blaaderen method for the synthesis of SNPs as in reference 10.*

Alkoxysilane derivatized dyes are used in order to achieve the covalent doping of the SNPs, but some limitations may rise from their solubility in ethanol/water mixtures.[10] The luminescence properties of these nanocolloidal systems are based on the mutual position of the dyes within the SNPs.[13] Previous reports showed that alkoxysilane pyrene derivatives undergo to self-compartmentalization during NP nucleation and growth processes, which can lead to spontaneous core-shell structures (Figure 2.3).[14] Two different modifications of the Stöber method have been developed:

(1) the use of amino acids as the hydrolytic catalyst and a phase transfer approach to modulate the TEOS provision into the reaction medium.[15] With this method it is possible to obtain very small nanoparticles (~ 10 nm) and multiple-shell monodisperse nanoparticles;

(2) the strategy developed by Wiesner and co-workers, which exploit a heterogeneous nucleation process where dyes reach cores act as seeds in the nucleation process.[16-18] The luminescent silica NPs obtained in this way, called *Cornell Dots* (or *C-Dots*), have a core-shell structure that allows the control over NPs monodispersity and dimension and protect the dyes from the solvent, thus increasing their photostability.[19-22]

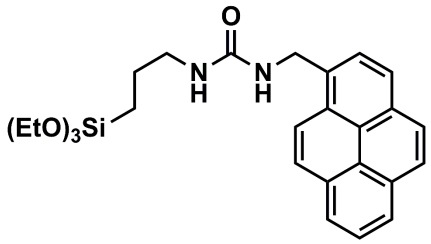


**Figure 2.3** *Molecular structure of the pyrene derivative as in reference 14.*

Colloidal suspension obtained by the Stöber methods are stabilized by electrostatic repulsion, since the deprotonation of the Si-OH groups on the SNPs surface yield nanoparticles with very negative ζ-potential values. Furthermore, it is possible to functionalize these NPs by chemical modifications on Si-OH groups with additional alkoxysilane components for several applications; the occurrence of aggregation and incomplete passivation of the surface can make this process quite tricky.

Purification steps are necessary to remove uncondensed dyes, catalysts, oligomers and, if necessary, to change suspending media. These processes may include precipitation-centrifugation steps, ultrafiltration (UF), dialysis, size exclusion chromatography (SEC) and other instrumental techniques as FlFFF (Flow Field Flow Fractionation).[23] The last three purification methods presented here are mild and contribute to preserve the SNPs monodispersity.

## 2.3 Reverse microemulsion method

In this approach a Stöber process is carried out in a reverse microemulsion: a thermodynamically stable, isotropic, and transparent solution of hydrocarbon, water and surfactant. The water droplets in the reverse microemulsion act as nanoreactors in a continuous domain of hydrocarbon, where the hydrolysis and condensation processes, that form the SNPs, take place.[24] Several synthetic protocols supply the nanoparticle synthesis and surface modification in the 15-200 nm dimensional range,[2,25] which depend upon the surfactant type (Figure 2.4) and on the surfactant-to-water molar ratio.[26] Unfortunately, this approach is suitable for positively charged water soluble dyes (Figure 2.5),[3,27,28] which can be entrapped in the nanoparticle silica core by electrostatic interactions; this is a strong limitation for the incorporation of poorly water soluble or negatively charged dyes.

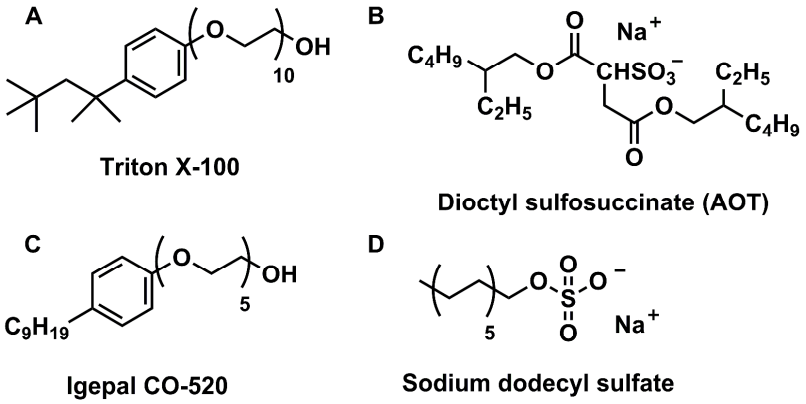


**Figure 2.4** *Molecular structures of more common surfactants used in the reverse microemulsion synthesis of silica nanoparticles as in reference 2 (A, B, C and D) and in reference 3 (C).*

This approach is particularly useful for the synthesis of SNPs with a layer-by-layer structure, to develop hybrid structures by covering nanoparticles of other materials (Q-Dots, metals, iron oxides, etc.) with a silica shell, and for the surface derivatization to increase the chemical stabilization or for bio-molecules targeting.[29]

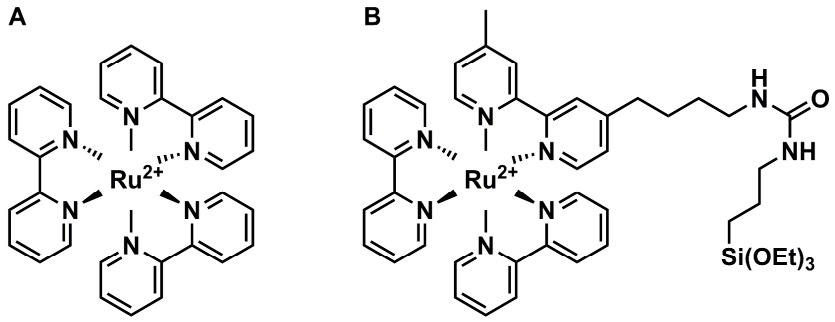


**Figure 2.5** Ru(II) complexes used *in the reverse microemulsion synthesis of silica nanoparticles as in reference 2 (A) and in reference 3 (B).*

These derivatizations are obtained by subsequent addition of reactants within the microemulsion, without intermediate purification steps,[2,25] which are necessary to remove the organic solvent and the surfactants from SNPs, and usually are carried through precipitation-centrifugation-sonication steps which can lead to irreversible aggregation among the nanoparticles (Figure 2.6).

The addition of appropriate ratios of inert functional groups (e.g., methylphosphonate) to active functional groups (e.g., amino groups) to the surface of silica nanoparticles results in very negative ζ-potential values, which can minimize nanoparticles aggregation and nonspecific binding.[25]

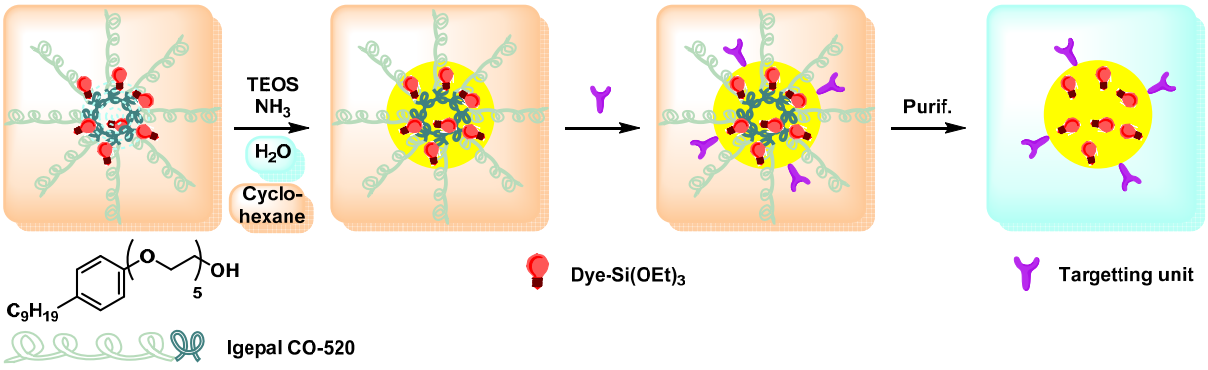


**Figure 2.6** *Schematization of the reverse microemulsion method for the synthesis of silica nanoparticles as in reference 3.*

## 2.4 Direct micelles assisted methods

### 2.4.1 ORMOSIL nanoparticles

With this approach the hydrolysis and condensation processes involving highly lipophilic silica precursors such as TEOS and organo-alkoxyilane take place in direct aggregates or

co-aggregates of surfactants in water. A large variety of dyes can be used to produce luminescent and very mono-disperse nanoparticles in water, with a dimensional range of 10-60 nm; this features make this method versatile for the development of luminescent nanocolloids for *in vivo* and *in vitro* applications.

This strategy has many advantages such as the possibility of using water as a solvent, and of lower surfactant (co-surfactant) quantities compared to the reverse microemulsion strategies. The direct micelles assisted methods differ from each other mainly in the molecular weight of the surfactant implicated in formation of the nanoparticles. Also in this case, SNPs purification procedures are necessary to remove silica oligomers, surfactants and dyes that have not been trapped in the particles.

With this approach Prasad and co-workers have made many nanoparticles in the 20-30 nm dimensional range that are often called ORMOSIL (Organic modified Silica), obtained using oil in water systems usually made by mixtures of surfactant, DMSO, 1-butanol and water.[30-33] The hydrolysis of the lipophilic silica precursor triethoxyvinylsilane (VTES) is catalysed by addition of (3-Aminopropyl)triethoxysilane (APTES) or ammonia, while the low molecular weight surfactants normally used are Tween 80[34] or Bis(2-ethylhexyl) sulfosuccinate sodium salt (AOT).[35-38] This SNPs have a certain degree of mesoporosity, due to the presence of the surfactant and to the low reticulation deriving from the trialkoxysilane precursor: for these reasons the covalent condensation of the doping agents (such as dyes[39] and PDT agents[35,40,41]) is needed to avoid leaching from the particle.[34,42] With the use of this strategy surface functionalization (-$NH_2$, -COOH, -SH also together with polyethylene glycol (PEG) chains) is readily accessible and allows for conjugation with bioactive molecules (Figure 2.7).[36,43,44] The incorporation of dyes, PDT agents, and the possibility of obtaining hybrid structures containing QDs[45] and $Fe_3O_4$ nanoparticles[46] make the ORMOSIL particles very versatile platforms for multimodal imaging and the development of theranostic nanoprobes.

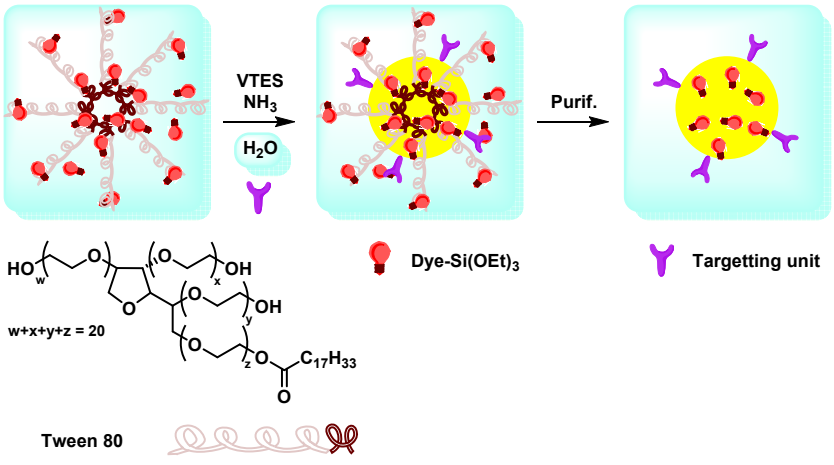


**Figure 2.7** Schematization of the *direct micelles assisted method for the synthesis of ORMOSIL nanoparticles as in reference 40.*

This last synthetic strategy can be used with high molecular weight surfactants, where the occurrence of entrapment-adsorption phenomena can cause the irreversible bond among the surfactant molecules and the silica matrix. Several groups took advantage of the template effect of high molar weight surfactants such as Pluronic F108 or Brij700 to obtain cross-linked micellar SNPs that have core-shell structures,[7,47,48] or to tune the SNP size using an organic swelling agent, such as trimethylbenzene.[49]

### 2.4.2 Pluronic F127 nanoparticles

Our research group proposed a strategy to obtain luminescent core-shell silica-PEG nanoparticles[6] which can be employed in several fields such as photophysical studies,[50] live cells fluorescence imaging,[51] *in vivo* imaging,[52] electrochemiluminescence (ECL) applications[7,53] and chemical sensors development.[54,55] This synthetic strategy relies on the formation of direct micelles of Pluronic F127 (Figure 2.8) in water.[47,56]

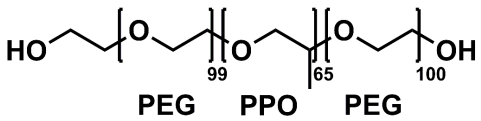


**Figure 2.8** *Molecular structure of Pluronic F127*

Pluronic surfactants represent a family of non-ionic tri-block A-B-A copolymers, bearing a poly(ethylene glycol)$_x$-poly(propylene oxide)$_y$-poly(ethylene glycol)$_x$ ($PEG_x$-$PPO_y$-$PEG_x$) structure, thus terminating in primary hydroxy groups.[57] Specifically, Pluronic F127 has an average molecular weight of 12.6 KDa, (x = 100 and y = 65), and Pluronic F127 micelles have a PPO hydrophobic core and a more hydrophilic PEG shell.[58,59]

When added to a Pluronic F127 aqueous solution, TEOS is able to diffuse and condensate in the hydrophobic PPO core: the central part of the micelle acts as a nanoreactor for the hydrolysis and condensation processes of TEOS and of triethoxysilane-derivatized dyes used as doping units. Hydrolysis-condensation processes are promoted by an acidic environment, using diluted acids such as HOAc[51] or HCl[47,57]: in these conditions (pH < 4) hydrolysis has faster kinetics compared with the condensation rate, leading to the occurrence of Si-O-Si chains in the early stages of polymerization,[60] that finally undergo cross-linking.[61] In this way, the confinement of the silica matrix occurs exclusively in the micellar environment, together with the entrapment and adsorption processes of the surfactant to the silica core, leading to the nanoparticle surface modification in a single synthetic process (Figure 2.9).

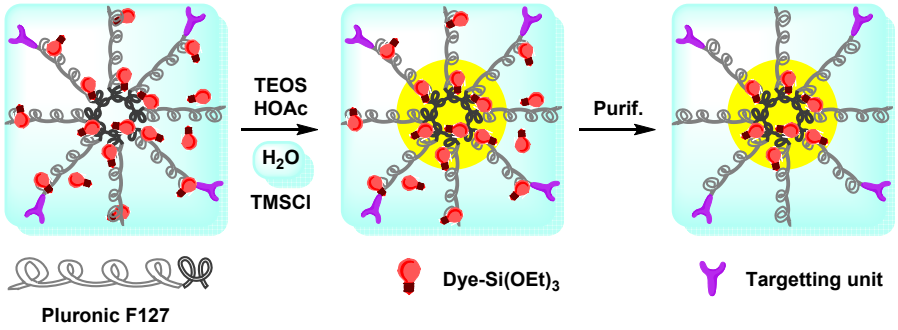


**Figure 2.9** Schematization of the *direct micelles assisted method for the synthesis of F127 nanoparticles.*

A terminating agent such as trimethylsilyl chloride (TMSCl) is added to the reaction mixture to stop the condensation of TEOS: TMSCl, in fact, supplies alkyl substituents for the end-capping of the silica surface.[62,63]

This synthetic strategy is useful to obtain luminescent core-shell silica-PEG nanoparticles with very high monodispersity and colloidal stability in water, bearing a silica core of about 10 nm (Figure 2.10) and an overall hydrodynamic diameter (including the PEG shell) of

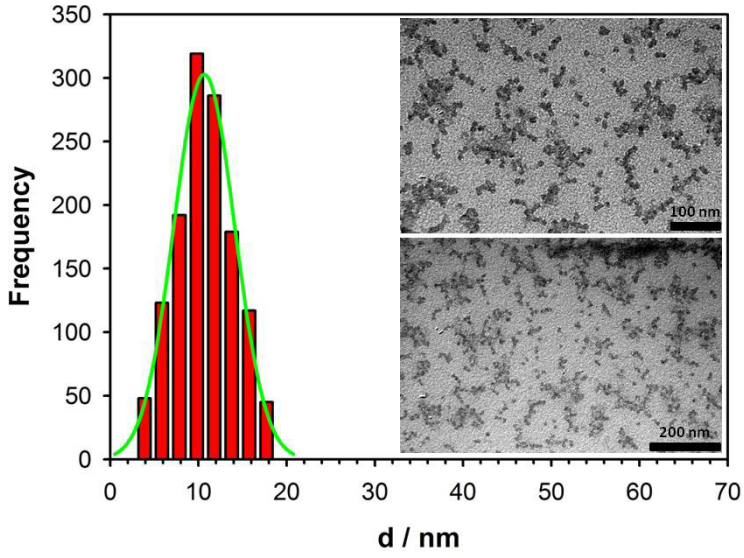


**Figure 2.10** *TEM images of silica core/PEG shell nanoparticles (silica core size distribution, $d_c$ = 11 ± 3 nm).*

about 25 nm (Figure 2.11).[64,65] This last feature, deriving from the entrapped Pluronic F127, together with the non-toxic properties of PEG are valuable characteristics able to confer stealth properties in biological environments.[66,67]

This synthetic method is applicable to a vast variety of trialkoxysilane derivatized dyes, since it is quite independent from their solubility properties.[68]

These core-shell silica-PEG nanoparticles can also act as labels modifying the Pluronic F127 hydroxy end groups (see Chapter 3, 6 and 8).[52,69] These modifications are carried out in the pristine Pluronic F127 surfactant, then used in the nanoparticle synthesis in the desired amount, so that no post nanoparticle functionalization is needed to introduce chemical functionalities (-COOH, $-NH_2$, -SH, $-N_3$, alkynes, etc.) for targeting and bio-molecule conjugation.[70,71] It is also possible to obtain charge insertion through silica core functionalization using a suitable silane reagent, to provide SNPs in which the charges are hidden by the PEG shell surrounding the silica core.[71] These features make SNPs highly adaptable for *in vitro* and *in vivo* imaging applications.

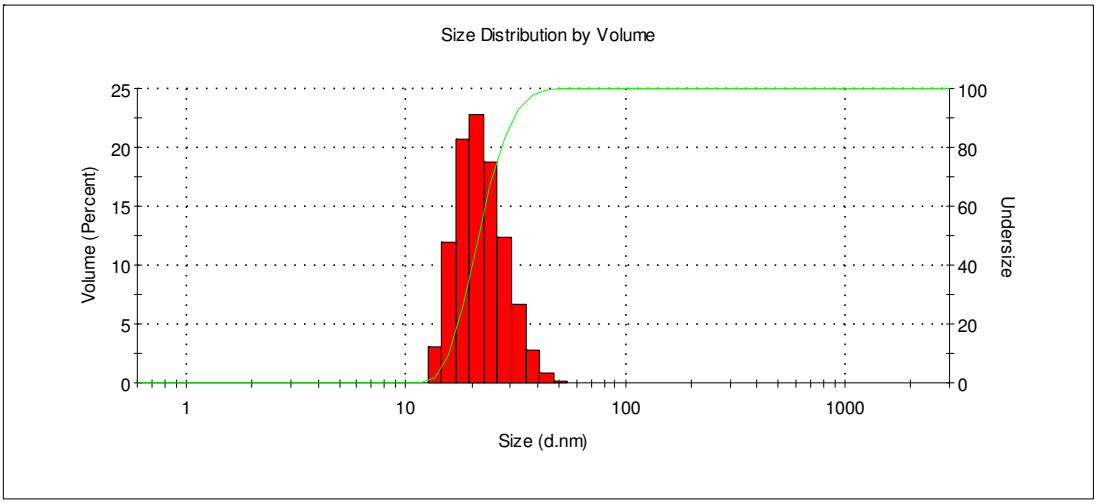


**Figure 2.11** *Dynamic light scattering diameter distribution by volume and undersize curve for silica core/PEG shell nanoparticles ($d_H$ = 25 nm; PdI = 0.04, water, 25°C).*

## 2.5 Conclusions

Luminescent silica nanoparticles in solution can be obtained mainly by Stöber, reverse microemulsion and direct micelles assisted methods. Every strategy has quite different characteristics, that can be exploited to tailor the final system to a specific application.

The direct micelles assisted strategy using Pluronic F127 has proven to be suitable for the synthesis of silica-core/PEG-shell nanoparticles with high reproducibility, stability and monodispersity. This characteristics make them extremely versatile for *in vitro* and *in vivo* imaging applications. By modification of the surfactant hydroxy end groups, and by functionalization of the silica core, in a one-pot procedure it is possible to introduce

functional groups on the surface and on the silica core of these nanoplatforms, with the objective of using them as devices for bioanalytical applications.

The possible use of the silica-core/PEG-shell nanoparticles as fluorescent labels will be shown in the next chapter.

## 2.6 Notes and references


(1) Hench, L. L.; West, J. K. *Chemical Reviews* **1990**, *90*, 33.
(2) Bagwe, R. P.; Yang, C.; Hilliard, L. R.; Tan, W. *Langmuir* **2004**, *20*, 8336.
(3) Zanarini, S.; Rampazzo, E.; Ciana, L. D.; Marcaccio, M.; Marzocchi, E.; Montalti, M.; Paolucci, F.; Prodi, L. *Journal of the American Chemical Society* **2009**, *131*, 2260.
(4) Arriagada, F. J.; Osseo-Asare, K. *Journal of Colloid and Interface Science* **1999**, *211*, 210.
(5) Osseo-Asare, K.; Arriagada, F. J. *Journal of Colloid and Interface Science* **1999**, *218*, 68.
(6) Bonacchi, S.; Genovese, D.; Juris, R.; Montalti, M.; Prodi, L.; Rampazzo, E.; Zaccheroni, N. *Angewandte Chemie International Edition* **2011**, *50*, 4056.
(7) Zanarini, S.; Rampazzo, E.; Bonacchi, S.; Juris, R.; Marcaccio, M.; Montalti, M.; Paolucci, F.; Prodi, L. *Journal of the American Chemical Society* **2009**, *131*, 14208.
(8) Yong, K. T.; Roy, I.; Swihart, M. T.; Prasad, P. N. *Journal of Materials Chemistry* **2009**, *19*, 4655.
(9) Van Blaaderen, A.; Imhof, A.; Hage, W.; Vrij, A. *Langmuir* **1992**, *8*, 1514.
(10) Verhaegh, N. A. M.; Blaaderen, A. v. *Langmuir* **1994**, *10*, 1427.
(11) Kolbe, G., 1956.
(12) van Blaaderen, A.; Vrij, A. *Journal of Colloid and Interface Science* **1993**, *156*, 1.
(13) Prasad, P. N. *Introduction to Nanomedicine and Nanobioengineering*; John Wiley & Sons, 2012; Vol. 1.
(14) Rampazzo, E.; Bonacchi, S.; Montalti, M.; Prodi, L.; Zaccheroni, N. *Journal of the American Chemical Society* **2007**, *129*, 14251.
(15) Wang, J.; Sugawara-Narutaki, A.; Fukao, M.; Yokoi, T.; Shimojima, A.; Okubo, T. *ACS Applied Materials & Interfaces* **2011**, *3*, 1538.
(16) Nyffenegger, R.; Quellet, C.; Ricka, J. *Journal of Colloid and Interface Science* **1993**, *159*, 150.
(17) Ow, H.; Larson, D. R.; Srivastava, M.; Baird, B. A.; Webb, W. W.; Wiesner, U. *Nano Letters* **2004**, *5*, 113.
(18) Larson, D. R.; Ow, H.; Vishwasrao, H. D.; Heikal, A. A.; Wiesner, U.; Webb, W. W. *Chemistry of Materials* **2008**, *20*, 2677.
(19) Burns, A. A.; Vider, J.; Ow, H.; Herz, E.; Penate-Medina, O.; Baumgart, M.; Larson, S. M.; Wiesner, U.; Bradbury, M. *Nano Letters* **2008**, *9*, 442.
(20) Herz, E.; Ow, H.; Bonner, D.; Burns, A.; Wiesner, U. *Journal of Materials Chemistry* **2009**, *19*, 6341.
(21) Cohen, B.; Martin, C.; Iyer, S. K.; Wiesner, U.; Douhal, A. *Chemistry of Materials* **2011**, *24*, 361.
(22) Pedone, A.; Prampolini, G.; Monti, S.; Barone, V. *Chemistry of Materials* **2011**, *23*, 5016.
(23) Montalti, M.; Prodi, L.; Zaccheroni, N.; Zattoni, A.; Reschiglian, P.; Falini, G. *Langmuir* **2004**, *20*, 2989.
(24) Zhao, X.; Bagwe, R. P.; Tan, W. *Advanced Materials* **2004**, *16*, 173.
(25) Bagwe, R. P.; Hilliard, L. R.; Tan, W. *Langmuir* **2006**, *22*, 4357.
(26) Arriagada, F. J.; Osseo-Asare, K. *Journal of Colloid and Interface Science* **1995**, *170*, 8.
(27) Wang, L.; Lofton, C.; Popp, M.; Tan, W. *Bioconjugate Chemistry* **2007**, *18*, 610.
(28) Wang, L.; Zhao, W.; O'Donoghu, M. B.; Tan, W. *Bioconjugate Chemistry* **2007**, *18*, 297.
(29) Chang, C.-L.; Fogler, H. S. *Langmuir* **1997**, *13*, 3295.
(30) Koo, Y.-E. L.; Cao, Y.; Kopelman, R.; Koo, S. M.; Brasuel, M.; Philbert, M. A. *Analytical Chemistry* **2004**, *76*, 2498.
(31) Xu, H.; Aylott, J. W.; Kopelman, R.; Miller, T. J.; Philbert, M. A. *Analytical Chemistry* **2001**, *73*, 4124.
(32) Koo Lee, Y.-E.; Smith, R.; Kopelman, R. *Annual Review of Analytical Chemistry* **2009**, *2*, 57.
(33) Kim, G.; Huang, S.-W.; Day, K. C.; O'Donnell, M.; Agayan, R. R.; Day, M. A.; Kopelman, R.; Ashkenazi, S. *BIOMEDO* **2007**, *12*, 044020.
(34) Ohulchanskyy, T. Y.; Roy, I.; Goswami, L. N.; Chen, Y.; Bergey, E. J.; Pandey, R. K.; Oseroff, A. R.; Prasad, P. N. *Nano Letters* **2007**, *7*, 2835.
(35) Roy, I.; Ohulchanskyy, T. Y.; Pudavar, H. E.; Bergey, E. J.; Oseroff, A. R.; Morgan, J.; Dougherty, T. J.; Prasad, P. N. *Journal of the American Chemical Society* **2003**, *125*, 7860.

(36) Roy, I.; Ohulchanskyy, T. Y.; Bharali, D. J.; Pudavar, H. E.; Mistretta, R. A.; Kaur, N.; Prasad, P. N. *Proceedings of the National Academy of Sciences of the United States of America* **2005**, *102*, 279.
(37) Kim, S.; Pudavar, H. E.; Prasad, P. N. *Chemical Communications* **2006**, 2071.
(38) Rio-Echevarria, I. M.; Selvestrel, F.; Segat, D.; Guarino, G.; Tavano, R.; Causin, V.; Reddi, E.; Papini, E.; Mancin, F. *Journal of Materials Chemistry* **2010**, *20*, 2780.
(39) Kim, S.; Huang, H.; Pudavar, H. E.; Cui, Y.; Prasad, P. N. *Chemistry of Materials* **2007**, *19*, 5650.
(40) Kim, S.; Ohulchanskyy, T. Y.; Pudavar, H. E.; Pandey, R. K.; Prasad, P. N. *Journal of the American Chemical Society* **2007**, *129*, 2669.
(41) Compagnin, C.; Bau, L.; Mognato, M.; Celotti, L.; Miotto, G.; Arduini, M.; Moret, F.; Fede, C.; Selvestrel, F.; Echevarria, I. M. R.; Mancin, F.; Reddi, E. *Nanotechnology* **2009**, *20*.
(42) Selvestrel, F.; Moret, F.; Segat, D.; Woodhams, J. H.; Fracasso, G.; Echevarria, I. M. R.; Bau, L.; Rastrelli, F.; Compagnin, C.; Reddi, E.; Fedeli, C.; Papini, E.; Tavano, R.; Mackenzie, A.; Bovis, M.; Yaghini, E.; MacRobert, A. J.; Zanini, S.; Boscaini, A.; Colombatti, M.; Mancin, F. *Nanoscale* **2013**, *5*, 6106.
(43) Bharali, D. J.; Klejbor, I.; Stachowiak, E. K.; Dutta, P.; Roy, I.; Kaur, N.; Bergey, E. J.; Prasad, P. N.; Stachowiak, M. K. *Proceedings of the National Academy of Sciences of the United States of America* **2005**, *102*, 11539.
(44) Kumar, R.; Roy, I.; Ohulchanskyy, T. Y.; Goswami, L. N.; Bonoiu, A. C.; Bergey, E. J.; Tramposch, K. M.; Maitra, A.; Prasad, P. N. *ACS Nano* **2008**, *2*, 449.
(45) Seddon, A.; Li Ou, D. *Journal of Sol-Gel Science and Technology* **1998**, *13*, 623.
(46) Law, W.-C.; Yong, K.-T.; Roy, I.; Xu, G.; Ding, H.; Bergey, E. J.; Zeng, H.; Prasad, P. N. *Journal of Physical Chemistry C* **2008**, *112*, 7972.
(47) Huo, Q.; Liu, J.; Wang, L.-Q.; Jiang, Y.; Lambert, T. N.; Fang, E. *Journal of the American Chemical Society* **2006**, *128*, 6447.
(48) Chi, F.; Guan, B.; Yang, B.; Liu, Y.; Huo, Q. *Langmuir* **2010**, *26*, 11421.
(49) Chi, F.; Guo, Y.-N.; Liu, J.; Liu, Y.; Huo, Q. *Journal of Physical Chemistry C* **2010**, *114*, 2519.
(50) Rampazzo, E.; Bonacchi, S.; Juris, R.; Montalti, M.; Genovese, D.; Zaccheroni, N.; Prodi, L.; Rambaldi, D. C.; Zattoni, A.; Reschiglian, P. *Journal of Physical Chemistry B* **2010**, *114*, 14605.
(51) Rampazzo, E.; Boschi, F.; Bonacchi, S.; Juris, R.; Montalti, M.; Zaccheroni, N.; Prodi, L.; Calderan, L.; Rossi, B.; Becchi, S.; Sbarbati, A. *Nanoscale* **2012**, *4*, 824.
(52) Rampazzo, E.; Voltan, R.; Petrizza, L.; Zaccheroni, N.; Prodi, L.; Casciano, F.; Zauli, G.; Secchiero, P. *Nanoscale* **2013**, *5*, 7897.
(53) Valenti, G.; Rampazzo, E.; Bonacchi, S.; Khajvand, T.; Juris, R.; Montalti, M.; Marcaccio, M.; Paolucci, F.; Prodi, L. *Chemical Communications* **2012**, *48*, 4187.
(54) Rampazzo, E.; Bonacchi, S.; Genovese, D.; Juris, R.; Sgarzi, M.; Montalti, M.; Prodi, L.; Zaccheroni, N.; Tomaselli, G.; Gentile, S.; Satriano, C.; Rizzarelli, E. *Chemistry – A European Journal* **2011**, *17*, 13429.
(55) Montalti, M.; Rampazzo, E.; Zaccheroni, N.; Prodi, L. *New Journal of Chemistry* **2013**, *37*, 28.
(56) Pedone, A.; Gambuzzi, E.; Barone, V.; Bonacchi, S.; Genovese, D.; Rampazzo, E.; Prodi, L.; Montalti, M. *Physical Chemistry Chemical Physics* **2013**, *15*, 12360.
(57) Liu, J.; Bai, S.; Zhong, H.; Li, C.; Yang, Q. *Journal of Physical Chemistry C* **2009**, *114*, 953.
(58) Kozlov, M. Y.; Melik-Nubarov, N. S.; Batrakova, E. V.; Kabanov, A. V. *Macromolecules* **2000**, *33*, 3305.
(59) Alexandridis, P.; Holzwarth, J. F.; Hatton, T. A. *Macromolecules* **1994**, *27*, 2414.
(60) Cushing, B. L.; Kolesnichenko, V. L.; O'Connor, C. J. *Chemical Reviews* **2004**, *104*, 3893.
(61) Gallagher, D.; Ring, T. A. *Chimia* **1989**, *43*, 298.
(62) Biffi, S.; Petrizza, L.; Rampazzo, E.; Voltan, R.; Sgarzi, M.; Garrovo, C.; Prodi, L.; Andolfi, L.; Agnoletto, C.; Zauli, G.; Secchiero, P. *RSC Advances* **2014**, *4*, 18278.
(63) Weng, X.; Bao, Z.; Zhang, Z.; Su, B.; Xing, H.; Yang, Q.; Yang, Y.; Ren, Q. *Journal of Materials Chemistry B* **2015**, *3*, 620.
(64) Desai, P. R.; Jain, N. J.; Sharma, R. K.; Bahadur, P. *Colloids and Surfaces A: Physicochemical and Engineering Aspects* **2001**, *178*, 57.
(65) Rampazzo, E.; Bonacchi, S.; Juris, R.; Montalti, M.; Genovese, D.; Zaccheroni, N.; Prodi, L.; Rambaldi, D. C.; Zattoni, A.; Reschiglian, P. *Journal of Physical Chemistry B* **2010**, *114*, 14605.
(66) He, X.; Nie, H.; Wang, K.; Tan, W.; Wu, X.; Zhang, P. *Analytical Chemistry* **2008**, *80*, 9597.
(67) Knop, K.; Hoogenboom, R.; Fischer, D.; Schubert, U. S. *Angewandte Chemie International Edition* **2010**, *49*, 6288.
(68) Rampazzo, E.; Bonacchi, S.; Genovese, D.; Juris, R.; Montalti, M.; Paterlini, V.; Zaccheroni, N.; Dumas-Verdes, C.; Clavier, G.; Méallet-Renault, R.; Prodi, L. *The Journal of Physical Chemistry C* **2014**, *118*, 9261.
(69) Soster, M.; Juris, R.; Bonacchi, S.; Genovese, D.; Montalti, M.; Rampazzo, E.; Zaccheroni, N.; Garagnani, P.; Bussolino, F.; Prodi, L.; Marchio, S. *International Journal of Nanomedicine* **2012**, *7*, 4797.

(70) Wang, X.-d.; Stolwijk, J. A.; Lang, T.; Sperber, M.; Meier, R. J.; Wegener, J.; Wolfbeis, O. S. *Journal of the American Chemical Society* **2012**, *134*, 17011.
(71) Helle, M.; Rampazzo, E.; Monchanin, M.; Marchal, F.; Guillemin, F.; Bonacchi, S.; Salis, F.; Prodi, L.; Bezdetnaya, L. *ACS Nano* **2013**, *7*, 8645.

# Chapter 3

# Silica nanoparticles as fluorescent labels

## 3.1 Introduction

In this part we present Silica-based luminescent nanoparticles (SNPs) designed to display neutral, positive or negative charges on their surface will be presented. The main purposes of this experimental work were: to improve the cell adhesion and internalization efficiency of SNPs; to study the kinetics and mechanism of cell internalization as well as the persistence of SNPs-cellular fluorescence (mainly by flow cytometric analyses); to evaluate their cytotoxicity by using several cellular models.

Nanoparticles are up-and-coming devices in nanomedicine nowadays, because of their applicability in essential topics such as early diagnosis of several diseases and targeted therapy.[1-8] However, a great limitation is that only a few types of multifunctional nanostructures have reached the stage of clinical trials.[9] A parameter which must be taken into account in the design of nanoparticles is the uncertainty about their cellular uptake, as well as their potential cytotoxicity in different cell models.[10-14]

In the field of nanomedicine, SNPs can provide very stunning solutions for several reasons.[15] Firstly, luminescence measurements are highly sensitive (down to single molecule detection), smoothly carried out and very versatile, providing submicrom spatial resolution and sub-millisecond temporal resolution.[16] This enables, in general, low detection limits, and could allow the tracking of biological events to show the origin and growth of various pathologies, including cancer. Theoretically, there are many different fluorescent nanocolloids that could represent a good alternative to SNPs, such as dye doped latex nanoparticles,[17-19] or quantum dots (QDs), that are intrinsically luminescent nanomaterials.[8,20,21] Nevertheless, SNPs can show unparalleled features for effective diagnostics and theranostic applications.[8,13,20,22-27] In fact, from a chemical viewpoint, SNPs are very stable platforms to incorporate dyes, increasing the resistance to photobleaching as well as the protection against enzymatic degradation. Since many dyes can be contained inside a nanoparticle, it is possible to have an increase in the brightness and in the signal-to-noise ratio, with the possibility, when required, to tune the signals spectral range.[12,28]

In conclusion, the main synthetic methods (see Chapter 2) share important features such as high versatility and reproducibility, low costs and mild synthetic conditions that can be tuned to a large number of applications.[7,23] In this context, Prodi and co-workers recently developed a new one-pot synthetic approach for SNPs that starts from the preparation of Pluronic F127 micelles in water.[24,29,30] The resulting SNPs dispersions are bright, photostable, highly monodisperse (d ~ 25 nm) and stable in water also in the presence of proteins, thus offering a valuable advantage compared to other nanostructures, which

require solvothermal approaches with the use of organic solvents, quite high temperatures and additional steps for surface stabilization and derivatization.[15]

Moreover, it is noteworthy that the structure and versatility of these SNPs offer the possibility to load external species such as photoswitches,[31] drugs,[29] and chemosensors.[32] In the present study, the possibility to tune the external SNP charge was then investigated to improve the efficiency of SNP-cell binding/cell uptake processes. In particular, with the aim to translate these SNPs for *in vivo* applications, was assessed the potential cellular toxicity by using a variety of cellular models. Moreover, were analysed the kinetics and mechanism of cell internalization were, as well as the persistence of SNP-cellular fluorescence, mainly by flow cytometric quantitative approaches. The results obtained provide interesting evidences, opening up the possibility for several *in vivo* applications of these derivatized fluorescent SNPs.

## 3.2 Result and discussion

### 3.2.1 Synthesis and characterization of nanoparticles

The surfactant Pluronic F127 was derivatized to obtain two derivatives: F127-carbo and F127-amino. These two compounds, along with the unmodified F127 (Table 3.1), were employed for the synthesis of SNPs having on their outer PEG shells negative, positive or neutral charges,[30] respectively, yielding NP-PEG-carbo, NP-PEG-amino and NP-PEG, as shown in Fig. 3.2. All the SNPs were covalently doped with a triethoxysilane derivative of the Rhodamine B (RhodB-Si): the covalent linking of the dyes to the silica matrix limits dye leaching in the biological environment and circumvents dye toxicity. In addition, the photophysical properties of this derivatized dye allow visualizationby both flow-cytometry and fluorescence microscopy (Fig. 3.1).

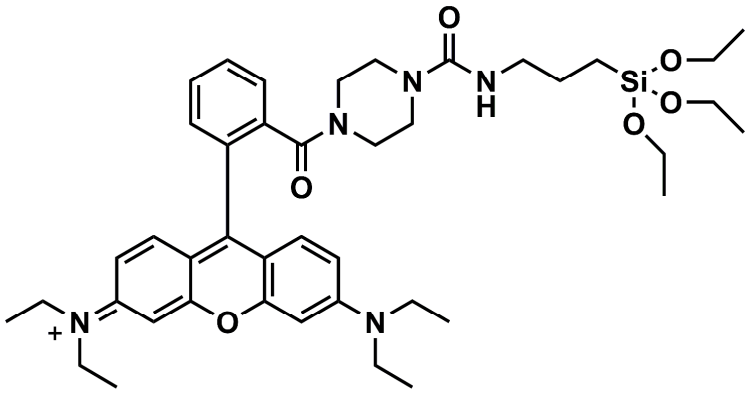


**Figure 3.1** *Molecular structure of RhodB-Si.*

In this context it is worth underlining that covalent linking of fluorophores to the NP silica

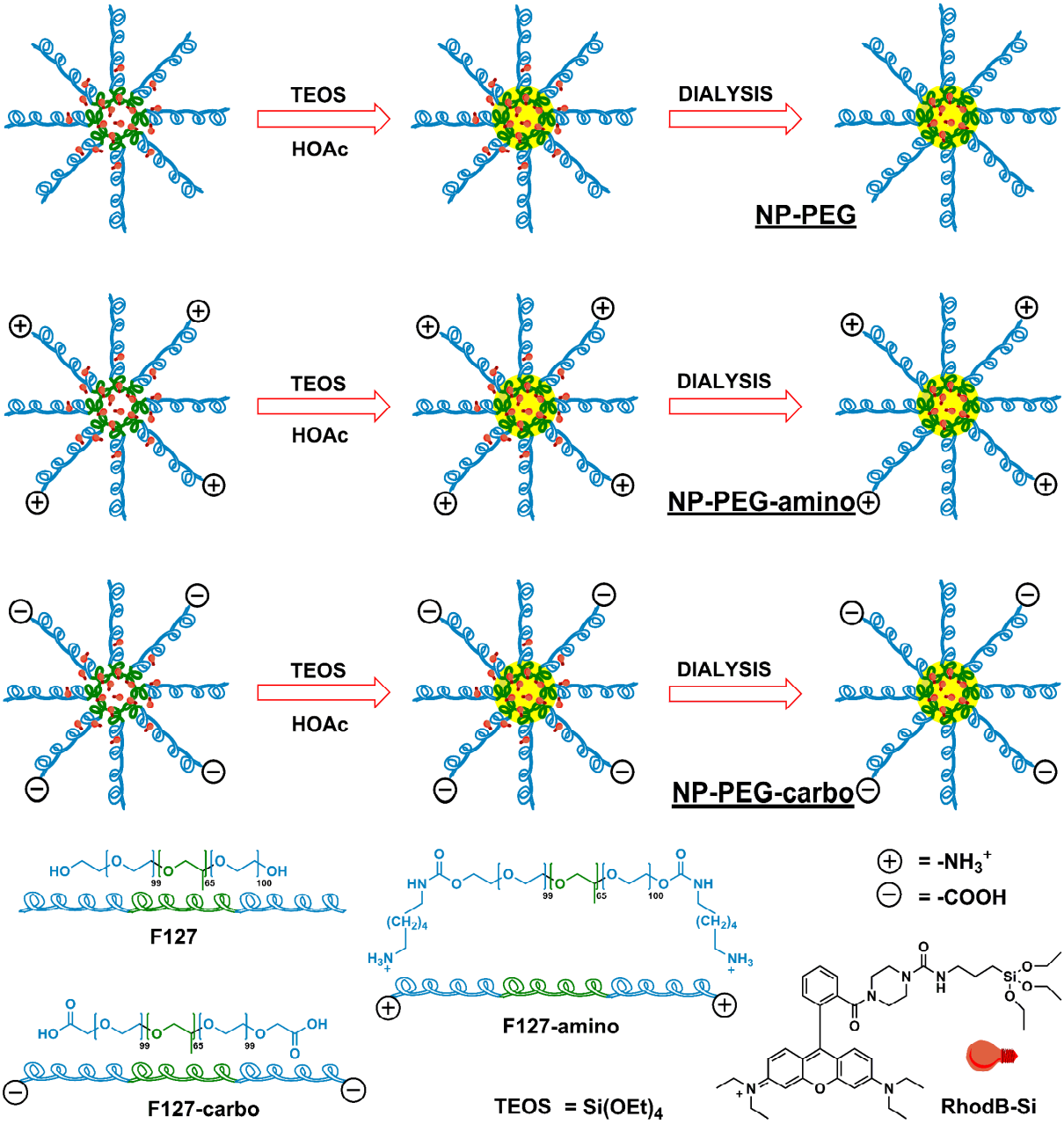


**Figure 3.2** *Schematic representation of the synthetic procedure and the main components of non-derivatized NP-PEG and derivatized NP-PEG-amino and NP-PEG-carbo.*

**Table 3.1** *Quantities of F127 surfactant and RhodB-Si used in SNPs preparations.*

| NPs sample | F127 (mg) | Derivatized F127 (mg) | RhodB-Si (mg) |
|---|---|---|---|
| *NP-PEG* | 200 | - | 2.9 |
| *NP-PEG-carbo* | 140 | F127-carbo 60 | 2.9 |
| *NP-PEG-amino* | 140 | F127-amino 60 | 2.9 |

matrix has manifold advantages, such as to circumvent dye toxicity, avoiding dye leaching in a biological environment, and therefore to securely fix fluorescent emission due to NPs in biological media.[33]

These nanoparticles are characterized by an absorption coefficient of $\varepsilon = 9.5 \times 10^5\ M^{-1}\ cm^{-1}$, with an average of ten RhodB-Si dye molecules inside each silica core. Furthermore, since a quantum yield of $\Phi = 0.52$ was measured in all samples, these SNPs showed a remarkable brightness ($B = 4.9 \times 10^5\ M^{-1}\ cm^{-1}$).[24,34] These photophysical parameters showed that at this concentration RhodB-Si give rise to negligible ground state interactions and to very low self-quenching processes (Figure 3.3).

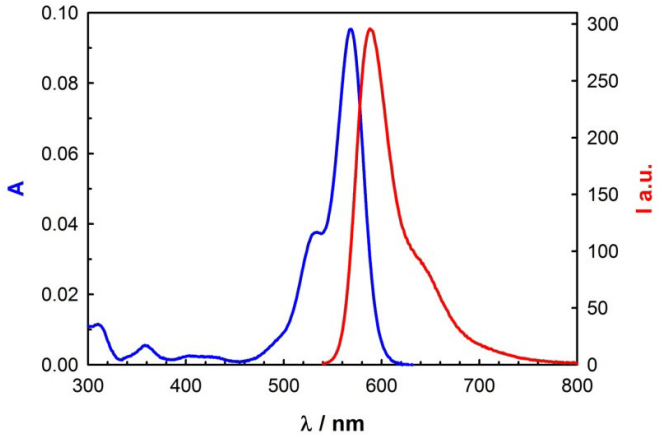


**Figure 3.3** *Representative absorption and emission spectra of SNPs doped with RhodB-Si in water.*

From a morphological viewpoint, the hydrodynamic diameter ($d_H$) measured by Dynamic Light Scattering (DLS) was less than 30 nm for NP-PEG and NP-PEG-carbo ($d_H$ = 25 and 28 nm, respectively), with a very low polydispersity index (PdI = 0.04 and 0.08, respectively); higher values of $d_H$ and PdI were found for NP-PEG-amino ($d_H$ = 69 nm and PdI = 0.2): this was probably due to H-bonding interactions between the SNPs (Figure 3.4 and Table 3.2). Morphological characterization by TEM images indicates a silica core diameter, $d_c = 12 \pm 2$ nm for NP-PEG-amino, $d_c = 11 \pm 2$ nm for NP-PEG-carbo and $d_c = 11 \pm 3$nm for NP-PEG (Figure 3.5 and Table 3.2).

**Table 3.2** *Mean silica core ($d_c \pm SD$) determined by TEM analysis, DLS hydrodynamic values ($d_H \pm SD$) and corresponding PdI for the SNPs described in this work. Standard deviation was calculated on five different measurements.*

| Sample | ($d_c \pm SD$) / nm | ($d_H \pm SD$) / nm | PdI |
|---|---|---|---|
| *NP-PEG* | 11 ± 3 | 25 ± 5 | 0.04 |
| *NP-PEG-carbo* | 11 ± 2 | 28 ± 8 | 0.08 |

| | | | |
|---|---|---|---|
| *NP-PEG-amino* | 12 ± 2 | 69 ± 30 | 0.20 |

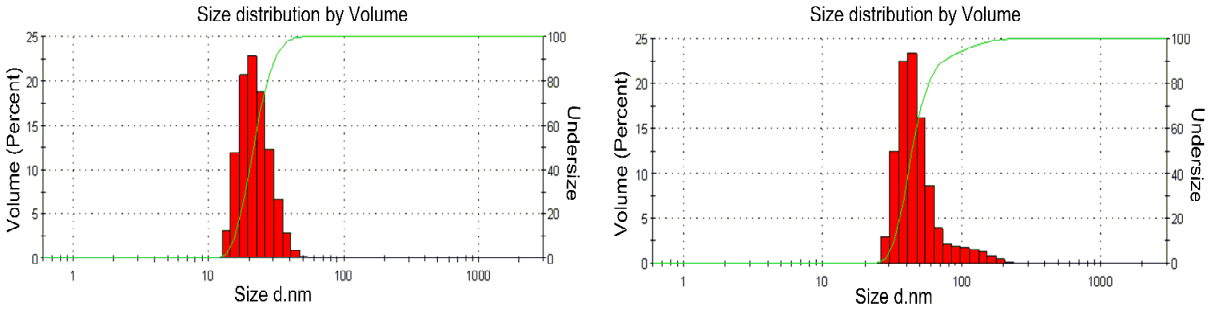


**Figure 3.4** *Dynamic light scattering diameter distributions by volume and undersize curves for SNPs: (left) NP-PEG-carbo ($d_H$ = 28 nm; PdI = 0.08, water, 25° C); (right) NP-PEG-amino ($d_H$ = 69 nm; PdI = 0.20, water, 25° C). For clarity, only results of experiments done with NP-PEG-carbo and NP-PEG-amino are shown.*

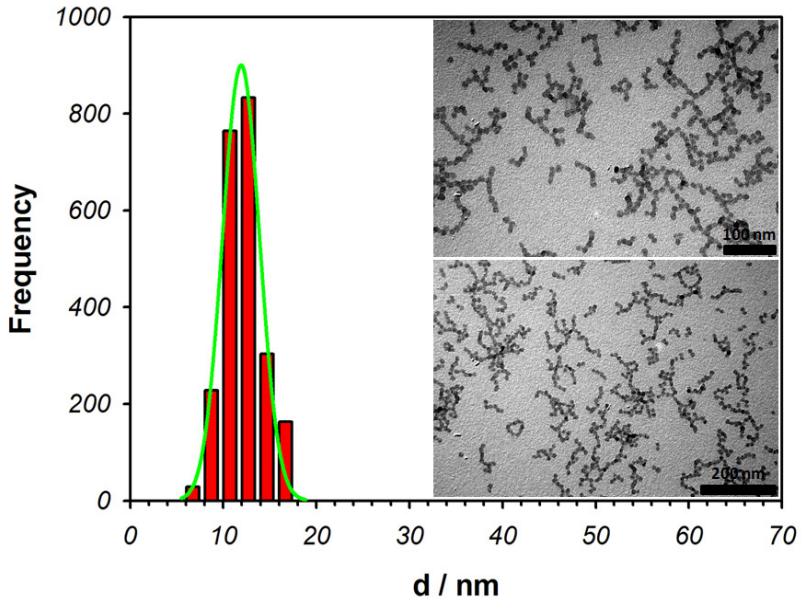


**Figure 3.5** *TEM images of SNPs NP-PEG-amino (silica core size distribution = 12 ± 2 nm). For clarity, only results of experiments done with NP-PEG-amino are shown.*

### 3.2.2 Evaluation of cell cytotoxicity

The cytotoxicity of SNPs functionalized on their surface with different charges (NP-PEG, NP-PEG-amino and NP-PEG-carbo) (Table 3.3), was evaluated in different cell models.

**Table 3.3** *Values of ζ-Potential ± SD (n=6) for SNPs samples. Conditions: [NPs] = 2 μM, [PB] = 1 mM, [KCl] = 1 mM, pH 7.4, 25° C.*

| NPs sample | ζ-Potential ± SD (mV) |
|---|---|
| *NP-PEG* | -4.3 ± 0.3 |
| *NP-PEG-carbo* | -6.5 ± 0.5 |
| *NP-PEG-amino* | -9.6 ± 0.4 |

It is important to emphasize that *in vitro* cell toxicity of SNPs is a significant topic in nanomedicine which depends on numerous factors, such as the testing techniques and treatment modalities;[35] previous studies reported that silica nanoparticles can have cytotoxic effects on diverse cell lines,[35-37] while other reports showed the absence of toxicity.[7,8,11,20,38]

In this work were used both tumor cell lines (leukemic JVM-2 cells and hepatocellular-carcinoma Huh7 cells) as well as primary normal cell models (peripheral blood mononuclear cells, PBMC, and human umbilical vein endothelial cells, HUVEC). By means of the Trypan blue dye exclusion test it was possible to evaluate the effects of SNPs on the viability of cells growing in suspension, namely leukemic JVM-2 and normal PBMC cells: a slight decrease in the cell availability (10%), that was not connected with the surface charge of the various SNPs, was observed after 48 hours of exposure at the maximal dose of 100 nM (Figure 3.6).

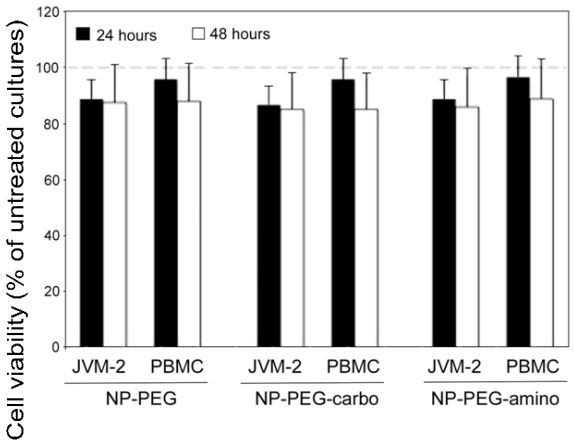


**Figure 3.6** *NP cytotoxicity evaluated on normal human PBMC and JVM-2 leukemic cells. Cells were cultured in the absence or presence of SNPs (100 nM). Cell viability was*

*calculated as a percentage with respect to the control vehicle cultures (set to 100% for each cell line). Data are reported as means ± SD of results from at least three independent experiments (different PBMC donors), performed in duplicate.*

Furthermore, the effects of SNPs on the viability of cells growing adherent to plastic, such as HUVEC (normal human umbilical vein endothelial cells) and hepatocellular-carcinoma Huh7 cells, were assessed using the xCELLigence real time cell analyzer (RTCA): the proliferation curves relative to the Cell Index of the cultures incubated with the NPs were comparable with those obtained using untreated cultures for both cell models investigated (Figure 3.7). In addition, it is interesting to note that the analysis of these proliferation curves show that cells treated with SNPs could maintain their morphology and viability even when treated for more than 48 hours with the highest concentration of SNPs (100 nM).

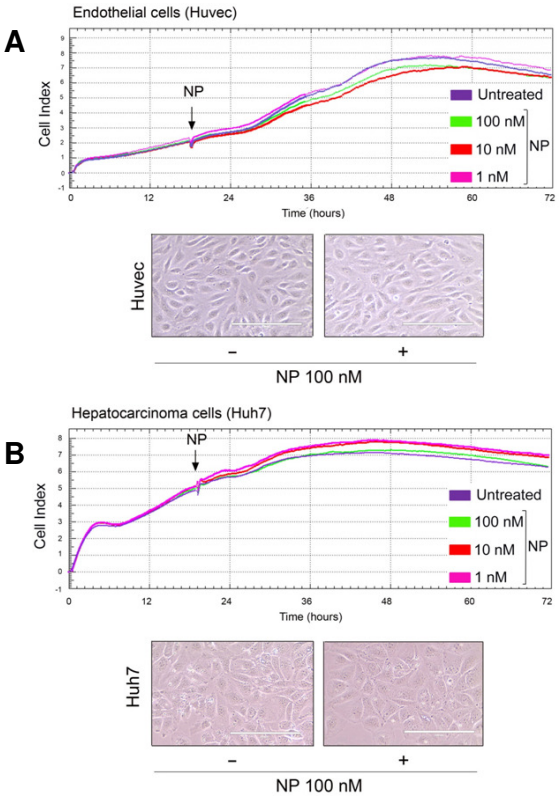


**Figure 3.7** *Adherent cell cultures (Huvec and Huh7) were exposed to SNPs used at the indicated concentrations. Cell proliferation/cytotoxicity was evaluated using the xCELLigence real time cell analyzer (RTCA) and was expressed as Cell Index. In parallel, the cell morphology was examined by using phase-contrast microscopy. In (A), cell proliferation/cytotoxicity was evaluated in endothelial primary cells (Huvec) seeded on pre-fibronectin-coated wells. In (B), cell proliferation/cytotoxicity was evaluated in hepatocellular carcinoma cells (Huh7). Representative Cell Index graphs (expressed as a*

*mean of quadruplicates) and microscopy images (original magnification: 20) of cultures from at least three independent experiments are shown. For clarity, only results of experiments done with NP-PEG-amino are shown.*

This negligible cytotoxicity was further shown by comparison with the effects due to the treatment with the kinase inhibitor Sorafenib, used as an inducer of cell toxicity. The effects produced by the inhibitor were visible not only on the proliferation curves, but also on the cell morphology and cell number, as shown by microscopy images (Figure 3.8).

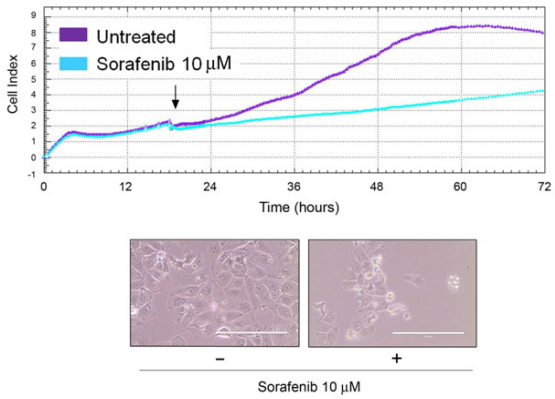


**Figure 3.8** *Cytotoxic effects (Cell Index reduction as well as morphological changes) induced by treatment with Sorafenib are shown for comparison. Representative Cell Index graphs (expressed as a mean of quadruplicates) and microscopy images (original magnification: 20 ) of cultures from at least three independent experiments are shown. For clarity, only results of experiments done with NP-PEG-amino are shown.*

Taken together, our results clearly indicate that, even upon surface derivatization, the SNPs display a very low grade of cytotoxicity, evaluated as alteration of cell viability and cell proliferation capacity. Of note, our results were derived from assays performed on different and relevant cell models of both normal and cancer origins, strengthening the notion of a potential use of SNPs in several biomedical applications.

### 3.2.3 Cell adhesion and internalization

The study of the SNPs cellular uptake is of fundamental importance because it can provide precise indications about their possible use as cell labels for *in vivo* applications and as carrier for active species, such as photoswitches,[31] drugs[29] and chemosensors.[32]

Firstly, the capacity of binding to the cells of the SNPs functionalized on their surface with neutral (NP-PEG), negative (NP-PEG-carbo) or positive (NP-PEG-amino) charges was

evaluated by means of incubation of leukemic JVM-2 cells with SNPs covalently doped with RhodB-Si for 30 minutes at 4° C, followed by washing with cold PBS before flow-cytometry analysis. The shifts in the graphs of the Rhodamine-positive populations demonstrated that all SNPs previously described were able to adhere to the cells in a dose-dependent fashion (Figure 3.9A). Secondly, the endocytosis process was induced by increasing the temperature from 4° C to 37° C. In this case, the negatively charged SNPs (NP-PEG- carbo) were less efficient than neutral (NP-PEG) and positively charged (NP-PEG-amino) SNPs in the overall process of binding and entry (Fig. 3.9A). These results showed that the highest efficiency of entry was verified for NP-PEG-amino, even at the lowest assessed concentration (10 nM) (Fig. 3.9A). It can be assumed that the better performance of NP-PEG-amino in this test can be due to electrostatic interactions among the cell membrane (negatively charged) and the amino groups (positively charged) present on the PEG shell of NP-PEG-amino, which facilitated the entry of attached SNPs.[39] The persistence of NP-PEG-amino connected to the cells until 48 hours has been documented by flow-cytometric analyses of the Rhodamine signal; a reduction of mean fluorescence intensity subsequently was noticed after 72 hours, probably attributable cell duplication process (Figure 3.9B).

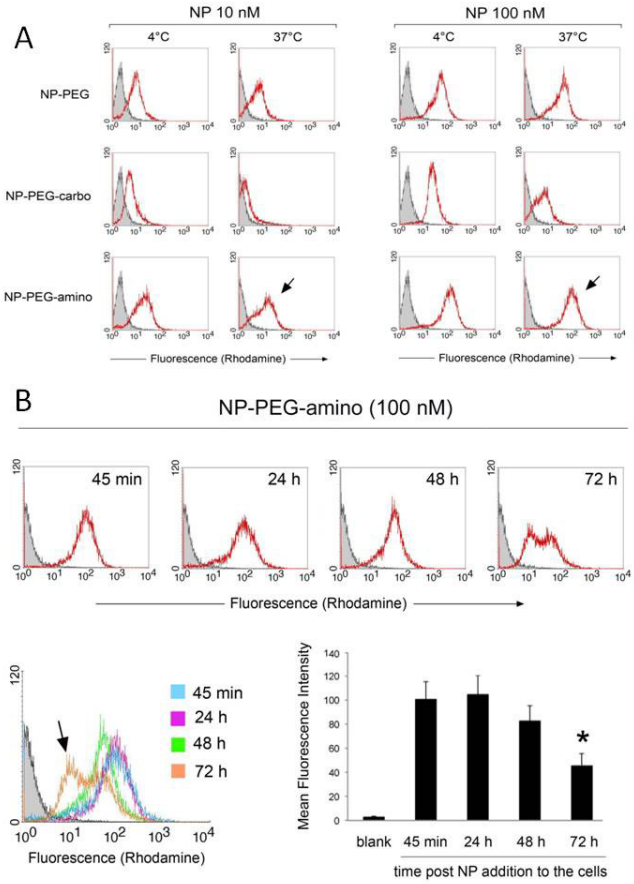


**Figure 3.9** *Binding to cell surface and persistence during time of Rhodamine-labeled SNPs. Cells incubated with Rhodamine-labeled SNPs were analyzed by flow cytometry. In*

*(A), JVM-2 cells were incubated with Rhodamine-labeled SNPs (10 nM and 100 nM) characterized for having different surface charge, and analyzed after 45 min incubation at 4°C and after washings and additional incubation over night at 37°C. Arrows indicate the best performing SNPs. In (B), kinetics analysis of the persistence of Rhodamine-labeled NP-PEG-amino signal into JVM-2 cells. Background signal from not-treated cells is in solid grey and specific Rhodamine signal is in color. Representative results out of three independent experiments are shown. The arrow indicates the loss of signal corresponding to a mean fluorescence intensity decrease after 72h, probably due to cellular duplication. In the histogram, flow cytometry analyses are expressed as Mean Fluorescence Intensity ± SD. Asterisk, p < 0.05 with respect to 24 hours of cultures.*

The ability of the SNPs to enter into cells has been further confirmed by the confocal fluorescence microscopy observation of Huh7 cells treated with Rhodamine-loaded SNPs. Cells were counterstained with FITC-conjugated phalloidin to mark intracellular actin, predominantly distributed alongside cell perimeters in these cells (Figure. 3.10A and B). As shown in Fig. 3.10A, SNPs showed red fluorescence mostly in the form of dots. In particular, after incubation at 4° C the 3D distribution of fluorescence obtained from the z-stack showed that the majority of SNPs were attached to the cell membrane, as evident from the arch drawn by the SNPs delineating the external border of the cells (Fig. 3.10B). Upon incubation at 37 °C, the SNPs were instead mostly localized inside the cells at the same depth of actin (Fig. 3.10B).

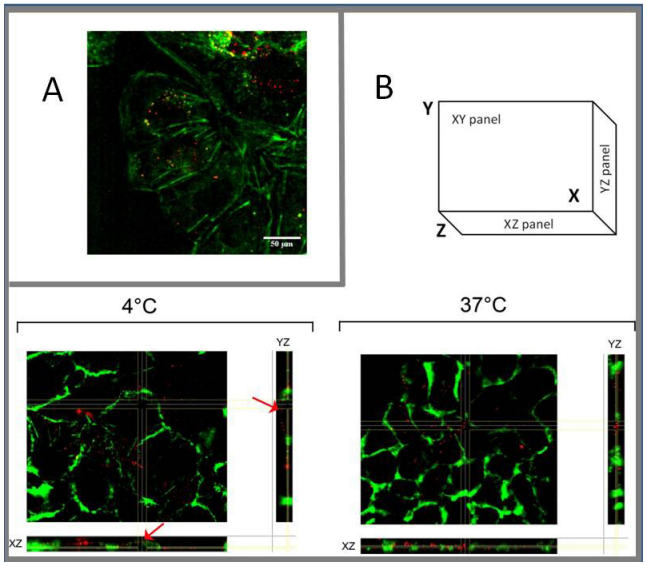


**Figure 3.10** *Fluorescence microscopy analysis of SiNP entry. Huh7 cells were incubated with Rhodamine-labeled SNPs (red) at 37°C and then counterstained with FITC-conjugated Phalloidin (to visualize intracellular actin, green). In (A), confocal 2D image of cells incubated with SNPs for 24 hours. A representative image merged of 21 sections is shown. Photographs were taken at a magnification of 60x. In (B), images of 21 subsequent*

*optical sections collected at 0.5 µm intervals (z-stack) were recorded and rearranged to a section view visualizing the 3D distribution of fluorescence inside the cells. A single 2D optical slice (horizontal median plane, XY panels) from the stack is in high magnification, while XZ and YZ panels show merged reconstruction of the stack along the Z axis (vertical plane originated from a slice through the stack, perpendicular to the XY image plane). The lines indicate the level at which the photographs were taken (X, Y, 5 µm). Examining the XZ and YZ panels, the arrows indicate the localization of SNPs delineating the external border of the cells after incubation at 4°C, while the SNPs show the same depth localization than intracellular actin indicating cell entry after incubation at 37°C. Photographs were taken at a magnification of 60x.*

To further validate these results and to define the mechanisms of SNP uptake, cells were pre-incubated with Genistein, a commonly used clathrin-independent caveolae-mediated endocytosis inhibitor[40] before assessing quantitatively the entry of Rhodamine-labeled SNPs by flow cytometry. As shown in Figure 3.11, the pretreatment with Genistein was able to interfere with the SNP uptake, as underlined by a significant reduction of fluorescence intensity in two different cell models represented by leukemic JVM-2 cells (growing in suspension) and by hepatocarcinoma Huh7 cells (growing in adhesion). The inhibitory effect was significant but not complete, due to the involvement of additional endocytosis mechanisms not inhibited by Genistein.[41] The multiparametric flow cytometry approach was preferred over that with confocal microscopy because it offered the advantage of analyzing a large population of cells (50000 in our study) instead of a small field of about 10-20 cells, and to rapidly quantify the inhibition of the entry.

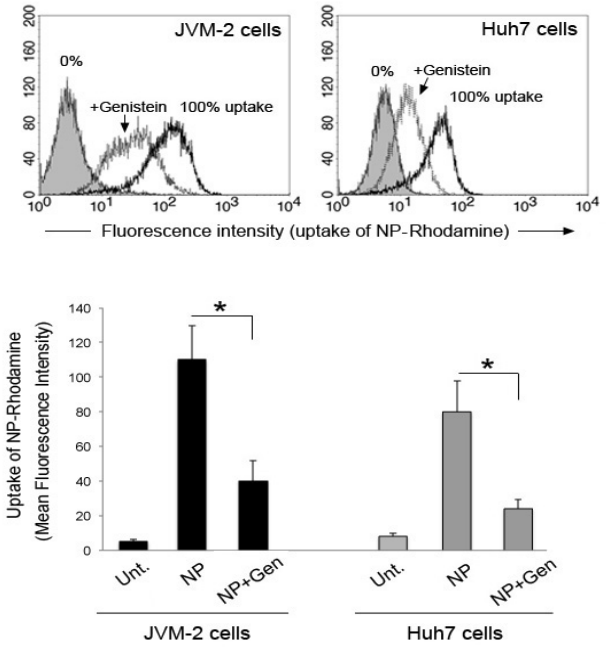

**Figure 3.11** *SNP entry is blocked by endocytosis inhibition. JVM-2 and Huh7 cells incubated with Rhodamine-labeled SNPs in the presence or absence of Genistein (Gen) were analyzed by flow cytometry. Background histograms from untreated cells are in solid grey (uptake 0%), specific Rhodamine-labeled NP signals are black (100% uptake) or dotted (Genistein addition) empty histograms. Analyses are expressed as Mean Fluorescence Intensity ± SD. Representative results out of three independent experiments are shown. Asterisk, p < 0.05.*

### 3.2.4 *In vivo* experiments

JVM-2 leukemic cells were loaded with Rhodamine-labeled NP-PEG-amino to evaluate not only the stability of SNPs inside the cells in the in vivo environment, but also to use them for cell traceability and detection in whole organisms (Figure 3.12A). After that, the labeled JVM-2 leukemic cells, at a pre-determined number, were injected intravenously in SCID immune-deficient mice. Twenty-four hours post-injection, mice circulating total blood cells were analyzed by flow-cytometry, after gating on the live cell populations (Figure 3.12B). As shown in Fig. 3.12B, we were able to detect in the peripheral blood of the injected mice a population of circulating cells positive for Rhodamine and showing a side and forward scatter characteristic of labeled JVM-2 human leukemic cells, which accounted for approximately 6% of the total peripheral blood population (Fig. 3.12B). Such a population was not present in the blood of mice injected with unlabeled JVM-2, used as control (Fig. 3.12B). In addition, the labeling with a FITC-conjugated antibody against human CD19 (expressed by the JVM-2 cells) confirms that the Rhodamine fluorescence was associated with JVM-2, further excluding a leaking of the SNP out from the injected JVM-2 and/or the uptake by different circulating cells (Fig. 3.12B).

There is growing interest in new methodologies which allow tracking of transplanted cells in animals and humans.[42] In this context, our in vitro data document a stable and intense fluorescence of the SNPs, a good efficiency of cell labeling capacity, and a stability of the SNPs in the intracellular microenvironment: together with our preliminary *in vivo* results, they support the potential application of SNPs for cell labeling and monitoring *in vivo*.

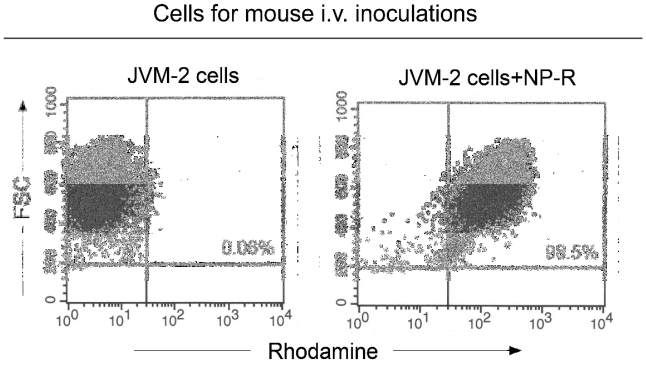

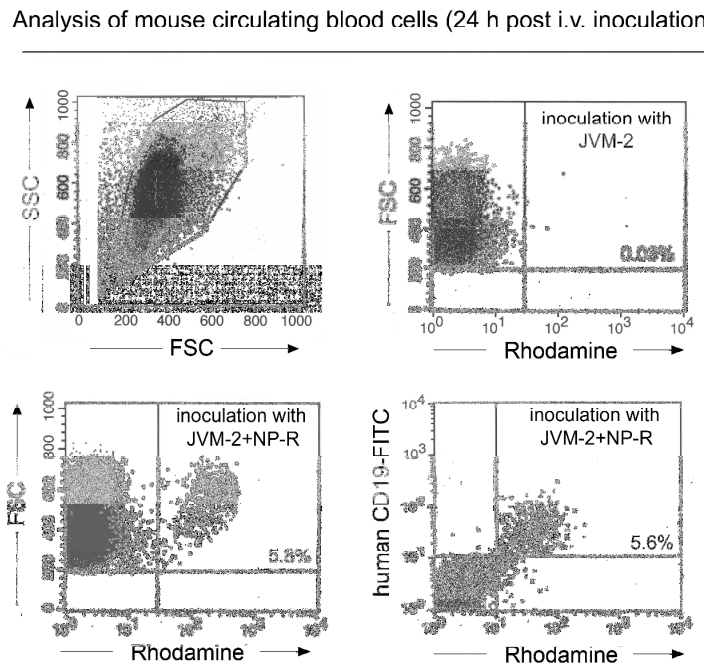


**Figure 3.12** *Cells loaded with Rhodamine-labeled SNPs are traceable after in vivo administration. SCID mice were i.v. injected with 5x106 JVM-2 cells or with JVM-2 cells pre-loaded with Rhodamine-labeled SNP (NP-R). In (A), JVM-2 cells were incubated for 24h with NP-R (100 nM) and before inoculation in mice the percentage of labeled cells was analyzed at flow cytometry. In (B), 24 hours post injection, mouse blood circulating cells were analyzed at flow cytometry for the presence of Rhodamine- positive and Rhodamine/hCD19-FITC double positive JVM-2 cells. A representative experiment is shown.*

## 3.3 Conclusions

Among the several possible approaches related to bio-analytical and imaging applications based on the use of NPs, the ones employed in the present study offer several advantages.[14,15] The possibility to obtain tiny NPs with a core-shell silica-PEG structure with a one pot synthesis is quite unique, moreover the synthetic approach is based on mild conditions in aqueous solution, is extremely reliable and it requires accessible and cheap components. The resulting SNPs are highly monodisperse, stable in physiological conditions and highly bright.[24] Furthermore, the structure of the SNPs offers the possibility to load external species such as drugs (see Chapter 7)[29] and chemosensors.[32] We have derivatized silica core/PEG shell SNPs with modified surfactants to obtain NP-PEG-amino and NP-PEG-carbo, having a different external charge. With the aim to characterize the behaviour of these SNP preparations (covalently doped with a Rhodamine B derivative) for potential in vivo applications, we have first demonstrated that none of these preparations showed toxicity on either suspension or adherent cell models of normal or cancer cell types. Within these families of nanoparticles, NP-PEG-amino exhibited the most efficient

kinetics of cell adhesion and internalization, coupled with high levels of SNP cell associated fluorescence persisting for more than 48 hours. The endocytosis of SNPs by a caveolae-mediated pathway was then demonstrated through significant inhibition by Genistein. Proper SNP cell internalization allowed cell traceability in vivo (upon blood analysis) of leukemic cells, pre-loaded in vitro with SNPs and intravenously injected into SCID mouse model.

It should be underlined that, although multiple approaches were used in order to investigate the different experimental aspects mentioned above, multiparametric flow cytometry offered a powerful tool to quantitatively evaluate aspects linked to the SNP adhesion and uptake by the cells as well as for the in vivo studies. We believe that our results strengthen the idea that derivatized fluorescent SNP are versatile non-toxic materials suitable for several in vivo applications, including cell labeling and monitoring.

## 3.4 Notes and references

The contents of this chapter are based on E. Rampazzo, R. Voltan, L. Petrizza, N. Zaccheroni, L. Prodi, F. Casciano, G. Zauli and P. Secchiero, *Nanoscale* **2013**, 5, 7897- Reproduced by permission of The Royal Society of Chemistry.


(1) Kim, D. K.; Dobson, J. *Journal of Materials Chemistry* **2009**, *19*, 6294.
(2) Riehemann, K.; Schneider, S. W.; Luger, T. A.; Godin, B.; Ferrari, M.; Fuchs, H. *Angewandte Chemie International Edition* **2009**, *48*, 872.
(3) Shi, D. L. *Adv. Funct. Mater.* **2009**, *19*, 3356.
(4) Shi, J. J.; Xiao, Z. Y.; Kamaly, N.; Farokhzad, O. C. *Accounts of Chemical Research* **2011**, *44*, 1123.
(5) Cuenca, A. G.; Jiang, H. B.; Hochwald, S. N.; Delano, M.; Cance, W. G.; Grobmyer, S. R. *Cancer* **2006**, *107*, 459.
(6) Doshi, N.; Mitragotri, S. *Adv. Funct. Mater.* **2009**, *19*, 3843.
(7) Gunasekera, U. A.; Pankhurst, Q. A.; Douek, M. *Targeted Oncology* **2009**, *4*, 169.
(8) Yong, K. T.; Roy, I.; Swihart, M. T.; Prasad, P. N. *Journal of Materials Chemistry* **2009**, *19*, 4655.
(9) Rai, P.; Mallidi, S.; Zheng, X.; Rahmanzadeh, R.; Mir, Y.; Elrington, S.; Khurshid, A.; Hasan, T. *Advanced Drug Delivery Reviews* **2010**, *62*, 1094.
(10) Kim, K.; Kim, J. H.; Park, H.; Kim, Y. S.; Park, K.; Nam, H.; Lee, S.; Park, J. H.; Park, R. W.; Kim, I. S.; Choi, K.; Kim, S. Y.; Kwon, I. C. *Journal of Controlled Release* **2010**, *146*, 219.
(11) Wang, M.; Thanou, M. *Pharmacological Research* **2010**, *62*, 90.
(12) Rosenholm, J. M.; Sahlgren, C.; Linden, M. *Nanoscale* **2010**, *2*, 1870.
(13) Benezra, M.; Penate-Medina, O.; Zanzonico, P. B.; Schaer, D.; Ow, H.; Burns, A.; DeStanchina, E.; Longo, V.; Herz, E.; Iyer, S.; Wolchok, J.; Larson, S. M.; Wiesner, U.; Bradbury, M. S. *Journal of Clinical Investigation* **2011**, *121*, 2768.
(14) Mahmoudi, M.; Hofmann, H.; Rothen-Rutishauser, B.; Petri-Fink, A. *Chemical Reviews* **2011**, *112*, 2323.
(15) Reddy, L. H.; Arias, J. L.; Nicolas, J.; Couvreur, P. *Chemical Reviews* **2012**, *112*, 5818.
(16) Prodi, L. *New Journal of Chemistry* **2005**, *29*, 20.
(17) Gong, Y. K.; Nakashima, K. *Chemical Communications* **2001**, 1772.
(18) Katz, L. C.; Burkhalter, A.; Dreyer, W. J. *Nature* **1984**, *310*, 498.
(19) Prilloff, S.; Fan, J. Y.; Henrich-Noack, P.; Sabel, B. A. *Eur. J. Neurosci.* **2010**, *31*, 521.
(20) Burns, A.; Ow, H.; Wiesner, U. *Chemical Society Reviews* **2006**, *35*, 1028.
(21) Medintz, I. L.; Uyeda, H. T.; Goldman, E. R.; Mattoussi, H. *Nat. Mater.* **2005**, *4*, 435.
(22) Bae, W.; Tan, W.; Hong, J.-I. *Chemical Communications* **2012**, *48*, 2270.
(23) Wang, L.; Wang, K. M.; Santra, S.; Zhao, X. J.; Hilliard, L. R.; Smith, J. E.; Wu, J. R.; Tan, W. H. *Analytical Chemistry* **2006**, *78*, 646.
(24) Bonacchi, S.; Genovese, D.; Juris, R.; Montalti, M.; Prodi, L.; Rampazzo, E.; Zaccheroni, N. *Angewandte Chemie, International Edition in English* **2011**, *50*, 4056.

(25) Bonacchi, S.; Genovese, D.; Juris, R.; Montalti, M.; Prodi, L.; Rampazzo, E.; Sgarzi, M.; Zaccheroni, N. In *Luminescence Applied in Sensor Science*; Prodi, L., Montalti, M., Zaccheroni, N., Eds. 2011; Vol. 300, p 93.
(26) Rampazzo, E.; Bonacchi, S.; Genovese, D.; Juris, R.; Marcaccio, M.; Montalti, M.; Paolucci, F.; Sgarzi, M.; Valenti, G.; Zaccheroni, N.; Prodi, L. *Coord. Chem. Rev.* **2012**, *256*, 1664.
(27) Montalti, M.; Rampazzo, E.; Zaccheroni, N.; Prodi, L. *New Journal of Chemistry* **2013**, *37*, 28.
(28) Ambrogio, M. W.; Thomas, C. R.; Zhao, Y. L.; Zink, J. I.; Stoddartt, J. F. *Accounts of Chemical Research* **2011**, *44*, 903.
(29) Rampazzo, E.; Bonacchi, S.; Juris, R.; Montalti, M.; Genovese, D.; Zaccheroni, N.; Prodi, L.; Rambaldi, D. C.; Zattoni, A.; Reschiglian, P. *Journal of Physical Chemistry B* **2010**, *114*, 14605.
(30) Soster, M.; Juris, R.; Bonacchi, S.; Genovese, D.; Montalti, M.; Rampazzo, E.; Zaccheroni, N.; Garagnani, P.; Bussolino, F.; Prodi, L.; Marchio, S. *International Journal of Nanomedicine* **2012**, *7*, 4797.
(31) Genovese, D.; Montalti, M.; Prodi, L.; Rampazzo, E.; Zaccheroni, N.; Tosic, O.; Altenhoner, K.; May, F.; Mattay, J. *Chemical Communications* **2011**, *47*, 10975.
(32) Rampazzo, E.; Bonacchi, S.; Genovese, D.; Juris, R.; Sgarzi, M.; Montalti, M.; Prodi, L.; Zaccheroni, N.; Tomaselli, G.; Gentile, S.; Satriano, C.; Rizzarelli, E. *Chemistry- A European Journal* **2011**, *17*, 13429.
(33) Ohulchanskyy, T. Y.; Roy, I.; Goswami, L. N.; Chen, Y.; Bergey, E. J.; Pandey, R. K.; Oseroff, A. R.; Prasad, P. N. *Nano Letters* **2007**, *7*, 2835.
(34) Rampazzo, E.; Boschi, F.; Bonacchi, S.; Juris, R.; Montalti, M.; Zaccheroni, N.; Prodi, L.; Calderan, L.; Rossi, B.; Becchi, S.; Sbarbati, A. *Nanoscale* **2012**, *4*, 824.
(35) Fede, C.; Selvestrel, F.; Compagnin, C.; Mognato, M.; Mancin, F.; Reddi, E.; Celotti, L. *Anal Bioanal Chem* **2012**, *404*, 1789.
(36) Stępnik, M.; Arkusz, J.; Smok-Pieniążek, A.; Bratek-Skicki, A.; Salvati, A.; Lynch, I.; Dawson, K. A.; Gromadzińska, J.; De Jong, W. H.; Rydzyński, K. *Toxicology and Applied Pharmacology* **2012**, *263*, 89.
(37) Kunzmann, A.; Andersson, B.; Thurnherr, T.; Krug, H.; Scheynius, A.; Fadeel, B. *Biochimica et Biophysica Acta (BBA) - General Subjects* **2011**, *1810*, 361.
(38) Malvindi, M. A.; Brunetti, V.; Vecchio, G.; Galeone, A.; Cingolani, R.; Pompa, P. P. *Nanoscale* **2012**, *4*, 486.
(39) Yeh, M.-K.; Hu, C.-s.; Chiang, C.-H.; Po-da, H. *International Journal of Nanomedicine* **2012**, 4861.
(40) Vercauteren, D.; Vandenbroucke, R. E.; Jones, A. T.; Rejman, J.; Demeester, J.; De Smedt, S. C.; Sanders, N. N.; Braeckmans, K. *Molecular Theraphy* **2010**, *18*, 561.
(41) Reno, F.; Carniato, F.; Rizzi, M.; Olivero, F.; Pittarella, P.; Marchese, L. *Nanotechnology* **2013**, *24*, 185101.
(42) Taylor, A.; Wilson, K. M.; Murray, P.; Fernig, D. G.; Levy, R. *Chemical Society Reviews* **2012**, *41*, 2707.
(43) Kaijzel, E. L.; van der Pluijm, G.; Lowik, C. W. *Clinical Cancer Research* **2007**, *13*, 3490.
(44) McIntyre, J. O.; Scherer, R. L.; Matrisian, L. M. *Methods in Molecular Biology* **2010**, *622*, 279.
(45) Agostinis, C.; Biffi, S.; Garrovo, C.; Durigutto, P.; Lorenzon, A.; Bek, A.; Bulla, R.; Grossi, C.; Borghi, M. O.; Meroni, P.; Tedesco, F. *Blood* **2011**, *118*, 4231.
(46) Day, K. E.; Sweeny, L.; Kulbersh, B.; Zinn, K. R.; Rosenthal, E. L. *Molecular Imaging and Biology* **2013**, *15*, 722.
(47) Ntziachristos, V.; Razansky, D. *Recent Results in Cancer Research* **2013**, *187*, 133.
(48) Byrne, W. L.; DeLille, A.; Kuo, C.; de Jong, J. S.; van Dam, G. M.; Francis, K. P.; Tangney, M. *Journal of Controlled Release* **2013**, *172*, 523.
(49) Schaafsma, B. E.; Mieog, J. S.; Hutteman, M.; van der Vorst, J. R.; Kuppen, P. J.; Lowik, C. W.; Frangioni, J. V.; van de Velde, C. J.; Vahrmeijer, A. L. *Journal of Surgical Oncology* **2011**, *104*, 323.
(50) Vahrmeijer, A. L.; Hutteman, M.; van der Vorst, J. R.; van de Velde, C. J.; Frangioni, J. V. *Nature Reviews Clinical Oncology* **2013**, *10*, 507.
(51) Helle, M.; Rampazzo, E.; Monchanin, M.; Marchal, F.; Guillemin, F.; Bonacchi, S.; Salis, F.; Prodi, L.; Bezdetnaya, L. *ACS Nano* **2013**, *7*, 8645.
(52) Burns, A. A.; Vider, J.; Ow, H.; Herz, E.; Penate-Medina, O.; Baumgart, M.; Larson, S. M.; Wiesner, U.; Bradbury, M. *Nano Letters* **2008**, *9*, 442.
(53) Ma, K.; Sai, H.; Wiesner, U. *Journal of the American Chemical Society* **2012**, *134*, 13180.
(54) Montalti, M.; Prodi, L.; Rampazzo, E.; Zaccheroni, N. *Chemical Society Reviews* **2014**, DOI: 10.1039/c3cs60433k.
(55) Lavis, L. D.; Raines, R. T. *ACS Chemical Biology* **2008**, *3*, 142.
(56) Gruber, H. J.; Hahn, C. D.; Kada, G.; Riener, C. K.; Harms, G. S.; Ahrer, W.; Dax, T. G.; Knaus, H.-G. *Bioconjugate Chemistry* **2000**, *11*, 696.
(57) Vivero-Escoto, J. L.; Huxford-Phillips, R. C.; Lin, W. *Chemical Society Reviews* **2012**, *41*, 2673.
(58) Deen, W. M.; Lazzara, M. J.; Myers, B. D. *American Journal of Physiology: Renal Physiology* **2001**, *281*, F579.

(59) Voltan, R.; Secchiero, P.; Ruozi, B.; Forni, F.; Agostinis, C.; Caruso, L.; Vandelli, M. A.; Zauli, G. *Clinical Cancer Research* **2013**, *19*, 3871.
(60) Maeda, H.; Wu, J.; Sawa, T.; Matsumura, Y.; Hori, K. *Journal of Controlled Release* **2000**, *65*, 271.
(61) Rampazzo, E.; Voltan, R.; Petrizza, L.; Zaccheroni, N.; Prodi, L.; Casciano, F.; Zauli, G.; Secchiero, P. *Nanoscale* **2013**, *5*, 7897.
(62) Genovese, D.; Rampazzo, E.; Bonacchi, S.; Montalti, M.; zaccheroni, N.; Prodi, L. *Nanoscale* **2013**, DOI: 10.1039/c3nr05599j.
(63) Genovese, D.; Bonacchi, S.; Juris, R.; Montalti, M.; Prodi, L.; Rampazzo, E.; Zaccheroni, N. *Angewandte Chemie International Edition* **2013**, *52*, 5965.

# Chapter 4

# NIR-emitting silica nanoparticles as fluorescent labels

## 4.1 Introduction

The field of biomedical imaging requires non-toxic, photostable and bright tools for fluorescence imaging. Optical imaging is actually broadly applied to obtain functional information *in vivo* over time for the preclinical assessment of protein expression, antibody binding, cell tracking and enzymatic activities. It represents, consequently, a rapidly improving technology that can be essential in a broad range of applications such as optical imaging that uses near-infrared (NIR) fluorescent light.[1-6] This application has emerged as a tool also in the clinical context because it provides real-time, intraoperative, high-contrast delineation of both normal and pathologic tissues and can offer new possibilities for both general and oncologic surgery.[7] Fluorescence-guided surgery has, certainly, the potential to improve cancer surgery outcomes and can also help surgeons in the identification and removal of malignant lesions. For these reasons, over the last years much effort has gone in clinical trials in this specific field.[8]

Today several optical imaging approaches have been developed but, in spite of this, there is an increasing need of more effective optical imaging probes beyond the approved indocyanine green (ICG).[7] A significant improvement in this field have led to a variety of fluorescent labeling probes based on nanomaterials (nanoparticles; NPs), which allow to store large payloads of imaging contrast agents and/or therapeutics within the NP core and "tissue specific targeting" molecules on NP surface.[9] The versatility of synthetic NPs allows to provide contrast improvement, binding specificity, enhanced stability and prolonged blood half-life.[10] Among the nanomaterials, fluorescent dye-doped NIR-emitting silica nanoparticles (NIR-SNPs) have demonstrated excellent potential for applications in advanced bioanalysis.[9-12] NIR-SNPs represent a precious tool in bioimaging, because they provide sufficient brightness and photostability and consist of hydrophilic non-toxic materials.[13-16]

Multiple dye-doped NIR emitting SNPs (m-NIR-SNPs) suitable for both time domain (TD) optical imaging and multiparametric flow cytometry analyses were developed. In order to characterize the optical properties and fluorescence imaging applications of these m-NIR-SNPs, we have characterized their performance by analyzing their *in vivo* biodistribution in healthy mice as well as in lymphoma bearing xenografts, and their suitability as contrast imaging agents for cell labeling and tracking.

## 4.2 Result and discussion

### 4.2.1 Synthesis and characterization of m-NIR-SNPs

Following the synthetic approach already shown in Section 3.2.1 (see also Section 8.9), in this work we synthesized silica nanoparticles, characterized by both long-term stability and low adhesion properties toward proteins. This synthetic approach allows to bind covalently to the silica matrix a large number of dyes, ensuring in this way an increase of the nanoparticle absorption coefficeint $\varepsilon$. Furthermore, the silica matrix protects the dyes that are incorporated within the particles from the external chemicals, increasing their photostability and, frequently, their luminescence quantum yield $\Phi$. Because of the reasons mentioned above, the SNPs are often characterized by high values of brightness.[10,14]

SNPs were covalently doped by using increasing doping ratios of the triethoxysilane derivative of Cy 5.5 dye (Cy5.5-Si, Figure 4.1A, Fig. 4.2, Fig. 4.3 and Table 4.1) to obtain NP-1 and NP-2, nanoplatforms suitable for both multiparametric flow cytometry analyses and time-domain optical imaging.

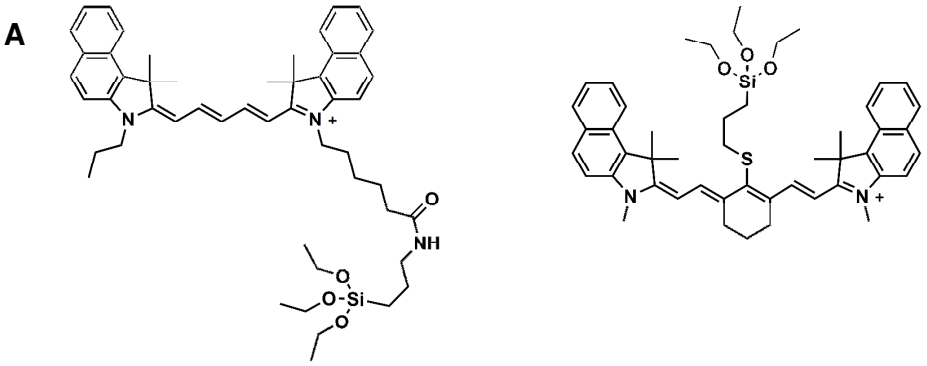


**Figure 4.1** *Molecular structure of: (A) Cy5.5-Si; (B) Cy7-Si.*

Cy5.5-Si was synthesized starting from 1,1,2-trimethylbenz[e]indole (1), that was alkylated with 1-Iodopropane in acetonitrile (MeCN) under reflux for two days to afford the compound (2), which was treated with malonaldehyde bis(phenylimine) monohydrochloride in acetic anhydride at 100°C for 1 h to obtain the hemicyanine intermediate (3). N-alkylation of (1) with 6-Bromohexanoic acid in MeCN under reflux for four days gave compound (4), which was treated with compound (3) to afford the compound (5).[17,18] The triethoxysilane function of Cy5.5-Si was introduced via a coupling reaction between the carboxylic moiety of (5) and the amino group of (3-Aminopropyl)triethoxysilane (Figure 4.2). Further details for this synthesis are given in Section 8.2.

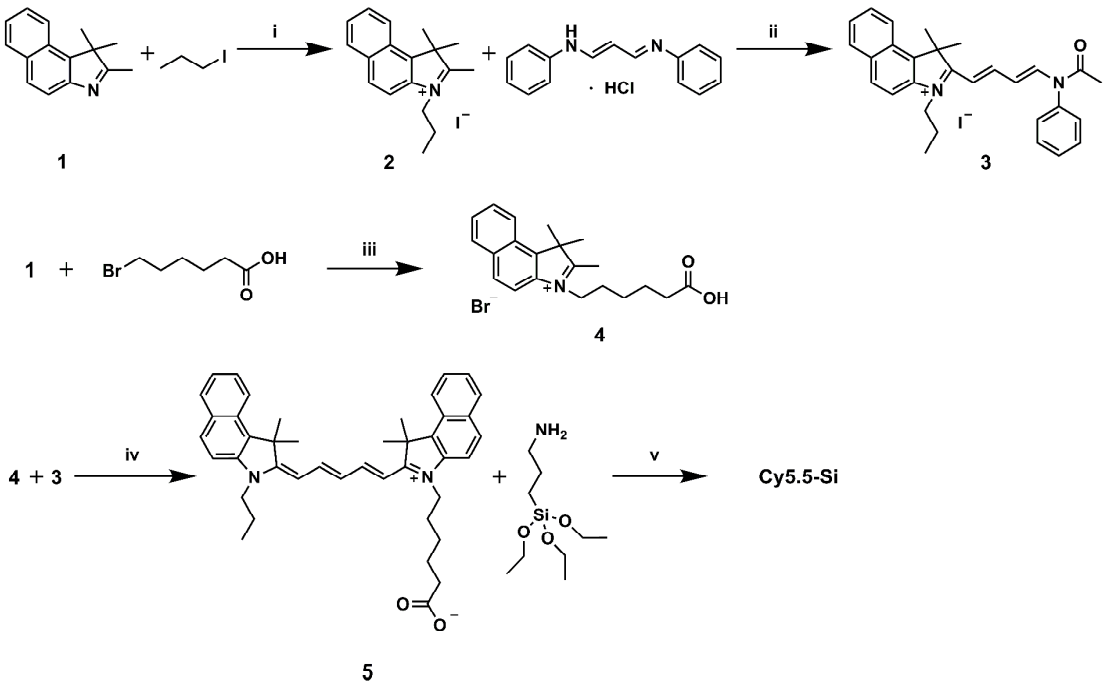


**Figure 4.2** *Schematization of the synthesis of Cy5.5-Si. Reagents and conditions: i) MeCN, reflux, 2 d; ii) $Ac_2O$, 100°C, 2 h; iii) MeCN, reflux, 4 d; iv) Pyridine, 40°C, 30 min; v) HATU, TEA, DCM, rt, 2 h.*

However, the dye showed a great tendency to aggregate, which has led to a scant loading of the dye within the silica matrix. This is also highlighted by the appearance of self-quenching processes,[15,16,19] which caused a decrease of the fluorescent quantum yield of the Cy5.5-Si dye inside the particles compared to the one noticed in solution. To overcome

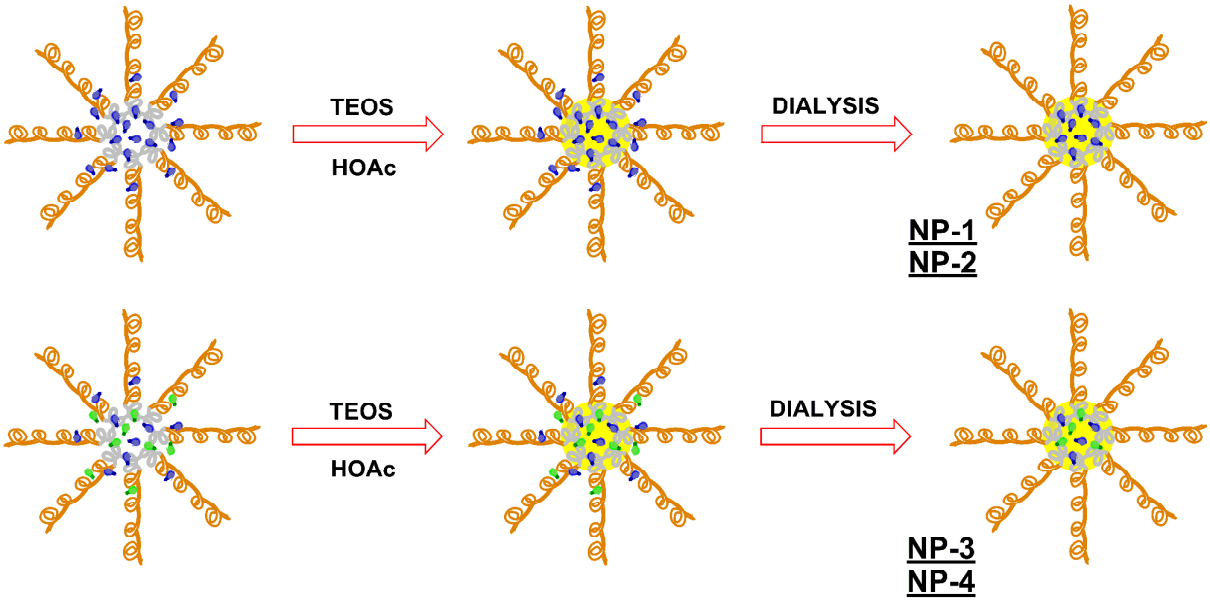

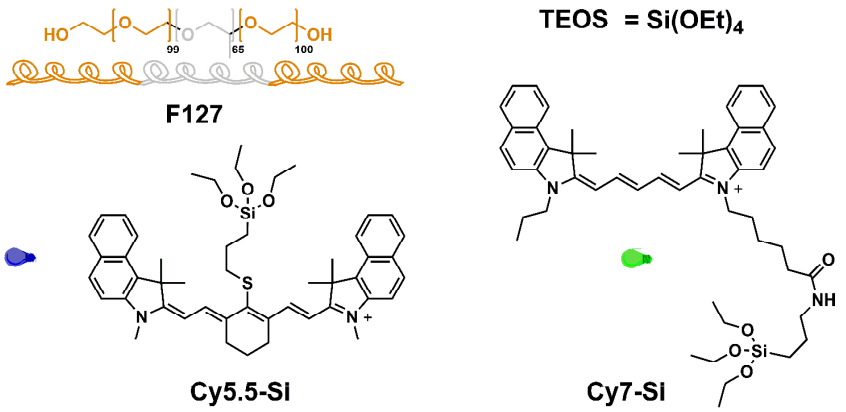


**Figure 4.3** *Doping dyes (Cy5.5-Si and Cy7-Si) and schematization of the synthetic procedure used for the synthesis of the NIR-SNPs (NP-1 and NP-2) and m-NIR-SNPs (NP-3 and NP-4) samples described in this work.*

**Table 4.1** *Doping characteristics of the SNPs samples presented in this study.*

| SNPs sample | %Dye[a] | TEOS mmol | Cy5.5-Si[b] µmol | Cy7-Si[b] µmol |
|---|---|---|---|---|
| *NP-1* | 0.1 Cy5.5-Si | 0.8 | 0.8 | - |
| *NP-2* | 0.2 Cy5.5-Si | 0.8 | 1.6 | - |
| *NP-3* | 0.2 Cy5.5-Si-0.1 Cy7-Si | 0.8 | 1.6 | 0.8 |
| *NP-4* | 0.2 Cy5.5-Si-0.2 Cy7-Si | 0.8 | 1.6 | 1.6 |

[a]*Doping ratio=[mol(dye)/mol(TEOS)]*100.* [b]*Cy5.5-Si and Cy7-Si were introduced in the reaction mixtures using pristine dichloromethane solutions.*

these problems, the idea was to dope the SNPs with the alkoxysilane derivative of Cy5.5 and an additional cyanine dye, to check whether the increase in the probability of aggregation with another dye could increase the number of Cy5.5 per nanoparticle and decrease the self-quenching processes. In addition, we also expected to have, at the same time, the beneficial effect of the presence of multiple signals.[9,20] For this objective, different SNPs preparatives were synthesized by using the derivative Cy5.5-Si in combination with the IR813 alkoxysilane dye derivative Cy7-Si (Figure 4.1B; NP-3 and NP-4, Fig. 4.3; Table 4.1, and Section 8.2) at two different Cy5.5-Si : Cy7-Si molecular ratios (2 : 1, 1 : 1) (Table 4.1). As shown in Figure 4.4, SNPs doped with both dyes showed the typical absorption maxima of Cy5.5 (693 nm) and Cy7 (828 nm). Additional photophysical properties of the SNPs preparatives are reported in Table 4.2.

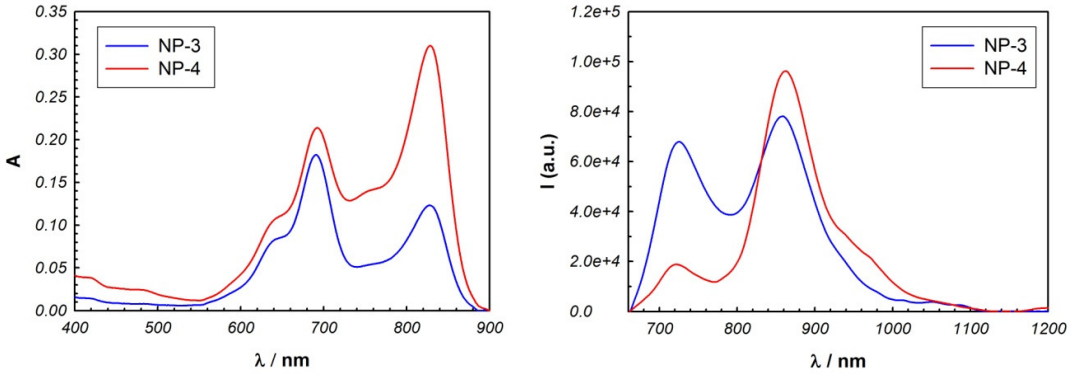


**Figure 4.4** *(A) Absorption spectra of aqueous suspensions of nanoparticles samples NP-3 and NP-4 ([NP-3] = 0.4 μM; [NP-4] = 0.4 μM). (B) Emission spectra of aqueous suspension of nanoparticles samples NP-3 and NP-4 ($\lambda_{ex}$ = 640 nm).*

**Table 4.2** *Spectral and emission properties of nanoparticles samples.*

| Sample | Abs. max./nm | Emi. max.[a]/nm | $\Phi_{em}$ | $\tau^{b,d}$ | $\tau^{c}$ | r (Δλ/nm) | r[e] (Δλ/nm) | $\eta_{ET}$ (%) |
|---|---|---|---|---|---|---|---|---|
| *Cy5.5-Si* | 685 | 717 | 0.07 | 1.6 | - | - | - | - |
| *Cy5.5*[f] | 683 | 707 | 0.2 | 1.4 | - | - | - | - |
| *Cy7-Si* | 819 | 860 | 0.03 | - | - | - | - | - |
| *NP-1* | 645, 688 | 722 | 0.02 | 1.5 | - | 0.3 (720-730)[d] | - | - |
| *NP-2* | 645, 688 | 722 | 0.03 | 1.4 | - | 0.008 (720-730)[d] | - | - |
| *NP-3* | 645, 693, 828 | 724, 860 | 0.08 | 1.0 | 1.1 | 0.4 (720-730)[e] | 0.4 (850-870) | 38 |
| *NP-4* | 645, 693, 828 | 724, 860 | 0.06 | 0.5 | 0.7 | 0.4 (720-730)[e] | 0.1 (850-870) | 70 |

*[a] $\lambda_{ex}$ = 650 nm; [b] $\lambda_{em}$ = 724 nm; [c] $\lambda_{em}$ = 860 nm; [d] $\lambda_{ex}$ = 640 nm; [e] $\lambda_{ex}$ = 650 nm; [f] Cy5.5 commercial dye (Cy5.5 GE) was purchased from GE Healthcare.*

Morphological characterization by TEM images (Figure 4.5) showed a silica core diameter $d_c$ = 10 nm for NP-1, $d_c$ = 9 nm for NP-2, $d_c$ = 10.5 nm for NP-3 and $d_c$ = 11 nm for NP-4. The hydrodynamic diameter ($d_H$) measured by dynamic light scattering (DLS) was very similar for NP-1, NP-2, NP-3 and NP-4 ($d_H$ = 25, 27, 25 and 27 nm, respectively), with relatively low polidispersity index (0.27, 0.27, 0.21 and 0.31, respectively) (Table 4.3).

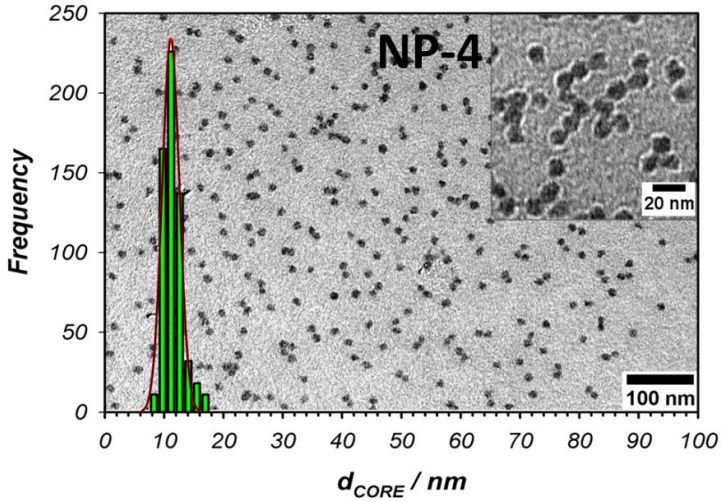


**Figure 4.5** *TEM images and silica core size distribution of NP-4. $d_c$ = (11.0 ± 1.5) nm. For clarity, only results of experiments done with NP-4 are shown.*

**Table 4.3** *Mean silica core - $d_c$ ± SD - determined by TEM analysis and DLS hydrodynamic values ($d_H$ ± SD) for the SNPs described in this work. Standard deviation was calculated on five different measurements.*

| Sample | ($d_c$ ± SD) / nm | ($d_H$ ± SD) / nm | PdI |
|---|---|---|---|
| *NP-1* | 10 ± 2 | 25 ± 13 | 0.27 |
| *NP-2* | 9 ± 2 | 27 ± 14 | 0.27 |
| *NP-3* | 10.5 ± 1.5 | 24 ± 11 | 0.21 |
| *NP-4* | 11.0 ± 1.5 | 27 ± 15 | 0.31 |

All SNPs synthesized were assessed both by flow-cytometry and optical imaging. In particular, for flow-cytometry assays, SNP samples were used for cell labeling, as shown in Section 3.2. SNPs doped with both dyes (NP-3 and NP-4, respectively) displayed a signal detectable in the FL4 channel of the flow-cytometer; moreover, their mean fluorescence intensity (NP-3 = 130; NP-4 = 100) was increased compared to that obtained with nanoparticels doped with only Cy5.5-Si (Figure 4.6A-B). These results confirmed that the approach selected in this work was very effective in increasing the fluorescence quantum yield and the number of Cy5.5 per nanoparticle and, as a consequence, the SNP brightness.

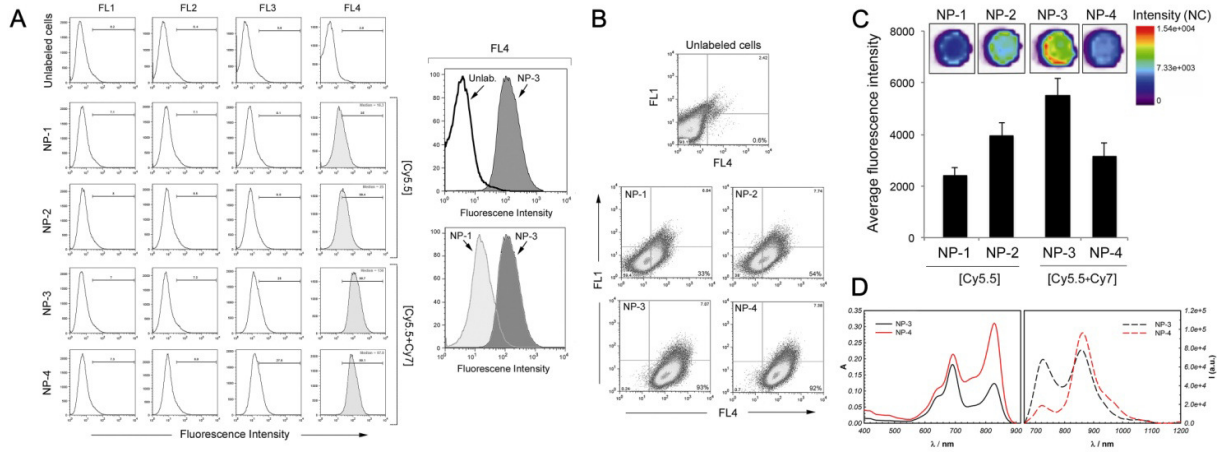


**Figure 4.6** *Characterization of the flow-cytometric and optical imaging performance of the NIR-SNPs and m-NIR-SNPs. (A-B) Cells were incubated with the indicated SNP at 37°C for 18 hours, to allow SNP cell internalization, before analyses by flow cytometry. (A) The fluorescence intensity of the NIR-SNPs- and m-NIR-SNPs-labeled cells, detected selectively on the FL4 channel, is indicated by the light grey histograms. On the right panels, the overlays compare the fluorescence intensity of the double dye-doped NP-3 [Cy5.5-Si+Cy7-Si] either with the unlabeled cells (Unlab.) or with the single dye-doped NP-1 [Cy5.5-Si]. (B) Flow-cytometric analyses of SNP-labeled cells are shown as dot plots; percentages of the positive cells (into the lower right quadrant) are indicated. (C) Equimolar aliquots of the SNP preparatives were placed on a paper substrate before analysis of the fluorescence with a time-domain fluorescence imager Optix. Results are expressed as means ± SD (experiments performed in triplicate). (D) Comparison of absorption and emission spectra of the double dye-doped [Cy5.5-Si+Cy7-Si] samples NP-3 and NP-4. (A-D) For each set of analyses, representative results out of three independent experiments are shown.*

By comparison of the fluorescence of the SNPs obtained with a small animal TD fluorescence imager, NP-3 sample exhibited the best result in terms of emission intensity. This performance was better compared to that obtained with NP-1 and NP-2, but also with respect to NP-4 sample, which had the same content of the Cy5.5-Si but the highest Cy7-Si content: this result was due to the fact that NP-3 and NP-4 samples had very similar quantum yields ($\Phi_{NP-3}$ = 0.08 and $\Phi_{NP-4}$ = 0.06), but not the same energy transfer efficiency (38% and 70%, respectively) (Table 4.2 and Figure 4.6C).

As can be seen from Figure 4.6D for the NP-3 sample, the lower Cy7 concentration promoted the increase in the Cy5.5 fluorescence intensity. On the other hand, the higher Cy7 concentration in NP-4 decreased the Cy5.5 fluorescence intensity, because the increased concentration of the energy acceptor Cy7 raised the energy transfer efficiency. For these reasons, NP-3 SNPs were chosen for the *in vivo* experiments relating to their biodistribution in healthy mice as well as in lymphoma bearing xenografts, and their suitability as contrast imaging agents for cell labeling and tracking.

### 4.2.2 Analysis of m-NIR-SNPs biodistribution

BALB/c mice were injected intravenously (i.v.) *via* the tail vein with 1 nmol of NP-3 sample and analyzed by optical imaging, in order to explore their biodistribution. A diffuse distribution throughout the body of the mouse was detected at few minutes after i.v. injection of the SNPs by whole-body fluorescence analysis. Moreover, within the first 24 hours, a strong signal was detectable in the liver and intestine decreasing over time (Figure 4.7).

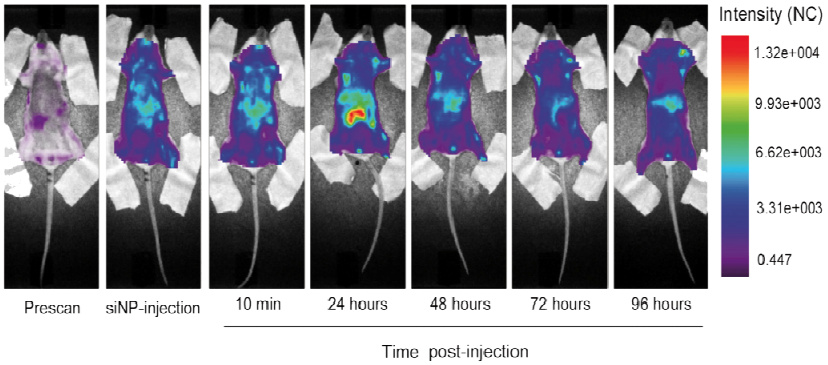


**Figure 4.7** *Biodistribution of m-NIR-SNPs. BALB/c mice were injected intravenously (i.v.) via the tail vein with 1 nmol of m-NIR-SNPs and analyzed by optical imaging. Whole-body scan of a representative mouse in supine position; fluorescence intensity images were acquired at the indicated time post-injection and are displayed in normalized counts (NC).*

To study deeply the degree of SNPs accumulation in the organs and tissues excluding any potential influence due to autofluorescence and scattering within the body and fur, consequently, to increase both specificity and sensitivity of the probe detection, mice were sacrificed at either 24 hours or 96 hours after i.v. injection of the NP-3 nanoparticles. In this way, the *ex vivo* optical imaging analysis of explanted organs (i.e. kidneys, heart, spleen, brain, lungs, stomach, intestine, liver) was carried out. As shown in Figure 4.8A-B, by comparison between the fluorescence intensity of explanted organs, it was possible to document that the highest fluorescence signal was in the liver followed by intestine, kidneys, stomach, heart and lungs, while the lowest signal was observed in the spleen and in the brain. At 96 hours after SNPs injection, despite an overall decrease of the signal compared to that observed within 24 hours after i.v. injection, the highest fluorescent signal was still in the liver and lowest in the heart and the brain; this analysis confirmed the preferential localization of SNPs in the liver, with a significant presence in the gastrointestinal tract.

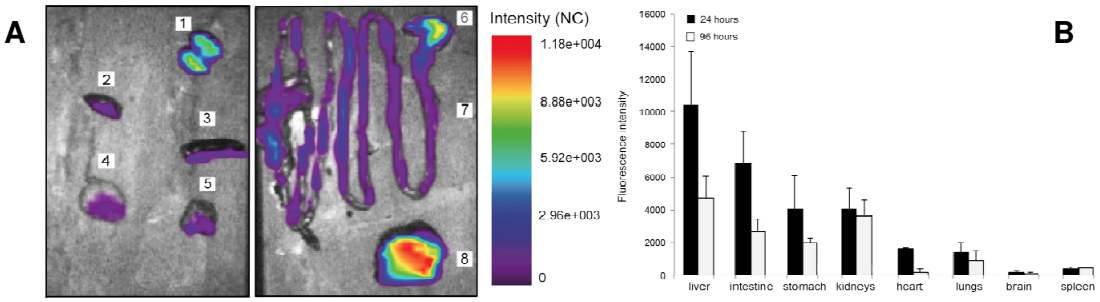


**Figure 4.8** *Mice were sacrificed at either 24 hours or 96 hours after i.v. injection of the m-NIR-SNPs, for ex vivo optical imaging analysis of the explanted organs. (A) Ex vivo imaging of organs explanted at 96 hours after m-NIR-SNPs administration are shown: 1, kidneys; 2, heart; 3, spleen; 4, brain; 5, lungs; 6, stomach; 7, intestine; 8, liver. (C) Ex vivo profile of m-NIR-SNPs distribution at 24 hours and 96 hours after i.v. injection. Data are expressed as means ± SD of three independent experiments.*

The validation of such localization occurred through the fluorescence microscopic examination of tissue cryosections obtained from the explanted organs at 24 hours after SNPs injection. Between the organs analyzed, the highest fluorescence signal was detected again in the liver, which displayed a homogeneous distribution of NIR fluorescence along with NIR fluorescent spots, attributable to clusters of SNPs in the hepatic parenchyma (Figure 4.9).

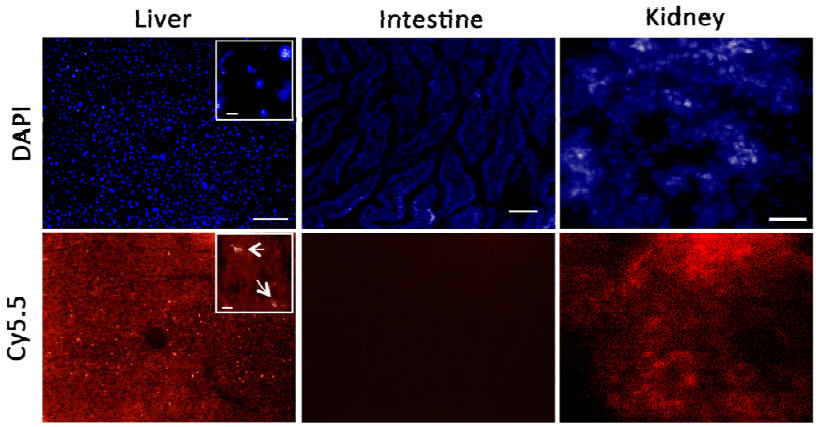


**Figure 4.9** *Representative fluorescence microscopy images of cryosections obtained from organs explanted from the m-NIR-SNPs injected mice. DAPI staining was carried out to visualize cell nuclei, which appear in blue, while m-NIR-SNPs appear in red; fluorescence images have identical exposure times to allow fluorescence comparison among tissues (liver, bar = 150μm; intestine, bar=100μm; kidney, 50μm). The arrows into the inset indicate SNPs-clusters in the hepatic parenchyma (bar = 5μm).*

Figure 4.9 also showed an irrelevant NIR fluorescence in the small intestine wall sections; nevertheless, this apparent contradiction of what *ex vivo* analysis of the organs underlined can be explained with the presence of the m-NIR-SNPs in the feces. It is of interest to note that the overall conclusions derived by whole-body and *ex vivo* analyses are consistent with the excretion of the silica based nanostructures by the hepatobiliary way.[10] Finally, although a fluorescent signal was revealed by microscopic examination of kidneys sections, no fluorescence was detected in urine samples: this observation confirmed data previously reported showing that molecules with a hydrodynamic diameter greater than 8 nm do not typically undergo to glomerular filtration.[21]

### 4.2.3 *In vivo* tumor imaging and cell tracking

With the aim to assess the possible tumor-targeting properties of SNPs, the JVM-2 human leukemic cells were injected subcutaneously in SCID mice ($10^7$ cells per mouse) to obtain the formation of a tumor of an average size of 0.6–0.7 cm diameter in 12–15 days after injection.[22,23] After that, subcutaneous tumor-bearing mice were i.v. injected with the NP-3 sample and monitored for up to 48 hours (Figure 4.10A). At 24 hours after injection, it was possible to note a clear accumulation of SNPs in the tumor site by the *in vivo* whole-body TD optical imaging. Previous observations were confirmed by the *ex vivo* analysis of the explanted tumor masses, which highlighted the localization of the m-NIR-SNPs fluorescence signal into the JVM-2-derived tumor mass (4.10B).

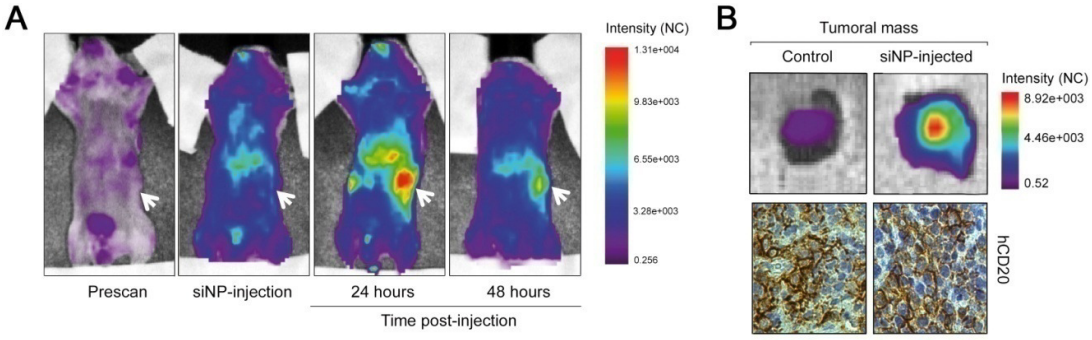


**Figure 4.10** *Application of m-NIR-SNPs as contrast agent for in vivo tumor imaging. SCID mice (n=8) were subcutaneously injected with JVM-2 cells ($10^7$ cells/mouse) and, when xenograft tumors reached the size of 0.6-0.7 cm diameter, mice were either left untreated or i.v. injected with the m-NIR-SNPs. (A) Whole-body scan of a representative tumor-bearing mouse. Fluorescence intensity images were acquired at the indicated time post-injection; arrows indicate the tumor site. (B) Ex vivo imaging of the tumor mass explanted from mouse either left untreated or injected with m-NIR-SNPs. IHC analysis documents that the tumors derive from the s.c. injected CD20 + JVM-2 cells (original magnification x200). Representative results are shown.*

At 48 hours after injection, although m-NIR-SNPs uptake was mainly in the liver, a fluorescence signal due to the SNPs was still noticeable. These results demonstrated the ability of the circulating SNPs to passively localize into solid tumors due to the enhanced permeability and retention (EPR) effect, which depends on numerous factors such as extensive angiogenesis and hence hypervasculature, defective vascular architecture and impaired lymphatic drainage/ recovery system.[24] Of course, the tumor-targeting properties of m-NIR-SNPs could be useful for important applications such as tumor imaging (for diagnostic purposes and for intraoperative image guidance) and/or to deliver drugs physically entrapped in the silica matrix of the SNPs (See Chapter 7) to the tumoral sites.

The possibility of using the SNPs for *in vivo* cell tracking of cells labeled with the SNPs was also investigated.[10,25] For this study, which represented a combination of flow-cytometry and optical imaging, JVM-2 cells were labeled with m-NIR-SNPs and the efficiency of the intracellular uptake was verfied by flow-cytometry, before s.c. injection in SCID mice (Figure 4.11).

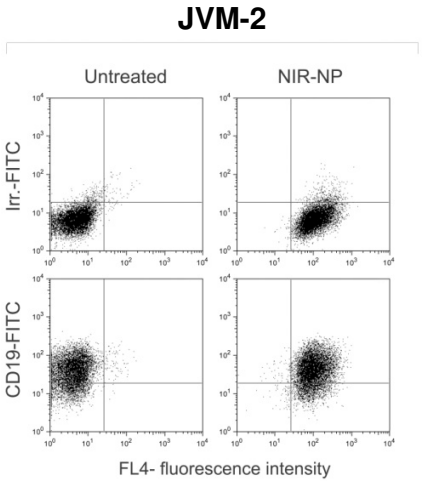


**Figure 4.11** *m-NIR-SNPs allow multiparametric analysis in flow-cytometry. Cells were either left untreated or incubated with m-NIR-SNPs at 37°C for 18 hours, to allow SNPs cell internalization, before analyses by flow cytometry in combination with antibodies (Ab) for cell surface antigens. JVM-2 cells were labelled with m-NIR-SNPs along with the B-cell specific CD19 Ab. Flow-cytometric analyses of multi-labeled cells were shown as two-colours dot plots in which co-expression (of either 2 different antigens or antigen + NP) was documented by localization of the cells in the upper right quadrant. Irr., isotype-matched control Ab. The results showed that m-NIR-SNPs fluorescence did not interfere with the fluorescence (FITC, PE) of Ab used for phenotypical cell characterization. Representative results out of three independent experiments are shown.*

Injected mice were then monitored daily by whole-body TD optical imaging. As can be noted from Figure 4.12A, a strong fluorescent signal was detectable in the injection site for 3 days after cell inoculation and, although the signal decreased progressively over time, it

was still visible for 12 days. It is important to note that the fluorescent signal was due to the to the m-NIR-SNPs-JVM-2 labeled cells, and not derived from cell-free nanoparticles, as demonstrated by two important evidences: (1) the co-localization of the fluorescence and of the human CD20 antigen (the marker of JVM-2 cells), respectively, was documented by *ex vivo* and IHC analyses of the explanted subcutaneous tissue (Fig. 4.12B); (2) a subcutaneous tumor mass became macroscopically detectable at the injection site from day 8 onward (Fig. 4.12C).

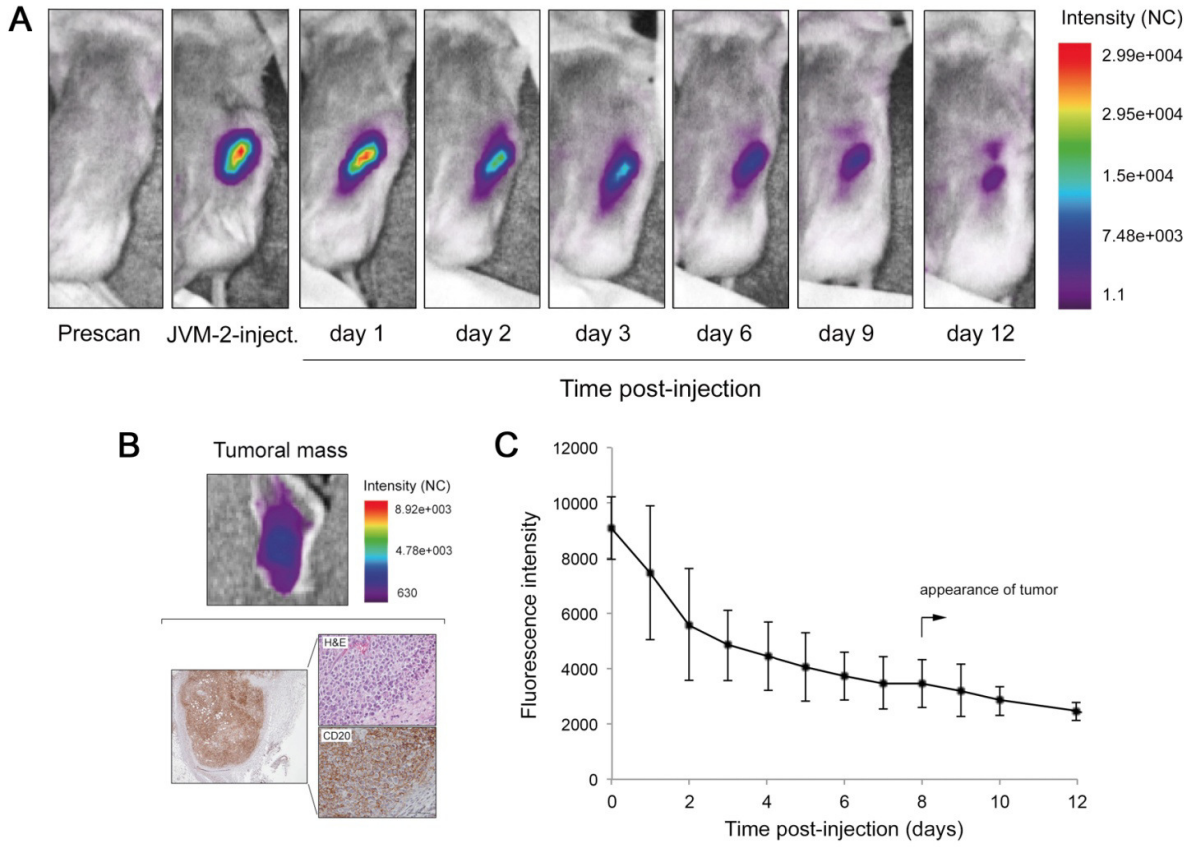


**Figure 4.12** *In vivo cell tracking using m-NIR-SNPs as cell labeling probe. JVM-2 leukemic cells were either left untreated or incubated with m-NIR-SNPs at 37°C for 18 hours, to allow SNPs cell internalization, before s.c. injection in SCID mice (107 cells/mouse). (A and B) Whole-body scan of a representative mouse injected with m-NIR-SNPs-labeled JVM-2 and ex vivo imaging of the explanted subcutaneous tumor mass. Microscopic analyses of tumor sections stained with haematoxylin and eosin (H&E) and anti-human CD20 staining (original magnification x200) confirm the co-localization of the in vivo and ex-vivo fluorescence signal with the s.c. injected CD20 + JVM-2 cells. (C) At the indicated time post-injection of the labeled cells, fluorescence intensity images were acquired from whole-body scan of 5 mice and results are expressed as means±SD.*

As a consequence, the tumor-forming capacity of m-NIR-SNPs- labeled cells can be a tool to monitor both the cell localization upon injection and the site of tumor development, with the possibility to anticipate and substitute eventual macroscopic manifestations or autoptic examinations in animal models.

## *4.3* Conclusions

In this work, a synthetic strategy based on the development of silica-core PEG-shell nanostructures doped with a donor-acceptor couple exhibiting a tunable intensity profile across the NIR spectrum was reported. This is a fundamental feature in view of applications such as whole-animal optical imaging and *in vitro* and *in vivo* cell labeling applications. In fact, this approach allows to increase the fluorescence signal *in vivo*, and to match in a versatile way the probe and instrumental setup spectral properties.

Moreover - respect to the single dye preparation - it will be possible a significant improvement of the signal-to-noise ratio of optical measurements, since large pseudo Stokes-shifts can be obtained exploiting efficient energy transfer processes within the particle.[24,26-29] These features will be useful in designing new application for imaging agents based on silica nanoparticles for different experimental disease models.

## 4.4 Notes and references

The contents of this chapter are based on S. Biffi, L. Petrizza, E. Rampazzo, R. Voltan, M. Sgarzi, C. Garrovo, L. Prodi, L. Andolfi, C. Agnoletto, G. Zauli and P. Secchiero, *RSC Adv.* **2014**, *4*, 18278 - Reproduced by permission of The Royal Society of Chemistry.


(1) Kaijzel, E. L.; van der Pluijm, G.; Lowik, C. W. *Clinical Cancer Research* **2007**, *13*, 3490.
(2) McIntyre, J. O.; Scherer, R. L.; Matrisian, L. M. *Methods in Molecular Biology* **2010**, *622*, 279.
(3) Agostinis, C.; Biffi, S.; Garrovo, C.; Durigutto, P.; Lorenzon, A.; Bek, A.; Bulla, R.; Grossi, C.; Borghi, M. O.; Meroni, P.; Tedesco, F. *Blood* **2011**, *118*, 4231.
(4) Day, K. E.; Sweeny, L.; Kulbersh, B.; Zinn, K. R.; Rosenthal, E. L. *Molecular Imaging and Biology* **2013**, *15*, 722.
(5) Ntziachristos, V.; Razansky, D. *Recent Results in Cancer Research* **2013**, *187*, 133.
(6) Byrne, W. L.; DeLille, A.; Kuo, C.; de Jong, J. S.; van Dam, G. M.; Francis, K. P.; Tangney, M. *Journal of Controlled Release* **2013**, *172*, 523.
(7) Schaafsma, B. E.; Mieog, J. S.; Hutteman, M.; van der Vorst, J. R.; Kuppen, P. J.; Lowik, C. W.; Frangioni, J. V.; van de Velde, C. J.; Vahrmeijer, A. L. *Journal of Surgical Oncology* **2011**, *104*, 323.
(8) Vahrmeijer, A. L.; Hutteman, M.; van der Vorst, J. R.; van de Velde, C. J.; Frangioni, J. V. *Nature Reviews Clinical Oncology* **2013**, *10*, 507.
(9) Bae, W.; Tan, W.; Hong, J.-I. *Chemical Communications* **2012**, *48*, 2270.
(10) Helle, M.; Rampazzo, E.; Monchanin, M.; Marchal, F.; Guillemin, F.; Bonacchi, S.; Salis, F.; Prodi, L.; Bezdetnaya, L. *ACS Nano* **2013**, *7*, 8645.
(11) Burns, A. A.; Vider, J.; Ow, H.; Herz, E.; Penate-Medina, O.; Baumgart, M.; Larson, S. M.; Wiesner, U.; Bradbury, M. *Nano Letters* **2008**, *9*, 442.
(12) Ma, K.; Sai, H.; Wiesner, U. *J. Am. Chem. Soc.* **2012**, *134*, 13180.
(13) Montalti, M.; Prodi, L.; Rampazzo, E.; Zaccheroni, N. *Chem Soc Rev* **2014**, *43*, 4243.
(14) Montalti, M.; Prodi, L.; Rampazzo, E.; Zaccheroni, N. *Chemical Society Reviews* **2014**, DOI: 10.1039/c3cs60433k.
(15) Lavis, L. D.; Raines, R. T. *ACS Chemical Biology* **2008**, *3*, 142.

(16) Gruber, H. J.; Hahn, C. D.; Kada, G.; Riener, C. K.; Harms, G. S.; Ahrer, W.; Dax, T. G.; Knaus, H.-G. *Bioconjugate Chemistry* **2000**, *11*, 696.
(17) Chipon, B.; Clavé, G.; Bouteiller, C.; Massonneau, M.; Renard, P.-Y.; Romieu, A. *Tetrahedron Letters* **2006**, *47*, 8279.
(18) Hirata, T.; Kogiso, H.; Morimoto, K.; Miyamoto, S.; Taue, H.; Sano, S.; Muguruma, N.; Ito, S.; Nagao, Y. *Bioorganic and Medicinal Chemistry* **1998**, *6*, 2179.
(19) Bonacchi, S.; Genovese, D.; Juris, R.; Montalti, M.; Prodi, L.; Rampazzo, E.; Zaccheroni, N. *Angewandte Chemie, International Edition in English* **2011**, *50*, 4056.
(20) Vivero-Escoto, J. L.; Huxford-Phillips, R. C.; Lin, W. *Chemical Society Reviews* **2012**, *41*, 2673.
(21) Deen, W. M.; Lazzara, M. J.; Myers, B. D. *American Journal of Physiology: Renal Physiology* **2001**, *281*, F579.
(22) Taylor, A.; Wilson, K. M.; Murray, P.; Fernig, D. G.; Levy, R. *Chem Soc Rev* **2012**, *41*, 2707.
(23) Voltan, R.; Secchiero, P.; Ruozi, B.; Forni, F.; Agostinis, C.; Caruso, L.; Vandelli, M. A.; Zauli, G. *Clinical Cancer Research* **2013**, *19*, 3871.
(24) Maeda, H.; Wu, J.; Sawa, T.; Matsumura, Y.; Hori, K. *Journal of Controlled Release* **2000**, *65*, 271.
(25) Rampazzo, E.; Voltan, R.; Petrizza, L.; Zaccheroni, N.; Prodi, L.; Casciano, F.; Zauli, G.; Secchiero, P. *Nanoscale* **2013**, *5*, 7897.
(26) Rampazzo, E.; Bonacchi, S.; Genovese, D.; Juris, R.; Sgarzi, M.; Montalti, M.; Prodi, L.; Zaccheroni, N.; Tomaselli, G.; Gentile, S.; Satriano, C.; Rizzarelli, E. *Chemistry- A European Journal* **2011**, *17*, 13429.
(27) Genovese, D.; Rampazzo, E.; Bonacchi, S.; Montalti, M.; zaccheroni, N.; Prodi, L. *Nanoscale* **2013**, DOI: 10.1039/c3nr05599j.
(28) Rampazzo, E.; Bonacchi, S.; Juris, R.; Montalti, M.; Genovese, D.; Zaccheroni, N.; Prodi, L.; Rambaldi, D. C.; Zattoni, A.; Reschiglian, P. *Journal of Physical Chemistry B* **2010**, *114*, 14605.
(29) Genovese, D.; Bonacchi, S.; Juris, R.; Montalti, M.; Prodi, L.; Rampazzo, E.; Zaccheroni, N. *Angew. Chem.-Int. Edit.* **2013**, *52*, 5965.

# Chapter 5

# Silica nanoparticles as agents for optoacoustic imaging

## 5.1 Introduction

In this work dye-doped near infrared-emitting silica nanoparticles (NIR-SNPs) were designed to study their potential application in the field of the optoacoustic imaging.

Optical imaging proved to be an important method for bioanalytical applications, operating on contrast mechanisms which permit the visualization of cellular and subcellular function and structure.[1] Optical imaging methods used different physical parameters of the interaction of light with tissue (Table 5.1). The image signal provided by these methods appears mainly as a function of internal contrast, which often shows a limited information content. A recent technique, however, has gained great popularity, as it offers molecular specificity to *in vivo* imaging technologies: fluorescence imaging. In fluorescence imaging, the light that comes from an external source is absorbed and immediately re-emitted at a longer wavelength (see Section 1.3). This technique can be performed with different resolutions and depth of penetration, ranging from micrometers (intravital microscopy) to centimeters (fluorescence molecular tomography, FMT) (Table 5.1).

**Table 5.1** *Optical in vivo imaging systems, as in reference 4.*

| Method[a] | Constrast[b] | Depth | Commonly used λ | Clinical potential[c] |
|---|---|---|---|---|
| *A-Epi* | Ab, Fl | 20 µm | Visible | ✓ |
| *A-Confocal* | Fl | 500 µm | Visible | ✓ |
| *A-Two-photons* | Fl | 800 µm | Visible | ✓ |
| *B-Opt. projection tomography* | Ab, Fl | 15 mm[d] | Visible | ✗ |
| *B-Opt. coherence tomography* | Sc | 2 mm | Visible, NIR | ✓ |
| *B-Laser speckle imaging* | Sc | 1 mm | Visible, NIR | ✓ |
| *C-Hyperspectral imaging* | Ab, Fl, Sc | <5 mm | Visible | ✓ |
| *C-Endoscopy* | Ab, Fl, Sc | <5 mm | Visible | ✓ |
| *C-Polarization imaging* | Ab, Sc | <1.5 cm | Visible, NIR | ✓ |
| *C-Fluor. reflectante imaging (FRI)* | Ab, Fl | <7 mm | NIR | ✓ |
| *C-Diffuse opt. tomography (DOT)* | Ab, Fl | <20 cm | NIR | ✓ |
| *D-Fluor. Resonance imaging (FRI)* | Ab, Fl | <7 mm | NIR | ✓ |
| *D-Fluor. molecular tomography (FMT)* | Fl | <20 cm | NIR | ✓ |
| *D-Bioluminescence imaging (BLI)* | Em | <3 cm | 500-600 nm | ✗ |

*[a]A=microscopic resolution; B=mesoscopic resolution; C=macroscopic resolution, intrinsic contrast; D=macroscopic resolution, molecular contrast. [b]Ab=absorption; Em=emission; Sc=scattering; Fl=fluorescence. [c] ✓=yes; ✗=no; ✓=experimental. [d] In cleared specimen.*

The recent development of a strong variety of fluorescent tags, which can display functional and molecular processes *in vivo,* showed the fascinating benefits of fluorescence for the optical imaging.[2]

In this context, the development of bright near-infrared (NIR) fluorescent probes, with excitation and emission spectra above 650 nm, allows more interesting applications,[3] such as whole body animal imaging. Indeed, it gives high sensitivity imaging through several millimeters of tissue, because hemoglobin (that is the principal absorber of visible light), water and lipids (that are the principal absorbers of infrared light) have their lowest absorption coefficient in the NIR spectral region (650–900 nm).[4]

Imaging in this wavelength range can have the additional advantage of minimizing tissue autofluorescence, thus increasing the signal-to-noise ratio.[5] A great multiplicity of probes operating in the NIR region have been developed, from fluorescent dyes (that are able to preferentially accumulate in tissues of interest) to activatable photoproteins.[3,6] Furthermore, several nanoparticles with optical contrast, such as gold or carbon nanoparticles, can be derivatized for specific cell targeting and molecular imaging.[7-10]

Conventional microscopy methods allow the visualization of *in vivo* imaging of optical reporter molecules, especially in cell monolayers or thin tissue slices. Over the last decade, in this field an increase in performance has occurred with the use of confocal and multiphoton microscopy for a deeper imaging than ever before in tissues.[11,12] Confocal microscopy can succeed in reaching depths of up to 100-200 μm when imaging highly scattering tissues *in vivo*, while two-photon and multiphoton microscopy can achieve 300-500 μm. However, these techniques, together with the Optical Projection Tomography (OPT)[13] and Selective Plane Illumination Microscopy (SPIM)[14] (which are very useful for volumetric imaging of low-scattering samples) are highly limited by tissue scattering.

As previously described, it is necessary to use optical reporter agents that work in the NIR region to reach a detection through up to few centimeters in tissues. Photon scattering process in tissues, however, can make imaging more difficult to achieve, yielding a significant resolution loss. A solution can be *macroscopic* optical tomography, that can resolve optical contrast in three-dimensions using optical measurements through multiple illumination and detection projections around the tissue of interest and, finally, mathematically combining these measurements to have a three-dimensional reconstruction of optical contrast images inside the investigated object.[15-17]

In recent years the accessibility to hybrid approaches, such as the combination with X-ray computed tomography (CT),[18,19] magnetic resonance imaging (MRI)[20] and optoacustic methods, leaded to improvements in macroscopic optical imaging performance, making these hybrid methods valuable and versatile for bioimaging. In this study, the interest has been directed to optoacoustic methods based on NIR-SNPs for imaging applications, with the aim to obtain a deeper penetration and higher spatial resolution that the ones achieved by optical microscopy.

Optoacoustic (or photoacoustic) imaging relies on the generation of acoustic waves following the absorption of light pulses of ultrashort duration. The optoacoustic

phenomenon has been known for over a century,[21] but only in the last decade has been used for bioanalytical applications.[22-24] The increase in the use of this technique was due to the coupling of the commercially available pulsed laser technology in the nanosecond range with sensitive acoustic detectors, yielding the generation of optoacoustic responses from tissue and the visualization of subsurface blood vessels with high resolution.[25-27]

In particular, MultiSpectral Optoacoustic Tomography (MSOT) is based on the spectral identification of chromophoric agents (such as molecules and particles) spread in tissue over background tissue absorption, and requires that the tissue of interest is illuminated with light pulses of time-shared multiple wavelengths of duration in the 1-100 ns range. The fast absorption of light pulses produces a response from photoabsorbing agents: indeed, the latter are designed to have an efficient and fast non radiative deactivation; this process leads to a thermoelastic expansion of the solvent around the dye that generates mechanical waves at ultrasonic frequencies. Acoustic detectors, placed in proximity to the illuminated tissue, can detect these waves. By modeling photon and acoustic propagation in tissues and using appropriate mathematical methods (inversion, or simply tomographic methods), it is possible to obtain images; if different dyes are present, it is also possible to spectrally separate their contribution to yield the biodistribution of all reporter molecules and tissue biomarkers (Figure 5.1).

Each light wavelength can generate images separately, but multiwavelength illumination and spectral processing are necessary for the identification of the unique spectral signatures of optical reporter agents of interest in the presence of intrinsic tissue chromophores. MSOT imaging requires agents with absorption spectra that show characteristic differences from the absorption of background tissue; for this reason,

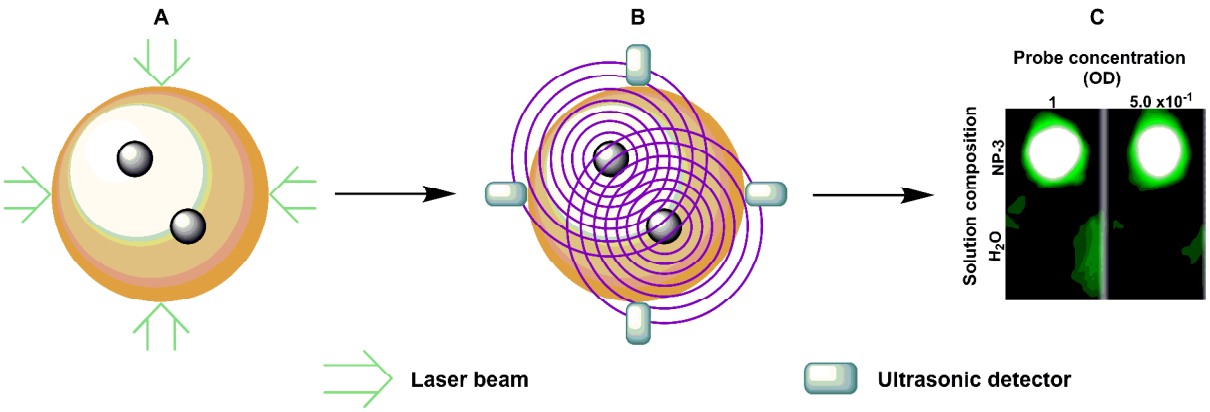


**Figure 5.1** *Principle of MSOT operation. (A) Light pulses of different time-shared multiple wavelengths illuminate the tissue of interest and achieve transient photon fields in tissue. (B) The fast absorption of light pulses produces a thermoelastic expansion that generates acoustic responses, that are then detected using acoustic detectors. (C) Tomographically reconstructed and spectrally unmixed images depicting the photoabsorbing agent (NIR-SNPs, in this case) and water signals detected by MSOT.*

molecules or nanoparticles that have steep absorption changes are preferible, since it is easier to resolve them by scanning narrow spectral bands. Reporter agents with molecular specificity without characteristic spectral signatures - such as agents with slow varying, broad absorption spectra - can also be detected in MSOT, using single wavelength measurements. In this case baseline measurements must be available, and this method is appropriate for highly absorbing agents with fast distribution or expression dynamics.[28]

Moreover, it is also necessary to evaluate the effects of light propagation in tissues accurately, to decompose the true probe concentration from variations of the optoacoustic signal due to light intensity variations in tissue.

In summary, with this method the spectral signature of the reporter dyes is distinguished with specificity from the nonspecific background absorption by multispectral separation. Suitable photoabsorbing agents display different spectra compared to the background absorption spectrum: as a consequence, compounds that have high molar extinction coefficients and can be detected above the intrinsic tissue optoacoustic signal are important for molecular imaging applications.[29] Previous reports showed that for these applications suitable agents could be conjugated plasmonic particles (e.g. gold nanorods),[7,9,10,30,31] targeted particles (e.g. carbon nanotubes, quantum dots),[8,32-34] fluorochromes and organic dyes (conjugated for targeting)[35,36] and agents used in other nonoptical imaging modalities (e.g. MRI) (Table 5.2).[37] In the next section, the design and synthesis of NIR-SNPs will be shown to assess their potential application as photoabsorbing agents for optoacoustic imaging.

**Table 5.2** *Optical Characteristics of Major Tissue Chromophores and Some Optoacoustic Molecular Contrast Agents. The actual values can change depending on the particular compound and its derivatization; therefore, representative examples are provided, as in references 8, 9, 28, 32, 34, and 36.*

| Chromophore | $\lambda_{exc}$ (nm) | $\varepsilon^a$ ($cm^{-1}$ $M^{-1}$) | $\Phi_{em}$ | Concentration-normalized absorptivity[b] [$cm^{-1}$/(mg/mL)] |
|---|---|---|---|---|
| *Oxygenated hemoglobin ($HbO_2$)* | 750 | $5.2 \times 10^2$ | 0 | 0.008 |
| | 550 | $58 \times 10^3$ | 0 | 0.9 |
| *Eumelanin* | 750 | $4.7 \times 10^2$ | 0 | 2.3 |
| | 550 | $1.2 \times 10^3$ | 0 | 5.8 |
| *NIR- organic dyes (AlexaFluor750)* | 750 | $2.5 \times 10^2$ | 0.12 | 169 |
| *Red-shifted fluor. protein (mCherry)* | 587 | $7.2 \times 10^4$ | 0.22 | 2.2 |
| *Single-walled carbon nanotubes* | 750 | $1.5 \times 10^7$ | 0 | 150 |
| *Gold nanorods* | 750 | $9.4 \times 10^8$ | 0 | 72 |
| *Activ. chromogenic assay (X-gal)* | 650 | $10^4$ | 0 | 24.5 |
| *NIR-Quantum dots* | 840 | $5 \times 10^6$ | 0.13 | 9.9 |

*[a]These numbers are provided per particle/molecule; [b]It is an estimate of a contrast agent's efficiency, with optical absorption coefficient in $cm^{-1}$, created in the target volume by a 1 mg/mL concentration of the contrast agent.*

## 5.2 Results and discussion

### 5.2.1 Synthesis and characterization of NIR-SNPs

In this work, dye-doped core-shell NIR-SNPs were synthesized using a one-pot synthetic approach (see Section 8.9), which starts from the preparation of surfactant Pluronic F127 micelles in water.[38-43] The resulting SNPs are photostable, showing high and durable monodispersity and colloidal stability,[44-48] displaying low adhesion properties toward proteins and that make them suitable for *in vitro* and *in vivo* experiments.[49,50]

Different dye-doped NIR-emitting silica nanoparticles (m-NIR-SNPs) were synthesized using increasing doping ratios of the triethoxysilane derivative Cy5.5-Si (Figure 5.2A) (see Section 4.2 and Section 8.2), utilized either alone (NPLP-2, -3, -4, -5 and -6, Figure 5.3) or together with the IR813 triethoxysilane dye derivative Cy7-Si (NP-3, -4 and -5, Fig. 5.2 and 5.3) to evaluate their suitability as optoacoustic imaging probes (Figure 5.3, Table 5.3).

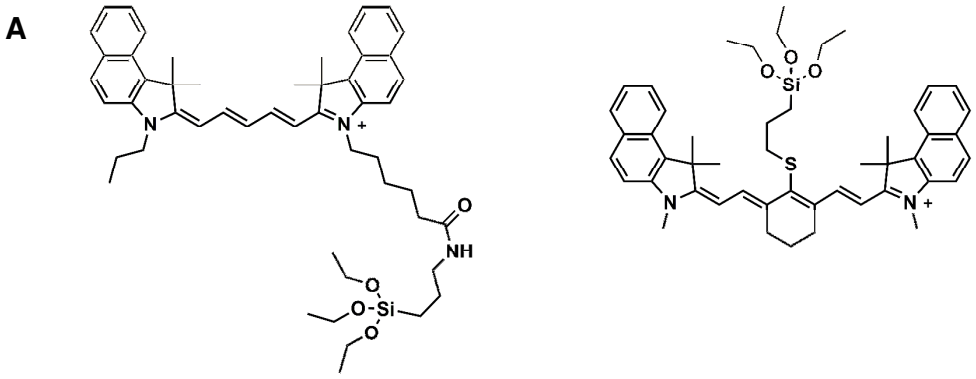


**Figure 5.2** *Molecular structure of: (A) Cy5.5-Si; (B) Cy7-Si.*

M-NIR-SNPs presented the distinctive absorption bands of the two Cyanine derivatives (693 nm, Cy5.5-Si; 828 nm, Cy7-Si, Figure 5.4). As can be seen from Table 5.4, m-NIR-SNPs with the highest Cy5.5-Si content (NPLP-5 and NPLP-6) exhibited the best results in terms of luminescence brightness, due to a higher fluorescence quantum yield and a higher molar absorption coefficient. This last property makes m-NIR-SNPs very promising tools for optoacoustic imaging. Additional photophysical properties of these SNPs are reported in Table 5.4. Moreover, from a morphological point of view, these nanoparticles have shown values comparable to those found in Section 4.2.1 (silica core diameter ($d_c$) ~

10 nm; hydrodynamic diameter ($d_H$) ~ 25 nm), with relatively low polidispersity index (PdI ~ 0.25).

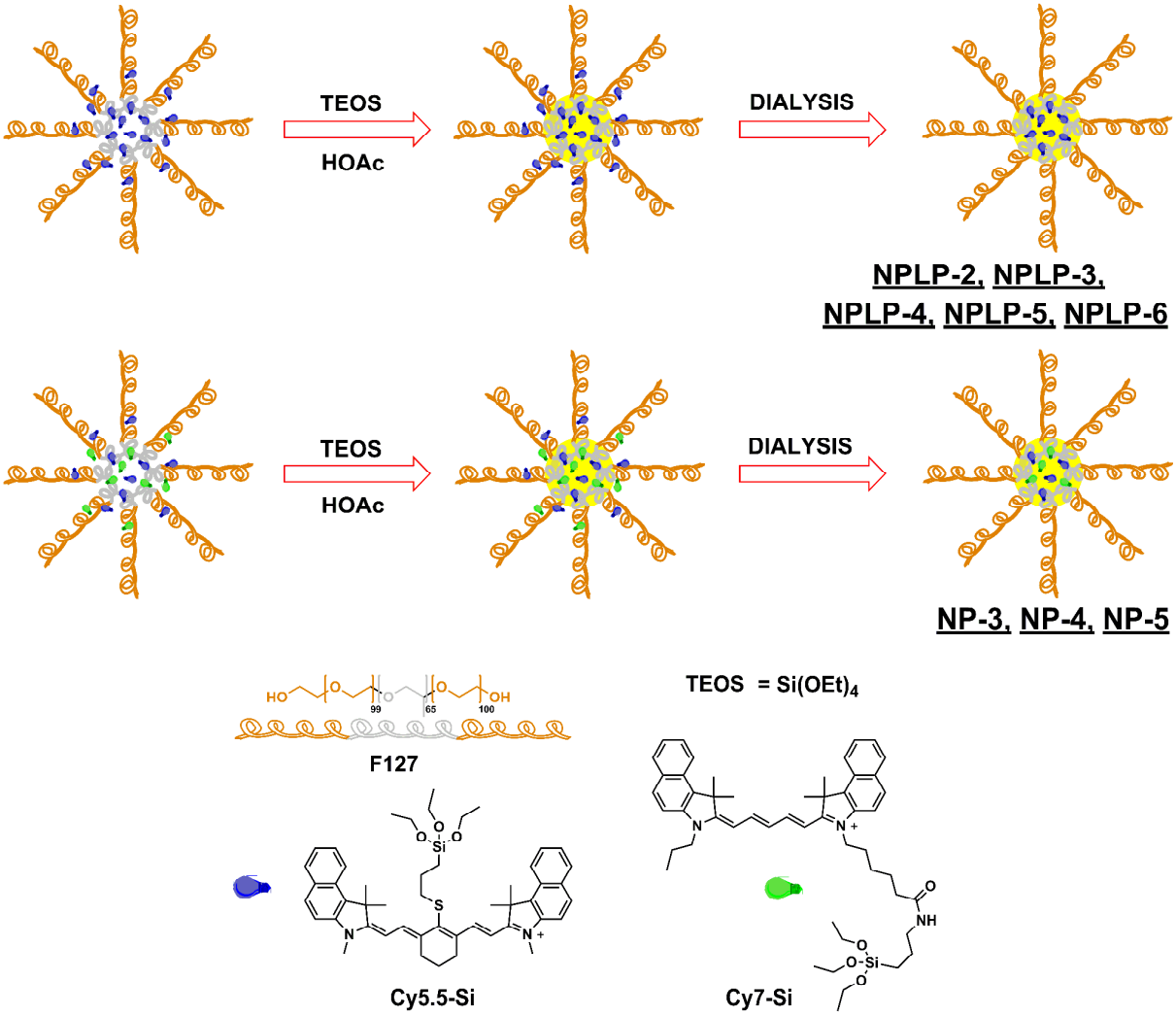


**Figure 5.3** *Doping dyes (Cy5.5-Si and Cy7-Si) and schematization of the synthetic procedure used for the synthesis of the m-NIR-SNPs (NPLP-2, -3, -4, -5 and -6; NP-3, -4 and -5) samples described in this work.*

**Table 5.3** *Doping characteristics of the SNPs samples presented in this study.*

| SNPs sample | %Dye[a] | TEOS mmol | Cy5.5-Si[b] µmol | Cy7-Si[b] µmol |
|---|---|---|---|---|
| *NP-3* | 0.2 Cy5.5-Si-<br>0.1 Cy7-Si | 0.8 | 1.6 | 0.8 |
| *NP-4* | 0.2 Cy5.5-Si-<br>0.2 Cy7-Si | 0.8 | 1.6 | 1.6 |
| *NP-5* | 0.4 Cy5.5-Si-<br>0.4 Cy7-Si | 0.8 | 3.2 | 3.2 |
| *NPLP-2* | 0.2 Cy5.5-Si- | 0.8 | 1.6 | - |
| *NPLP-3* | 0.5 Cy5.5-Si- | 0.8 | 4 | - |
| *NPLP-4* | 1 Cy5.5-Si- | 0.8 | 8 | - |

| | | | |
|---|---|---|---|
| *NPLP-5* | 2 Cy5.5-Si- | 16 | - |
| *NPLP-6* | 5 Cy5.5-Si- | 40 | - |

*[a]Doping ratio=[mol(dye)/mol(TEOS)]*100. [b]Cy5.5-Si and Cy7-Si were introduced in the reaction mixtures using pristine dichloromethane solutions.*

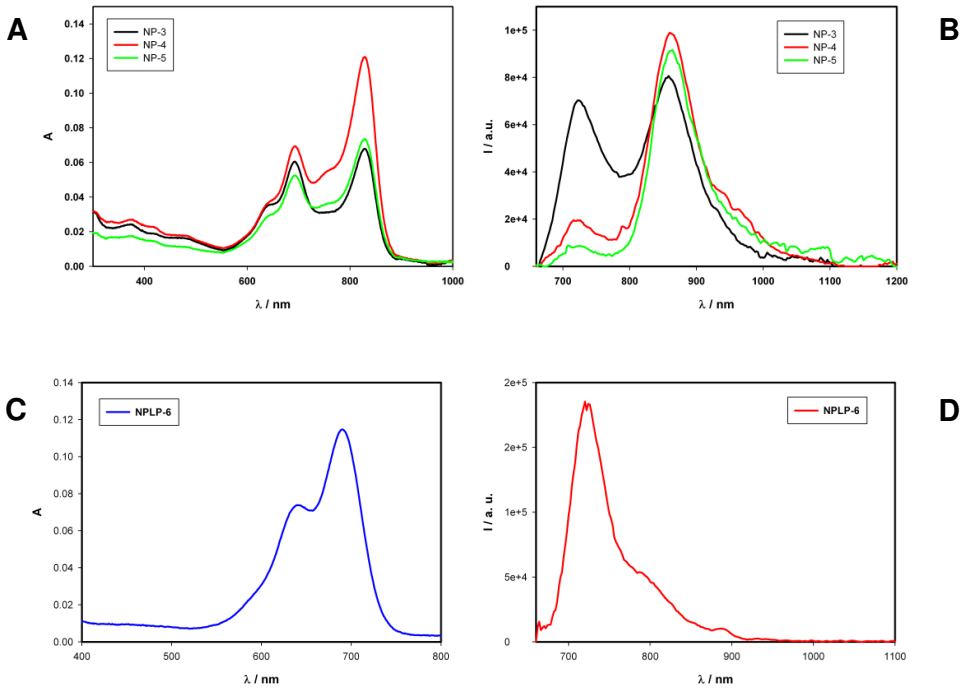


**Figure 5.4** *(A) Absorption spectra of aqueous suspensions of nanoparticles samples NP-3, NP-4 and NP-5 ([NP-3] = 0.4 μM; [NP-4] = 0.2 μM; [NP-5] = 0.1 μM ). (B) Emission spectra of aqueous suspension of nanoparticles samples NP-3, NP-4 and NP-5 ($\lambda_{ex}$ = 650 nm). (C) Absorption spectra of aqueous suspensions of NPLP-6 ([LPSC-6] 0.1 μM. (D) Emission spectra of aqueous suspension of NPLP-6 ($\lambda_{ex}$ = 650 nm).*

**Table 5.4** *Spectral and emission properties of nanoparticles samples.*

| Sample | Abs. max./nm | Emi. max.[a]/nm | $\Phi_{em}$ | $\tau^{b,d}$ | $\tau^{c}$ | r (Δλ/nm) | r[e] (Δλ/nm) |
|---|---|---|---|---|---|---|---|
| *Cy5.5-Si* | 685 | 717 | 0.07 | 1.6 | - | - | - |
| *Cy5.5*[f] | 683 | 707 | 0.2 | 1.4 | - | - | - |
| *Cy7-Si* | 819 | 860 | 0.03 | - | - | - | - |
| *NP-3* | 645, 693, 828 | 724, 860 | 0.08 | 1.0 | 1.1 | 0.4 (720-730)[e] | 0.4 (850-870) |
| *NP-4* | 645, 693, 828 | 724, 860 | 0.06 | 0.5 | 0.7 | 0.4 (720-730)[e] | 0.1 (850-870) |
| *NP-5* | 645, 693, 828 | 724, 860 | 0.06 | 0.5 | 0.7 | 0.4 (720-730)[e] | 0.006 (850-870) |
| *NPLP-2* | 645, 688 | 722 | 0.03 | 1.4 | - | 0.008 (720-730)[d] | |
| *NPLP-3* | 645, 688 | 712 | 0.05 | 1.4 | - | 0.3 (710-720)[e] | |

| | | | | | | |
|---|---|---|---|---|---|---|
| *NPLP-4* | 645, 691 | 716 | 0.07 | 1.2 | - | 0.1 (710-720)[e] |
| *NPLP-5* | 645, 691 | 720 | 0.07 | 1.2 | - | 0.2 (714-724)[e] |
| *NPLP-6* | 645, 691 | 721 | 0.12 | 0.8 | - | 0.1 (720-730)[e] |

*[a] $\lambda_{ex}$ = 650 nm; [b] $\lambda_{em}$ = 724 nm; [c] $\lambda_{em}$ = 860 nm; [d] $\lambda_{ex}$ = 640 nm; [e] $\lambda_{ex}$ = 650 nm; [f] Cy5.5 commercial dye (Cy5.5 GE) was purchased from GE Healthcare*

### 5.2.2 In vitro optoacoustic experiments

In the first set of experiments, SNPs doped with both fluorophores (NP-3, NP-4 and NP-5) were analyzed to evaluate the possibility of obtaining a detectable optoacoustic signal. For this purpose water solutions of the three probes were placed into the scattering MSOT phantom *(1.5% agar, 1% intralipid)* to determine their optoacoustic spectra (Figure 5.5).

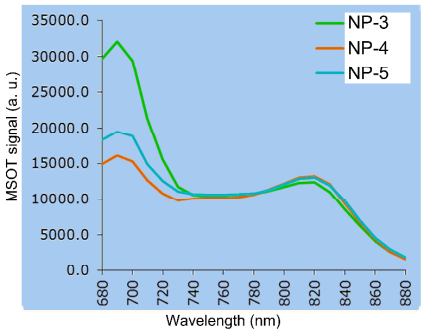


**Figure 5.5** *Optoacoustic spectrum of NP-3, NP-4 and NP-5 samples. Water dilutions of the three probes were placed into a scattering MSOT phantom (1.5% agar, 1% intralipid) to determine their optoacoustic spectrum (insertion diameter: 3 mm).*

The MSOT optoacoustic spectrum resembled the absorption spectrum of analyzed SNPs with regard to peak wavelengths and signal strength at 690 nm, while the peak at 830 nm produced a weak optoacoustic signal.

The analysis of tomographically reconstructed and spectrally unmixed images depicting NP-3, NP-4 and NP-5 samples detected by MSOT in combination with the MSOT quantification revealed that:

- NP-3, NP-4 and NP-5 samples generated a signal detectable by means of MSOT imaging;
- 2) the SNPs preparatives share very low lower limit of quantification (LLOQ) (NP-3 = 9.1 nM; NP-4 = 18 nM; NP-5 = 19 nM) and high linearity between the optoacoustic signal and the concentration (Figure 5.6).

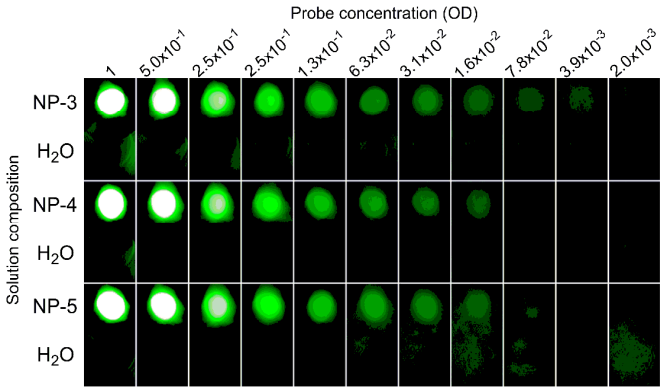


| | Concentration (µM) | | |
|---|---|---|---|
| **OD** | **NP-3** | **NP-4** | **NP-5** |
| 1.0 | 4.6 | 2.4 | 2.4 |
| $5.0x10^{-1}$ | 2.3 | 1.2 | 1.2 |
| $2.5x10^{-1}$ | 1.2 | $5.9x10^{-1}$ | $5.9x10^{-1}$ |
| $1.3x10^{-1}$ | $5.8x10^{-1}$ | $2.9x10^{-1}$ | $3.0x10^{-1}$ |
| $6.3x10^{-2}$ | $2.9x10^{-2}$ | $1.5x10^{-1}$ | $1.5x10^{-1}$ |
| $3.1x10^{-2}$ | $1.4x10^{-2}$ | $7.4x10^{-2}$ | $7.4x10^{-2}$ |
| $1.6x10^{-2}$ | $7.2x10^{-2}$ | $3.7x10^{-2}$ | $3.7x10^{-2}$ |
| $7.8x10^{-3}$ | $3.6x10^{-3}$ | $1.8x10^{-2}$ | $1.9x10^{-2}$ |
| $3.9x10^{-3}$ | $1.8x10^{-3}$ | $9.2x10^{-3}$ | $9.3x10^{-3}$ |
| $2.0x10^{-3}$ | $9.1x10^{-3}$ | $4.6x10^{-3}$ | $4.6x10^{-3}$ |

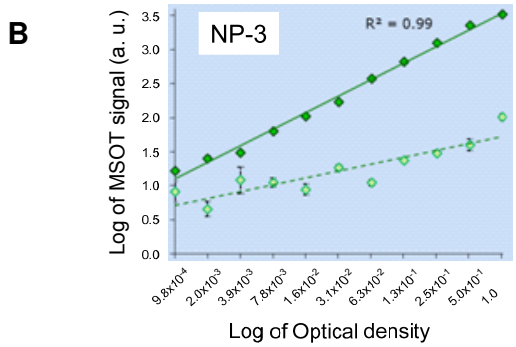


**Figure 5.6** *Tomographically reconstructed and spectrally unmixed images of m-NIR-SNPs and water signals detected by MSOT in single cross-sections for each dilution. A) Dilutions of NP-3, NP-4 and NP-5 samples in water (starting concentration 1 OD; OD = Optical Density) were inserted in a scattering agar phantom (1.5% agar and 1% Intralipid; 2 cm diameter) along with water as a control. MSOT acquisition was performed in five imaging planes (~800µm cross-section) with a 2 mm step size. B) MSOT quantifications of m-NIR-SNPs. Regions of interest were drawn around the probe and water phantom insertions and the spectrally unmixed signal was quantified. Error bars: standard error o the mean of 5 measurements. For clarity, only results of experiments done with NP-3 are shown.*

To further investigate the possibility to use the m-NIR-SNPs for *in vivo* evaluation, the photoacoustic spectrum of nanoparticles doped with Cy5.5-Si (NPLP-2, -3, -4, -5, -6) was acquired in the wavelength range from 680 to 970 nm using PBS spectrum as reference for background values (Figure 5.7). Higher values were in the wavelength range from 680 to 730 nm. While NPLP-2 and -3 displayed spectra similar to the PBS, NPLP-4, -5 and -6 samples showed greater photoacoustic intensity (PAI) values with NPLP-6 showing the highest signal.

Similar results were obtained with spectra recorded after dilution with PBS (dilution factor = 2), with NPLP-6 exhibiting the best result in terms of photoacoustic intensity.

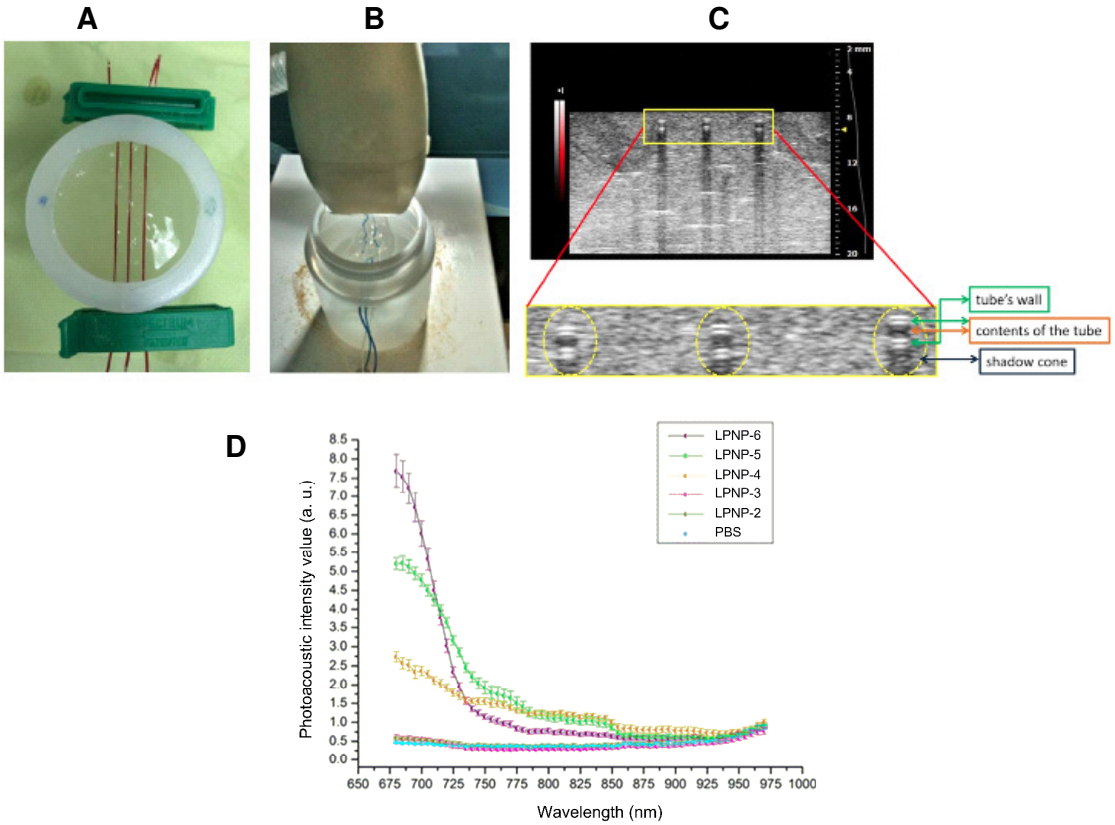


**Figure 5.7** *Optoacoustic spectrum of NPLP-2, -3, -4, -5 and -6 samples. A) and B) The phantom for the optoacoustic in vitro tests is a polyurethane tubing (outer diameter: 0.9 mm; inner diameter: 0.6 mm) submerged in a vinyl and borax gel. C) The acquisitions were performed along the major axis of the tube, obtaining content tube axial sections images. D) Comparison with PBS spectrum. [m-NIR-SNPs] = 20µM.*

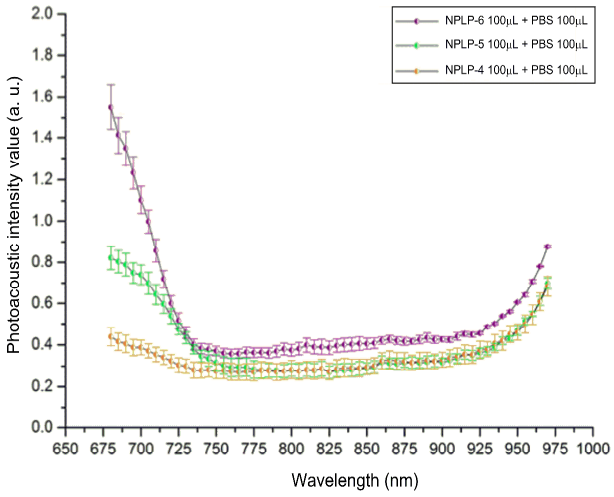

**Figure 5.8** *Optoacoustic spectrum of NPLP-4, -5, -6 samples after dilutions with PBS. Final [m-NIR-SNPs] = 10µM.*

The results showed an important decrease of photoacoustic intensity (PAI) values (~ 80%) that was not proportional to dilution (Figure 5.8).

Subsequently, blood spectrum was recorded and compared with the NPLP-4, -5 and -6 spectrum, showing that at the wavelength of interest for *in vivo* testing (range from 680 to 730 nm) there was no interference from blood signal (Figure 5.9).

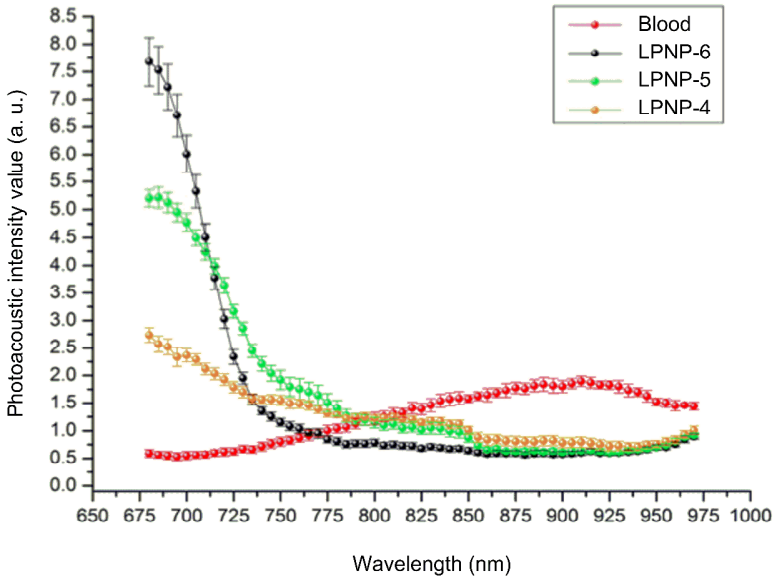


**Figure 5.9** Comparison between *NPLP-4, -5, -6 samples and blood optoacoustic spectrum. [m-NIR-SNPs] = 20µM.*

Finally, LPNP-4, -5 and -6 were diluted with blood (dilution factors = 2 for NPLP-4, -5 and -6; 3 and 3.5 for NPLP-6), displaying a decrease in the PAI signal that was again not proportional to dilution (Figure 5.10). As showed in Fig. 5.10, also after dilution with blood, the best results were obtained from the sample with the highest Cy5.5-Si content, suggesting its use in further experiments *in vivo*.

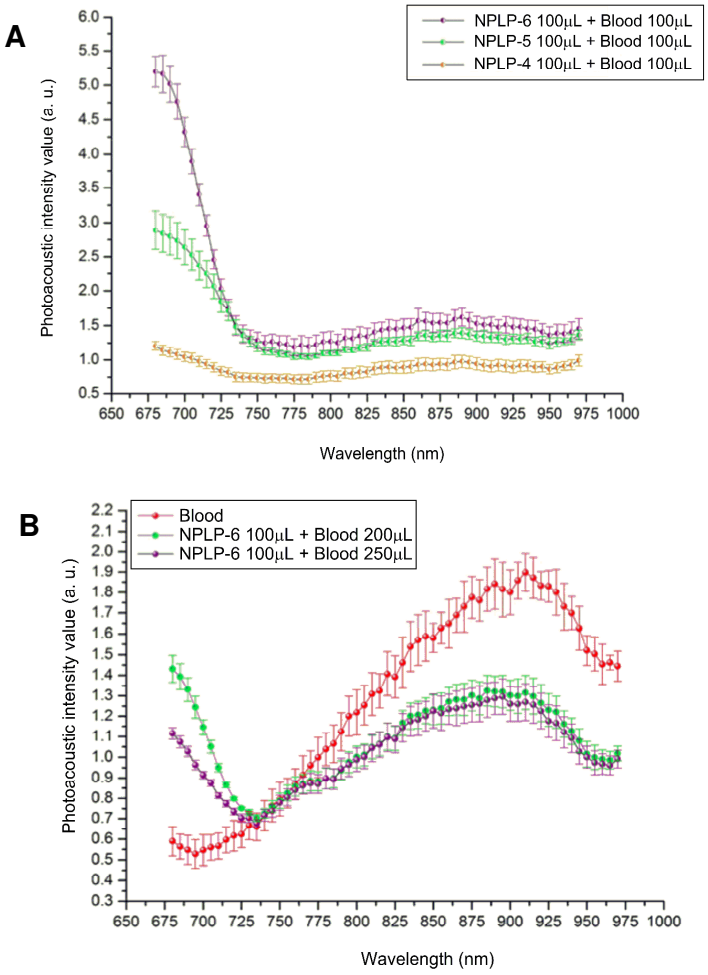


**Figure 5.10** *Optoacoustic spectrum of NPLP-4, -5, -6 samples after dilutions with blood. A) Final [m-NIR-SNPs] = 10µM. B) Final [NPLP-6] = 6.7µM and 5.7 µM.*

## 5.3 Conclusions

In this work, we have reported a synthetic strategy to develop silica-PEG core-shell nanostructures doped with two cyanine dyes displaying a tunable intensity profile across the NIR spectrum.

The synthetic approach shown in this chapter has enabled to synthesize SNPs suitable for *in vitro* optoacoustic imaging, as it permitted to increase the m-NIR-SNPs extinction coefficient value, resulting in a significant improvement of the photoacoustic intensity. Indeed, these SNPs showed a signal detectable by means of MSOT imaging, even when the samples were diluted with PBS and blood. These results represent an interesting starting point for the design of new platforms for optoacoustic imaging *in vivo* based on silica nanoparticles.

Furthermore, these results open the way for a possible use of these nanoparticles as sensitisers for phototherapeutic modalities for the treatment of solid tumours, such as the PhotoThermal Therapy (PTT).[51,52]

## 5.4 Notes and references


(1) Kaur, S.; Venktaraman, G.; Jain, M.; Senapati, S.; Garg, P. K.; Batra, S. K. *Cancer Letters* **2012**, *315*, 97.
(2) Giepmans, B. N. G.; Adams, S. R.; Ellisman, M. H.; Tsien, R. Y. *Science* **2006**, *312*, 217.
(3) Shu, X.; Royant, A.; Lin, M.; Aguilera, T.; Lev-Ram, V.; Steinbach, P.; Tsien, R. *Science* **2009**, *324*, 804.
(4) Weissleder, R.; Ntziachristos, V. *Nat Med* **2003**, *9*, 123.
(5) Müller, M. G.; Georgakoudi, I.; Zhang, Q.; Wu, J.; Feld, M. S. *Applied Optics* **2001**, *40*, 4633.
(6) Weissleder, R.; Pittet, M. *Nature* **2008**, *452*, 580.
(7) Rayavarapu, R.; Petersen, W.; Ungureanu, C.; Post, J.; van Leeuwen, T.; Manohar, S. *Int. J. Biomed. Imaging* **2007**, *2007*, 29817.
(8) De la Zerda, A.; Zavaleta, C.; Keren, S.; Vaithilingam, S.; Bodapati, S.; Liu, Z.; Levi, J.; Smith, B.; Ma, T.; Oralkan, O.; Cheng, Z.; Chen, X.; Dai, H.; Khuri-Yakub, B.; Gambhir, S. *Nat. Nanotechnol.* **2008**, *3*, 557.
(9) Eghtedari, M.; Oraevsky, A.; Copland, J.; Kotov, N.; Conjusteau, A.; Motamedi, M. *Nano Lett.* **2007**, *7*, 1914.
(10) Li, P.; Wang, C.; Shieh, D.; Wei, C.; Liao, C.; Poe, C.; Jhan, S.; Ding, A.; Wu, Y. *Opt. Express* **2008**, *16*, 18605.
(11) Webb, R. H. *Confocal Microscopy*, 1999; Vol. 307.
(12) Helmchen, F.; Denk, W. *Nat. Methods* **2005**, *2*, 932.
(13) Sharpe, J.; Ahlgren, U.; Perry, P.; Hill, B.; Ross, A.; Hecksher-Sorensen, J.; Baldock, R.; Davidson, D. *Science* **2002**, *296*, 541.
(14) Huisken, J.; Swoger, J.; Del Bene, F.; Wittbrodt, J.; Stelzer, E. H. K. *Science* **2004**, *305*, 1007.
(15) Ntziachristos, V.; Ripoll, J.; Wang, L. V.; Weissleder, R. *Nat. Biotechnol.* **2005**, *23*, 313.
(16) Ntziachristos, V.; Tung, C.; Bremer, C.; Weissleder, R. *Nat. Med.* **2002**, *8*, 757.
(17) Ntziachristos, V.; Razansky, D. *Chemical Reviews* **2010**, *110*, 2783.
(18) Hyde, D.; de Kleine, R.; MacLaurin, S. A.; Miller, E.; Brooks, D. H.; Krucker, T.; Ntziachristos, V. *Neuroimage* **2009**, *44*, 1304.
(19) Schulz, R. B.; Ale, A.; Sarantopoulos, A.; Freyer, M.; Soehngen, E.; Zientkowska, M.; Ntziachristos, V. *IEEE Trans. Med. Imaging* **2010**, *29*, 465.
(20) Davis, S. C.; Pogue, B. W.; Springett, R.; Leussler, C.; Mazurkewitz, P.; Tuttle, S. B.; Gibbs-Strauss, S. L.; Jiang, S. S.; Dehghani, H.; Paulsen, K. D. *Rev. Sci. Instrum.* **2008**, *79*, 10.
(21) Bell, A. G. *Am. J. Sci.* **1881**, *20*, 305.
(22) Bowen, T.; Nasoni, L.; Pifer, A. E.; Sembroski, G. H. *Proc. IEEE Ultrasonics Symp.* **1981**, *2*, 823.
(23) Oraevsky, A. A.; Jacques, S. L.; Esenaliev, R. O.; Tittel, F. K. *Proc. SPIE* **1994**, *2134A*, 122.
(24) Rosencwaig, A. *Science* **1973**, *181*, 657.
(25) Wang, X.; Pang, Y.; Ku, G.; Xie, X.; Stoica, G.; Wang, L. *Nat. Biotechnol.* **2003**, *21*, 803.
(26) Wang, L. V.; Ieee, J. *Sel. Top. Quantum Electron.* **2008**, *14*, 171.
(27) Wang, L. V. *Nat. Photonics* **2009**, *3*, 503.
(28) Razansky, D.; Vinegoni, C.; Ntziachristos, V. *Opt. Lett.* **2007**, *32*, 2891.
(29) Patterson, M. S.; Chance, B.; Wilson, B. C. *Appl. Opt.* **1989**, *28*, 2331.
(30) Wang, B.; Yantsen, E.; Larson, T.; Karpiouk, A.; Sethuraman, S.; Su, J.; Sokolov, K.; Emelianov, S. *Nano Lett.* **2009**, *9*, 2212.
(31) Chamberland, D. L.; Agarwal, A.; Kotov, N.; Fowlkes, J. B.; Carson, P. L.; Wang, X. *Nanotechnology* **2008**, *19*, 095101.
(32) Li, L.; Zemp, R.; Lungu, G.; Stoica, G.; Wang, L. *J. Biomed. Opt.* **2007**, *12*, 020504.
(33) Shashkov, E. V.; Everts, M.; Galanzha, E. I.; Zharov, V. P. *Nano Lett.* **2008**, *8*, 3953.
(34) Kim, S.; Lim, Y.; Soltesz, E.; De Grand, A.; Lee, J.; Nakayama, A.; Parker, J.; Mihaljevic, T.; Laurence, R.; Dor, D.; Cohn, L.; Bawendi, M.; Frangioni, J. *Nat. Biotechnol.* **2004**, *22*, 93.
(35) Li, M. L.; Oh, J. T.; X, X.; G, K.; Wang, W.; Li, C.; Lungu, G.; Stoica, G.; Wang, L. V. *Proc. IEEE* **2008**, *96*, 481.

(36) Razansky, D.; Distel, M.; Vinegoni, C.; Ma, R.; Perrimon, N.; Koster, R.; Ntziachristos, V. *Nat. Photonics* **2009**, *3*, 412.
(37) Bouchard, L.; Anwar, M.; Liu, G.; Hann, B.; Xie, Z.; Gray, J.; Wang, X.; Pines, A.; Chen, F. *Proc. Natl. Acad. Sci. U. S. A.* **2009**, *106*, 4085.
(38) Rampazzo, E.; Bonacchi, S.; Juris, R.; Montalti, M.; Genovese, D.; Zaccheroni, N.; Prodi, L.; Rambaldi, D. C.; Zattoni, A.; Reschiglian, P. *Journal of Physical Chemistry B* **2010**, *114*, 14605.
(39) Bonacchi, S.; Genovese, D.; Juris, R.; Montalti, M.; Prodi, L.; Rampazzo, E.; Zaccheroni, N. *Angewandte Chemie International Edition* **2011**, *50*, 4056.
(40) Genovese, D.; Bonacchi, S.; Juris, R.; Montalti, M.; Prodi, L.; Rampazzo, E.; Zaccheroni, N. *Angew. Chem.-Int. Edit.* **2013**, *52*, 5965.
(41) Genovese, D.; Rampazzo, E.; Bonacchi, S.; Montalti, M.; zaccheroni, N.; Prodi, L. *Nanoscale* **2013**, DOI: 10.1039/c3nr05599j.
(42) Genovese, D.; Montalti, M.; Prodi, L.; Rampazzo, E.; Zaccheroni, N.; Tosic, O.; Altenhoner, K.; May, F.; Mattay, J. *Chemical Communications* **2011**, *47*, 10975.
(43) Montalti, M.; Rampazzo, E.; Zaccheroni, N.; Prodi, L. *New Journal of Chemistry* **2013**, *37*, 28.
(44) Rampazzo, E.; Bonacchi, S.; Montalti, M.; Prodi, L.; Zaccheroni, N. *J. Am. Chem. Soc.* **2007**, *129*, 14251.
(45) Rampazzo, E.; Bonacchi, S.; Genovese, D.; Juris, R.; Montalti, M.; Paterlini, V.; Zaccheroni, N.; Dumas-Verdes, C.; Clavier, G.; Méallet-Renault, R.; Prodi, L. *The Journal of Physical Chemistry C* **2014**, *118*, 9261.
(46) Rampazzo, E.; Voltan, R.; Petrizza, L.; Zaccheroni, N.; Prodi, L.; Casciano, F.; Zauli, G.; Secchiero, P. *Nanoscale* **2013**, *5*, 7897.
(47) Biffi, S.; Petrizza, L.; Rampazzo, E.; Voltan, R.; Sgarzi, M.; Garrovo, C.; Prodi, L.; Andolfi, L.; Agnoletto, C.; Zauli, G.; Secchiero, P. *RSC Advances* **2014**, *4*, 18278.
(48) Montalti, M.; Prodi, L.; Zaccheroni, N.; Zattoni, A.; Reschiglian, P.; Falini, G. *Langmuir* **2004**, *20*, 2989.
(49) Montalti, M.; Prodi, L.; Rampazzo, E.; Zaccheroni, N. *Chemical Society Reviews* **2014**, DOI: 10.1039/c3cs60433k.
(50) Helle, M.; Rampazzo, E.; Monchanin, M.; Marchal, F.; Guillemin, F.; Bonacchi, S.; Salis, F.; Prodi, L.; Bezdetnaya, L. *ACS Nano* **2013**, *7*, 8645.
(51) Camerin, M.; Rello, S.; Villanueva, A.; Ping, X.; Kenney, M. E.; Rodgers, M. A. J.; Jori, G. *European Journal of Cancer* **2005**, *41*, 1203.
(52) Camerin, M.; Jori, G.; Della Ciana, L.; Fabbroni, S.; Bonacchi, S.; Montalti, M.; Prodi, L. *Photochemical & Photobiological Sciences* **2009**, *8*, 1422.

# Chapter 6

# Silica nanoparticles as fluorescent chemosensors

## 6.1 Introduction

In this study dye-doped silica-core/PEG-shell nanoparticles (DSNPs) were designed to develop a chemosensor for the sensing of the Glutathione and the Caspase-3 enzyme.

One of the most important topics in nanomedicine is represented by luminescent chemosensors, able to monitor *in vitro* and *in vivo* biologically relevant analytes. A luminescent chemosensor is the combination of different components: (i) a recognition site (receptor) able to recognize the analyte; (ii) a signaling unit (luminophore) apt to signal the binding event, and (iii), in most cases, a linker between the receptor and the luminophore (Figure 6.1).

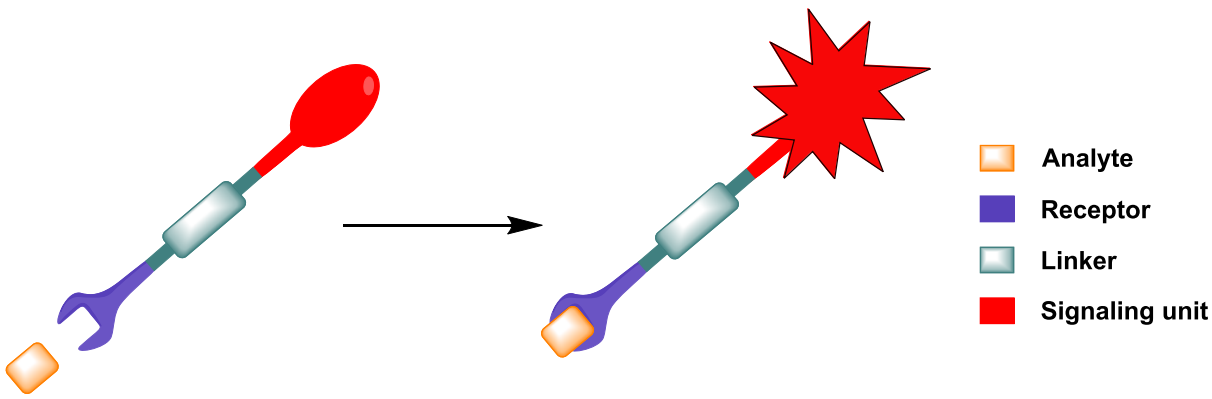


**Figure 6.1** *Schematic representation of a luminescent chemosensor.*

To investigate the functions and the possible alterations of target analytes in living systems, these probes can take advantage of the high sensitivity and spatio-temporal resolution provided by fluorescence techniques.[1-4] In addition to a high signal-to-noise ratio and selectivity, the ideal chemosensor should also avoid the perturbation of the cellular methabolism, descreasing, for instance, the concentration of analytes such as metal ions.[5]

Among the available nanostructures, that include Quantum Dots (QDs)[6-10] and gold nanoparticles,[11-15] DSNPs play a promising role,[16-18] circumventing several restrictions of conventional chemosensors.[2,19-25] One of the unique advantages that SNPs can offer in the field of sensing is signal amplification and to lower the detection limits using energy- and electron-transfer processes. Indeed, because of their collective nature, it is very challenging to obtain these functions following a supramolecular approach, with a

receptor-linker(s)-luminophore(s) structure.[1] In this context, the group of Prodi and co-workers developed SNPs doped with a chemosensor having the dansil-polyamine as fluorophore-receptor couple; this system was used to quench 13 fluorescent units upon the complexation of a single copper ion.[26] To amplify the quenching luminescence response to the presence of Cu (II) ions, Tonellato *et al.* proposed an alternative approach based on the assembly of fluorescent dyes and receptors on the SNPs surface; due to their proximity, the dye-receptor couple was able to allow intercomponent photoinduced processes, with the need of a direct covalent bond.[27,28]

The previous example revealed that the amplification of the luminescence signal is an important objective for SNPs-based chemosensors. An example was shown by using a 6-methoxy-8-p-toluensulfonamidequinoline (TSQ) derivative as a probe for Zn (II) ions:[29] short distances for homo- and hetero-energy transfer processes - that produced the amplified enhancement of the luminescence signal - were obtained by grafting the different components on the nanoparticles surface (Figure 6.2).[30]

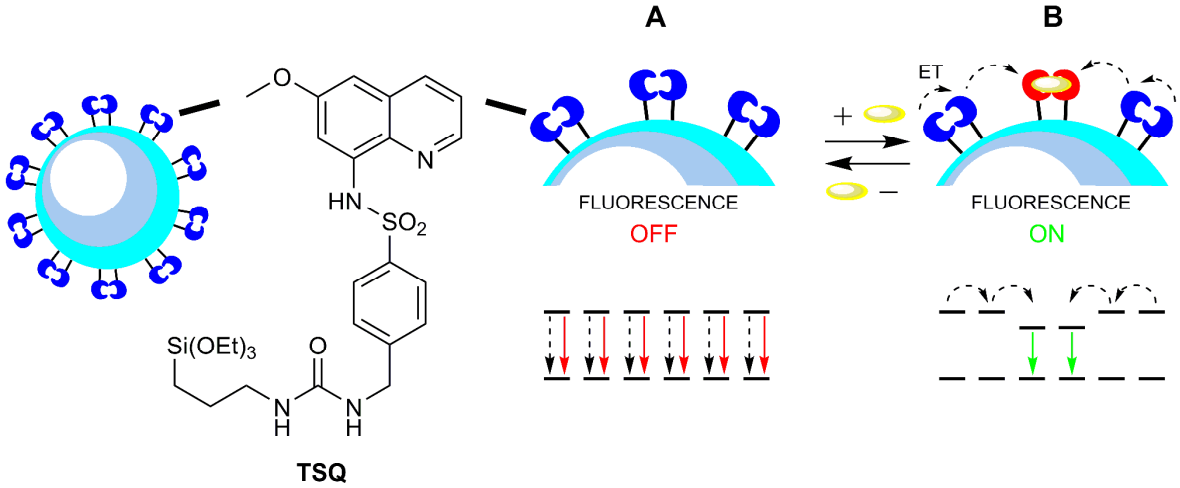


**Figure 6.2** *Schematization of functionalized SNPs and triethoxysilane TSQ derivative as in reference 29. A) In the absence of zinc ions, TSQ excited states deactivate mostly in a nonradiative way (black dashed arrows), because the radiative path (red arrows) is inefficient. B) At low zinc concentration, [$TSQ_2Zn$] complexes are formed and the fluorescence of the complexed units is switched on (green arrows): as a result of energy transfer processes (ET), the excitation energy absorbed is funneled towards the fluorescent excited states.*

More recently, our group proposed a new, very efficient strategy to monitor Cu(I) ions in biological samples, achieving both signal amplification and affinity increase.[31] A bodipy-based chemosensor[32] was added to a water solution of DSNPs doped with a coumarin derivative. The doping fluorescent units were chosen in order to have an efficient energy transfer process between the dyes inside the nanoparticles and the bodipy derivative when hosted by the nanostructutre. The chemosensor, due to its lipophilic nature, in fact, was

able to be hosted by the SNPs. The signal transduction mechanism of this nanosensor was based on the modulation of the energy transfer efficiency by the Cu(I) complexation (Figure 6.3). This system also showed additional benefits: (i) the increase in separation between the excitation and emission wavelengths, leading to the enhancement of the signal-to-noise ratio and (ii) the use of water insoluble chemosensors in aqueous media, which is a general advantage of using DSNPs in sensing. Indeed, this approach was later exploited also with various chemosensors for sensing Hg (II) ions in different milieu.[33,34]

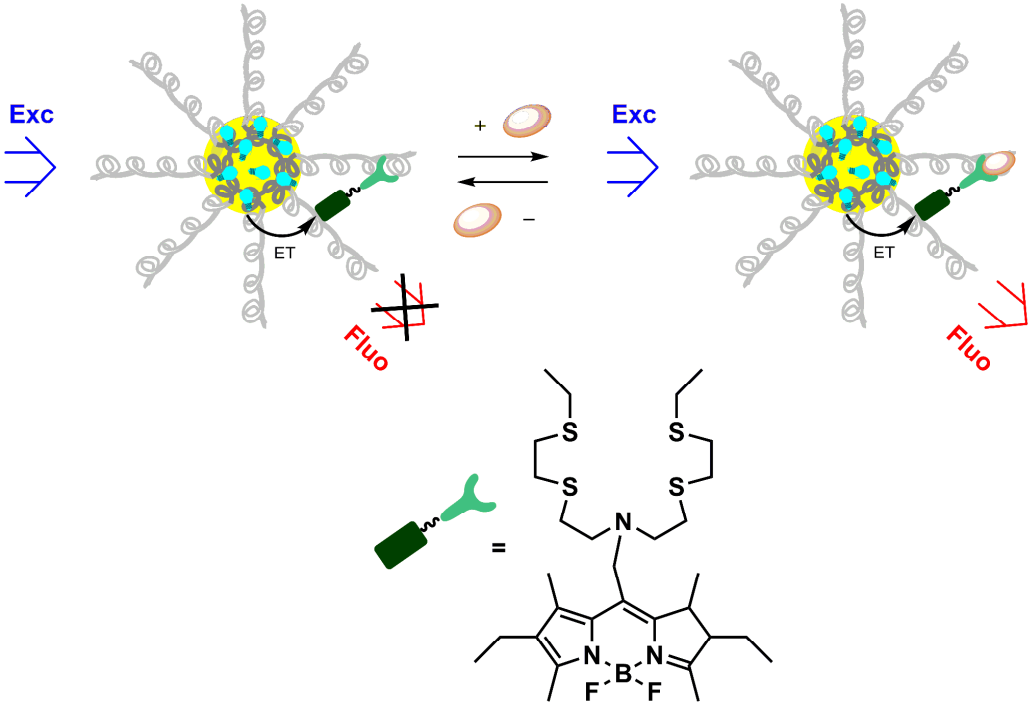


**Figure 6.3** *Schematization of the transduction mechanism in the sensing system for Cu(I) ions as in reference 31.*

The previous examples showed the two main advantages for sensing applications provided by DSNPs: versatility and multi-functionality. In this work, these features will be exploited for the design of a chemosensor for the Caspase-3 enzyme (Cas-3) and the Glutathione (GSH).

## 6.2 Results and discussion

### 6.2.1 Design of biosensor for Cas-3 based on DSNPs

Apoptosis - the programmed cell death - is a highly regulated process which occurs in multicellular organisms.[35-40] This essential physiological process has an astonishing role in the development of multicellular organisms, regulation of the immune system, and

clearance of abnormal cells. Shortcomings in cell death regulation may compromise homeostasis causing several diseases such as neurodegenerative disorders, cancer, autoimmune diseases, atherosclerosis and myocardial infarction. Consequently, monitoring apoptosis is crucial to the early identification of therapy efficiency and the assessment of disease progression.[41-45]

Caspases are a family of ubiquitously expressed cysteine proteases involved in the initiation and execution of apoptosis, which are present in cells as inactive zymogens. Pro-apoptotic signals activate initiator caspases, which cleave downstream effector caspases, causing a proteolytic cascade that leads to cell death.[46-53]

The activation of Caspase-3 (Cas-3) is essential for the neural cells apoptosis, since it is the key activator in the self-propagation of positive feedback cycle composed by other caspases in the apoptotic pathway. However, there is the need for sensors with high specificity to detect Cas-3 *in vitro* or *in vivo,* as its activation mechanism is not completely understood.[53-58]

As Cas-3 recognizes and cleaves with high specificity the N-terminus of the tetra-peptide sequence Asp-Glu-Val-Asp (DEVD), it is possible to use this sequence for Cas-3 detection. DEVD-containing peptides have been combined with nanomaterials such as quantum dots (QDs),[59,60] graphene oxide,[61] carbon nanotubes,[62] manganese oxide[63] and gold nanoparticles.[64,65] In this work NPs doped with a triethoxysilane derivative of Rhodamine B (RhodB-Si, Figure 6.5) were covalently linked to a DEVD-containing peptide (G-DEVD-Pra, Figure 6.4), which was functionalized with a nonfluorescent quencher (Black Hole Quencher, BHQ) derivative. This peptide was close enough to the DSNPs core to enable an energy transfer process between the rhodamines and the BHQ. After proteolitic cleavage, rhodamine dyes and quencher were separated, resulting in an increased fluorescent signal (Figure 6.5).

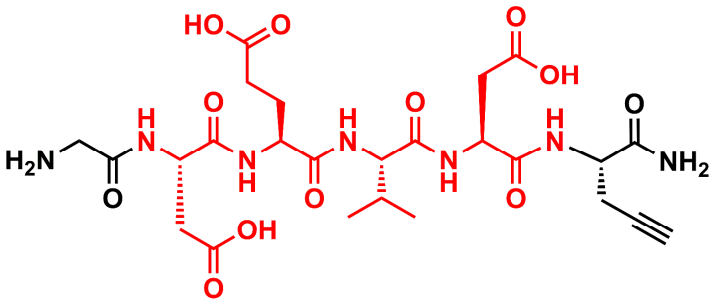


**Figure 6.4** *Molecular structure of G-DEVD-Pra (DEVD) peptide synthesized for the present work. Abbreviations were used for amino acids: G=glycine; D=aspartic acid; E=glutamic acid; Pra=propargyl glycine.*

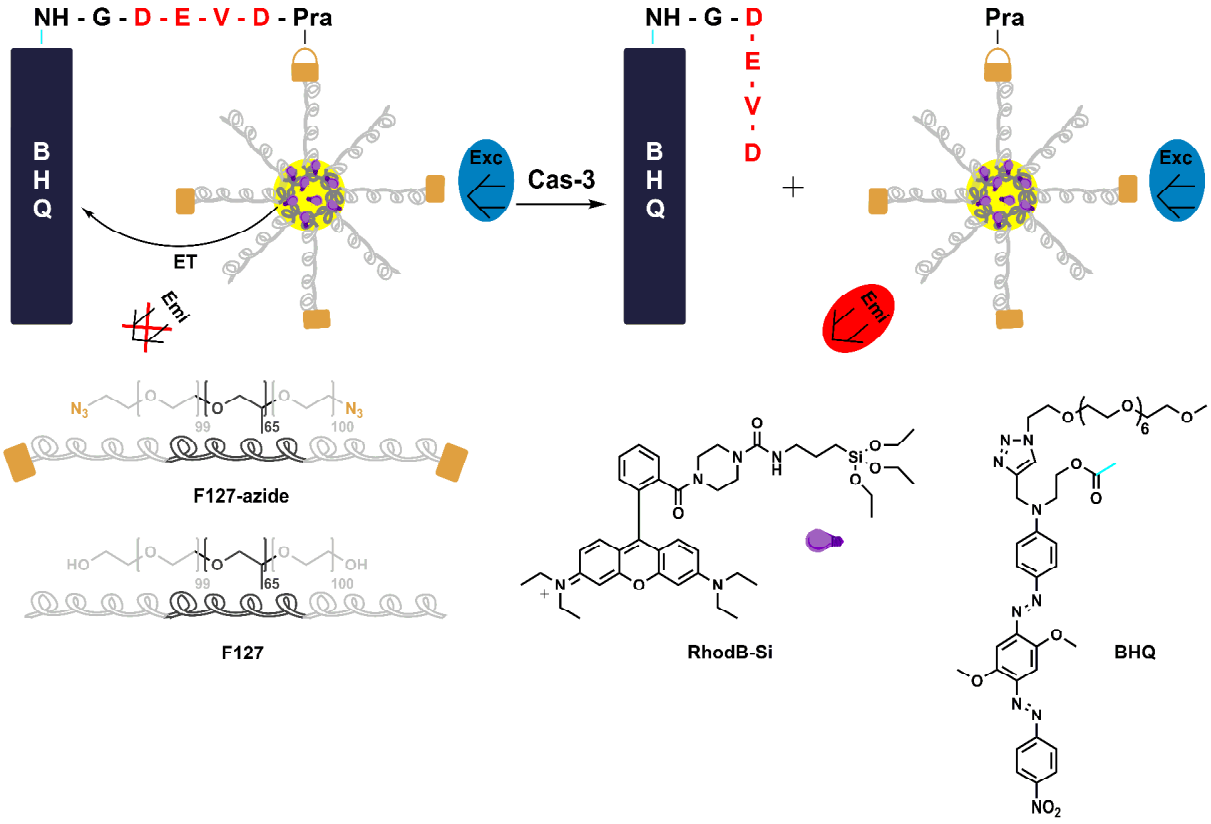


**Figure 6.5** *Schematization of the main components of the Cas-3 sensor based on DSNPs.*

### 6.2.2 Design of biosensor for GSH based on DSNPs

In this work we have also designed a sensor for the detection of the Glutathione (GSH) based on DSNPs.

GSH is a thiolated tripeptide that is the main redox buffering system of the cell (Figure 6.6). It is present at concentrations up to 10 mM in the cellular environment, with several functions, such as the regulation of intracellular redox activity, the protection of DNA and RNA from free radicals and the maintenance of xenobiotic metabolism and gene regulation.[66-68]

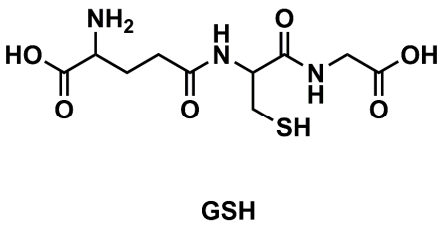


**Figure 6.6** *Molecular structure of Glutathione (GSH).*

Abnormal levels of GSH can cause serious diseases, including liver damage, Alzheimer's disease, autism, cancer and AIDS.[69] As a consequence, the development of luminescent biosensors for detection of GSH has special importance to understand its vital functions and has become a crucial topic of current chemical research,[70-73] involving nanomaterials such as carbon nanodots,[74] QDs,[69,75,76] upconversion nanoparticles (UCPs)[77] and manganese oxide,[78,79] gold[80] and silver nanoparticles.[81]

In the present study, we used a system very similar to the one previously described for Cas-3 detection to achieve the sensor for GSH; in this case the nucleophilic $GS^-$ was able to attack one of the two sulfur atoms of disulfide bond (S-S) which was positioned between the DSNP and the BHQ derivative, leading to the increase in the fluorescent signal (Figure 6.7).

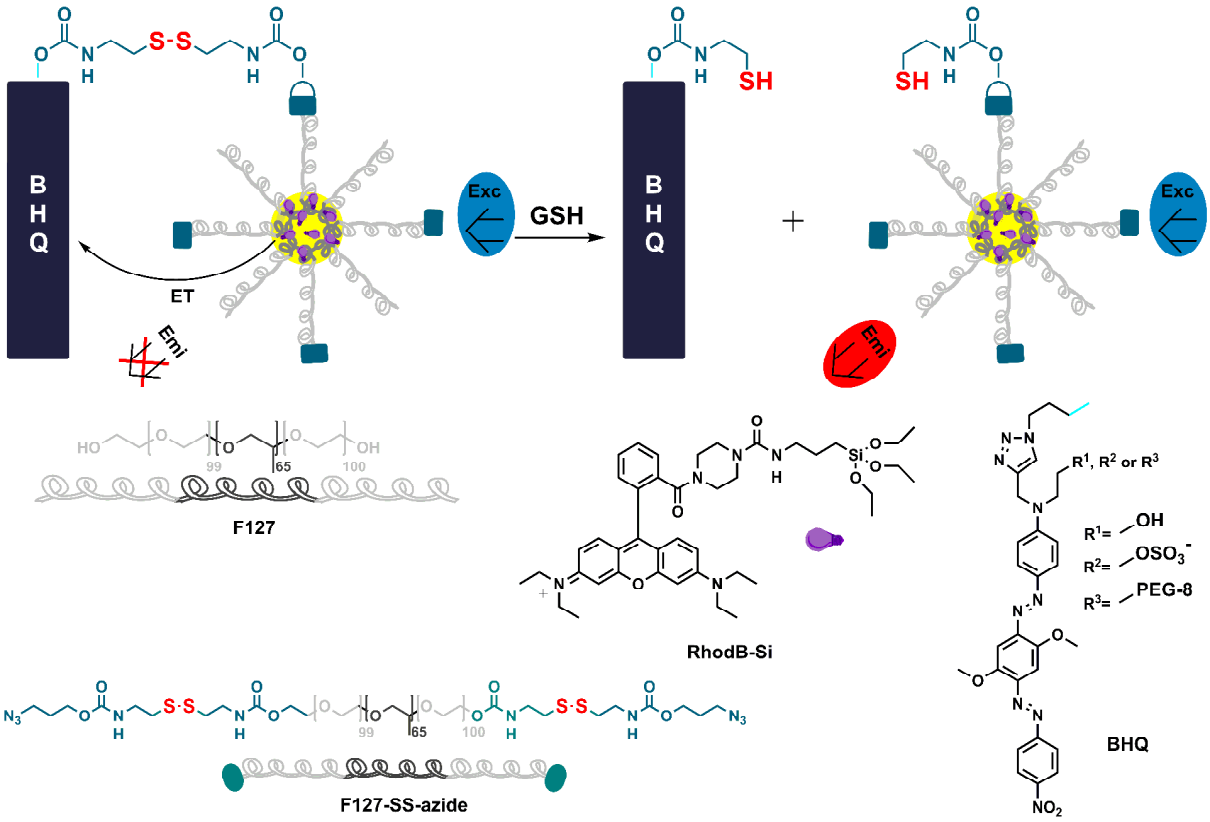


**Figure 6.7** *Schematization of the main components of the GSH sensor based on DSNPs.*

### 6.2.3 Synthesis of F127-BHQ derivatives

Non-fluorescent BHQ-2 quenchers are widely used to achieve FRET-based bioprobes,[82-86] as they exhibit a broad absorption spectrum which covers the blue-red - ca. 400-600 nm - part of the visible spectrum (according to the solvent and substitution pattern of the aniline).[87,88]

Four different BHQ-2 derivatives (Figure 6.8) were synthesized to carry out the quenching of the rhodamines loaded within the DSNPs (Fig. 6.5 and 6.7). Sulfonate (BHQ-sul), alcohol (BHQ-alc) and PEG (BHQ-PEG) moieties were used to decrease their lipophilic nature - due to the aromatic bis-diazo scaffold - and to increase their water solubility up to a concentration range compatible with bio-applications involving FRET probes (µm to mm).

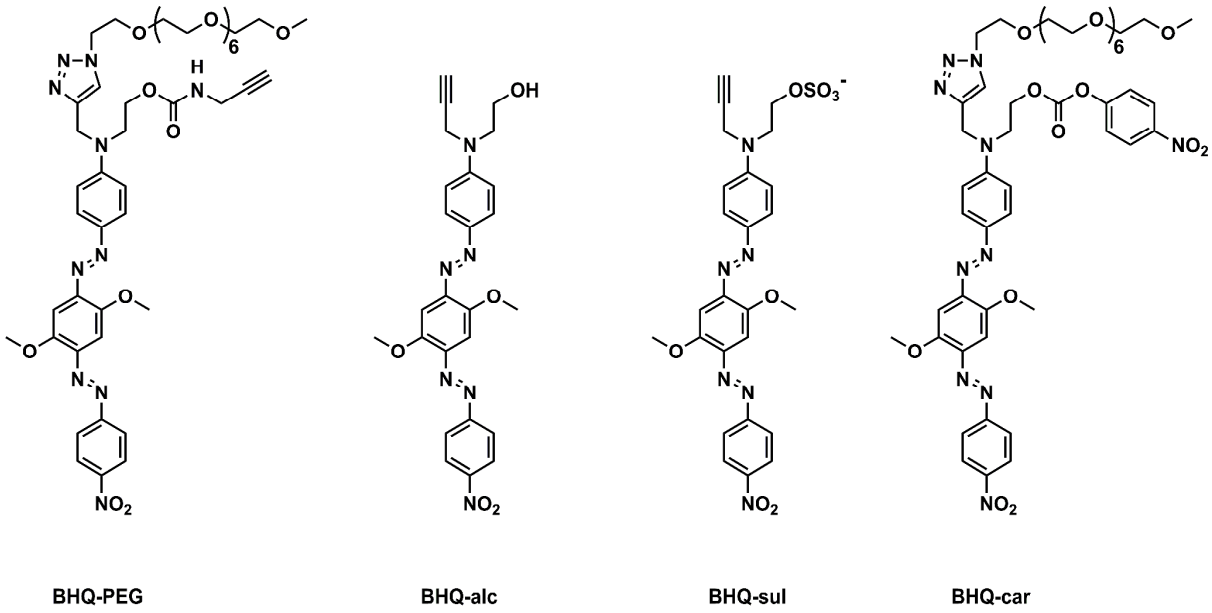


**Figure 6.8** *Molecular structure of BHQ-PEG, BHQ-alc, BHQ-sul and BHQ-car derivatives.*

As can be seen from Figure 6.8, BHQ-PEG, -alc and -sul derivatives were functionalized with an alkyne group to perform azide-alkyne cycloaddition reactions ("click" reactions)[89] with the "clickable" F127-SS-azide, allowing the covalent linking of quenchers to the surfactant Pluronic F127 (Figure 6.9). The resulting F127 derivatives (F127-SS-BHQ-PEG, -sul and –alc) were used to develop a sensing system for GSH based on SNPs.

The click approach has also been used for the reaction between the GDP-BHQ-PEG and the F127-azide derivative, leading to the BHQ-derivatized surfactant F127-D-BHQ-PEG which was involved in the synthesis of SNPs suitable for the detection of Cas-3 enzyme (Figure 6.10).

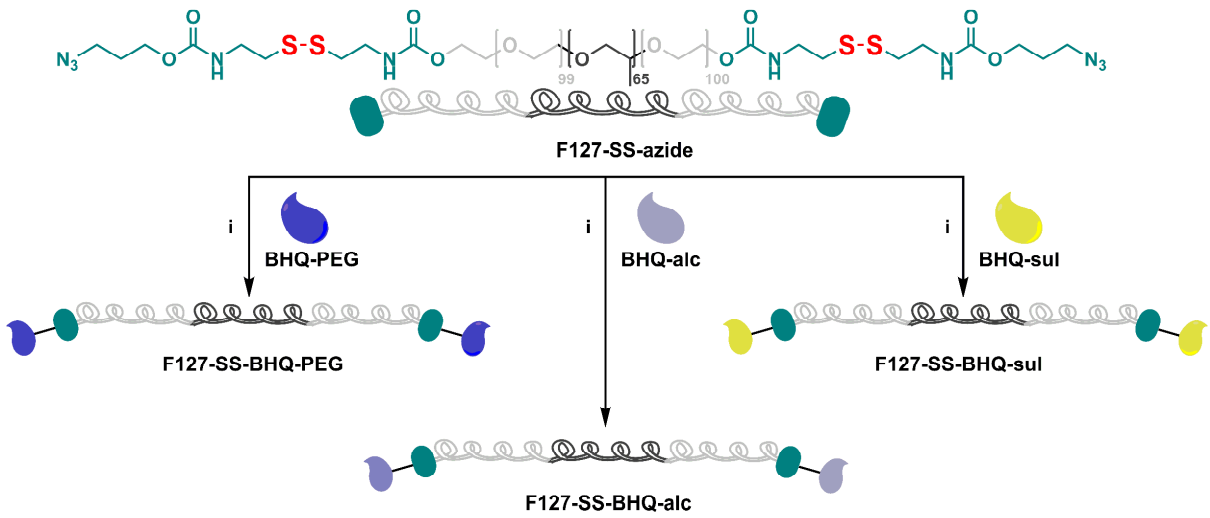


**Figure 6.9** *Schematization of the synthesis of F127-SS-BHQ-PEG, -alc and –sul derivatives. Reagents and conditions: i) Na ascorbate, Cu(II) sulfate pentahydrate, 1,4-Dioxane/$H_2O$, room temperature, 8 h.*

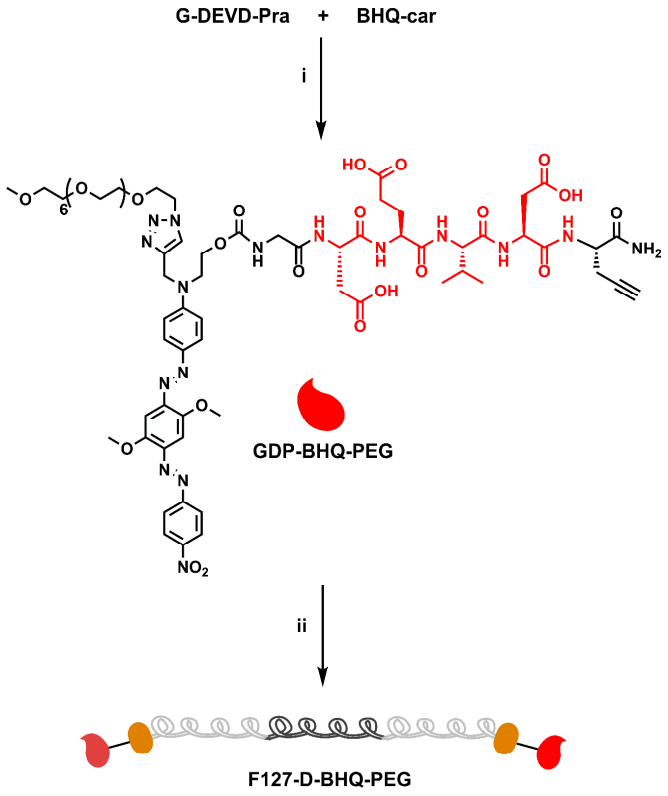


**Figure 6.10** *Schematization of the synthesis of F127-D-BHQ-PEG derivative. Reagents and conditions: i) DIPEA, DMF, room temperature, 16 h; ii) F127-azide, Na ascorbate, Cu(II) sulfate pentahydrate, DMF, room temperature, 8 h.*

### 6.2.4 Synthesis and characterization of SNPs

On the basis of a one pot synthetic approach that we have recently developed (Section 8.9),[90-92] we designed a family of SNPs by using suitably derivatized surfactant, F127-SS-BHQ-PEG, -sul, -alc (Figure 6.9) and F127-D-BHQ-PEG (Figure 6.10 and Table 6.1). In this way, the outer shells of the nanoparticles were decorated with SS-BHQ-PEG, alcohol, sulfonate and D-BHQ-PEG moieties yielding NPGP, NPGa, NPGs and NPDP, as schematically represented in Figure 6.11. Different SNPs preparatives were synthesized by using increasing amounts of derivatized surfactant (NP-16 and NP-32); furthermore, non-derivatized SNPs (NP-PEG, see Section 3.2.1) were prepared and used in the fluorescence experiments for comparison (Table 6.1). All SNPs were covalently doped with the triethoxysilane derivative of Rhodamine B (RhodB-Si, Fig 6.6, 6.7, 6.11 and Table 6.1).

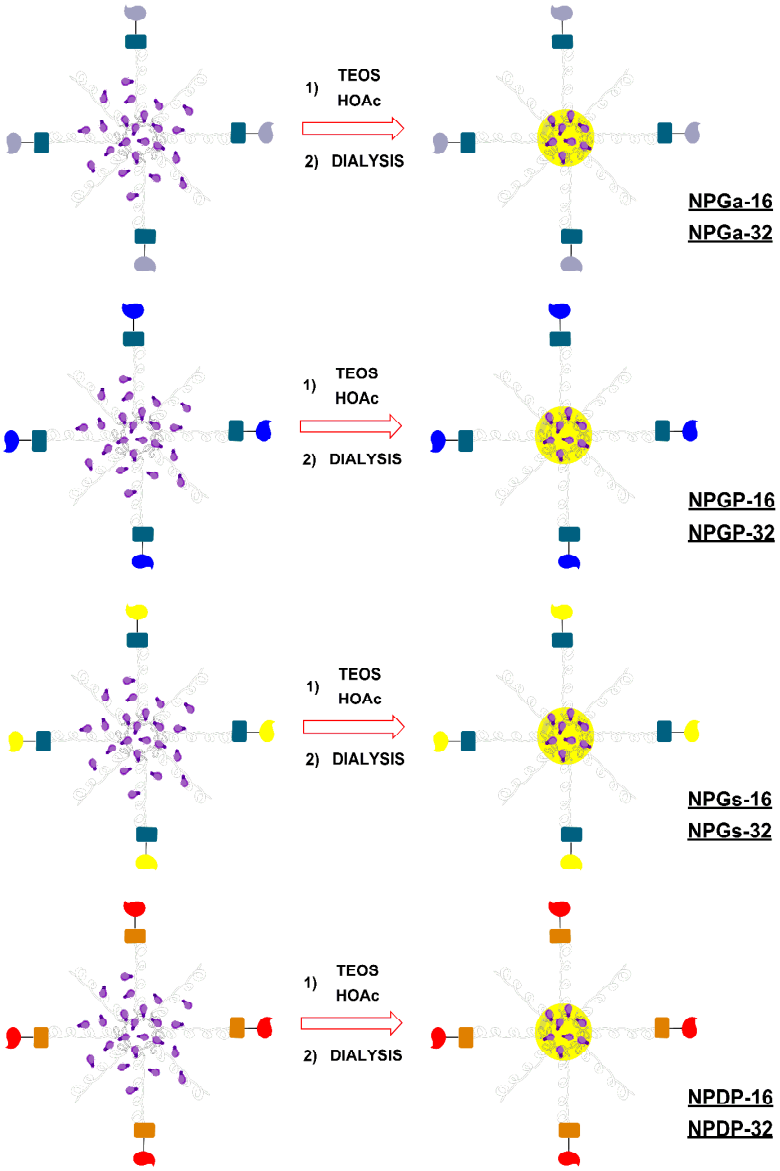

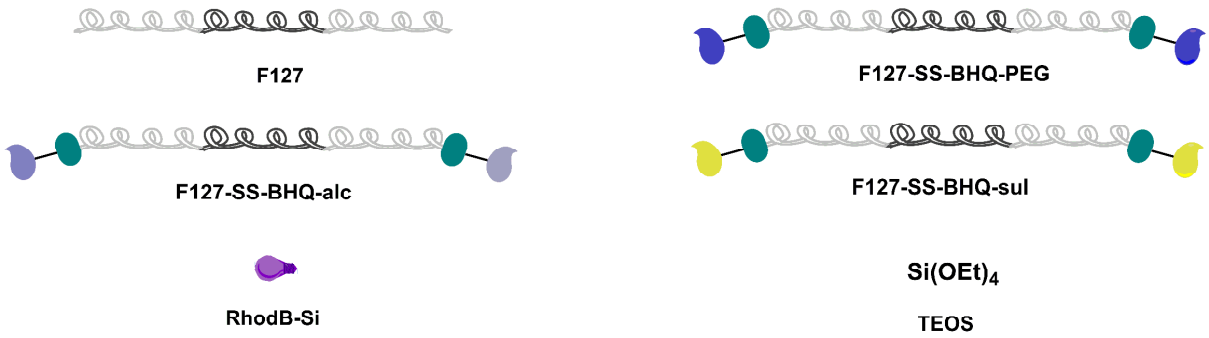


**Figure 6.11** *Schematic representation of the synthetic procedure and the main components of derivatized NPGa, NPGs, NPGP and NPDP.*

**Table 6.1** *Quantities of F127 surfactant and RhodB-Si used in SNPs preparations. RhodB-Si was introduced in the reaction mixtures using pristine methanol solutions.*

| NPs sample | F127 (mg) | Derivatized F127 | (mg) | RhodB-Si (mg) |
|---|---|---|---|---|
| *NP-PEG* | 100 | - | | 1.45 |
| *NPGP-16* | 84 | F127-SS-BHQ-PEG | 16 | 1.45 |
| *NPGP-32* | 68 | F127-SS-BHQ-PEG | 32 | 1.45 |
| *NPGs-16* | 84 | F127-SS-BHQ-sul | 16 | 1.45 |
| *NPGs-32* | 68 | F127-SS-BHQ-sul | 32 | 1.45 |
| *NPGa-16* | 84 | F127-SS-BHQ-alc | 16 | 1.45 |
| *NPGa-32* | 68 | F127-SS-BHQ-alc | 32 | 1.45 |
| *NPDP-16* | 84 | F127-D-BHQ-PEG | 16 | 1.45 |
| *NPDP-32* | 68 | F127-D-BHQ-PEG | 32 | 1.45 |

Morphological characterization by TEM images (Figure 6.12) showed that the silica core ($d_c$) was very similar for all samples, with values ranging from 10 to 12 nm. The hydrodynamic diameter ($d_H$) measured by dynamic light scattering (DLS) (Figure 6.13) was very similar for NP-PEG, NPGP-16, NPGP-32 and NPGs-16 ($d_H$ = 24, 26, 26 and 27 nm, respectively) with a very low polydispersity index (PdI = 0.02, 0.03, 0.06 and 0.09, respectively). Slight aggregation among particles was instead observed in the case of NPGa-16 and NPGa-32 ($d_H$ = 38 and 34 nm; PdI = 0.25 and 0.30, respectively) and for NPGs-32, NPDP-16 and NPDP-32 ($d_H$ = 65, 83 and 86 nm; PdI = 0.28, 0.49 and 0.23, respectively) , probably due to H-bonding interactions among the SNPs (Table 6.2).

**Table 6.2** *Mean silica core ($d_c$ ± SD) determined by TEM analysis and DLS hydrodynamic values ($d_H$ ± SD) for the SNPs described in this work. Standard deviation was calculated on five different measurements.*

| Sample | ($d_c$ ± SD) / nm | ($d_H$ ± SD) / nm | PdI |
|---|---|---|---|
| *NP-PEG* | 10 ± 1 | 24 ± 3 | 0.02 |
| *NPGP-16* | 11 ± 3 | 26 ± 4 | 0.03 |
| *NPGP-32* | 10 ± 2 | 26 ± 6 | 0.06 |
| *NPGs-16* | 11 ± 2 | 27 ± 8 | 0.09 |
| *NPGs-32* | 11 ± 2 | 65 ± 30 | 0.28 |
| *NPGa-16* | 12 ± 3 | 38 ± 20 | 0.25 |
| *NPGa-32* | 11 ± 2 | 34 ± 20 | 0.30 |
| *NPDP-16* | 12 ± 2 | 83 ± 60 | 0.49 |
| *NPDP-32* | 11 ± 3 | 86 ± 40 | 0.23 |

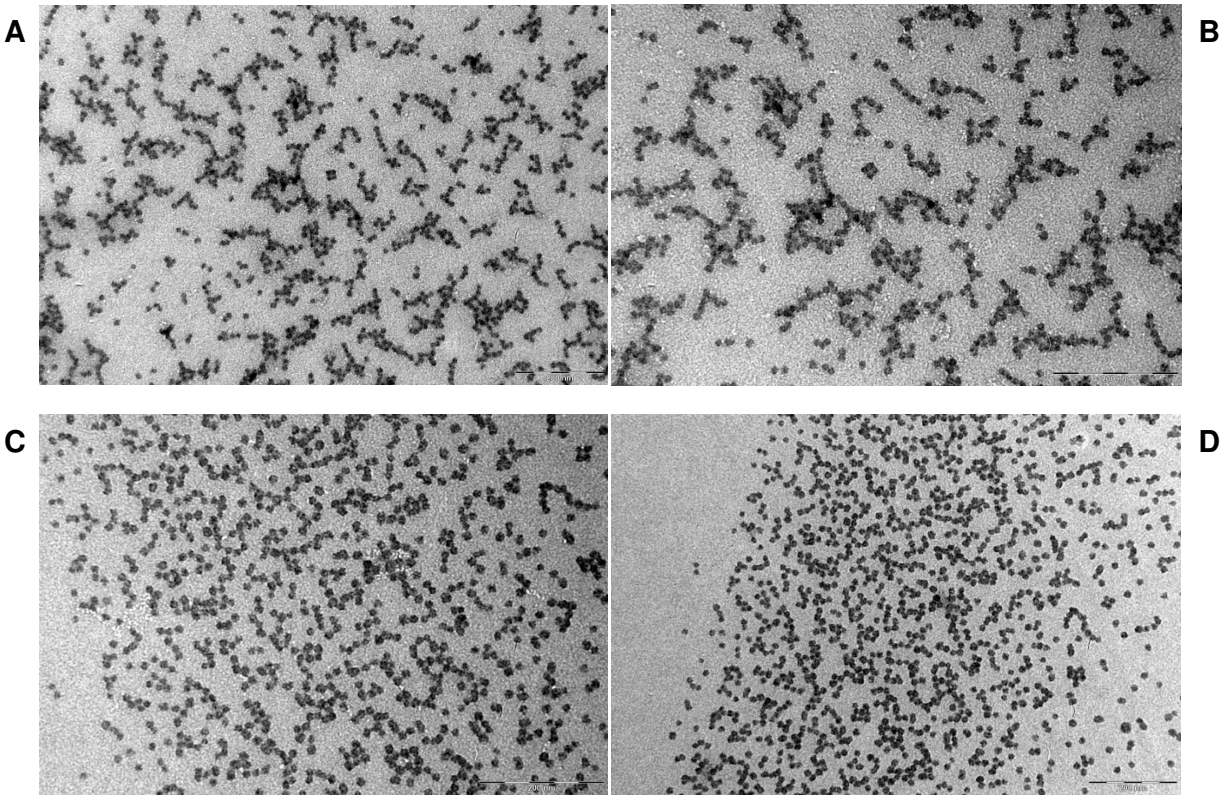


**Figure 6.12** *TEM images and silica core size distribution of: A) NPGP-16 ($d_c$ = 11 ± 3 nm); B) NPGs-32 ($d_c$ = 11 ± 2 nm); C) NPGa-16 ($d_c$ = 12 ± 3 nm); D) NPDP-32 ($d_c$ = 11 ± 3 nm). For clarity, only results of experiments done with NPGP-16, NPGs-32, NPGa-16 and NPDP-32 are shown.*

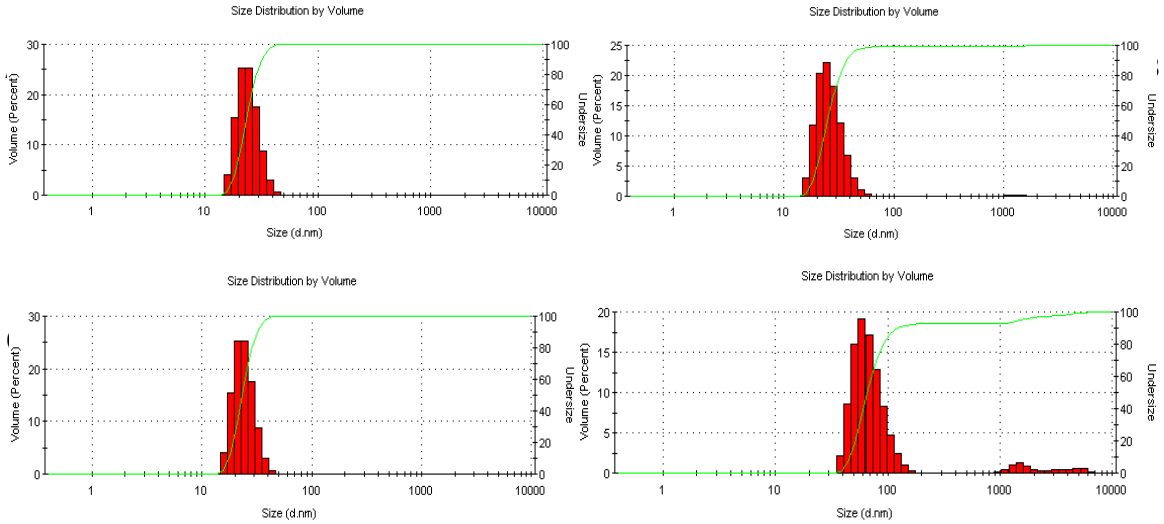


**Figure 6.13** *DLS diameter distribution by volume and undersize curve for: A) NPGP-16 ($d_H$ = 26 ± 4 nm); B) NPGs-32 ($d_H$ = 65 ± 30 nm); C) NPGa-16 ($d_H$ = 38 ± 20 nm); D) NPDP-32 ($d_H$ = 86 ± 40 nm). For clarity, only results of experiments done with NPGP-16, NPGs-32, NPGa-16 and NPDP-32 are shown.*

### 6.2.5 Evaluation of quenching efficiency

Fluorescence spectra were recorded to evaluate the decrease of emission intensity of NPGP, NPGs, NPGa and NPDP samples with respect to the unquenched NP-PEG. Interestingly, normalized integral emission intensities of SNPs-16 (Figure 6.14) revealed that BHQ-2 quenchers were efficient at quenching RhodB-Si with a general value of nearly 80% for NPG samples (NPGP-16 = 82%; NPGs-16 = 81%; NPGa-16 = 78%) and 66% for NPDP-16.

SNPs-32 provided an increase in quenching efficiency, with NPDP-32 exhibiting the best results - 90 % - with respect to the other nanoparticles (NPGP-32 = 87%; NPGs-32 = 89%; NPGa-32 = 84%, Table 6.3). Subsequently, NPGP-32, NPGs-32 and NPGa-32 were treated with Tris(2-CarboxyEthyl)Phosphine (TCEP), able to reduce organic disulfides to thiols in water.[93-95] Interestingly, the quenching effect due to BHQ was removed in about an hour, leading to a complete restoration of the NPs fluorescence (Figure 6.15).

FRET-based sensors are widely used in bioassay sensors.[96,97] Taken together, our quenching data - that indicated the increase in SNPs quenching efficiency up to 90% - represent a promising starting point for potential *in vitro* and *in vivo* detection of the Cas-3 and GSH.

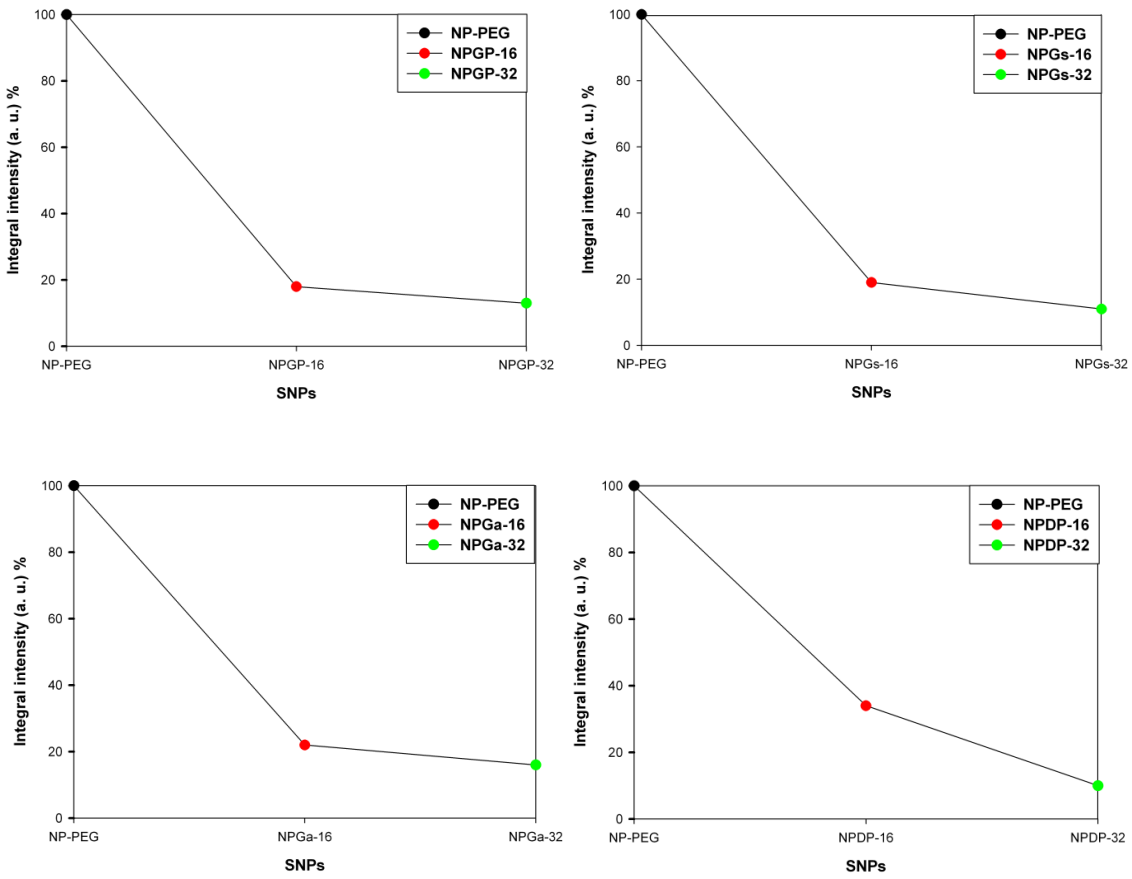


**Figure 6.14** *Decrease of emission intensity of derivatized NPGa, NPGs, NPGP and NPDP with respect to the unquenched NP-PEG. A) NPGP-16 and NPGP-32; B) NPGs-16 and NPGP-32; C) NPGa-16 and NPGa-32; D) NPDP-16 and NPDP-32.*

**Table 6.3** *Quenching efficiency % of derivatized NPGa, NPGs, NPGP and NPDP with respect to the unquenched NP-PEG (NP-PEG = 100%).* $\lambda_{ex}$ *= 530 nm. [SNPs] = 0.1 μM.*

| Sample | Quenching efficiency % |
|---|---|
| *NP-PEG* | - |
| *NPGP-16* | 82 |
| *NPGP-32* | 87 |
| *NPGs-16* | 81 |
| *NPGs-32* | 89 |
| *NPGa-16* | 78 |
| *NPGa-32* | 84 |
| *NPDP-16* | 66 |
| *NPDP-32* | 90 |

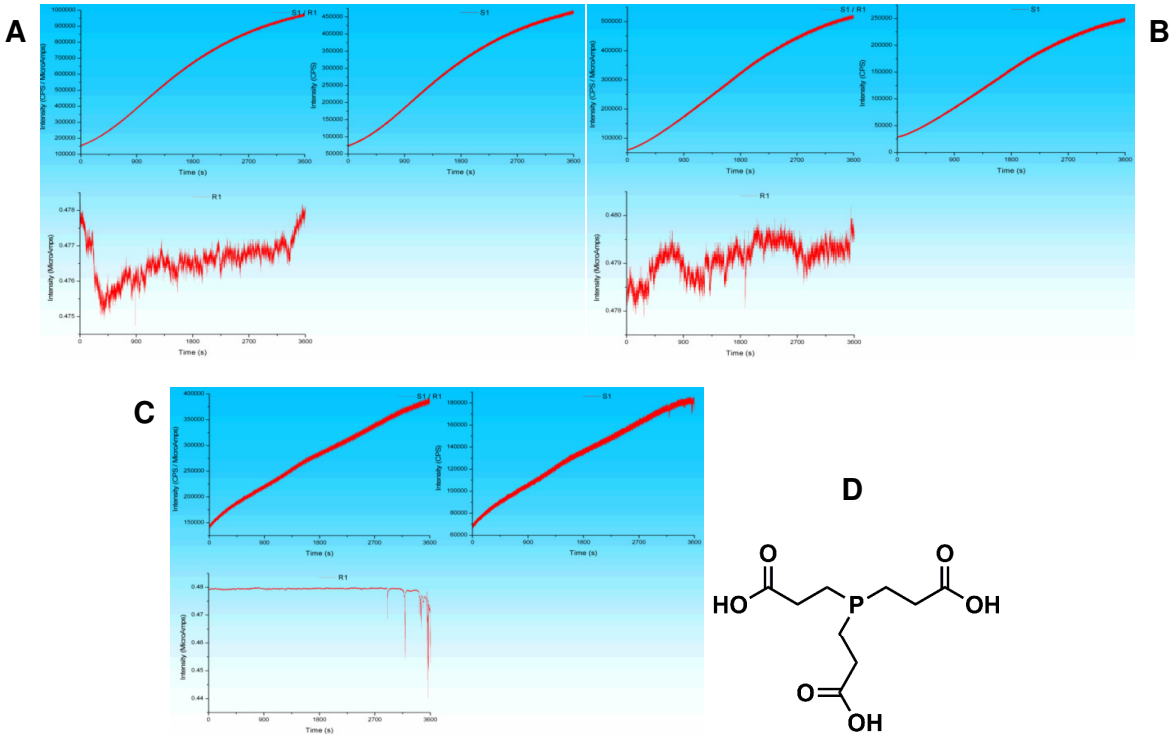


**Figure 6.15** Fluorescence recovery of (A) NPGa-32, (B) NPGs-32, (C) NPGP-32 in water after the addition of TCEP (D). [NPs] = 13 nM; [TCEP] = 14 mM.

## 6.3 Conclusions

In the present work we displayed a synthetic strategy based on the development of silica-core PEG-shell nanoparticles covalently doped with a triethoxysilane derivative of Rhodamine B. The resulting SNPs were highly bright and monodisperse, displaying high stability under physiological conditions.[91,98]

These SNPs were covalently linked to a DEVD-containing peptide that was functionalized with a nonfluorescent quencher (GPD-BHQ-PEG), to obtain FRET-based nanoplatforms suitable for the detection of Cas-3 (NPGP, NPGs and NPGa). By using a system similar to the one described for Cas-3 detection, it was possible to synthesize a sensor for the detection of GSH based on SNPs (NPDP). BHQ-2 quenchers were very efficient at quenching RhodB-Si, yielding quenching efficiency values up to 90%.

These results are very encouraging in view of the next steps planned for this study, namely (i) the analysis of photophysical parameters to determine the nature of the quenching and (ii) the *in vitro* and *in vivo* detection of the Cas-3 and GSH.

## 6.4 Notes and references

(1) Prodi, L. *New Journal of Chemistry* **2005**, *29*, 20.

(2) Bonacchi, S.; Genovese, D.; Juris, R.; Montalti, M.; Prodi, L.; Rampazzo, E.; Sgarzi, M.; Zaccheroni, N. *Topics in Current Chemistry* **2011**, *300*, 93.
(3) Que, E. L.; Domaille, D. W.; Chang, C. J. *Chemical Reviews* **2008**, *108*, 1517.
(4) Lodeiro, C.; Capelo, J. L.; Mejuto, J. C.; Oliveira, E.; Santos, H. M.; Pedras, B.; Nunez, C. *Chemical Society Reviews* **2010**, *39*, 2948.
(5) Qin, Y.; Miranda, J. G.; Stoddard, C. I.; Dean, K. M.; Galati, D. F.; Palmer, A. E. *ACS Chemical Biology* **2013**.
(6) Wu, P.; Yan, X.-P. *Chemical Society Reviews* **2013**, *42*, 5489.
(7) Lesnyak, V.; Gaponik, N.; Eychmuller, A. *Chemical Society Reviews* **2013**, *42*, 2905.
(8) Taylor, A.; Wilson, K. M.; Murray, P.; Fernig, D. G.; Levy, R. *Chemical Society Reviews* **2012**, *41*, 2707.
(9) Amelia, M.; Lincheneau, C.; Silvi, S.; Credi, A. *Chemical Society Reviews* **2012**, *41*, 5728.
(10) Wang, Y.; Hu, R.; Lin, G.; Roy, I.; Yong, K.-T. *ACS Applied Materials & Interfaces* **2013**, *5*, 2786.
(11) Dykman, L.; Khlebtsov, N. *Chemical Society Reviews* **2012**, *41*, 2256.
(12) Sperling, R. A.; Rivera Gil, P.; Zhang, F.; Zanella, M.; Parak, W. J. *Chemical Society Reviews* **2008**, *37*, 1896.
(13) Dreaden, E. C.; Alkilany, A. M.; Huang, X.; Murphy, C. J.; El-Sayed, M. A. *Chemical Society Reviews* **2012**, *41*, 2740.
(14) Das, M.; Shim, K.; An, S.; Yi, D. *Toxicol. Environ. Health Sci.* **2011**, *3*, 193.
(15) Giljohann, D. A.; Seferos, D. S.; Daniel, W. L.; Massich, M. D.; Patel, P. C.; Mirkin, C. A. *Angewandte Chemie International Edition* **2010**, *49*, 3280.
(16) Doussineau, T.; Schulz, A.; Lapresta-Fernandez, A.; Moro, A.; Korsten, S.; Trupp, S.; Mohr, G. J. *Chemistry- A European Journal* **2010**, *16*, 10290.
(17) Zhu, S.; Fisher, T.; Wan, W.; Descalzo, A. B.; Rurack, K. *Topics in Current Chemistry* **2011**, *300*, 51.
(18) Bau, L.; Tecilla, P.; Mancin, F. *Nanoscale* **2011**, *3*, 121.
(19) Bonacchi, S.; Genovese, D.; Juris, R.; Montalti, M.; Prodi, L.; Rampazzo, E.; Zaccheroni, N. *Angewandte Chemie International Edition* **2011**, *50*, 4056.
(20) Burns, A.; Ow, H.; Wiesner, U. *Chemical Society Reviews* **2006**, *35*, 1028.
(21) Wang, L.; Wang, K. M.; Santra, S.; Zhao, X. J.; Hilliard, L. R.; Smith, J. E.; Wu, J. R.; Tan, W. H. *Analytical Chemistry* **2006**, *78*, 646.
(22) Sokolova, V.; Epple, M. *Nanoscale* **2011**, *3*, 1957.
(23) Schulz, A.; McDonagh, C. *Soft Matter* **2012**, *8*, 2579.
(24) Schaferling, M. *Angewandte Chemie International Edition* **2012**, *51*, 3532.
(25) Jung, J. H.; Lee, J. H.; Shinkai, S. *Chemical Society Reviews* **2011**, *40*, 4464.
(26) Montalti, M.; Prodi, L.; Zaccheroni, N. *Journal of Materials Chemistry* **2005**, *15*, 2810.
(27) Rampazzo, E.; Brasola, E.; Marcuz, S.; Mancin, F.; Tecilla, P.; Tonellato, U. *Journal of Materials Chemistry* **2005**, *15*, 2687.
(28) Brasola, E.; Mancin, F.; Rampazzo, E.; Tecilla, P.; Tonellato, U. *Chemical Communications* **2003**, 3026.
(29) Bonacchi, S.; Rampazzo, E.; Montalti, M.; Prodi, L.; Zaccheroni, N.; Mancin, F.; Teolato, P. *Langmuir* **2008**, *24*, 8387.
(30) Teolato, P.; Rampazzo, E.; Arduini, M.; Mancin, F.; Tecilla, P.; Tonellato, U. *Chemistry – A European Journal* **2007**, *13*, 2238.
(31) Rampazzo, E.; Bonacchi, S.; Genovese, D.; Juris, R.; Sgarzi, M.; Montalti, M.; Prodi, L.; Zaccheroni, N.; Tomaselli, G.; Gentile, S.; Satriano, C.; Rizzarelli, E. *Chemistry – A European Journal* **2011**, *17*, 13429.
(32) Zeng, L.; Miller, E. W.; Pralle, A.; Isacoff, E. Y.; Chang, C. J. *Journal of the American Chemical Society* **2005**, *128*, 10.
(33) Oliveira, E.; Genovese, D.; Juris, R.; Zaccheroni, N.; Capelo, J. L.; Raposo, M. M. M.; Costa, S. P. G.; Prodi, L.; Lodeiro, C. *Inorganic Chemistry* **2011**, *50*, 8834.
(34) Bazzicalupi, C.; Caltagirone, C.; Cao, Z.; Chen, Q.; Di Natale, C.; Garau, A.; Lippolis, V.; Lvova, L.; Liu, H.; Lundström, I.; Mostallino, M. C.; Nieddu, M.; Paolesse, R.; Prodi, L.; Sgarzi, M.; Zaccheroni, N. *Chemistry – A European Journal* **2013**, *19*, 14639.
(35) Brindle, K. *Nat Rev Cancer* **2008**, *8*, 94.
(36) Blankenberg, F. G. *Journal of Nuclear Medicine* **2008**, *49*, 81S.
(37) Jiang, X.; Wang, X. *Annual Review of Biochemistry* **2004**, *73*, 87.
(38) Riedl, S. J.; Shi, Y. *Nat Rev Mol Cell Biol* **2004**, *5*, 897.
(39) Ye, D.; Shuhendler, A. J.; Cui, L.; Tong, L.; Tee, S. S.; Tikhomirov, G.; Felsher, D. W.; Rao, J. *Nat Chem* **2014**, *6*, 519.
(40) Favaloro, B.; Allocati, N.; Graziano, V.; Di Ilio, C.; De Laurenzi, V. *Aging (Albany NY)* **2012**, *4*, 330.
(41) Brunelle, J. K.; Zhang, B. *Drug Resistance Updates*, *13*, 172.

(42) Löser, R.; Abbenante, G.; Madala, P. K.; Halili, M.; Le, G. T.; Fairlie, D. P. *Journal of Medicinal Chemistry* **2010**, *53*, 2651.
(43) Irvine, G. B.; El-Agnaf, O. M.; Shankar, G. M.; Walsh, D. M. *Molecular Medicine* **2008**, *14*, 451.
(44) Jankovic, J. *Journal of Neurology, Neurosurgery & Psychiatry* **2008**, *79*, 368.
(45) Taylor, R. C.; Cullen, S. P.; Martin, S. J. *Nat Rev Mol Cell Biol* **2008**, *9*, 231.
(46) Martinez, M. M.; Reif, R. D.; Pappas, D. *Analytical Methods* **2010**, *2*, 996.
(47) Li, J.; Yuan, J. *Oncogene* **0000**, *27*, 6194.
(48) Zorn, J. A.; Wells, J. A. *Nat Chem Biol* **2010**, *6*, 179.
(49) Wolan, D. W.; Zorn, J. A.; Gray, D. C.; Wells, J. A. *Science* **2009**, *326*, 853.
(50) Lamkanfi, M.; Festjens, N.; Declercq, W.; Berghe, T. V.; Vandenabeele, P. *Cell Death Differ* **2006**, *14*, 44.
(51) Johnson, J. R.; Kocher, B.; Barnett, E. M.; Marasa, J.; Piwnica-Worms, D. *Bioconjugate Chemistry* **2012**, *23*, 1783.
(52) Nguyen, Q.-D.; Smith, G.; Glaser, M.; Perumal, M.; Årstad, E.; Aboagye, E. O. *Proceedings of the National Academy of Sciences* **2009**, *106*, 16375.
(53) Edgington, L. E.; Berger, A. B.; Blum, G.; Albrow, V. E.; Paulick, M. G.; Lineberry, N.; Bogyo, M. *Nat Med* **2009**, *15*, 967.
(54) Jun, Y.-w.; Sheikholeslami, S.; Hostetter, D. R.; Tajon, C.; Craik, C. S.; Alivisatos, A. P. *Proceedings of the National Academy of Sciences* **2009**, *106*, 17735.
(55) Mader, H. S.; Link, M.; Achatz, D. E.; Uhlmann, K.; Li, X.; Wolfbeis, O. S. *Chemistry- A European Journal* **2010**, *16*, 5416.
(56) Shekhawat, S. S.; Campbell, S. T.; Ghosh, I. *ChemBioChem* **2011**, *12*, 2353.
(57) Maxwell, D.; Chang, Q.; Zhang, X.; Barnett, E. M.; Piwnica-Worms, D. *Bioconjugate Chemistry* **2009**, *20*, 702.
(58) Callahan, B. P.; Stanger, M. J.; Belfort, M. *ChemBioChem* **2010**, *11*, 2259.
(59) Boeneman, K.; Mei, B. C.; Dennis, A. M.; Bao, G.; Deschamps, J. R.; Mattoussi, H.; Medintz, I. L. *J. Am. Chem. Soc.* **2009**, *131*, 3828.
(60) Prasuhn, D. E.; Feltz, A.; Blanco-Canosa, J. B.; Susumu, K.; Stewart, M. H.; Mei, B. C.; Yakovlev, A. V.; Loukou, C.; Mallet, J.-M.; Oheim, M.; Dawson, P. E.; Medintz, I. L. *ACS Nano* **2010**, *4*, 5487.
(61) Wang, H.; Zhang, Q.; Chu, X.; Chen, T.; Ge, J.; Yu, R. *Angewandte Chemie International Edition* **2011**, *50*, 7065.
(62) Zhang, J.-J.; Zheng, T.-T.; Cheng, F.-F.; Zhu, J.-J. *Chemical Communications* **2011**, *47*, 1178.
(63) Yu, C.; Zhou, Z.; Wang, J.; Sun, J.; Liu, W.; Sun, Y.; Kong, B.; Yang, H.; Yang, S. *Journal of Hazardous Materials* **2015**, *283*, 519.
(64) Pan, Y.; Guo, M.; Nie, Z.; Huang, Y.; Peng, Y.; Liu, A.; Qing, M.; Yao, S. *Chemical Communications* **2012**, *48*, 997.
(65) Chen, W.-H.; Luo, G.-F.; Xu, X.-D.; Jia, H.-Z.; Lei, Q.; Han, K.; Zhang, X.-Z. *Nanoscale* **2014**, *6*, 9531.
(66) Lu, S. C. *Molecular Aspects of Medicine* **2009**, *30*, 42.
(67) Chen, X.; Zhou, Y.; Peng, X.; Yoon, J. *Chemical Society Reviews* **2010**, *39*, 2120.
(68) Chakravarthi, S.; Jessop, C. E.; Bulleid, N. J. *EMBO Reports* **2006**, *7*, 271.
(69) Banerjee, S.; Kar, S.; Perez, J. M.; Santra, S. *J. Phys. Chem. C* **2009**, *113*, 9659.
(70) Meng, H.-M.; Jin, Z.; Lv, Y.; Yang, C.; Zhang, X.-B.; Tan, W.; Yu, R.-Q. *Analytical Chemistry* **2014**, *86*, 12321.
(71) Zheng, L.-Q.; Li, Y.; Yu, X.-D.; Xu, J.-J.; Chen, H.-Y. *Analytica Chimica Acta* **2014**, *850*, 71.
(72) Li, M.; Wu, X.; Wang, Y.; Li, Y.; Zhu, W.; James, T. D. *Chemical Communications* **2014**, *50*, 1751.
(73) Niu, L.-Y.; Guan, Y.-S.; Chen, Y.-Z.; Wu, L.-Z.; Tung, C.-H.; Yang, Q.-Z. *Chemical Communications* **2013**, *49*, 1294.
(74) Mandani, S.; Sharma, B.; Dey, D.; Sarma, T. K. *Nanoscale* **2015**, *7*, 1802.
(75) Liu, J.; Bao, C.; Zhong, X.; Zhao, C.; Zhu, L. *Chem. Commun.* **2010**, *46*, 2971.
(76) Zhang, Y.; Li, Y.; Yan, X. P. *Anal. Chem.* **2009**, *81*, 5001.
(77) Deng, R.; Xie, X.; Vendrell, M.; Chang, Y. T.; Liu, X. *J. Am. Chem. Soc.* **2011**, *133*, 20168.
(78) He, D.; He, X.; Wang, K.; Yang, X.; Yang, X.; Zou, Z.; Li, X. *Chemical Communications* **2015**, *51*, 776.
(79) Li, N.; Diao, W.; Han, Y.; Pan, W.; Zhang, T.; Tang, B. *Chemistry – A European Journal* **2014**, *20*, 16488.
(80) Shi, Y.; Pan, Y.; Zhang, H.; Zhang, Z.; Li, M.-J.; Yi, C.; Yang, M. *Biosensors and Bioelectronics* **2014**, *56*, 39.
(81) Ouyang, L.; Zhu, L.; Jiang, J.; Tang, H. *Analytica Chimica Acta* **2014**, *816*, 41.
(82) Li, H.; Wang, M.; Wang, C.; Li, W.; Qiang, W.; Xu, D. *Analytical Chemistry* **2013**, *85*, 4492.
(83) Ma, J.; Chen, Y.; Hou, Z.; Jiang, W.; Wang, L. *Biosensors and Bioelectronics* **2013**, *43*, 84.

(84) Xiang, D.-S.; Zhou, G.-H.; Luo, M.; Ji, X.-H.; He, Z.-K. *Analyst* **2012**, *137*, 3787.
(85) Taniguchi, Y.; Koga, Y.; Fukabori, K.; Kawaguchi, R.; Sasaki, S. *Bioorganic & Medicinal Chemistry Letters* **2012**, *22*, 543.
(86) Chen, J.; Tsai, A.; Petrov, A.; Puglisi, J. D. *Journal of the American Chemical Society* **2012**, *134*, 5734.
(87) Crisalli, P.; Hernández, A. R.; Kool, E. T. *Bioconjugate Chemistry* **2012**, *23*, 1969.
(88) Chevalier, A.; Renard, P.-Y.; Romieu, A. *Tetrahedron Letters* **2014**, *55*, 6764.
(89) Kolb, H. C.; Finn, M. G.; Sharpless, K. B. *Angewandte Chemie International Edition* **2001**, *40*, 2004.
(90) Soster, M.; Juris, R.; Bonacchi, S.; Genovese, D.; Montalti, M.; Rampazzo, E.; Zaccheroni, N.; Garagnani, P.; Bussolino, F.; Prodi, L.; Marchio, S. *International Journal of Nanomedicine* **2012**, *7*, 4797.
(91) Rampazzo, E.; Voltan, R.; Petrizza, L.; Zaccheroni, N.; Prodi, L.; Casciano, F.; Zauli, G.; Secchiero, P. *Nanoscale* **2013**, *5*, 7897.
(92) Biffi, S.; Petrizza, L.; Rampazzo, E.; Voltan, R.; Sgarzi, M.; Garrovo, C.; Prodi, L.; Andolfi, L.; Agnoletto, C.; Zauli, G.; Secchiero, P. *RSC Advances* **2014**, *4*, 18278.
(93) Burns, J. A.; Butler, J. C.; Moran, J.; Whitesides, G. M. *The Journal of Organic Chemistry* **1991**, *56*, 2648.
(94) Lai, Y.-J.; Tseng, W.-L. *Talanta* **2012**, *91*, 103.
(95) Wang, K.; Peng, H.; Wang, B. *Journal of Cellular Biochemistry* **2014**, *115*, 1007.
(96) Carrasquilla, C.; Li, Y.; Brennan, J. D. *Analytical Chemistry* **2011**, *83*, 957.
(97) Tuleuova, N.; Jones, C. N.; Yan, J.; Ramanculov, E.; Yokobayashi, Y.; Revzin, A. *Analytical Chemistry* **2010**, *82*, 1851.
(98) Montalti, M.; Prodi, L.; Rampazzo, E.; Zaccheroni, N. *Chemical Society Reviews* **2014**, *43*, 4243.

# Chapter 7

# Silica nanoparticles for drug delivery

## 7.1 Introduction

In this study luminescent silica-core/PEG-shell nanoparticles (DSNps) were designed to assess their potential application in drug delivery.

Nanotechnology is a discipline in rapid and continuous evolution, as it seeks to offer solutions to current social, environmental and health problems. In this regard, one of its most important applications is to develop multifunctional platforms suitable for cancer treatment, within a broader context concerning theranostics, i.e., the simultaneous diagnosis and therapy.

Particularly, we believe that DSNPs offers very appealing solutions in this field for several reasons. Firstly, luminescence measurements are very sensitive (down to single molecule detection), easily performed, and versatile, offering submicron spatial resolution and sub millisecond temporal resolution.[1] This enables, in general, low detection limits (and thus, early diagnosis), and could permit the tracking of biological events to reveal the origin and growth of different pathologies, including cancer. Secondly, compared to magnetic resonance imaging (MRI), optical imaging is much easier to use and more cost-effective, and can be applied to cancer diagnosis with high resolution.[2] This could lead to direct visualization of tumour tissues in real-time during the surgical process, providing direct guidance to surgeons for effective and complete tumour resection.[3] Finally, since optical fibres are currently used in the investigation of some tumours (such as colorectal cancer), near infrared (NIR) imaging can be quickly and easily introduced into clinical practice.[4]

There are many different nanocolloids that could offer a valuable alternative to SNPs, such as dye-doped latex nanoparticles[5-7] or intrinsically luminescent nanomaterials, such as the so-called quantum dots (QDs).[3,8,9] However, in our opinion, silica is the only one capable of offering all the required features for effective diagnostic and theranostic applications.[3,8,10-16] Silica is intrinsically not toxic, although more in-depth investigations are under way to completely rule out possible hazards related to the tiny dimensions of nanoparticles. Preliminary experiments point in favour of their benign nature, even supporting their use for in vivo imaging and therapy.[3,4,8,11] Silica nanoparticles constitute a robust domain also under different external stimuli, providing increased mechanical strength and chemical stability to the loaded species, as well as protection against enzymatic degradation, an enhanced resistance to photobleaching and an almost constant chemical environment.[17,18] Since silica is photophysically inert, it is transparent to visible light and is not involved in energy- and electron-transfer processes that may quench the luminescence of the dyes linked to the matrix. In addition, each silica nanoparticle can contain many active species, which can induce collective effects to increase the brightness and the signal-to-noise ratio. Moreover, the great versatility offered by the different synthetic strategies, typically

requiring inexpensive reagents and mild conditions, is an extremely valuable characteristic since it opens up the possibility to adapt these materials for a large number of applications.[4,11]

While some nanomedicine-based drug/dye delivery systems have already been marketed and others are in clinical trials, most remain in the stage of preclinical development. Mesoporous silica nanoparticles have been highlighted as an interesting drug delivery platform, due to their flexibility and high drug load potential, and have therefore been extensively investigated as delivery systems. In spite of considerable interest in the biomedical applications of such nanoparticles, the knowledge of their *in vivo* biocompatibility, toxicity and bio-distribution remains limited, which has delayed the onset of human clinical trials.

Within this context, in the present study we have evaluated the possible application of dye-doped silica-core/PEG-shell nanoparticles (DSNPs) as drug delivery systems, by using Dasa-10 (Dasa), i.e., an anticancer drug that belongs to the family of substituted N,N'-diarylsulfonamides (Figure 7.1).[19] The synthesis of such a drug, as well as that of the DSNPs, will be analyzed in the next section.

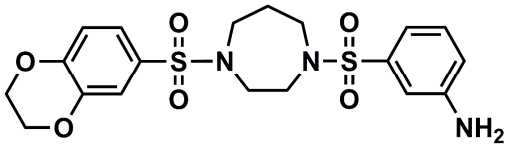


**Figure 7.1** *Molecular structure of Dasa.*

## 7.2 Results and discussion

### 7.2.1 Dasa: synthesis and preliminary study of loading

Dasa is a promising anticancer agent because it is a pharmacological activator[20-23] of the tumor cell specific pyruvate kinase isozyme that is known as PKM2.[19,24-27] To understand the importance of this activator, it is necessary to analyze the differences in metabolic requirements of differentiated and proliferative tissues (Figure 7.2).

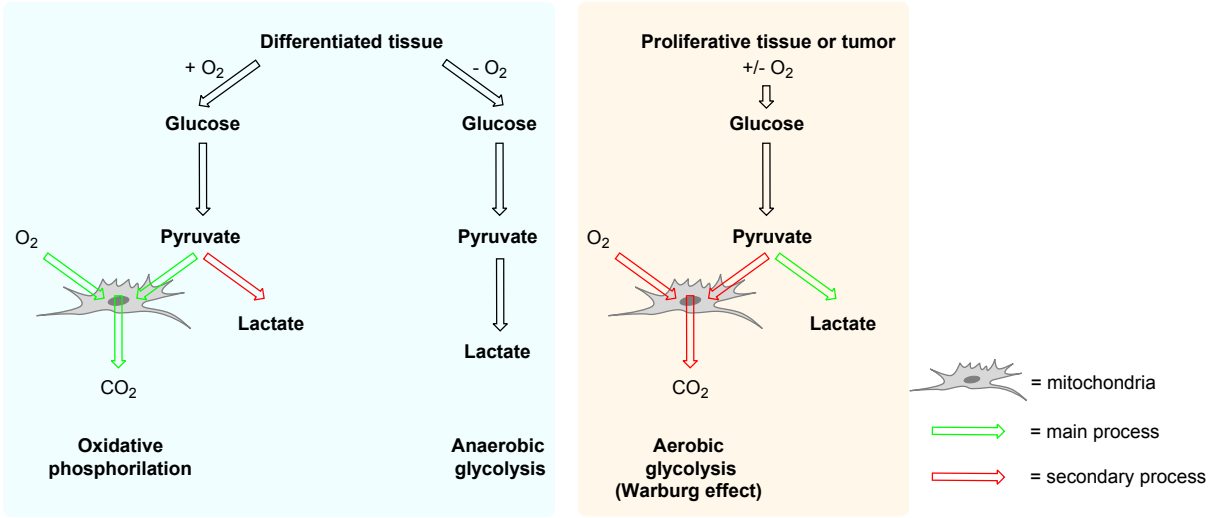


**Figure 7.2** Schematic representation of the differences between oxidative phosphorylation, anaerobic glycolysis, and aerobic glycolysis (Warburg effect).

In the presence of oxygen, differentiated tissues first metabolize glucose to pyruvate via glycolysis and then completely oxidize most of that pyruvate in the mitochondria to $CO_2$ during the process of oxidative phosphorylation. Oxygen is essential for this process because it is required as the final electron acceptor to completely oxidize the glucose. When oxygen is limiting, cells can redirect the pyruvate generated by glycolysis away from mitochondrial oxidative phosphorylation by generating lactate in a process called anaerobic glycolysis. This generation of lactate during anaerobic glycolysis allows glycolysis to continue. Warburg observed that cancer cells - and normal proliferative tissues - have increased rates of lactate production even in the presence of oxygen (aerobic glycolysis).[28-32] This altered metabolism is thought to give tumor cells a selective growth advantage compared to normal cells.

PKM2 is usually inactive in tumor cells. Substituted N,N'-diarylsulfonamides, such as Dasa, are pharmacological activators of PKM2, directing glucose towards oxidative metabolism; in this way it is possible to alter the Warburg effect, yielding a therapeutic potential in the treatment of cancer and other metabolic diseases.[19]

Dasa was synthesized by using a strategy based on an efficient sequence of coupling reaction, deprotection, and a second coupling reaction as detailed in Figure 7.3.[19]

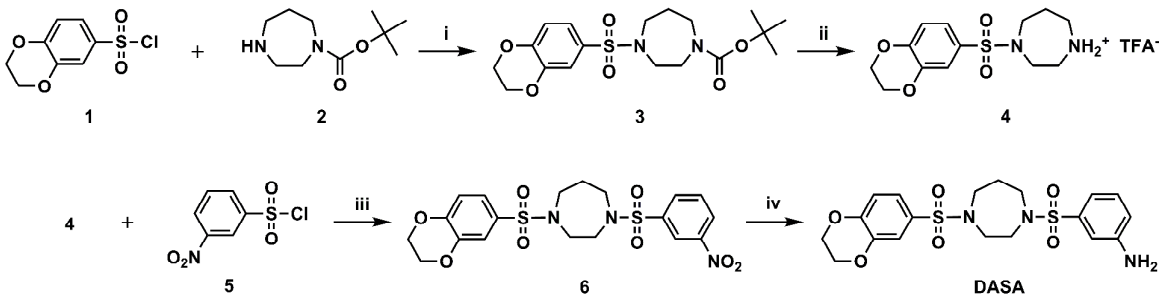

**Figure 7.3** *Schematization of the synthesis of Dasa. Reagents and conditions: i) and iii) TEA, DCM, 0°C, 1 h; ii) TFA, DCM, 0°C, 1 h; iv) $SnCl_2{\cdot}2H_2O$, EtOH, 70°C, 50 min.*

In particular, the monoboc protected diazepine (2) was coupled to aryl sulfonyl chloride (1) to provide the corresponding boc-protected N-arylsulfonamide (3). These intermediate was deprotected and subsequently coupled to the second aryl sulfonyl chloride (5) to provide the N,N'-diarylsulfonamide derivative (6) that was reduced to yield Dasa (for more details see Section 8.3).

On the basis of a one-pot synthetic approach that our group recently developed,[33-35] we designed SNPs covalently doped with the triethoxysilane derivative of Rhodamine B (RhodB-Si), which allows visualization by both fluorescence microscopy and flow-cytometry.[36] Multifunctional NPs were realized by adding Dasa in the same synthetic step, to be confined - due to its lipophilic nature - within the apolar silica core of NPs; indeed, in view of a potential application of the above-mentioned nanoparticles in the field of drug delivery, it was necessary that Dasa was simply physically entrapped in the SNP structure. The non-covalent entrapment of the drug, however, increases the likelihood of leaching from the particle; for this reason, a high Dasa : NP doping ratio (50 : 1) was chosen for a preliminary study, yielding NPT-1-D50. (Table 7.1 and Figure 7.4).

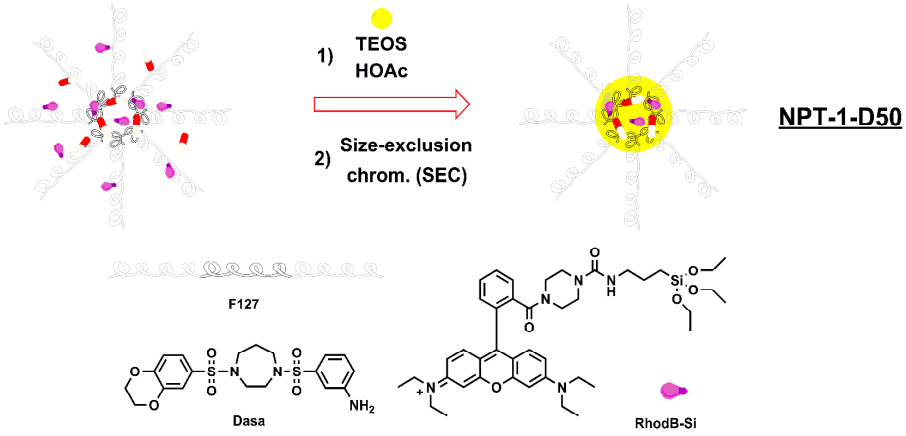


**Figure 7.4** Schematic representation of the synthetic procedure and the main components of NPT-1-D50.

**Table 7.1** *Doping characteristics of the SNPs sample presented in this study.*

| SNPs sample | Doping ratio[a] | SNPs µmol | TEOS mmol | RhodB-Si[b] µmol | Dasa µmol |
|---|---|---|---|---|---|
| *NPT-50* | 50 | 0.2 | 1.6 | 2 | 10 |

[a]*Doping ratio= [mol(drug)/mol(NP)].* [b]*RhobB-Si was introduced in the reaction mixture using pristine dichloromethane solutions.*

By means of absorbance measurements of NPT-50 ($\varepsilon_{Dasa}$ = 5.65 x $10^3$ $M^{-1}$ $cm^{-1}$ at $\lambda_{max}$ = 292 nm) and considering the NP concentration obtained with this synthetic method,[37] we found that the loading of Dasa inside the silica matrix (5 molecules of Dasa per NP) was lower than expected; this was probably due to a difficulty of entrapment of the drug in the silica matrix, which led quickly to leaching of Dasa from the particle.

### 7.2.2 Synthesis and characterization of SNPs

In light of the results of this preliminary test, we decided to design different NPs with improved properties using three different silica precursors (Figure 7.5) with the following objectives: (i) the synthesis of SNPs that had increased lipophilic nature on their silica core by using the derivative BTSE; indeed, as can be seen from Fig. 7.5, the presence of an ethylene moiety makes this derivative more apolar than TEOS. BTSE was utilized either in combination with TEOS (NPB-1, NPB-2 and NPB-3) at three different BTSE : TEOS molecular ratios (1 : 3, 1 : 1 and 3 : 1) or alone (NPB-4) (Table 7.2); (ii) the synthesis of SNPs capable of establishing H-bonding interactions between their silica core and the hosted molecule by using the derivative BUPS, which had an ureidic moiety suitable for this purpose. BUPS was employed in combination with TEOS (NPU-1 and NPU-2) at two different BUPS : TEOS molecular ratios (1 : 3 and 1 : 9). Non derivatized SNPs were also prepared and used in subsequent experiments for comparison (NPT-1) (Figure 7.5 and Table 7.2).

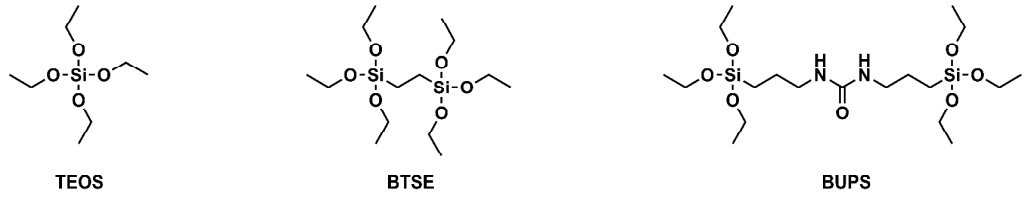


**Figure 7.5** *Molecular structure of silica precursors TEOS, BTSE and BUPS.*

**Table 7.2** *Doping characteristics, mean silica core - $d_c$ ± SD - determined by TEM analysis and DLS hydrodynamic values ($d_H$ ± SD) for the SNPs described in this work. Standard deviation was calculated on five different measurements*

| SNPs sample | TEOS | | BTSE | | BUPS | | ($d_c$ ± SD) / nm | ($d_H$ ± SD) / nm | PdI |
|---|---|---|---|---|---|---|---|---|---|
| | mmol | % | mmol | % | mmol | % | | | |
| *NPT-1* | 1.6 | 100 | - | - | - | - | 11 ± 2 | 20 ± 4 | 0.04 |
| *NPB-1* | 1.2 | 75 | 0.2 | 25 | - | - | 11 ± 4 | 23 ± 9 | 0.15 |
| *NPB-2* | 0.8 | 50 | 0.4 | 50 | - | - | 10 ± 3 | 25 ± 12 | 0.22 |
| *NPB-3* | 0.4 | 25 | 0.6 | 75 | - | - | 11 ± 4 | 35 ± 12 | 0.12 |
| *NPB-4* | - | - | 0.8 | 100 | - | - | 11 ± 4 | 35 ± 24 | 0.48 |
| *NPU-1* | 1.2 | 75 | - | - | 0.2 | 25 | 11 ± 3 | 17 ± 8 | 0.21 |
| *NPU-2* | 1.44 | 90 | - | - | 0.08 | 10 | 12 ± 4 | 23 ± 12 | 0.26 |

Morphological characterization by TEM images showed that all SNPs shared a low polydispersion index (PdI) and that the dimensions of the silica core (ca. 12 nm) were not influenced by the silica precursor used (Table 7.2, Figure 7.6). The hydrodynamic diameter ($d_H$), measured by dynamic light scattering (DLS), was similar for all samples, with values ranging between 17 and 35 nm (Table 7.2, Figure 7.7). These data confirmed the possibility of applying such nanoplatforms to evaluate if the possibility to tune the polarity of their silica core could increase the loading and retention of Dasa within the particles.

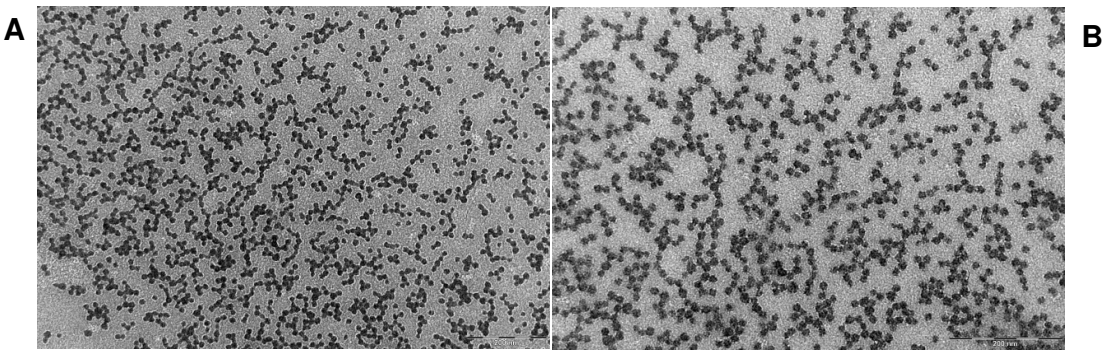


**Figure 7.6** *TEM images and silica core size distribution of: A) NPT-1 ($d_c$ = 12 ± 4 nm); B) NPB-4 ($d_c$ = 11 ± 4 nm). For clarity, only results of experiments done with NPT-1 and NPB-4 are shown.*

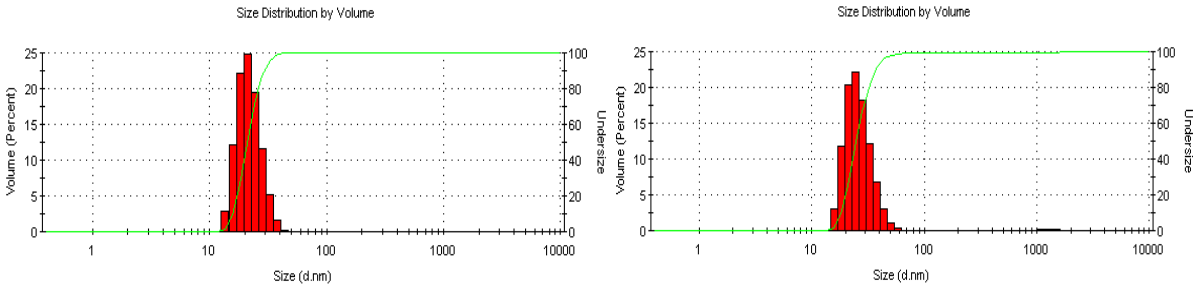

**Figure 7.7** *DLS diameter distribution by volume and undersize curve for: A) NPT-1 ($d_H$ = 20 ± 4 nm); B) NPB-4 ($d_H$ = 35 ± 24 nm). For clarity, only results of experiments done with NPT-1 and NPB-4 are shown.*

### 7.2.3 Synthesis and characterization of DSNPs with Dasa

A selection of the samples shown previously, NPT-1, NPB-2, NPB-4 and NPU-1 was chosen to synthesize DSNPs covalently doped with RhodB-Si; drug loading was carried out by using increasing Dasa : NP doping ratio (50 : 1, 100 : 1 and 300 :1), yielding NP-D50, NP-D100 and NP-D300 preparatives (Table 7.3 and Figure 7.8).

**Table 7.3** *Doping characteristics of the SNPs sample presented in this study.*

| SNPs sample | TEOS | | BTSE | | BUPS | | Rhod B-Si[a] | Dasa initial d. ratio[b] | Dasa final d. ratio[c] |
|---|---|---|---|---|---|---|---|---|---|
| | mmol | % | mmol | % | mmol | % | µmol | | |
| *NPT-1-D50* | 1.6 | 100 | - | - | - | - | 2 | 50 | 5 |
| *NPT-1-D100* | 1.6 | 100 | - | - | - | - | 2 | 100 | 9 |
| *NPT-1-D300* | 1.6 | 100 | - | - | - | - | 2 | 300 | 11 |
| *NPB-2-D50* | 0.8 | 50 | 0.4 | 50 | - | - | 2 | 50 | 2 |
| *NPB-2-D100* | 0.8 | 50 | 0.4 | 50 | - | - | 2 | 100 | 4 |
| *NPB-2-D300* | 0.8 | 50 | 0.4 | 50 | - | - | 2 | 300 | 17 |
| *NPB-4-D50* | - | - | 0.8 | 100 | - | - | 2 | 50 | 7 |
| *NPB-4-D100* | - | - | 0.8 | 100 | - | - | 2 | 100 | 8 |
| *NPB-4-D300* | - | - | 0.8 | 100 | - | - | 2 | 300 | 23 |
| *NPU-1-D50* | 1.2 | 75 | - | - | 0.2 | 25 | 2 | 50 | 4 |
| *NPU-1-D100* | 1.2 | 75 | - | - | 0.2 | 25 | 2 | 100 | 8 |
| *NPU-1-D300* | 1.2 | 75 | - | - | 0.2 | 25 | 2 | 300 | 33 |

[a]*RhobB-Si was introduced in the reaction mixture using pristine dichloromethane solutions.* [b]Initial Doping *ratio=[mol(drug)/mol(NP)];* [c]Final doping *ratio=[mol(drug)/mol(NP)] after the purification step by means of size-exclusion chromatography (see Section 8.1.2).*

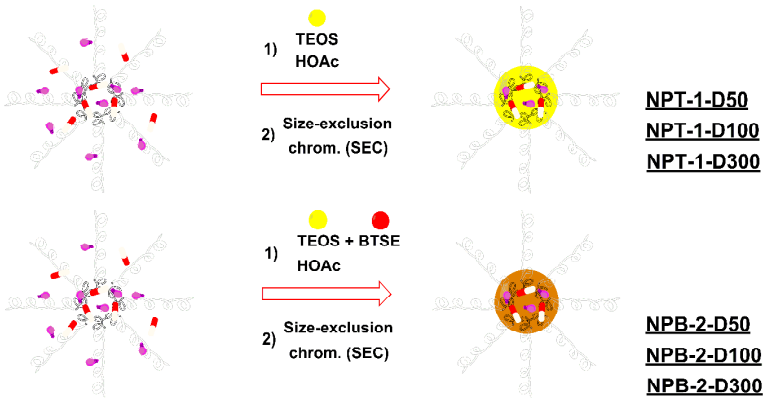

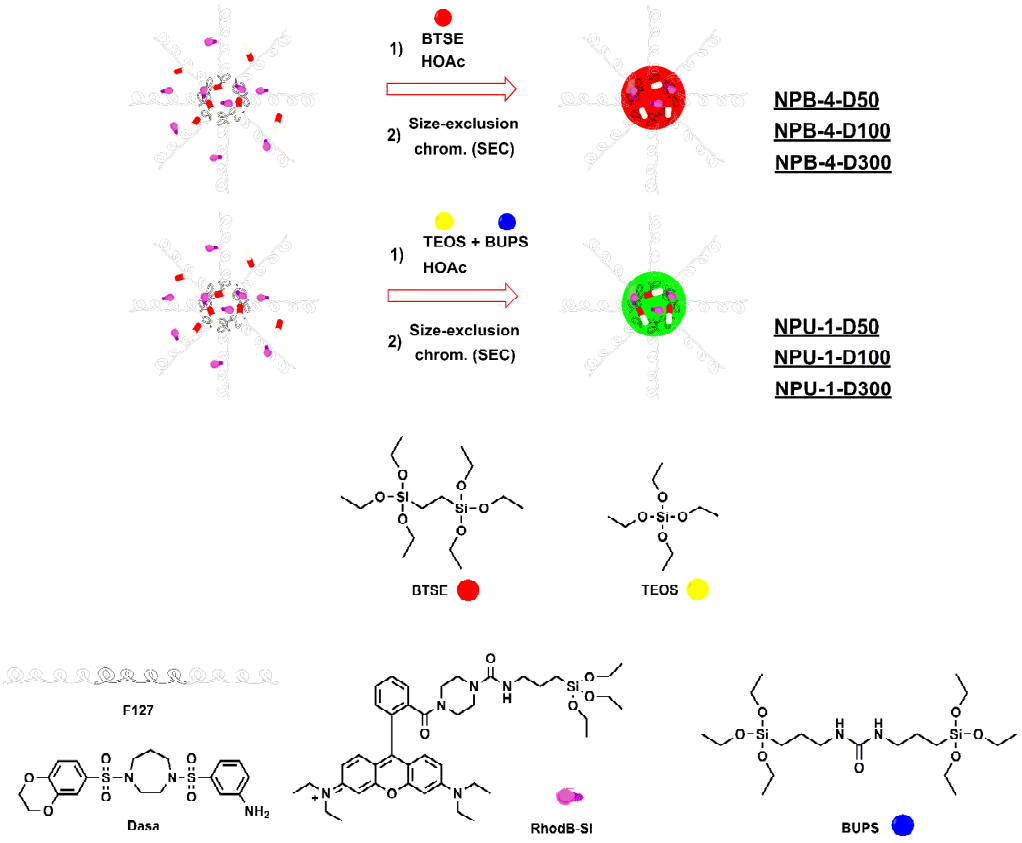


**Figure 7.8** *Schematic representation of the synthetic procedure and the main components of NPT-1, NPB-2, NPB-4 and NPU-1 loaded with Dasa.*

The results obtained clearly demonstrated that the loading of Dasa within the nanoparticles increased in a nonlinear way upon increasing the initial Dasa : NP molecular ratio; the lack of linearity was probably due to the saturation of the porous sites present in the silica core and to the differences in release rate of the drug at different loading level. Finally, the analysis of data relating to particles having the highest initial doping ratio (NPT-1-D300, NPB-2-D300, NPB-4-D300 and NPU-1-D300) revealed that the increase of the apolarity detected by employing a mixed system TEOS/BTSE in place of the one containing the only TEOS could almost double the units of drug per particle. The best loading of Dasa was found in sample NPU-1-D300, due to the presence of a precursor containing an ureidic moiety capable of giving H-bonding interactions between the silica core and the hosted molecule.

## 7.3 Conclusions

Fluorescence imaging techniques are becoming essential in biomedical applications and the research of suitable tools for in vitro and in vivo measurements is gaining increasing attention. Nanotechnology is supplying many solutions for present limitations in the field

and, in particular, luminescent nanoparticles are one of the most promising materials proposed for future diagnostic implementations.

In this contribution we have focused our attention on dye doped silica nanoparticles, since they are able to merge different materials to combine various functionalities. That is, to act as a basis for multifunctional medicine dedicate nanoplatforms, enabling multimodal imaging and simultaneous diagnosis and therapy.

In particular, we tested the ability of the particles to load biologically active molecules such as Dasa, an anti cancer drug capable of altering the Warburg effect, yielding a therapeutic potential in the treatment of cancer and other metabolic diseases. DSNPs were synthesized in increasing degree of lipophilicity and ability to establish hydrogen bond interactions in their silica core, resulting in an increased loading capacity of the drug within the silica core. However, this step, that is crucial for pratical applications, is only the first one towards a potential application of these systems in clinical trials. Therefore, this study will continue in the coming months in order to synthesize novel silica derivatives and multimodal/multifunctional nanoparticles suitable for theranostics.

## 7.4 Notes and references


(1) Prodi, L. *New Journal of Chemistry* **2005**, *29*, 20.
(2) Shi, D. L. *Adv. Funct. Mater.* **2009**, *19*, 3356.
(3) Yong, K. T.; Roy, I.; Swihart, M. T.; Prasad, P. N. *Journal of Materials Chemistry* **2009**, *19*, 4655.
(4) Gunasekera, U. A.; Pankhurst, Q. A.; Douek, M. *Targ. Oncol.* **2009**, *4*, 169.
(5) Gong, Y. K.; Nakashima, K. *Chem. Commun.* **2001**, 1772.
(6) Katz, L. C.; Burkhalter, A.; Dreyer, W. J. *Nature* **1984**, *310*, 498.
(7) Prilloff, S.; Fan, J. Y.; Henrich-Noack, P.; Sabel, B. A. *Eur. J. Neurosci.* **2010**, *31*, 521.
(8) Burns, A.; Ow, H.; Wiesner, U. *Chemical Society Reviews* **2006**, *35*, 1028.
(9) Medintz, I. L.; Uyeda, H. T.; Goldman, E. R.; Mattoussi, H. *Nat. Mater.* **2005**, *4*, 435.
(10) Bae, W.; Tan, W.; Hong, J.-I. *Chem. Commun.* **2012**, *48*, 2270.
(11) Wang, L.; Wang, K. M.; Santra, S.; Zhao, X. J.; Hilliard, L. R.; Smith, J. E.; Wu, J. R.; Tan, W. H. *Analytical Chemistry* **2006**, *78*, 646.
(12) Benezra, M.; Penate-Medina, O.; Zanzonico, P. B.; Schaer, D.; Ow, H.; Burns, A.; DeStanchina, E.; Longo, V.; Herz, E.; Iyer, S.; Wolchok, J.; Larson, S. M.; Wiesner, U.; Bradbury, M. S. *J. Clin. Invest.* **2011**, *121*, 2768.
(13) Bonacchi, S.; Genovese, D.; Juris, R.; Montalti, M.; Prodi, L.; Rampazzo, E.; Zaccheroni, N. *Angew. Chem. Int. Ed.* **2011**, *50*, 4056.
(14) Bonacchi, S.; Genovese, D.; Juris, R.; Montalti, M.; Prodi, L.; Rampazzo, E.; Sgarzi, M.; Zaccheroni, N. In *Luminescence Applied in Sensor Science*; Prodi, L., Montalti, M., Zaccheroni, N., Eds. 2011; Vol. 300, p 93.
(15) Rampazzo, E.; Bonacchi, S.; Genovese, D.; Juris, R.; Marcaccio, M.; Montalti, M.; Paolucci, F.; Sgarzi, M.; Valenti, G.; Zaccheroni, N.; Prodi, L. *Coord. Chem. Rev.* **2012**, *256*, 1664.
(16) Montalti, M.; Rampazzo, E.; Zaccheroni, N.; Prodi, L. *New Journal of Chemistry* **2013**, *37*, 28.
(17) Ambrogio, M. W.; Thomas, C. R.; Zhao, Y. L.; Zink, J. I.; Stoddartt, J. F. *Acc. Chem. Res.* **2011**, *44*, 903.
(18) Rosenholm, J. M.; Sahlgren, C.; Linden, M. *Nanoscale* **2010**, *2*, 1870.
(19) Boxer, M. B.; Jiang, J.-k.; Vander Heiden, M. G.; Shen, M.; Skoumbourdis, A. P.; Southall, N.; Veith, H.; Leister, W.; Austin, C. P.; Park, H. W.; Inglese, J.; Cantley, L. C.; Auld, D. S.; Thomas, C. J. *Journal of Medicinal Chemistry* **2010**, *53*, 1048.
(20) Xu, Y.; Liu, X.-H.; Saunders, M.; Pearce, S.; Foulks, J. M.; Parnell, K. M.; Clifford, A.; Nix, R. N.; Bullough, J.; Hendrickson, T. F.; Wright, K.; McCullar, M. V.; Kanner, S. B.; Ho, K.-K. *Bioorganic & Medicinal Chemistry Letters* **2014**, *24*, 515.

(21) Parnell, K. M.; Foulks, J. M.; Nix, R. N.; Clifford, A.; Bullough, J.; Luo, B.; Senina, A.; Vollmer, D.; Liu, J.; McCarthy, V.; Xu, Y.; Saunders, M.; Liu, X.-H.; Pearce, S.; Wright, K.; O'Reilly, M.; McCullar, M. V.; Ho, K.-K.; Kanner, S. B. *Molecular Cancer Therapeutics* **2013**, *12*, 1453.
(22) Anastasiou, D.; Yu, Y.; Israelsen, W. J.; Jiang, J.-k.; Boxer, M. B.; Hong, B. S.; Tempel, W.; Dimov, S.; Shen, M.; Jha, A.; Yang, H.; Mattaini, K. R.; Metallo, C. M.; Fiske, B. P.; Courtney, K. D.; Malstrom, S.; Khan, T. M.; Kung, C.; Skoumbourdis, A. P.; Veith, H.; Southall, N.; Walsh, M. J.; Brimacombe, K. R.; Leister, W.; Lunt, S. Y.; Johnson, Z. R.; Yen, K. E.; Kunii, K.; Davidson, S. M.; Christofk, H. R.; Austin, C. P.; Inglese, J.; Harris, M. H.; Asara, J. M.; Stephanopoulos, G.; Salituro, F. G.; Jin, S.; Dang, L.; Auld, D. S.; Park, H.-W.; Cantley, L. C.; Thomas, C. J.; Vander Heiden, M. G. *Nature chemical biology* **2012**, *8*, 839.
(23) Kung, C.; Hixon, J.; Choe, S.; Marks, K.; Gross, S.; Murphy, E.; DeLaBarre, B.; Cianchetta, G.; Sethumadhavan, S.; Wang, X.; Yan, S.; Gao, Y.; Fang, C.; Wei, W.; Jiang, F.; Wang, S.; Qian, K.; Saunders, J.; Driggers, E.; Woo, H. K.; Kunii, K.; Murray, S.; Yang, H.; Yen, K.; Liu, W.; Cantley, L. C.; Vander Heiden, M. G.; Su, S. M.; Jin, S.; Salituro, F. G.; Dang, L. *Chemistry & biology* **2012**, *19*, 1187.
(24) Filipp, F. V. *Journal of Carcinogenesis* **2013**, *12*, 14.
(25) Warner, S. L.; Carpenter, K. J.; Bearss, D. J. *Future Medicinal Chemistry* **2014**, *6*, 1167.
(26) Prigione, A.; Rohwer, N.; Hoffmann, S.; Mlody, B.; Drews, K.; Bukowiecki, R.; Blümlein, K.; Wanker, E. E.; Ralser, M.; Cramer, T.; Adjaye, J. *STEM CELLS* **2014**, *32*, 364.
(27) Mazurek, S. *The International Journal of Biochemistry & Cell Biology* **2011**, *43*, 969.
(28) Warburg, O. *Science* **1956**, *123*, 309.
(29) Yang, W.; Lu, Z. *Cell Cycle* **2013**, *12*, 3343.
(30) Yang, W.; Zheng, Y.; Xia, Y.; Ji, H.; Chen, X.; Guo, F.; Lyssiotis, C. A.; Aldape, K.; Cantley, L. C.; Lu, Z. *Nature cell biology* **2012**, *14*, 1295.
(31) Palsson-McDermott, Eva M.; Curtis, Anne M.; Goel, G.; Lauterbach, Mario A. R.; Sheedy, Frederick J.; Gleeson, Laura E.; van den Bosch, Mirjam W. M.; Quinn, Susan R.; Domingo-Fernandez, R.; Johnston, Daniel G. W.; Jiang, J.-k.; Israelsen, William J.; Keane, J.; Thomas, C.; Clish, C.; Vander Heiden, M.; Xavier, Ramnik J.; O'Neill, Luke A. J. *Cell Metabolism* **2015**, *21*, 347.
(32) Zong, H.; Zhang, Y.; You, Y.; Cai, T.; Wang, Y. *Med Oncol* **2015**, *32*, 1.
(33) Biffi, S.; Petrizza, L.; Rampazzo, E.; Voltan, R.; Sgarzi, M.; Garrovo, C.; Prodi, L.; Andolfi, L.; Agnoletto, C.; Zauli, G.; Secchiero, P. *RSC Advances* **2014**, *4*, 18278.
(34) Montalti, M.; Prodi, L.; Rampazzo, E.; Zaccheroni, N. *Chemical Society Reviews* **2014**, *43*, 4243.
(35) Rampazzo, E.; Bonacchi, S.; Genovese, D.; Juris, R.; Montalti, M.; Paterlini, V.; Zaccheroni, N.; Dumas-Verdes, C.; Clavier, G.; Meallet-Renault, R.; Prodi, L. *Journal of Physical Chemistry C* **2014**, *118*, 9261.
(36) Rampazzo, E.; Voltan, R.; Petrizza, L.; Zaccheroni, N.; Prodi, L.; Casciano, F.; Zauli, G.; Secchiero, P. *Nanoscale* **2013**, *5*, 7897.
(37) Rampazzo, E.; Bonacchi, S.; Juris, R.; Montalti, M.; Genovese, D.; Zaccheroni, N.; Prodi, L.; Rambaldi, D. C.; Zattoni, A.; Reschiglian, P. *Journal of Physical Chemistry B* **2010**, *114*, 14605.

# Chapter 8

# Experimental section

## 8.1 Materials and methods

### 8.1.1 Chemicals

1-Iodopropane (99%), Malonaldehyde bis(phenylimine) monohydrochloride (97%), Acetic anhydride (≥ 99%), 6-Bromohexanoic acid (97%), Dimethylformamide (DMF ≥ 99.8%, over molecular sieve, $H_2O$ ≤ 0.01%), Pyridine (≥ 99.8%), 1-[Bis(dimethylamino)methylene]-1H-1,2,3-triazolo[4,5-b]pyridinium3-oxidhexafluorophosphate (HATU, 97%), 1-Hydroxybenzotriazole hydrate (HOBt ≥ 99%) IR-813 perchlorate (80%), (3-Mercaptopropyl)triethoxysilane (≥ 80%), Acetonitrile (MeCN, 99.8%), Diethyl ether ($Et_2O$, ≥ 99.8%), Methanol (MeOH, ≥ 99.8%), Magnesium sulfate (≥ 99.5%), Dichloromethane (DCM, ≥ 99.8%), Ethyl acetate (EtOAc, ≥ 99.5%), Sodium hydroxide (≥ 98%), Piperidine (≥ 99.5%), Pluronic F127, Tetraethyl orthosilicate (TEOS, 99.99%), Copper(II) sulfate pentahydrate (≥ 98%), N,N-Diisopropylethylamine (≥ 99%), Chlorotrimethylsilane (TMSCl, ≥ 98%), Acetic acid (HOAc, ≥ 99.7 %), HCl (≥ 37 %), 4-(Dimethylamino)pyridine (DMAP, ≥ 99%), HBTU (≥ 98%), N,N'-Disuccinimidyl carbonate, Propargyl bromide solution (80 wt. % in toluene), DSC ( ≥ 98%), 1,6-Diaminohexane (98%), Tin(II) chloride dehydrate (98%), Trifluoroacetic acid (TFA, 99%), N-(2-Hydroxyethyl)aniline (98%), Sodium bicarbonate (≥ 99.7%), sodium sulfate (≥ 99%), 1,4-Dioxane (≥ 99%), reagent grade Ethanol (EtOH), DMF, $Et_2O$, DCM, Thionyl chloride, Acetone, Dimethyl sulfoxide (DMSO), Cyclohexane, Chloroform, Heptane were purchased from Sigma-Aldrich.

Triisopropylsilane (TIS, 99%), 3-Azido-1-propanol (97%) 3-(Triethoxysilyl)propyl isocyanate (95%), 1,2-Bis(triethoxysilyl)ethane (96%), 3-Nitrobenzenesulfonyl chloride (97%), 1,4-Benzodioxan-6-sulfonyl chloride (95%), 1-Boc-hexahydro-1,4-diazepine (98%), Fmoc-tBu-Gly-OH (≥ 98%), Fmoc-Glu(OtBu)-OH (≥ 98%), Fmoc-Val-OH (98%), Fmoc-Asp(OtBu)-OH (≥ 98%), Sulfur trioxide triethylamine complex (≥ 95%), Propargylamine (98%), 4-Nitrophenyl chloroformate (96%), 1,1′-Carbonyldiimidazole (≥ 97%), 3-Bromo-1-propanol (97%), Sodium azide (≥ 99%) and Methanesulfonyl chloride (98%) were purchased from Aldrich.

Lithium chloride (≥ 99%), Sodium phosphate monobasic (≥ 98 %), Fluorescamine (≥ 98 %) and Sodium ascorbate (≥ 99%) was purchased from Sigma.

Octaethylene glycol monomethyl ether (≥ 96%) was purchased from TCI.

(Fmoc-Pra-OH) was purchased from ChemPep Inc.

Cystamine dihydrochloride (≥ 98 %), Methoxypolyethylene glycol amine (PEG-NH2, MW 750 g/mol), (3-Aminopropyl)triethoxysilane (APTES, ≥ 98%), Fast Black K salt, N,N-Diisopropylethylamine (DIPEA, ≥ 98%), Triethylamine (TEA, ≥ 99.5%), NaCl and Silica on

Reference Cy5.5 commercial dye (Cy5.5 GE) was purchased from GE Healthcare (Amersham FluoroLinkTM Cy5.5 Monofunctional dye, Code: PA25501).

Resin Rink amide AM was purchased from Activotec

### 8.1.2 Purifications

Dialysis was performed vs. water at room temperature under gentle stirring with regenerated cellulose dialysis tubing (Sigma, mol wt. cut-off > 12 KDa, avg. diameter 33 mm).

After dialysis, all luminescent nanoparticles samples were passed through hydrophilic Durapore membrane filters (0.45, 0.22 and 0.1 μm pore size) purchased from Millipore.

Size-Exclusion Chromatography (SEC) was performed on Sephadex G-25 (nanoparticles for drug delivery, see Chapter 7), or Sephadex LH-20, that were purchased from Sigma.

Flash chromatography was performed on silica gel 60, 230-400 and 35-70 mesh. Thin layer chromatography was carried out on silica gel supported on aluminum foils, containing a fluorescent indicator at 254 nm. These products were purchased from Fluka.

Semipreparative HPLC chromatography was performed on SunFire C18 column (5 μm, 19 × 150 mm) on Gilson PLC2020.

### 8.1.3 NMR measurements

Unless otherwise specified, NMR measurements were recorded at 25 °C, in $CDCl_3$, on a Varian Mercury Plus 200, 300 and 400 MHz spectrometer. Chemical shifts are reported in δ from $Me_4Si$ (δ = 0.00 ppm) or from CDCl3 (δ = 7.27 ppm for $^1$H-Nmr or δ = 77.0 ppm for $^{13}$C-NMR). Multiplicities are reported using the following abbreviations: s (singlet); d (doublet); t (triplet); q (quartet), m (multiplet); br (broad), or a suitable combination. All coupling constants *J* are expressed in Hz. In case of uncertainty or ambiguity, proton assignments were determined by means of two-dimensional $^1$H,$^1$H-Cosy experiments.

### 8.1.4 Photophysical measurements

UV-VIS absorption spectra were recorded at 25°C by means of Perkin-Elmer Lambda 45 spectrophotometer. The fluorescence spectra were recorded with a Perkin-Elmer Lambda LS 55 fluorimeter and with a modular UV-VIS-NIR spectrofluorimeter Edinburgh Instruments FLS920 equipped with a photomultiplier Hamamatsu R928P. The latter instrument connected to a PCS900 PC card was used for the Time Correlated Single Photon Counting (TCSPC) experiments.

Chapter 4 and 5 - Corrected fluorescence emission and excitation spectra (450 W Xe lamp) were obtained with the same instrument equipped with both a Hamamatsu R928P P photomultiplier tube (for the 500-850 nm spectral range) and an Edinburgh Instruments Ge detector (for the 800-1600 nm spectral range).

Quartz cuvettes with optical path length of 1 cm were used for both absorbance and emission measurements.

Nanoparticles solutions were diluted with Milli-Q® water.

Luminescence quantum yields (uncertainty ± 15%) were recorded on air-equilibrated solutions (absorbance < 0.1 in the whole spectral region to avoid auto-absorption), with rhodamine 101 in ethanol ($\Phi$ = 0.1) and cyanine IR-125 (from Acros Organics) in ethanol ($\Phi$ = 0.05) as a reference.[1] Corrections for instrumental response, inner filter effects and phototube sensitivity were performed.[2]

All fluorescence anisotropy measurements were performed on an Edinburgh FLS920 equipped with Glan-Thompson polarizers. Anisotropy measurements were collected using an L-format configuration, and all data were corrected for polarization bias using the G-factor. Four different spectra were acquired for each sample combining different orientation of the excitation and emission polarizers: $I_{VV}$, $I_{VH}$, $I_{HH}$, $I_{HV}$ (where V stands for vertical and H for horizontal; the first subscript refers to the excitation polarizer and the second subscript refers to the emission one). The spectra were used to calculate the G-factor and the anisotropy r: $G = I_{HV}/I_{HH}$, $r = (I_{VV} - GI_{VH})/(I_{VV} + 2GI_{VH})$.

### 8.1.5 Trasmission Electron Microscopy

A Philips CM 100 transmission electron microscope operating at 80 kV was used. For TEM investigations a 3.05 mm copper grid (400 mesh) covered by a Formvar support film was dried up under vacuum after deposition of a drop of nanoparticles solution diluted with water (1:50). The SiNP TEM images show that only the silica cores present sufficient contrast to appear in the images. The size distribution was obtained analyzing images with a block of several hundred nanoparticles. The obtained histogram was fitted according to a Gaussian distribution obtaining the average diameter for the silica nanoparticles core.

### 8.1.6 Dynamic Light Scattering

Chapter 3, 6 and 7 - SNP hydrodynamic diameter ($d_H$) distributions determination was carried out through Dynamic Light Scattering measurements with a Malvern Nano ZS instrument equipped with a 633 nm laser diode. Samples were housed in disposable polystyrene cuvettes of 1 cm optical path length, using water as solvent.

Chapter 4 and 5 - SNP hydrodynamic diameter ($d_H$) distributions determination was carried out at 25°C through Dynamic Light Scattering measurements using a NICOMP Model 370

Submicron Particle Sizer (Nicomp International, Orlando, FL) equipped with a 488 nm Argon laser. This laser source and equipment was used to minimize interferences due to absorption-emission processes during the DLS measurements.

Samples were housed in small disposable glass test tubes, using water as solvent.

The width of DLS hydrodynamic diameter distribution is indicated by the standard deviation of five different measurement. The Polydispersion Index values (in case of monomodal distribution $PdI=(\sigma/Z_{avg})^2$, where $\sigma$ is the width of the distribution and $Z_{avg}$ is average diameter of the particles population respectively) are also reported.

### 8.1.7 ζ-Potential experiments

SNPs ζ-Potential values were determined using a Malvern Nano ZS instrument. Samples were housed in disposable polycarbonate folded capillary cell (750 µL, 4 mm optical path length). Electrophoretic determination of ζ-Potential was made under Smoluchowski approximation in acqueous media at moderate electrolyte concentration.

### 8.1.8 Cells

Chapter 3 - Blood samples were collected in heparin-coated tubes from 6 healthy blood donors following informed consent, in accordance with the Declaration of Helsinki and in agreement with institutional guidelines. Peripheral blood mononuclear cells (PBMC) from healthy donors were isolated by gradient centrifugation with lymphocyte cell separation medium (Cedarlane Laboratories, Hornby, ON) and were routinely cultured in RPMI-1640 medium containing 10% FBS, L-glutamine and Penicillin/Streptomycin (all from Gibco, Life Technologies Corporation, Paisley, UK). The JVM-2 B leukemic line was purchased from DSMZ (Deutsche Sammlung von Mikroorganismen und Zellkulturen GmbH, Braunschweig, Germany) and cultured, as previously described[3] in RPMI-1640 medium containing 15% FBS, L-glutamine, Penicillin/Streptomycin, supplemented with glucose 4.5 g/L, sodium pyruvate 1 mM, sodium bicarbonate 1.5 g/L, HEPES 10 mM (Gibco). Huh7 hepatocellular-carcinoma cell line (European Collection of Cell Cultures, Salisbury, UK) was cultured in Dulbecco's Modified Eagle Medium (DMEM) containing 10% FBS, L-glutamine and penicillin/streptomycin (Gibco). Human umbilical vein endothelial cells (HUVEC) were purchased from BioWhittaker (Lonza, Walkersville, MD), grown in EGM2 medium (Lonza) on tissue culture plates coated with 1µg/cm2 of human fibronectin (BD, Becton Dickinson, San Jose, CA) and used between the 3rd and 5th passage in vitro, as previously described.[4]

Chapter 4 - JVM-2 B leukemic cell line was purchased from DSMZ (Deutsche Sammlung von Mikroorganismen und Zellkulturen GmbH, Braunschweig, Germany) and cultured in RPMI-1640 medium containing 15% FBS, L-glutamine, penicillin/streptomycin, supplemented with glucose 4.5 gL-1, sodium pyruvate 1 mM, sodium bicarbonate 1.5 gL-1, HEPES 10 mM (Gibco, Grand Island, NY). Human bone marrow-derived mesenchymal

stromal cells (MSC) were isolated as previously reported.[5] MSC cell preparations were homogenously CD105+, CD90+, CD34-, CD45-, CD14-, which is a typical MSC surface antigen profile, and were routinely cultured in MSC-Growth Medium (MSC-GM; Lonza, Walkersville, MD).

### 8.1.9 Assessment of cell viability

At different time points (24-96 hours) post treatment with SNPs used at different concentrations (range 1-100 nM), cell survival was evaluated by Trypan blue dye exclusion, as previously described.[6,7] Moreover, the degree of apoptosis was evaluated by double-staining with PI and FITC-conjugated Annexin V (Alexis Biochemical, Enzo Life Sciences, Lausen, Switzerland,) according to the manufacturer's instructions and analyzed by flow cytometry as previously detailed.[8,9] These assays were performed on 0.5 ml of cells suspension, for PBMC and JMV-2 cultures. For cells growing in adhesion (HUVEC, Huh7 and MSC), adherent cells were recovered with 0.25% trypsin-EDTA (Gibco) and pooled with floating cells to analyze the degree of cell death and apoptosis in the entire cell population.[10] In addition, for adherent cell types (HUVEC and Huh7), cell proliferation was analyzed by using the DP version of the xCELLigence real time cell analyzer RTCA, (Roche Diagnostics, Mannheim, Germany), which records changes in impedance (reported as Cell Index) over a prolonged time course in a non-invasive system. All data were then analyzed using the xCELLigence software (version 1.2.1). Briefly, the background impedance of RTCA DP E-Plates 16 was performed using a standard protocol provided in the software with 100 µL of cell culture medium (pre-coating with fibronectin was performed for HUVEC). Cells were seeded at a pre-defined optimal concentration in a final volume of 200 µL in quadruplicate before treatment with SNP preparations or, in some experiments, with Sorafenib 10µM as positive control of cellular cytotoxicity.[11] Cell cultures treated in parallel in normal 96 well plates were analyzed for cell shape and growth changes and phase-contrast images were recorded with EVOS digital inverted microscope (Advanced Microscopy Group, Bothel, WA).

### 8.1.10 Flow cytometric analysis

Chapter 3 - The binding efficiency of SNPs to the cell surface membrane was investigated by flow cytometry (FACSCalibur Analyzer, BD), as previously described.[12] JVM-2 cells, seeded at 106/mL, were incubated with Rhodamine-labeled SNPs (10-100 nM) for 45 min at 4°C, washed three times in ice-cold PBS, suspended in fresh medium and placed at 37°C, 5% $CO_2$. At different time points, cells were analyzed for the evaluation of Rhodamine signal persistence. SNP entry on adherent cell types (HUVEC and Huh7) was evaluated on cells treated as described above with Rhodamine-labeled SNPs. Flow cytometry analysis was performed following incubation of cells with 0.25% trypsin-EDTA to remove eventual residue of SNPs still attached to the outside of cells and to detach cells from the flask.[13] In some experiments, cells were treated with the endocytosis inhibitor Genistein (0.4 mM, Sigma-Aldrich, Saint Luis, MO) starting from 2 hours before addition of

Rhodamine-labeled SNPs.[14] Nonspecific fluorescence was evaluated on not-treated cells. Data files were collected and analyzed using the CellQuest Pro software.

Chapter 4 - Cell labeling performance and/or efficiency of the single and m-NIR-SNPs was quantitatively evaluated by flow cytometry using a FACSCalibur Analyzer (Becton-Dickinson, San Jose, CA) equipped with a 488 nm laser and a 635 nm laser, spatially separated. The filters used in our FACSCalibur provide the measurement of green (515-545 nm; FL1), yellow (564-606 nm; FL2), red (> 670 nm; FL3) fluorescences excited at 488 nm. The FL4 filter (653-669 nm) is used to measure the red fluorescence excited at 635 nm. This is possible because of the particular hardware/elettronic setting, which allows the detection by the FL4 detector of the signals that have been exited by the 635 nm laser. For labeling of JVM-2, cells were seeded at 106 mL-1 in fresh medium before the addition of SNPs (10 nM). JVM-2 cultures were then placed at 37°C, 5% $CO_2$, for 18 hours. For cell labeling of adherent MSC cultures, SNPs were directly added to the medium of sub-confluent cell layer. Cultures were then kept at 37°C, 5% $CO_2$ for 18 hours. After 18 hours of incubation, cells were washed with PBS and incubated with 0.25% trypsin–EDTA (to remove any eventual residue of SNPs attached to the outside of cells and/or to detach MSC cells from the flask) and analyzed by flow cytometry. For multiparametric analysis, JVM-2 and MSC cultures, either left untreated or labeled with siNPs, were then incubated with the following monoclonal antibodies (Ab) recognizing cell-type specific surface antigens: FITC-conjugated anti-human-CD19 and PE-conjugated anti-human-CD105 (Immunotech; Marseille, France), FITC-conjugated anti-human-CD90 (Miltenyi Biotech, Auburn, CA). For cell surface staining, 5×105 cells were resuspended in 200 µL of PBS containing 1% BSA (Sigma-Aldrich, St Louis, MO) and incubated 30 minutes at 4°C with the conjugated monoclonal Ab (CD19 for the JVM-2 B cells; CD90 and CD105 for the MSC). Non-specific fluorescence was assessed by incubation of cells with isotype-matched conjugated Ab (Becton-Dickinson). Data files were collected and analysed using the CellQuest Pro software and displayed as single histograms and as two-colours dot plots to measure the proportion of double-positive cells.

### 8.1.11 Fluorescence microscopy

For fluorescence microscopy observation, Huh-7 adherent cells were seeded over night at 1.5x105/well on 6 well plates containing glass coverslips and treated with Rhodamine-labeled SNPs (100-300 nM). At different time points, cells were fixed in paraformaldehyde 4%, permeabilized with 0.1% Triton X-100 and stained with FITC-conjugated Phalloidin (all from Sigma-Aldrich) to mark intracellular actin.[15] Cells were then mounted on slides with anti-fading and anti-photobleaching solution Vectashield Mounting Medium (Vector Laboratories, Burlingame, CA). Cells were examined using an inverted Swept Field Nikon (Nikon Corporation, Tokyo, Japan) confocal microscope equipped with 60x plan apoVC objective and Andor DU885 EM-CCD camera (Andor Technology Ltd, Belfast, Northen Ireland). Images were captured with Nikon NIS Elements software and analyzed using the Image-J 1.43m software (NIH, Bethesda, MA). In parallel, additional images were taken using the Xcellence® Olympus imaging platform (Olympus, Vienna, Austria) equipped with

Hamamatsu ORCA CCD camera and 60x oil immersion objective. For each field 21 planes of 0.5 µm each were acquired. Z-stacks were then visualized using the extended slice function on Bitplane Imaris 4.0 software (Bitplane AG, Zurich, Switzerland).

### 8.1.12 *In vivo* experiments

Chapter 3 - Female SCID mice (5 weeks-old) were purchased from Charles River Laboratories (Hollister, CA) and were maintained in accordance with the guide for the care and use of laboratory animals at the animal facility of the University of Ferrara. Mice were housed in vented cabinet with food and water ad libitum. The procedures involving animals and their care were approved by the institutional animal ethical care committee (CEASA) of the University of Ferrara and by the Italian Ministry of Health. JVM-2 (5x106) cells were treated for 24 hours with Rhodamine-labeled SNPs (100 nM), harvested, washed and suspended in PBS before intravenous injection (in a volume of 100 µL of PBS) into the lateral tail vein of adult mice. Controls were represented by mice injected with JVM-2 not loaded with SNPs. Twentyfour hours post inoculations, peripheral blood of mice was taken by intracardiac puncture performed under deep anesthesia followed by euthanasia of animals. Clot of blood was inhibited by addition of 10mg/ml EDTA. Before flow-cytometry analysis on mouse whole blood and evaluation of Rodamine-positive cells, red cells were lysed in lysing buffer (BD) following vendor's instructions.

Chapter 4 - Female BALB/c and SCID mice (4-6 weeks old) were purchased from Harlan (Italy) and maintained under pathogen-free conditions with ad libitum food and water, in accordance with the guide for the care and use of laboratory animals. All the experimental procedures were performed in compliance with the guidelines of European (86/609/EEC) and Italian (D.L.116/1992) laws and were approved by the institutional animal ethical care committee of the University of Trieste and by the Italian Ministry of Health. BALB/c mice were used for the biodistribution analysis of the m-NIR-SNPs in normal (healthy) settings, by i.v. injection of m-NIR-SNPs (1 nmol in 150 µL PBS, corresponded to 4.2 nmol of Cy5.5-Si). SCID mice were used to establish xenograft tumor models by subcutaneous (s.c.) inoculation on the left flank of 107 human leukemic cells (JVM-2) resuspended in 100 µL of PBS. Explanted subcutaneous tumor masses, after ex vivo imaging acquisitions, were fixed in 10% buffered-formalin solution and embedded in paraffin for histological analysis.

### 8.1.13 Optical imaging assessment

Equimolar aliquots (20 µM) of the fluorescent single or m-NIR-SNPs preparatives were placed on a paper substrate and comparatively analyzed with a time-domain fluorescence imager Optix MX2 preclinical NIRF-imager (Advanced Research Technologies, Montreal, CA). The same equipment was adopted for the acquisition of in vivo data in mouse models, as previously described.[16] Briefly, mice were shaved prior to the scanning procedure in order to reduce scattering of the signal from fur. Throughout all imaging

sessions, mice were anesthetized with vaporized isoflurane at 1.8-2.0 volume % (Sigma). The anesthetized mice were placed inside the acquisition system and gently fixed on a heated block (37°C) for the entire duration of data acquisition. Two-dimensional regions of interest (ROIs) were selected, and laser power, integration time (repetition time of the excitation per raster point) and scan step size were optimized according to the emitted signal. Prior to injection of the contrast agent (either m-NIR-SNPs or m-NIR-SNPs-labeled cells), mice were scanned to obtain background images. The background signal intensity, recorded with the baseline image for each animal, was subtracted from each post injection image. For ex vivo optical imaging, the last in vivo whole-body imaging session was followed by euthanasia of animals. The organs were explanted and imaged with the same Optix system. For each explanted organ, the average fluorescence intensity was calculated within a region of interest covering the whole sample and subtracted by the average fluorescence intensity within a region of the same area in the corresponding explanted organ of a control mouse (uninjected mouse). For selected mice, explanted organs were snap-frozen in isopentane and cooled at -80°C for tissue analysis.

Optical imaging results were analyzed by reporting fluorescence intensity values in normalized counts (NC) representing the photon count for unit excitation laser power and unit exposure time, allowing comparison among different images. Fluorescence lifetime results were obtained by fitting every fluorescence decay curve corresponding to each pixel measured by Optix using the Levenberg Marquet least squares method.[17]

### 8.1.14 Tissue analysis

For fluorescence microscopy, sections of 7- and 12-µm thickness were cut from frozen organs with a cryostat at -20°C. Glass slides were kept at 4°C at dark and Vectashield Mounting Medium with DAPI (Vector Laboratories, Burlingame, CA), diluted 1:1 with PBS, was used to stain cell nuclei. Fluorescent images were acquired by using an inverted microscope with a CCD camera (DVC-1412AM monochrome digital camera QE > 62% at 550nm) and the objectives lens 10x, 40x and 63x (NA 1.63) immersion oil.

For histological analysis, 5 µm thick sections were cut from paraffin blocks and stained with haematoxylin-eosin. Immunohistochemistry was performed by using the primary Ab for human CD20 (clone L26; NovocastraTM; Leica Biosystems Newcastle Ltd, Newcastle Upon Tyne, UK), associated to the NovoLinkTM Polymer Detection System (Novocastra), which was used for the visualization of the primary Ab, following manufacturer's instruction. After staining, the slides were examined under a Leica DM2000 optical microscope and microphotographs were taken using a Leica DFC320 digital camera.

### 8.1.15 Statistical analysis

Results from at least three independent experiments are reported as the means ± SD and analyzed for statistical significance by the two-tail Student's t-test and Mann-Witney rank-sum test. Differences were considered significant when p value was < 0.05.

### 8.1.16 Photoacoustic measurements

*In vitro* photoacoustic experiments were carried out by Vevo LZ250 transducer (Vevo® LAZR Photoacoustic Imaging System). Axial resolution: 75 µm. Broadband frequency: 13 MHz-24 MHz.

## 8.2 Synthesis and characterization of dyes

### 8.2.1 Cy 7 derivative

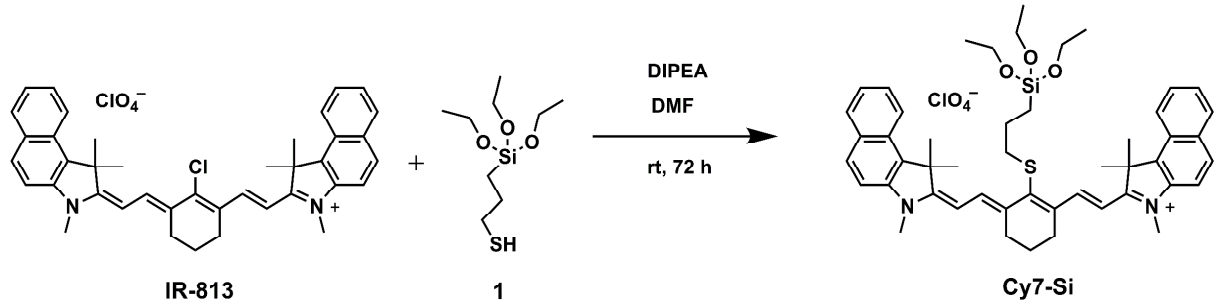


**Figure 8.1** *Schematization of the synthesis of the triethoxysilane derivative of Cy 7 dye (Cy7-Si)*

2-[2-[2-Thio-[3-(triethoxysilyl)propyl]-3-[2-(1,3-dihydro-1,1,3-trimethyl-2H-benzo[e]-indol-2-ylidene)-ethylidene]-1-cyclohexen-1-yl]-ethenyl]-1,1,3-trimethyl-1H-benzo[e]indolium perchlorate **Cy7-Si**: this compound was synthesized adapting reported procedures.[18] In a flamed 25 mL round bottom flask dried under vacuum, to a solution of 2-[2-[2-Chloro-3-[2-(1,3-dihydro-1,1,3-trimethyl-2H-benzo[e]-indol-2-ylidene)-ethylidene]-1-cyclohexen-1-yl]-ethenyl]-1,1,3-trimethyl-1H-benzo[e]indolium perchlorate (**IR-813** perchlorate, 0.064 g, 94 µmol) in DMF (6 mL) was added N,N-Diisopropylethylamine (DIPEA, 20 µL, 113 µmol) and (3-Mercaptopropyl)triethoxysilane (**1**) (68 µL, 282 µmol) and the reaction mixture was stirred at room temperature for 72 h. The reaction mixture was then diluted with Brine and extracted three times with DCM. The combined organic phases are dried over Sodium sulfate, concentrated with the rotary evaporator and desiccated in vacuum, affording a green solid substance. Purification was carried out by silica gel chromatography eluting with EtOAc/MeOH (9:1-1:9) to give the compound **Cy7-Si** as a dark green solid (0.053 g, yield 64 %).

- **Chemical formula**: $C_{49}H_{61}ClN_2O_7SSi$;

- **Molecular Weight**: 885.6;
- **$^{1}$H-NMR** (400 MHz, $CDCl_3$, 25°C): δ = 8.91 (2H, d, J = 16 Hz, C*H*), 8.11 (2H, d, J = 8 Hz, ar. C*H*), 7.93 (4H, d, J = 8 Hz, ar. C*H*), 7.47-7.43 (2H, m, ar. C*H*), 7.41 (2H, d, J = 8 Hz, ar. C*H*), 6.23 (2H, d, J = 12 Hz, C*H*), 3.77 (6H, q, J = 6.7 Hz, -OC*H*$_2$CH$_3$), 3.77 (6H, s, N-C*H*$_3$) overlapped, 2.83 (2H, t, J = 8 Hz, -SC*H*$_2$-), 2.68 (4H, t, J = 8 Hz, -C*H*$_2$CH$_2$C*H*$_2$-), 2.03 (12H, s, -C*H*$_3$), 1.96-1.92 (2H, m, -SCH$_2$C*H*$_2$CH$_2$-), 1.81-1.74 (2H, q, -CH$_2$C*H*$_2$CH$_2$-), 1.17 (9H, t, J = 6 Hz, -OCH$_2$C*H*$_3$), 0.75-0.70 (2H, m, -CH$_2$CH$_2$C*H*$_2$Si);
- **$^{13}$C-NMR** (100 MHz, $CDCl_3$, 25°C): δ = 139.8, 139.2, 135.7, 132.5, 131.5, 128.1, 125.6, 124.9, 124.5, 123.1, 105.0, 70.0, 64.5, 57.4, 30.7, 29.3, 27.14, 27.13, 27.0, 17.6, 7.9;
- **ESI-MS**: m/z calculated for $C_{49}H_{61}N_2O_3SSi^+$ is 785.4; obs: 786.4.

### 8.2.2 Cy 5.5 derivative

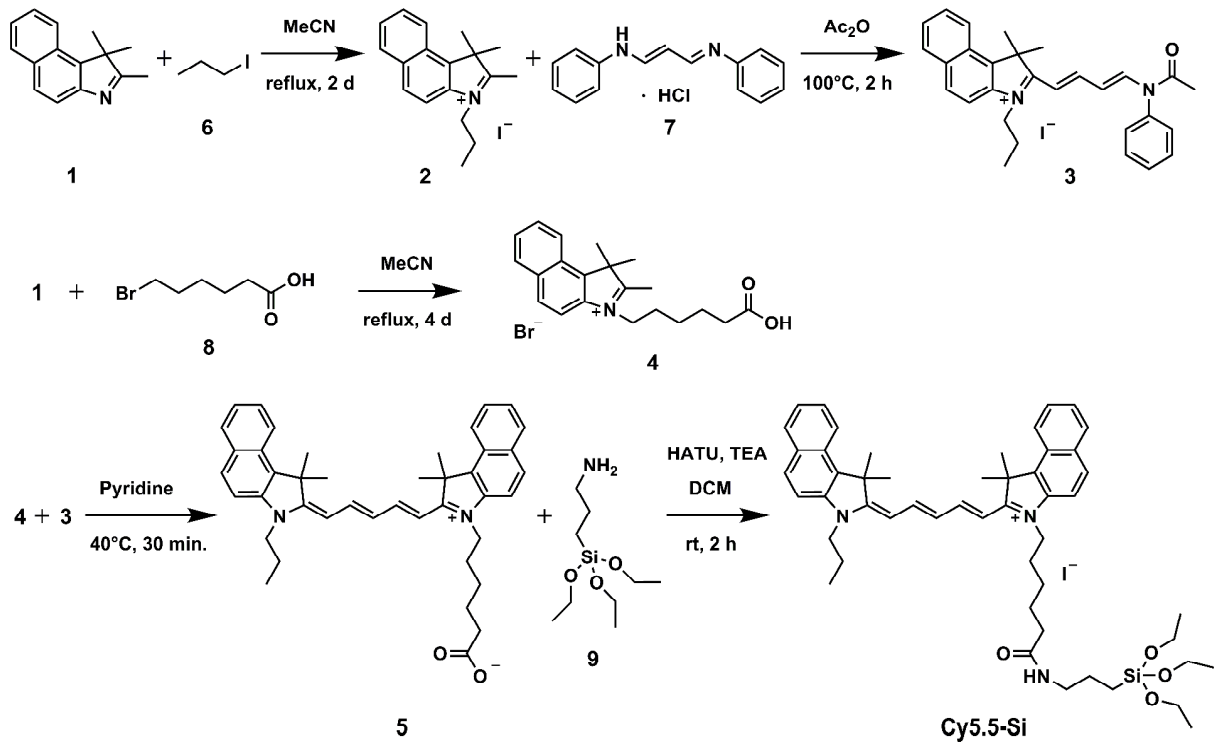


**Figure 8.2** *Schematization of the synthesis of (Cy5.5-Si).*

3-propyl-1,1,2-trimethyl-1H-benz[e]indolium iodide salt **2**: this compound was synthesized adapting reported procedures.[19] In a 100 mL flamed round bottom flask dried under vacuum, to a solution of 1,1,2-Trimethylbenz[e]indole (**1**) (1.0 g, 4.8 mmol) in MeCN (36 mL) was added 1-Iodopropane (**1**) (702 µL, 7.2 mmol) and the reaction mixture was

heated under reflux for two days. After cooling down to room temperature, the reaction mixture was concentrated in vacuo and the resulting oil was washed several times with $Et_2O$ to obtain compound **2** as dark brown solid (1.34 g, yield 97 %).

- **Chemical formula**: $C_{18}H_{22}IN$;
- **Molecular Weight**: 379.3;
- **$^1$H-NMR** (400 MHz, $CDCl_3$, 25°C): δ = 8.08 (2H, t, *J* = 8 Hz, ar. C*H*) and 8.04 (1H, d, *J* = 8 Hz, ar. C*H*) part. overlapped, 7.92 (1H, d, *J* = 8 Hz, ar. C*H*), 7.83 (1H, d, *J* = 8 Hz, ar. C*H*), 7.66 (1H, t, *J* = 8 Hz, ar. *CH*), 4.80 (2H, t, *J* = 8 Hz, -NC*H*$_2$-), 3.20 (3H, s, -C*H*$_3$), 2.11-2.02 (2H, m, -NCH$_2$C*H*$_2$CH$_2$), 1.87 (6H, s, -C*H*$_3$), 1.11 (3H, t, *J* = 8 Hz, -NCH$_2$CH$_2$C*H*$_3$);
- **$^{13}$C-NMR** (100 MHz, $CDCl_3$, 25°C): δ = 195.3, 189.7, 150.1, 138.5, 138.0, 136.9, 133.5, 132.1, 131.2, 130.0, 127.3, 55.8, 55.2, 22.6, 21.6, 16.8, 11.2;
- **ESI-MS**: m/z calculated for $C_{18}H_{22}N^+$ is 252.2; obs: 253.2.

2-[4-(N-Phenyl-N-acetylamino)1,3-pentadienyl]-1,1-dimethyl-3-propyl-1H-benz[e]indolium iodide salt **3**: this compound was synthesized adapting reported procedures.[19,20] In a flamed 50 mL round bottom flask dried under vacuum, a suspension of compound (**2**) (1.0 g, 3.5 mmol) and malonaldehyde bis(phenylimine) monohydrochloride (**7**) (906 mg, 3.5 mmol) in Acetic anhydride (17 mL) was heated at 100°C for 2 h. After cooling down to room temperature, the reaction mixture was poured into 190 mL $Et_2O$. The dark brown precipitate **3** (1.51 g, yield 79 %) was then filtered and used in the next step without further purification.

- **Chemical formula**: $C_{29}H_{31}IN_2O$;
- **Molecular Weight**: 550.5;
- **ESI-MS**: m/z calculated for $C_{29}H_{31}N_2O^+$ is 423.2; obs: 423.2.

1,1,2-Trimethyl-3-(6-carboxylatohexyl)benz[e]indolium bromide salt **4**: this compound was synthesized adapting reported procedures.[19,20] In a flamed 100 mL round bottom flask dried under vacuum, to a solution of compound (**1**) (1.0 g, 4.8 mmol) in MeCN (40 mL) was added 6-Bromohexanoic acid (**8**) (1.21 g, 6.2 mmol) and the reaction mixture was heated under reflux for four days. After cooling down to room temperature, the reaction mixture was poured into 150 mL of $Et_2O$ and kept in fridge overnight. The obtained solid was filtered and washed three times with diethyl ether to obtain the compound **4** as blue-green solid (0.522 g, yield 34 %).

- **Chemical formula**: $C_{21}H_{26}NO_2^+$;
- **Molecular Weight**: 324.4;
- **$^1$H-NMR** (400 MHz, $CDCl_3$, 25°C): δ = 8.33 (1H, d, *J* = 8 Hz, ar. C*H*), 8.25 (1H, d, *J* = 8 Hz, ar. C*H*), 8.17 (1H, d, *J* = 8 Hz, ar. C*H*), 8.01 (1H, d, *J* = 8 Hz, ar. C*H*), 7.83-7.79 (1H, m, ar. C*H*), 7.75-7.71 (1H, m, ar. C*H*), 4.64 (2H, t, *J* = 8 Hz, -NC*H*$_2$-), 2.36 (2H, t, *J* = 6 Hz, -C*H*$_2$COOH), 2.10-2.01 (2H, m, -NCH$_2$C*H*$_2$), 1.85 (6H, s, -C*H*$_3$), 1.79-1.76 (2H, m, -C*H*$_2$CH$_2$COOH), 1.62-1.54 (2H, m, -CH$_2$C*H*$_2$CH$_2$-);

- **$^{13}$C-NMR** (100 MHz, $CDCl_3$, 25°C): δ = 197.7, 175.8, 139.9, 138.9, 135.4, 132.6, 131.2, 129.9, 129.29, 128.93, 124.57, 113.92, 57.5, 34.52, 34.41, 28.9, 27.21, 27.16, 25.58, 25.55, 22.5;
- **ESI-MS** m/z calculated for $C_{21}H_{26}NO_2^+$ is 324.2; obs.: 324.2.

2-[7-(1,3-Dihydro-1,1-dimethyl-3-propylbenz[e]indolin-2-ylidene)-1,3,5-pentatrienyl]-1,1-dimethyl-3-(6-carboxylatohexyl)-1H-benz[e]indolium inner salt **5**: this compound was synthesized adapting reported procedures.[19,20] In a flamed 10 mL round bottom flask dried under vacuum, to a solution of compound (**4**) (0.150 g, 0.46 mmol) in Pyridine (3 mL) was added compound (**3**) (0.255 g, 0.46 mmol) and the reaction mixture was heated at 40°C for 30 min. After cooling down to room temperature, the reaction mixture was concentrated in vacuo and the residue was purified by silica gel chromatography eluting with DCM/MeOH (99:1-90:10) to give the compound **5** as a blue solid (0.147 g, yield 49 %).

- **Chemical formula**: $C_{42}H_{46}N_2O_2$;
- **Molecular Weight**: 610.8;
- **$^1$H-NMR** (400 MHz, $CDCl_3$, 25°C): δ = 8.33-8.11 (4H, m, ar. C*H*), 7.90 (4H, d, *J* = 8 Hz, ar. C*H*), 7.59 (2H, q, *J* = 6.7 Hz, ar. C*H*), 7.45 (2H, q, *J* = 6.7 Hz, ar. C*H*), 7.32 (2H, t, *J* = 8 Hz, C*H*), 6.99 (1H, t, *J* = 12 Hz, C*H*), 6.54 (1H, d, *J* = 12 Hz, C*H*), 6.37 (1H, d, *J* = 16 Hz, C*H*), 4.19 (2H, t, *J* = 8 Hz, -NC*H*$_2$-) and 4.15 (2H, t, *J* = 8 Hz, -NC*H*$_2$-) par. overlapped, 2.15 (2H, t, *J* = 8 Hz, -C*H*$_2$COOH), 2.05-2.03 (12H, d, -C*H*$_3$), 1.93-1.86 (4H, m, -NCH$_2$C*H*$_2$CH$_2$ and -C*H*$_2$CH$_2$COOH), 1.80-1.76 (2H, m, -NCH$_2$C*H*$_2$), 1.61-1.57 (2H, m, -CH$_2$C*H*$_2$CH$_2$-), 1.08 (3H, t, *J* = 8 Hz, -NCH$_2$CH$_2$C*H*$_3$);
- **$^{13}$C-NMR** (100 MHz, $CDCl_3$, 25°C): δ = 202.0, 173.9, 152.2, 135.9, 130.9, 130.8, 130.3, 129.2, 128.1, 127.0, 125.4, 125.3, 125.2, 124.5, 123.6, 122.5, 122.4, 120.1, 110.9, 110.8, 110.6, 104.4, 103.7, 58.6, 51.4, 51.2, 46.3, 44.6, 34.1, 28.1, 26.4, 24.3, 21.5, 15.1, 11.7;
- **ESI-MS** m/z calculated for $C_{42}H_{47}N_2O_2^+$ is 611.4; obs.: 611.2.

2-[7-(1,3-Dihydro-1,1-dimethyl-3-propylbenz[e]indolin-2-ylidene)-1,3,5-pentatrienyl]-1,1-dimethyl-3-[6-[N-(3-(triethoxysilyl)propyl]hexanamide]-1H-benz[e]indolium iodide salt **Cy5.5-Si**: this compound was synthesized adapting reported procedures.[19] In a flamed 25 mL round bottom flask dried under vacuum, to a solution of compound (**5**) (0.118 g, 0.19 mmol) in DCM (12 mL) was added 1-[Bis(dimethylamino)methylene]-1H-1,2,3-triazolo[4,5-b]pyridinium 3-oxid hexafluorophosphate (**HATU**) (0.087 g, 0.24 mmol), (3-Aminopropyl)triethoxysilane (**9**) (0.049 mL, 0.21 mmol) and TEA (0.053 mL, 0.38 mmol) and the reaction mixture was stirred at room temperature for 2 h. The reaction mixture was concentrated in vacuo and the residue was purified by silica gel chromatography eluting with EtOAc/MeOH (95:5-80:20) to give the compound **Cy5.5-Si** as blue solid (0.102 g, yield 66 %).

- **Chemical formula**: $C_{51}H_{68}IN_3O_4Si$;

- **Molecular Weight**: 942.1;
- **$^1$H-NMR** (400 MHz, $CDCl_3$, 25°C): δ = 8.33-8.11 (4H, m, ar. C*H*), 7.90 (4H, d, *J* = 8 Hz, ar. C*H*), 7.59 (2H, q, *J* = 6.7 Hz, ar. C*H*), 7.45 (2H, q, *J* = 6.7 Hz, ar. C*H*), 7.32 (2H, t, *J* = 8 Hz, C*H*), 6.99 (1H, t, *J* = 12 Hz, C*H*), 6.54 (1H, d, *J* = 12 Hz, C*H*), 6.37 (1H, d, *J* = 16 Hz, C*H*), 4.19 (2H, t, *J* = 8 Hz, -NC$H_2$-) and 4.15 (2H, t, *J* = 8 Hz, -NC$H_2$-) par. overlapped, 3.77 (6H, q, *J* = 6.7 Hz, -OC$H_2$$CH_3$) - (6H, s, N-C$H_3$) overlapped, 2.15 (2H, t, *J* = 8 Hz, -C$H_2$COOH), 2.05-2.03 (12H, d, -C$H_3$), 1.96-1.92 (2H, m, -NHCH$_2$C$H_2$CH$_2$-) and 1.93-1.86 (4H, m, -NCH$_2$C$H_2$CH$_2$ and -C$H_2$CH$_2$COOH) overlapped, 1.80-1.76 (2H, m, -NCH$_2$C$H_2$), 1.81-1.74 (2H, q, -CH$_2$C$H_2$CH$_2$-), 1.61-1.57 (2H, m, -CH$_2$C$H_2$CH$_2$-), 1.17 (9H, t, *J* = 6 Hz, -OCH$_2$C$H_3$), 1.08 (3H, t, *J* = 8 Hz, -NCH$_2$CH$_2$C$H_3$), 0.75-0.70 (2H, m, -C$H_2$CH$_2$C$H_2$Si);
- **$^{13}$C-NMR** (100 MHz, $CDCl_3$, 25°C): δ = 12.1, 13.9, 18.5, 21.6, 23.5, 24.4, 25.0, 25.3, 27.5, 27.7, 34.3, 43.1, 49.4, 49.7, 52.8, 53.3, 58.4, 104.5, 104.8, 113.7, 117.6, 121.0, 122.0, 124.9, 125.5, 125.6, 125.8, 126.1, 126.3, 126.5, 126.9, 127.0, 128.6, 130.4, 132.5, 132.6, 133.5, 137.4, 143.1, 148.4, 170.7, 172.8;
- **ESI-MS** m/z calculated for $C_{51}H_{68}N_3O_4Si^+$ is 814.5; obs.: 816.4.

The triethoxysilane derivative of Rhodamine B, **RhodB-Si**, was synthesized following reported procedures.[21]

## 8.3 Synthesis and characterization of Dasa

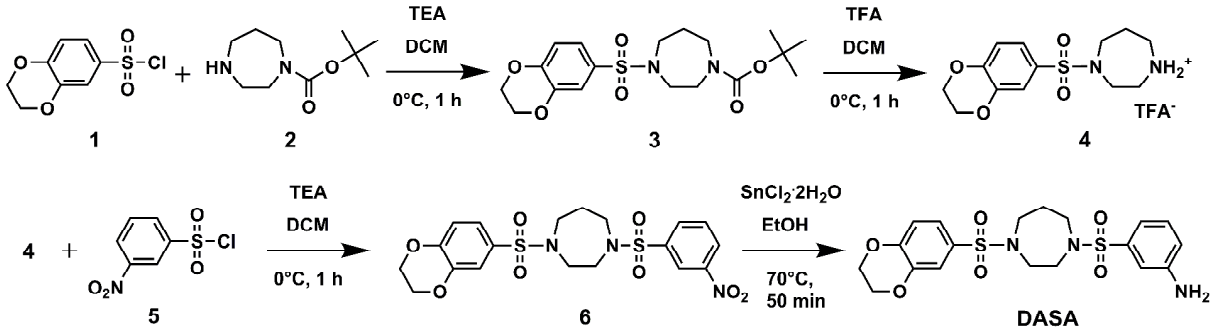


**Figure 8.3** *Schematization of the synthesis of **Dasa**.*

1-((2,3-dihydrobenzo[b][1,4]dioxin-6-yl)sulfonyl)-4-((3-nitrophenyl)sulfonyl)-1,4-diazepane **6** was synthesized adapting reported procedures.[22] In a flamed 25 mL round bottom flask dried under vacuum, compound (**4**) (0.287 g, 0.697 mmol) was dissolved in DCM (4 mL) and cooled in an ice bath. TEA (0.810 mL, 2.93 mmol) was added followed by portionwise addition of 3-Nitrobenzenesulfonyl chloride (**5**) (0.173 g, 0.8 mmol) and the reaction mixture was stirred at 0°C for 1 h. The reaction was quenched with saturated aqueous Ammonium chloride (6 mL). The organic layer was washed twice with saturated

Ammonium chloride, once with Brine, dried over Sodium sulfate and concentrated in vacuo and the residue was purified by silica gel chromatography eluting with Cyclohexane/EtOAc (1:1-1:9) to give the compound **6** as a white solid (0.256 g, yield 76 %).

- **Chemical formula:** $C_{19}H_{21}N_3O_8S_2$;
- **Molecular Weight:** 483.5;
- **$^1$H-NMR** (400 MHz, $CDCl_3$, 25°C): δ = 8.62 (1H, s, ar. C*H*), 8.45 (1H, d, *J* = 8.0 Hz, ar. C*H*), 8.11 (1H, d, *J* = 7.6 Hz, ar. C*H*), 7.76 (1H, t, *J* = 8.0 Hz, ar. C*H*), 7.28 (1H, s, ar. C*H*), 7.24 (1H, s, ar. C*H*), 6.95 (1H, d, *J* = 8.0 Hz, ar. C*H*), 4.31 (4H, s, -OC*H*$_2$-), 3.35 (8H, m, -NC*H*$_2$CH$_2$-), 1.95 (2H, m, -CH$_2$C*H*$_2$CH$_2$-);

3-((4-((2,3-dihydrobenzo[b][1,4]dioxin-6-yl)sulfonyl)-1,4-diazepan-1-yl)sulfonyl)aniline
**DASA** was synthesized adapting reported procedures.[23] In a 50 mL flamed round bottom flask dried under vacuum, to a solution of compound (**6**) (0.256 g, 0.53 mmol) in EtOH (15 mL) was added $SnCl_2 \cdot 2H_2O$ (0.597 g, 2.64 mmol) and the reaction mixture was heated at 70°C for 50 min. After cooling down to room temperature, the reaction mixture was quenched with NaOH 0.2 M and extracted three times with DCM. The combined organic phases were dried over Sodium sulfate, concentrated in vacuo and the residue was purified by silica gel chromatography eluting with Cyclohexane/EtOAc (7:3-5:5) to give the compound **DASA** as a white solid (0.166 g, yield 69 %).

- **Chemical formula:** $C_{19}H_{23}N_3O_6S_2$;
- **Molecular Weight:** 453.5;
- **$^1$H-NMR** (400 MHz, $CDCl_3$, 25°C): δ = 7.43 (1H, d, *J* = 8.4, ar. C*H*), 7.37 (2H, m, ar. C*H*), 7.25 (2H, m, ar. C*H*), 7.19 (1H, d, *J* = 7.6 Hz, ar. C*H*), 6.95 (1H, d, *J* = 8.0 Hz, ar. C*H*), 4.31 (4H, s, -OC*H*$_2$-), 3.96 (2H, br, -N*H*$_2$), 3.37 (8H, m, -NC*H*$_2$CH$_2$-), 1.95 (2H, m, -CH$_2$C*H*$_2$CH$_2$-);
- **$^{13}$C-NMR** (100 MHz, $CDCl_3$, 25°C): δ = 147.4, 147.0, 143.6, 140.0, 131.3, 130.1, 120.5, 119.0, 117.8, 116.5, 116.4, 112.7, 64.5, 64.1, 50.9, 50.8, 47.2, 29.0;
- **ESI-MS** m/z calculated for $C_{19}H_{23}N_3O_6S_2^+$ is 453.1; obs.: 454.1.

tert-butyl-4-((2,3-dihydrobenzo[b][1,4]dioxin-6-yl)sulfonyl)-1,4-diazepane-1-carboxylate **3** and 4-((2,3-dihydrobenzo[b][1,4]dioxin-6-yl)sulfonyl)-1,4-diazepan-1-ium 2,2,2-trifluoroacetate **4** were synthesized following reported procedures.[22]

## 8.4 Synthesis and characterization of BUPS

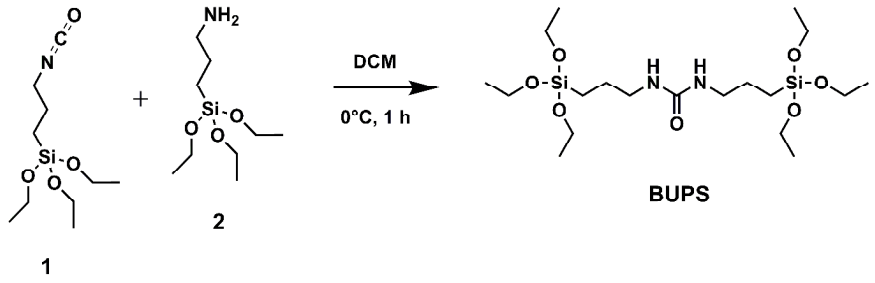


**Figure 8.4** *Schematization of the synthesis of BUPS.*

1,3-bis(3-(triethoxysilyl)propyl)urea **BUPS**: in a flamed 25 mL round bottom flask dried under vacuum, 3-(Triethoxysilyl)propyl isocyanate (**1**) (0.469 mL, 2 mmol) was dissolved in DCM (5 mL) and cooled in an ice bath. 3-(Aminopropyl)triethoxysilane (**2**) (0.457 mL, 2 mmol) was added and the reaction mixture was stirred at 0°C for 1 h. The reaction was concentrated in vacuo to give the compound **BUPS** as a white solid (0.906 g, yield 97 %).

- **Chemical formula:** $C_{19}H_{44}N_2O_7Si_2$;
- **Molecular Weight:** 468.7;
- **$^1$H-NMR** (400 MHz, $CDCl_3$, 25°C): δ = 6.00 (2H, s, -N*H*), 3.81 (12H, dd, *J* = 7.2 and 14 Hz, -OC$H_2$), 3.17 (4H, t, *J* = 6.8, -NC$H_2$-), 1.63 (4H, t, *J* = 7.6 Hz, -$CH_2CH_2CH_2$-), 1.24 (18H, dd, *J* = 7.2 and 14.0 Hz, -$CH_2CH_3$), 0.64 (4H, t, *J* = 7.6 Hz, -SiC$H_2$-);
- **$^{13}$C-NMR** (100 MHz, $CDCl_3$, 25°C): δ = 158.2, 58.4, 43.0, 23.6, 18.3, 7.6.
- **ESI-MS** m/z calculated for $C_{19}H_{44}N_2O_7Si_2^+$ is 468.2; obs.: 469.1.

## 8.5 Synthesis and characterization of DEVD

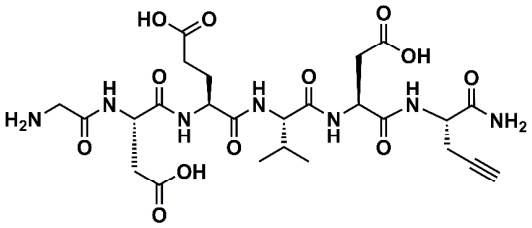

**Figure 8.5** *Molecular structure of **DEVD** peptide.*

(3S,6S,9S,12S,15S)-3-(2-aminoacetamido)-15-carbamoyl-6-(2-carboxyethyl)-12-(carboxymethyl)-9-isopropyl-4,7,10,13-tetraoxo-5,8,11,14-tetraazaoctadec-17-ynoic acid **DEVD**: this peptide was synthesized manually on a Rink Amide AM resin using the Fmoc-based strategy. Solid-phase reactions were performed in polypropylene tubes equipped with polyethylene frits and polypropylene caps using an orbital agitator shaking device. The overall yields for the solid-phase syntheses were calculated based on the initial loading provided by the supplier (0.58 mmol/g). The initial amount of resin was 1g. Amino

acids were introduced protected in the following order: Fmoc-Pra-OH, Fmoc-Asp(OtBu)-OH, Fmoc-Val-OH, Fmoc-Glu(OtBu)-OH, Fmoc-Asp(OtBu)-OH and Fmoc-Gly-OH. The cleavages of Fmoc protecting groups were performed in 20% piperidine/DMF (2 times for 15 min). The completion of couplings and Fmoc cleavages was monitored with the color Kaiser test. Coupling reactions of Fmoc amino acids were performed for 2 h in DMF (7 mL) under gentle stirring using a molar ratio of amino acid/HBTU/HOBt/DIEA/resin (5:5:5:5:1). Boc and resin cleavage was carried out by a mixture consisting of 95% TFA:2.5% $H_2O$:2.5% TIS (7 mL) for 2 h under gentle stirring. The reaction mixture was then concentrated in vacuo. $Et_2O$ was added (10 mL), the resulting precipitate was filtered and washed three times with $Et_2O$ to obtain **DEVD** as a transparent gel (0.280 g, yield 77 %).

- **Chemical formula:** $C_{25}H_{37}N_7O_{12}$;
- **Molecular Weight:** 627.6;
- **ESI-MS** m/z calculated for $C_{25}H_{37}N_7O_{12}^+$ is 627.2; obs.: 628.2.

## 8.6 Synthesis and characterization of BHQ derivatives

### 8.6.1 BHQ-alc

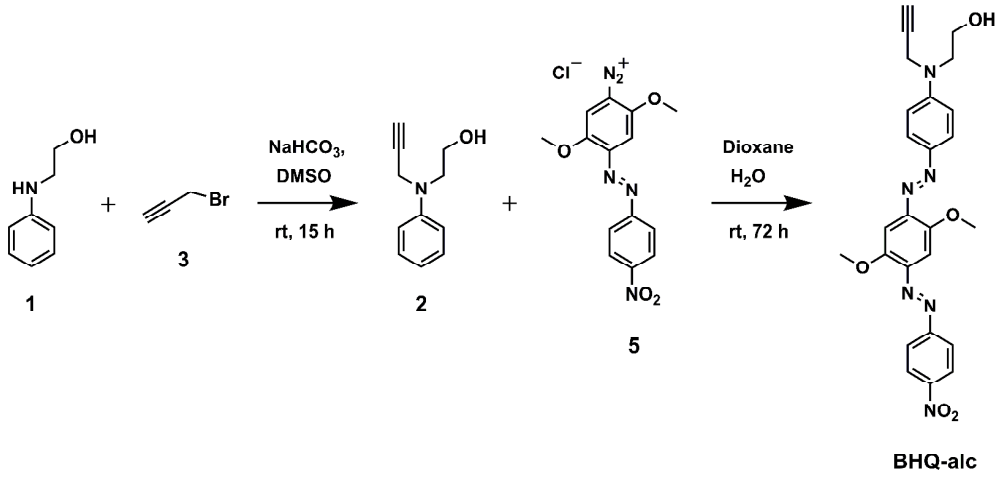


**Figure 8.6** *Schematization of the synthesis of the alcoholic derivative of BHQ (BHQ-alc).*

2-(phenyl(prop-2-yn-1-yl)amino)ethan-1-ol **2**: in a flamed 250 mL round bottom flask dried under vacuum, to a solution of N-(2-Hydroxyethyl)aniline (**1**) (5 g, 36.45 mmol) in Dimethyl sulfoxide (DMSO) (40 mL) was added Propargyl bromide (**3**) (solution 80 wt. % in toluene) (4.8 mL, 43.10 mmol) and Sodium bicarbonate (6.13 g, 73 mmol) and the reaction mixture was stirred at room temperature for 15 h. The reaction mixture was then diluted with $H_2O$ (40 mL) and extracted four times with EtOAc. The combinated organic phases were washed two times with $H_2O$ and one time with Brine, dried over Sodium sulfate and

concentrated in vacuo to give the title compound **2** as a yellow-brown oil (6.219 g, yield 98 %).

- **Chemical formula:** $C_{11}H_{13}NO$;
- **Molecular Weight:** 175.2;
- **$^{1}$H-NMR** (400 MHz, $CDCl_3$, 25°C): δ = 7.31 (2H, t, *J* = 8.2 Hz, ar. C*H*), 6.95 (2H, d, *J* = 8.0 Hz, ar. C*H*), 6.87 (1H, t, *J* = 7.3 Hz, ar. C*H*), 4.11 (2H, s, -NC*H*$_2$-), 3.86 (2H, t, *J* = 5.3 Hz, -NC*H*$_2$CH$_2$-), 3.59 (2H, t, *J* = 5.5 Hz, -CH$_2$C*H*$_2$OH), 2.28 (1H, s, -CC*H*);
- **$^{13}$C-NMR** (100 MHz, $CDCl_3$, 25°C): δ = 148.3, 129.4, 119.0, 114.8, 80.1, 72.6, 60.2, 54.0, 41.1;
- **ESI-MS** m/z calculated for $C_{11}H_{13}NO^+$ is 175.1; obs.: 176.1.

2-((4-((E)-(2,5-dimethoxy-4-((E)-(4-nitrophenyl)diazenyl)phenyl)diazenyl)phenyl)(prop-2-yn-1-yl)amino)ethan-1-ol **BHQ-alc**: in a flamed 1 L round bottom flask dried under vacuum, the compound (**2**) (5.077 g, 29 mmol) was solubilized with 100 mL of 1,4-Dioxane. Fast Black K salt (**5**) (30% dye content, 20.4 g, 14.64 mmol) was solubilized in a mixture 1,4-Dioxane/$H_2O$ (7/3, 400 mL) and added to the previous solution, and the reaction mixture was stirred at room temperature for 72 h. 1,4-Dioxane was then removed in vacuo; a black solid was attached to the flask, and the water was discarded. The residue was purified by silica gel chromatography eluting with EtOAc/Heptane (5:5-9:1) to give the compound **BHQ-alc** as a purple solid (1.417 g, yield 10 %).

- **Chemical formula:** $C_{25}H_{24}N_6O_5$;
- **Molecular Weight:** 488.5;
- **$^{1}$H-NMR** (400 MHz, $CDCl_3$, 25°C): δ = 8.39 (2H, d, *J* = 8.9 Hz, ar. C*H*), 8.06 (2H, d, *J* = 8.8 Hz, ar. C*H*), 7.99 (2H, d, *J* = 8.9 Hz, ar. C*H*), 7.48 (1H, s, ar. C*H*), 7.45 (1H, s, ar. C*H*), 6.99 (2H, d, *J* = 9.7 Hz, ar. C*H*), 4.25 (2H, s, -NC*H*$_2$C-), 4.10 (3H, s, -OC*H*$_3$), 4.06 (3H, s, -OC*H*$_3$), 3.95 (2H, t, *J* = 5.3 Hz, -NC*H*$_2$CH$_2$OH), 3.74 (2H, t, *J* = 5.3 Hz, -CH$_2$C*H*$_2$OH), 2.34 (1H, s, -CC*H*);
- **$^{13}$C-NMR** (100 MHz, $CDCl_3$, 25°C): δ = 156.6, 153.7, 151.3, 151.0, 148.6, 146.6, 145.7, 142.6, 126.0, 124.9, 123.8, 113.1, 101.3, 100.3, 79.5, 73.0, 60.6, 57.0, 56.9, 53.9, 41.3;
- **ESI-MS** m/z calculated for $C_{25}H_{24}N_6O_5^+$ is 488.2; obs.: 489.2.

### 8.6.2 BHQ-sul

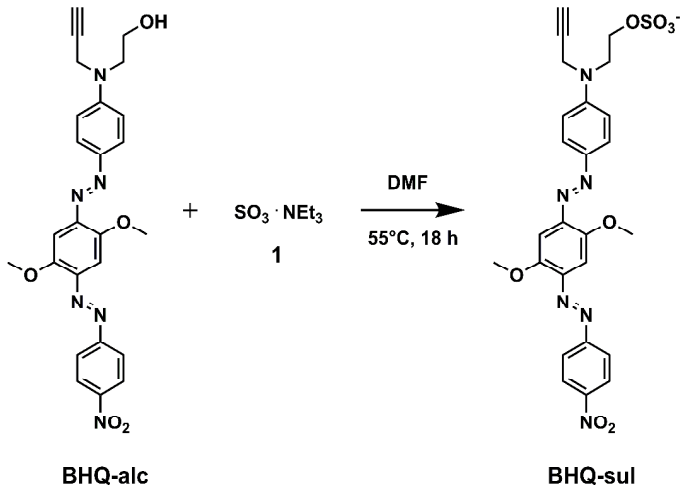


**Figure 8.7** *Schematization of the synthesis of the sulfonic derivative of BHQ (BHQ-sul).*

2-((4-((E)-(2,5-dimethoxy-4-((E)-(4-nitrophenyl)diazenyl)phenyl)diazenyl)phenyl)(prop-2-yn-1-yl)amino)ethyl sulfate **BHQ-sul**: in a flamed 50 mL round bottom flask dried under vacuum, to a solution of (**BHQ-alc**) (0.2 g, 0.41 mmol) in DMF (15 mL) was added Sulfur trioxide triethylamine complex (**1**) (0.8 g, 4.4 mmol) and the reaction mixture was heated at 55°C for 18 h. After cooling down to room temperature, the reaction mixture was then concentrated in vacuo and the residue was purified by silica gel chromatography eluting with DCM/MeOH (9:1-8:2) to give the compound **BHQ-sul** as a purple solid (0.202 g, yield 87 %).

- **Chemical formula:** $C_{25}H_{23}N_{6O}8S^-$;
- **Molecular Weight:** 567.5;
- **$^1$H-NMR** (400 MHz, $CDCl_3$, 25°C): δ = 8.38 (2H, d, *J* = 8.9 Hz, ar. C*H*), 8.05 (2H, d, *J* = 9.0 Hz, ar. C*H*), 7.95 (2H, d, *J* = 9.1 Hz, ar. C*H*), 7.51 (1H, s, ar. C*H*), 7.46 (1H, s, ar. C*H*), 6.96 (2H, d, *J* = 9.2 Hz, ar. C*H*), 4.34 (2H, t, *J* = 6.2 Hz, -$CH_2CH_2$OS-), 4.25 (2H, s, -NC$H_2$C-), 4.10 (3H, s, -OC$H_3$), 4.05 (3H, s, -OC$H_3$), 3.87 (2H, t, *J* = 5.3 Hz, -NC$H_2CH_2$OS-), 2.26 (1H, s, -CC*H*);
- **$^{13}$C-NMR** (100 MHz, $CDCl_3$, 25°C): δ = 156.4, 153.5, 151.0, 148.4, 146.5, 145.1, 142.3, 132.3, 125.8, 124.7, 123.6, 112.7, 101.1, 100.2, 72.4, 64.8, 56.8, 50.5, 46.1;
- **ESI-MS** m/z calculated for $C_{25}H_{23}N_{6O}8S^+$ is 567.1; obs.: 568.1.

### 8.6.3 BHQ-PEG

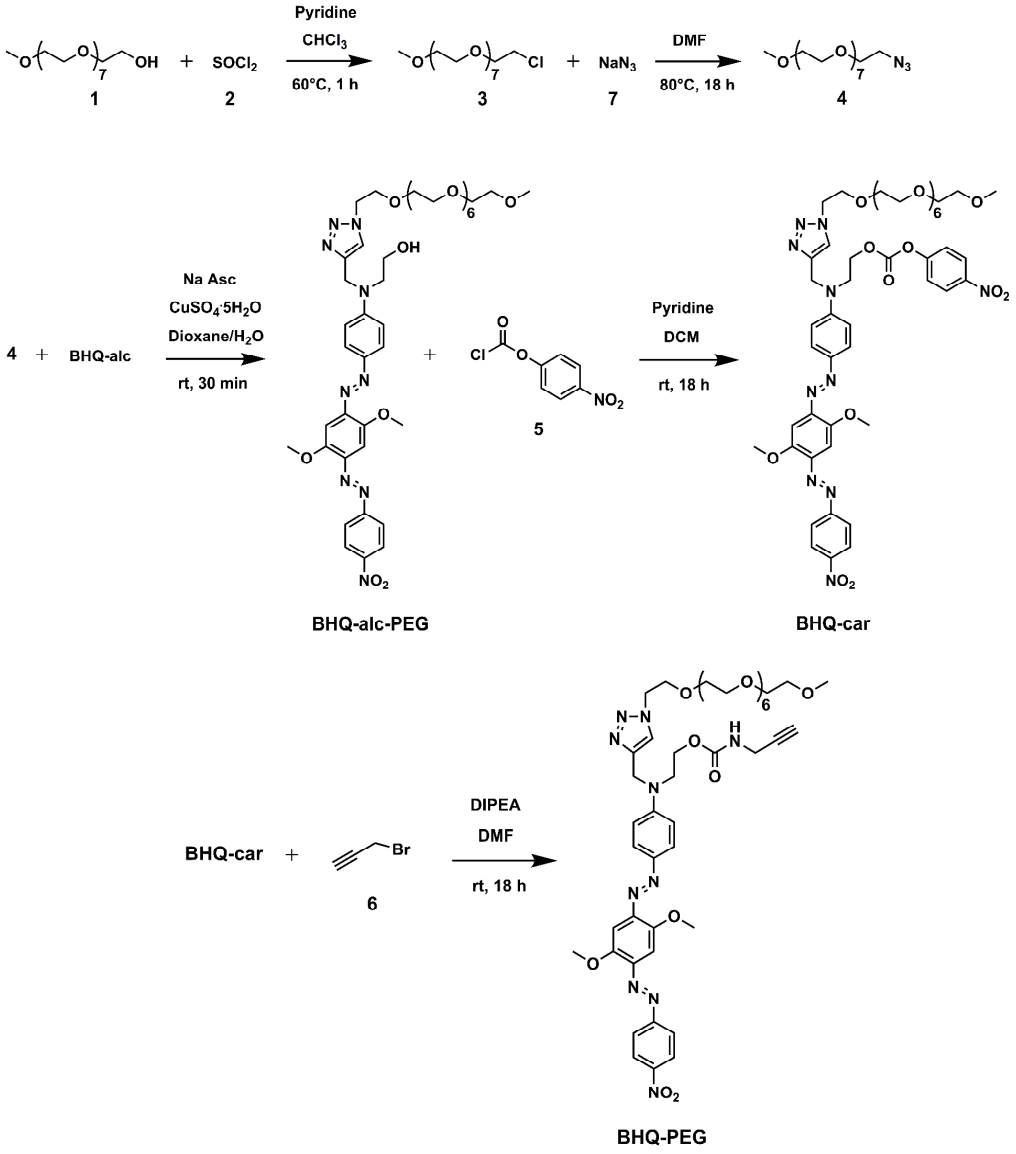


**Figure 8.8** Schematization of the *synthesis of the PEGylated derivative of BHQ (BHQ-PEG).*

25-chloro-2,5,8,11,14,17,20,23-octaoxapentacosane **3**: in a flamed 25 mL round bottom flask dried under vacuum, to a solution of Octaethylene glycol monomethyl ether (**1**) (0.5 g, 1.3 mmol) in Chloroform ($CHCl_3$, 5 mL) was added Pyridine (0.105 mL, 1.3 mmol) and Thionyl chloride (**2**) (0.142 mL, 1.95 mmol) and the reaction mixture was heated at 60°C for 1 h. After cooling down to room temperature, the reaction mixture was then concentrated in vacuo to give the compound **3** as a yellow oil (0.445 g, yield 85 %).

- **Chemical formula:** $C_{17}H_{35}ClO_8$;
- **Molecular Weight:** 402.9;
- **$^1$H-NMR** (400 MHz, $CDCl_3$, 25°C): δ = 3.76 (2H, t, *J* = 6.0 Hz, -C*H*$_2$Cl), 3.69-3.64 (28H, m, -OC*H*$_2$C*H*$_2$O-), 3.55 (2H, t, *J* = 4.9 Hz, -C*H*$_2$CH$_2$Cl), 3.38 (3H, s, -OC*H*$_3$);

- **$^{13}$C-NMR** (100 MHz, $CDCl_3$, 25°C): δ = 71.7, 71.1, 70.4, 70.3, 70.2, 58.8, 42.6;
- **ESI-MS** m/z calculated for $C_{17}H_{35}ClO_8^+$ is 402.2; obs.:403.2.

25-azido-2,5,8,11,14,17,20,23-octaoxapentacosane **4**: in a flamed 25 mL round bottom flask dried under vacuum, to a solution of (**3**) (0.969 g, 2.4 mmol) in DMF (9.5 mL) was added Sodium azide (**7**) (0.313 g, 4.8 mmol) and the reaction mixture was heated at 80°C for 18 h. After cooling down to room temperature, the reaction mixture was then concentrated in vacuo and the obtained residue was redisperded with 5 mL of $H_2O$ and extracted four times with DCM. The combinated organic phases were dried over Sodium sulfate and concentrated in vacuo to give the compound **4** as a yellow oil (0.908 g, yield 93 %).

- **Chemical formula:** $C_{17}H_{35}N_3O_8$;
- **Molecular Weight:** 409.5;
- **$^1$H-NMR** (400 MHz, $CDCl_3$, 25°C): δ = 3.66 (30H, t, *J* = 2.8 Hz, -OC*H*$_2$C*H*$_2$O-), 3.55 (2H, t, *J* = 4.3 Hz, -C*H*$_2$N$_3$), 3.38 (3H, s, -OC*H*$_3$);
- **$^{13}$C-NMR** (100 MHz, $CDCl_3$, 25°C): δ = 71.2, 70.6, 69.9, 69.8, 69.7, 69.3, 56.2, 49.9, 42.1;
- **ESI-MS** m/z calculated for $C_{17}H_{35}N_3O_8^+$ is 409.2; obs.:427.3 $(M+NH_4)^+$.

2-(((1-(2,5,8,11,14,17,20,23-octaoxapentacosan-25-yl)-1H-1,2,3-triazol-4-yl)methyl)(4-((E)-(2,5-dimethoxy-4-((E)-(4-nitrophenyl)diazenyl)phenyl)diazenyl)phenyl)amino)ethan-1-ol **BHQ-alc-PEG**: in a flamed 250 mL round bottom flask dried under vacuum, (**BHQ-alc**) (0.709 g, 1.45 mmol) and the compound (**4**) (0.714 g, 1.74 mmol) were solubilized with 65 mL of 1,4-Dioxane. Copper(II) sulfate pentahydrate (0.181 g, 0.73 mmol) and Sodium ascorbate (0.201 mg, 1.02 mmol) were solubilized with 3 mL of $H_2O$ and added to the previous solution, and the reaction mixture was stirred at room temperature for 30 min. The reaction mixture was then concentrated in vacuo and the residue was purified by silica gel chromatography eluting with DCM/MeOH (9:1) to give the compound **BHQ-alc-PEG** as a purple solid (0.975 g, yield 75 %).

- **Chemical formula:** $C_{42}H_{59}N_9O_{13}$;
- **Molecular Weight:** 898.0;
- **$^1$H-NMR** (400 MHz, $CDCl_3$, 25°C): δ = 8.36 (2H, d, *J* = 9.0 Hz, ar. C*H*), 8.03 (2H, d, *J* = 9.1 Hz, ar. C*H*), 7.89 (2H, d, *J* = 9.0 Hz, ar. C*H*) - 7.87 (1H, s, -NC*H*) overlapped, 7.47 (1H, s, ar. C*H*), 7.43 (1H, s, ar. C*H*) 6.92 (2H, d, *J* = 7.4 Hz, ar. C*H*), 4.82 (2H, s, -NC*H*$_2$C-), 4.52 (2H, t, *J* = 5.0 Hz, -NC*H*$_2$CH$_2$O-), 4.06 (3H, s, -OC*H*$_3$), 4.02 (3H, s, -OC*H*$_3$), 3.95 (2H, t, *J* = 4.6 Hz, -NC*H*$_2$CH$_2$OH), 3.83 (2H, t, *J* = 4.8 Hz, -CH$_2$C*H*$_2$OH), 3.64-3.60 (30H, m, -OC*H*$_2$C*H*$_2$O-), 3.35 (3H, s, -CH$_2$OC*H*$_3$);
- **$^{13}$C-NMR** (100 MHz, $CDCl_3$, 25°C): δ = 156.6, 153.7, 151.2, 151.1, 148.6, 146.8, 145.1, 145.0, 142.4, 126.0, 124.9, 123.7, 123.6, 112.4, 101.2, 100.3, 72.1, 71.5, 70.8, 70.7, 69.5, 60.7, 59.2, 57.0, 55.8, 50.7, 47.7, 42.9;

- **ESI-MS** m/z calculated for $C_{42}H_{59}N_9O_{13}^+$ is 897.4; obs.:898.4.

2-(((1-(2,5,8,11,14,17,20,23-octaoxapentacosan-25-yl)-1H-1,2,3-triazol-4-yl)methyl)(4-((E)-(2,5-dimethoxy-4-((E)-(4-nitrophenyl)diazenyl)phenyl)diazenyl)phenyl)amino)ethyl (4-nitrophenyl) carbonate **BHQ-car**: in a flamed 100 mL round bottom flask dried under vacuum, (**BHQ-alc-PEG**) (0.975 g, 1.09 mmol), Pyridine (0.264 mL, 3.27 mmol) and 4-Nitrophenyl chloroformate (**5**) (0.659 g, 3.27 mmol) were solubilized with 36 mL of DCM and the reaction mixture was stirred at room temperature for 18 h. The reaction mixture was then concentrated in vacuo and the residue was purified by silica gel chromatography eluting with EtOAc/Acetone (1:1) to give the compound **BHQ-car** as a purple oil (0.819 g, yield 71 %).

- **Chemical formula:** $C_{49}H_{62}N_{10}O_{17}$;
- **Molecular Weight:** 1063.1;
- **$^1$H-NMR** (400 MHz, $CDCl_3$, 25°C): δ = 8.36 (2H, d, *J* = 9.1 Hz, ar. C*H*), 8.25 (2H, d, *J* = 9.1 Hz, ar. C*H*), 8.03 (2H, d, *J* = 9.0 Hz, ar. C*H*), 7.94 (2H, d, *J* = 8.8 Hz, ar. C*H*), 7.69 (1H, s, -NC*H*), 7.51 (1H, s, ar. C*H*), 7.51 (1H, s, ar. C*H*), 7.33 (2H, d, *J* = 9.2 Hz, ar. C*H*), 6.98 (2H, d, *J* = 8.9 Hz, ar. C*H*), 4.85 (2H, s, -NC$H_2$C-), 4.58 (2H, t, *J* = 5.6 Hz, -OC$H_2$C$H_2$N-), 4.53 (2H, t, *J* = 4.9 Hz, -NC$H_2$C$H_2$O-), 4.10 (3H, s, -OC$H_3$), 4.06 (3H, s, -OC$H_3$), 4.0 (2H, t, *J* = 5.1 Hz, -NC$H_2$C$H_2$O-), 3.65-3.54 (30H, m, -OC$H_2$C$H_2$O-), 3.38 (3H, s, -C$H_2$OC$H_3$);
- **$^{13}$C-NMR** (100 MHz, $CDCl_3$, 25°C): δ = 158.0, 156.1, 153.4, 150.9, 151.0, 148.4, 148.1, 146.3, 145.7, 145.5, 144.4, 142.9, 126.2, 125.2, 125.1, 124.4, 123.1, 123.0, 122.3, 121.9, 110.4, 101.8, 101.2, 71.4, 70.6, 69.6, 66.3, 59.1, 56.8, 50.7, 49.4, 48.8, 42.9, 29.7;
- **ESI-MS** m/z calculated for $C_{49}H_{62}N_{10}O_{17}^+$ is 1062.4; obs.:1063.4.

2-(((1-(2,5,8,11,14,17,20,23-octaoxapentacosan-25-yl)-1H-1,2,3-triazol-4-yl)methyl)(4-((E)-(2,5-dimethoxy-4-((E)-(4-nitrophenyl)diazenyl)phenyl)diazenyl)phenyl)amino)ethyl prop-2-yn-1-ylcarbamate **BHQ-PEG**: in a flamed 25 mL round bottom flask dried under vacuum, to a solution of (**BHQ-car**) (0.1 g, 0.094 mmol) in DMF (5 mL) was added DIEA (0.065 mL, 0.376 mmol) and Propargylamine (**6**) (0.024 mL, 0.376 mmol) and the reaction mixture was stirred at room temperature for 18 h. The reaction mixture was then diluted with $H_2O$ (5 mL) and extracted three times with DCM. The combinated organic phases were washed three times with a saturated solution of Sodium bicarbonate, dried over Sodium sulfate and concentrated in vacuo to give the compound **BHQ-PEG** as a purple oil (0.074 g, yield 81 %).

- **Chemical formula:** $C_{46}H_{62}N_{10}O_{14}$;
- **Molecular Weight:** 979.1;
- **$^1$H-NMR** (400 MHz, $CDCl_3$, 25°C): δ = 8.39 (2H, d, *J* = 9.1 Hz, ar. C*H*), 8.06 (2H, d, *J* = 9.0 Hz, ar. C*H*), 7.93 (2H, d, *J* = 9.1 Hz, ar. C*H*), 7.62 (1H, s, -NC*H*), 7.50 (1H, s, ar. C*H*), 7.45 (1H, s, ar. C*H*), 6.91 (2H, d, *J* = 8.9 Hz, ar. C*H*), 4.81 (2H, s, -

NC$H_2$C-), 4.52 (2H, t, *J* = 4.8 Hz, -OC$H_2$C$H_2$N-), 4.36 (2H, t, *J* = 5.2 Hz, -NC$H_2$C$H_2$O-), 4.10 (3H, s, -OC$H_3$), 4.05 (3H, s, -OC$H_3$), 3.97 (2H, t, *J* = 5.2 Hz, -NC$H_2$C$H_2$O-), 3.86 (2H, s, NHC$H_2$C-), 3.65-3.53 (30H, m, -OC$H_2$C$H_2$O-) + (1H, s, CC*H*) overlapped, 3.38 (3H, s, -C$H_2$OC$H_3$);

- **$^{13}$C-NMR** (100 MHz, $CDCl_3$, 25°C): δ = 156.4, 155.8, 153.5, 151.1, 150.9, 148.4, 146.4, 145.1, 144.5, 142.3, 126.0, 124.7, 123.5, 123.1, 112.2, 101.0, 100.1, 79.8, 71.9, 71.7, 71.4, 70.7, 70.6, 70.5, 70.4, 69.4, 62.4, 59.0, 56.8, 50.3, 47.3, 42.7, 30.8, 29.7;
- **ESI-MS** m/z calculated for $C_{46}H_{62}N_{10}O_{14}^+$ is 978.4; obs.: 979.4.

### 8.6.4 GDP-BHQ-PEG

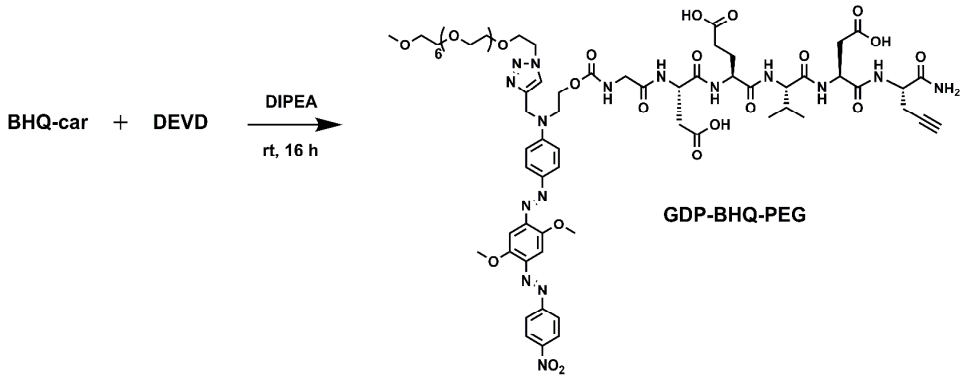


**Figure 8.9** *Schematization of the synthesis of the GDO-BHQ-PEG derivative.*

(11S,14S,17S,20S)-1-(1-(2,5,8,11,14,17,20,23-octaoxapentacosan-25-yl)-1H-1,2,3-triazol-4-yl)-20-(((S)-1-amino-1-oxopent-4-yn-2-yl)carbamoyl)-14-(2-carboxyethyl)-11-(carboxymethyl)-2-(4-((E)-(2,5-dimethoxy-4-((E)-(4-nitrophenyl)diazenyl)phenyl)diazenyl)phenyl)-17-isopropyl-6,9,12,15,18-pentaoxo-5-oxa-2,7,10,13,16,19-hexaazadocosan-22-oic acid **GDP-BHQ-PEG**: in a flamed 25 mL round bottom flask dried under vacuum, to a solution of (**BHQ-car**) (0.531 g, 0.5 mmol) in DMF (5 mL) was added DIEA (0.017 mL, 0.1 mmol) and (**DEVD**) (**6**) (0.024 mL, 0.376 mmol) and the reaction mixture was stirred at room temperature for 16 h. The reaction mixture was then concentrated in vacuo and the residue was purified by semi-preparative HPLC chromatography eluted with solvent B in solvent A: 20% for 5 min, then from 20% to 60% in 25 min to give the compound **BHQ-PEG** as a purple solid (0.066 g, yield 39 %). Solvent B (0.1% TFA in MeCN, v/v); solvent A (0.1% TFA in $H_2O$, v/v).

- **Chemical formula:** $C_{68}H_{94}N_{16}O_{26}$;
- **Molecular Weight:** 1551.6;
- **ESI-MS** m/z calculated for $C_{68}H_{94}N_{16}O_{26}^+$ is 1550.6; obs.: 1551.6.

## 8.7 Synthesis and characterization of F127 derivatives

### 8.7.1 F127-amino

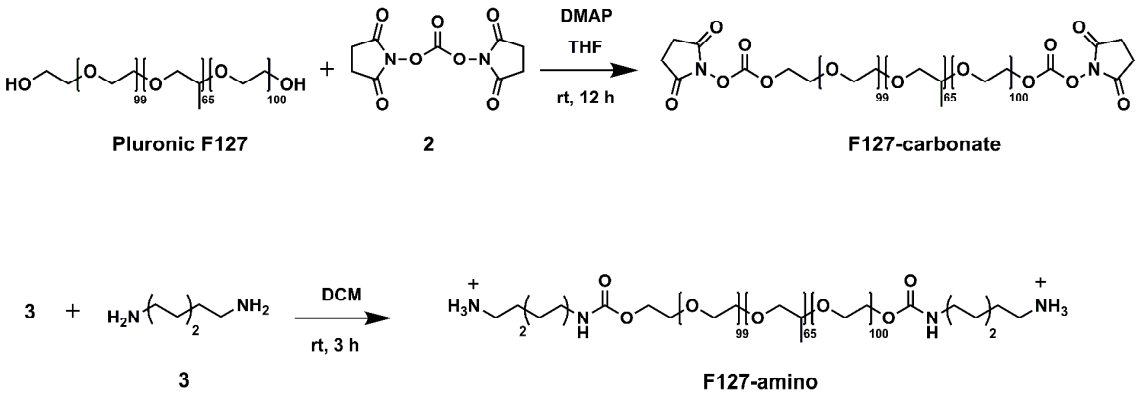


**Figure 8.10** *Schematization of the synthesis of F127-amino.*

Pluronic F127 N-disuccinimydil carbonate **F127-carbonate** was synthesized adapting reported procedures.[24] A toluene solution of Pluronic F127 (4.01 g, 0.32 mmol, 1.0 eq, 100 mL) was distilled under reduced pressure at 50-60°C in a 250 mL round bottom flask. The residue was dried under vacuum and finally solubilized with 15 mL of dry THF. N,N'-disuccinimidyl carbonate (**2**) (0.80 g, 3.1 mmol), solubilized in 7.0 mL of acetone was added. DMAP (0.41 g, 3.32 mmol) was then slowly added at room temperature under stirring by a dropping funnel. After 12 hours, **F127-carbonate** was precipitated with $Et_2O$ and recovered by centrifugation (25 minutes, 5000 rpm). The precipitate was resuspended and centrifugated several times with acetone (20 mL), until no trace of the excess reagent (TLC, chloroform-methanol 5:1) was present. The product was finally dried under vacuum and directly used for amine functionalization.

Pluronic F127-di-yl bis ((6-aminoesyl)carbamate) **F127-amino** was synthesized adapting reported procedures.[24] In a flamed 100 mL round bottom flask dried under vacuum, 1,6-Diaminohexane (**3**) (1.908 g, 16.4 mmol) was solubilized with 10 mL of dry DCM. A 10 mL DCM solution of (**F127-carbonate**) (2.0 g, 0.16 mmol) was then slowly added under stirring at room temperature. After 3 hours the reaction mixture was distilled under reduced pressure and the residue was solubilized with 20 mL of water. The resulting solution was dialyzed vs. Milli-Q water (regenerated cellulose, 12 KDa) for about 20 h under gentle stirring. The dialyzed solution was evaporated under reduced pressure and finally dried under vacuum, obtaining 0.84 g of white solid (yield 42%).

- **$^1$H-NMR** (300 MHz, $CDCl_3$, 25°C): δ = 8.21 (2H, s, -N*H*CO-), 5.09 (4H, s, -N$H_2$), 4.14 (4H, s, -C$H_2$OCO-), 3.76-3.75 (4H, m, -C$H_2$CH$_2$OH), 3.58 (s, -OCH$_2$CH$_2$O-) + 3.51-3.42 (m, -OC$H_2$CCH$_3$) + 3.33 (m, -OCH$_2$C*H*CH$_3$) ~1000H, 3.09 (4H, s, -C$H_2$NH$_2$), 1.45 (8H, s, -NHCH$_2$C$H_2$CH$_2$CH$_2$C$H_2$CH$_2$NH$_2$), 1.25–1.24 (8H, s, -NHCH$_2$CH$_2$C$H_2$C$H_2$CH$_2$CH$_2$NH$_2$), 1.08 (s, -OCH$_2$CHC$H_3$) ~195H;
- **$^{13}$C-NMR** (100 MHz, $CDCl_3$, 25°C): δ = 75.7, 75.6, 75.4, 75.3, 73.6, 73.5, 72.2-73.0 (m), 70.0, 17.7, 17.5.

The dicarboxylic acid derivative of Pluronic F127 **F127-carbo** was synthesized following reported procedures.[25]

### 8.7.2 F127-SS-azide

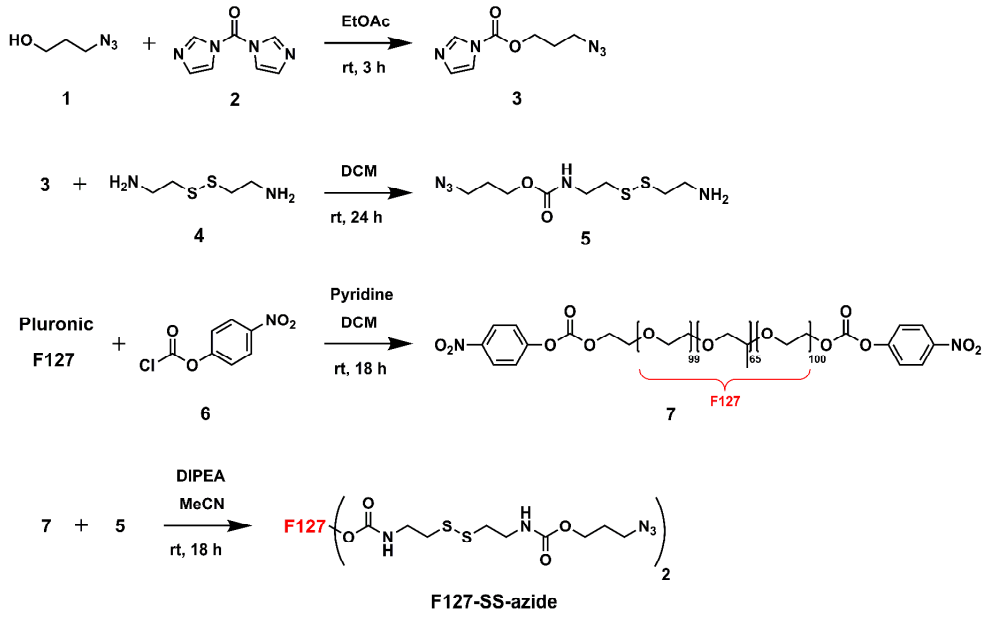


**Figure 8.11** *Schematization of the synthesis of F127-SS-azide.*

3-azidopropyl (2-((2-aminoethyl)disulfanyl)ethyl)carbamate **5** was syntyesized adapting reported procedures.[26,27] Cystamine dihydrochloride was neutralized by 4 M NaOH and extracted three times with DCM to yield cystamine (**4**). In a flamed 50 mL round bottom flask dried under vacuum, to a solution of (**4**) (1.267 g, 8.3 mmol) in DCM (20 mL) was added 3-azidopropyl 1H-imidazole-1-carboxylate (**3**) and the reaction mixture was stirred at room temperature for 24 h. The reaction mixture was concentrated in vacuo, and the residue was treated with $NaH_2PO_4$ (50 mL, 1.0 M) and extracted three times with $Et_2O$. The reaction mixture was then concentrated in vacuo to give the compound **5** as a yellow solid (0.412 g, yield 22 %).

- **Chemical formula:** $C_8H_{17}N_5O_2S_2$;
- **Molecular Weight:** 279.4;
- **$^1$H-NMR** (400 MHz, $CDCl_3$, 25°C): δ = 4.14 (2H, t, *J* = 6.0 Hz, -OC*H*$_2$CH$_2$-), 3.52-3.47 (2H, m, C*H*$_2$N$_3$), 3.36 (2H, t, *J* = 6.6 Hz, -OCNHC*H*$_2$-), 3.01 (2H, t, *J* = 6.2 Hz, -C*H*$_2$NH$_2$), 2.78-2.74 (4H, m, -C*H*$_2$SSC*H*$_2$-), 1.90-1.84 (2H, m, -CH$_2$C*H*$_2$CH$_2$-);
- **$^{13}$C-NMR** (100 MHz, $CDCl_3$, 25°C): δ = 156.4, 134.9, 121.4, 61.4, 47.7, 41.1, 41.0, 39.7, 39.5, 37.5, 28.1;

- **ESI-MS** m/z calculated for $C_8H_{17}N_5O_2S_2^+$ is 279.1; obs.: 280.1.

- Dicarbamate derivative of Pluronic F127 **7**: in a flamed 100 mL round bottom flask dried under vacuum, (**F127**) (6.3 g, 0.5 mmol), Pyridine (0.242 mL, 3 mmol) and 4-Nitrophenyl chloroformate (**6**) (0.605 g, 3 mmol) were solubilized with 30 mL of DCM and the reaction mixture was stirred at room temperature for 18 h. The reaction mixture was then concentrated in vacuo, then the residue was redispersed with HCl 0.1 M and extracted five times with DCM. The combined organic phases were dried over Sodium sulfate, concentrated in vacuo to give the compound **7** as a white solid (5.85 g, yield 91 %).
- **$^1$H-NMR** (400 MHz, $CDCl_3$, 25°C): δ = 8.25 (2H, d, *J* = 9.1 Hz, ar. C*H*), 8.06 (2H, d, *J* = 9.1 Hz, ar. C*H*), 7.36 (2H, d, *J* = 9.2 Hz, ar. C*H*), 6.88 (2H, d, *J* = 9.1 Hz, ar. C*H*), 4.42-4.39 (4H, m, -C*H*$_2$COO-), 3.79-3.77 (4H, m, -C*H*$_2$CH$_2$COO-), 3.63-3.59 (-OC*H*$_2$C*H*$_2$O-) + 3.57-3.49 (m, -OC*H*$_2$CH-) + 3.41-3.39 (m, -C*H*CH$_3$) ~1000H, 1.12-1.09 (~195H, m, -CHC*H*$_3$);
- **$^{13}$C-NMR** (100 MHz, $CDCl_3$, 25°C): δ = 166.2, 155.5, 152.4, 145.3, 139.1, 126.2, 125.2, 121.8, 116.3, 75.5, 75.3, 75.1, 73.3, 72.9, 70.5, 68.5, 68.3, 17.4, 17.3.

- Disulfide-azide derivative of Pluronic F127 **F127-SS-azide**: in a flamed 100 mL round bottom flask dried under vacuum, compound (**7**) (1.75 g, 0.135 mmol), DIPEA (0.092 mL, 0.54 mmol) and compound (**5**) (0.151 g, 0.54 mmol) were solubilized with 20 mL of MeCN and the reaction mixture was stirred at room temperature for 18 h. The reaction mixture was concentrated in vacuo, then the residue was redispersed with water and purification was carried out by means of dialysis against water (72 h) to give the compound **F127-SS-azide** as a yellow solid (1.075 g, yield 61 %).
- **$^1$H-NMR** (400 MHz, $CDCl_3$, 25°C): δ = 4.24-4.12 (8H, m, -C*H*$_2$OOCNH-), 3.80 (4H, t, J = 4.3 Hz, -NHCOOCH$_2$C*H*$_2$O-), 3.63-3.61 (m, (-OC*H*$_2$C*H*$_2$O-) + 3.57-3.46 (m, -OC*H*$_2$CH-) + 3.52-3.47 (4H, m, C*H*$_2$N$_3$) + 3.41-3.35 (m, -C*H*CH$_3$) + 3.36 (8H, m, -OCNHC*H*$_2$-) ~1000H, 2.80 (8H, t, *J* = 6.0 Hz, -C*H*$_2$SSC*H*$_2$-), 1.93-1.86 (4H, m, -CH$_2$C*H*$_2$CH$_2$N$_3$), 1.13-1.10 (~195H, m, -CHC*H*$_3$) ;
- **$^{13}$C-NMR** (100 MHz, $CDCl_3$, 25°C): δ = 156.3, 155.4, 75.4, 75.2, 75.0, 73.2, 72.8, 72.7, 70.7, 69.5, 69.4, 68.5, 68.2, 61.7, 48.1, 39.7, 39.6, 38.0, 17.3, 17.2.

Diazidic derivative of Pluronic F127) **F127-azide** was synthesized following reported procedures (see Section 6.2.2).[28]

3-azidopropyl 1H-imidazole-1-carboxylate **3** was synthesized following reported procedures.[26]

## 8.8 Synthesis and characterization of F127-BHQ derivatives

### 8.8.1 F127-SS-BHQ derivatives

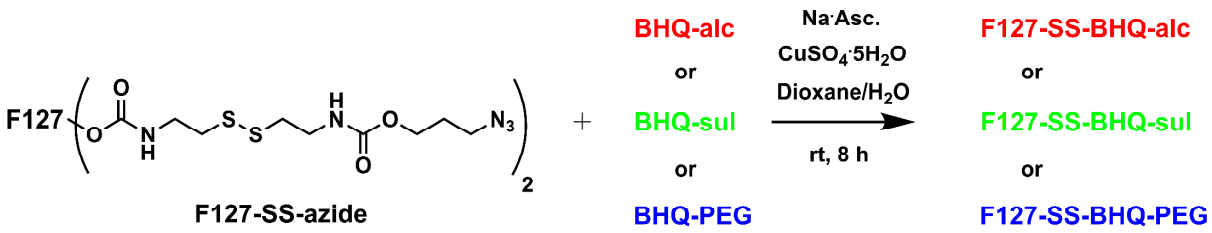


**Figure 8.12** *Schematization of the general procedure for F127-BHQ derivatives.*

General procedure: in a flamed 20 mL round bottom flask dried under vacuum, (**F127-SS-azide**) (1 eq., 0.012 mmol) was solubilized with 3 mL of Dioxane. Copper(II) sulfate pentahydrate (5 eq.) and Sodium ascorbate (7 eq.) were solubilized with 1 mL of $H_2O$ and added to the previous solution, and the reaction mixture was stirred at room temperature for 8 h. The reaction mixture was concentrated in vacuo, then the residue was purificated by means of Size-exclusion chromatography (LH-20) eluting with DCM/MeOH (1:1) to obtain the desired compound.

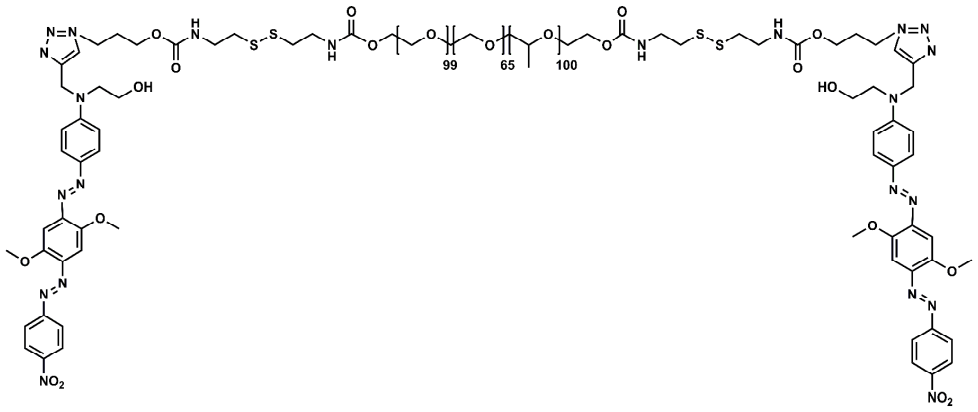

**Figure 8.13** *Molecular structure of F127-SS-BHQ-alc.*

Di-BHQ-alcohol derivative of F127 **F127-SS-BHQ-alc** (yield 68 %).

- **$^1$H-NMR** (400 MHz, $CDCl_3$, 25°C): δ = 8.37 (4H, d, *J* = 8.9 Hz, ar. C*H*), 8.04 (4H, d, *J* = 8.9 Hz, ar. C*H*), 7.87 (4H, d, *J* = 8.9 Hz, ar. C*H*), 7.61 (2H, s, -CC*H*-), 7.48 (2H, s, ar. C*H*), 7.42 (2H, s, ar. C*H*), 6.82 (4H, d, *J* = 8.9 Hz, ar. C*H*), 4.81 (4H, s, -NC$H_2$C-), 4.34 (4H, t, *J* = 6.0 Hz, -NC$H_2$C$H_2$C$H_2$-), 4.22-4.18 (8H, m, -C$H_2$OOCNH-), 4.07 (6H, s, -OC$H_3$-), 4.03 (6H, s, -OC$H_3$-), 3.96-3.94 (4H, m, -NC$H_2$C$H_2$OH), 3.82-3.80 (4H, m, -NCH$_2$C$H_2$OH) + (4H, m, -NHCOOCH$_2$C$H_2$O-) overlapped, 3.64-3.62 (m, -C$H_2$OCH$_2$-) + 3.57-3.49 (m, -OC$H_2$CH-) + 3.41-3.39 (m, -C*H*CH$_3$) + 3.36

(8H, m, -OCNHC*H*$_2$-) ~1000H, 2.83 (8H, t, *J* = 6.3 Hz, -C*H*$_2$SSC*H*$_2$-), 2.17-2.16 (4H, m, -NCH$_2$C*H*$_2$CH$_2$O-), 1.14-1.12 (~195H, m, -CHC*H*$_3$) ;

- **$^{13}$C-NMR** (100 MHz, $CDCl_3$, 25°C): δ = 177.3, 168.1, 164.4, 158.0, 156.3, 156.2, 151.8, 146.6, 143.3, 125.9, 125.8, 125.7, 125.6, 123.5, 123.4, 112.9, 112.0, 100.9, 97.2, 73.2, 72.8, 72.7, 70.4, 685, 68.4, 68.1, 63.9, 63.5, 61.5, 56.7, 39.7, 38.0, 17.3, 17.2.

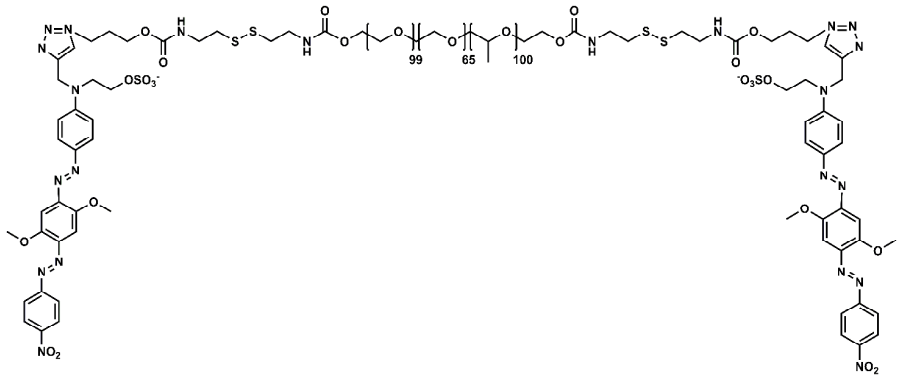

**Figure 8.14** *Molecular structure of F127-SS-BHQ-sul. For clarity, only molecular structure of F127-SS-BHQ-sul and F127-SS-BHQ-alc are shown.*

Di-BHQ-sulfonate derivative of Pluronic F127 **F127-SS-BHQ-sul** (yield 68 %)

- **$^{1}$H-NMR** (400 MHz, $CDCl_3$, 25°C): δ = 8.40 (4H, d, *J* = 8.4 Hz, ar. C*H*), 8.04 (4H, d, *J* = 8.8 Hz, ar. C*H*), 7.86 (4H, d, *J* = 7.6 Hz, ar. C*H*), 7.49-7.43 (2H, s, -CC*H*-) + (2H, s, ar. C*H*) + (2H, s, ar. C*H*) overlapped, 6.93 (4H, d, *J* = 8.4 Hz, ar. C*H*), 4.84 (4H, s, -NC*H*$_2$C-), 4.45-4.40 (4H, m, -C*H*$_2$OS-), 4.35-4.30 (4H, m, -NC*H*$_2$CH$_2$CH$_2$-), 4.24-4.19 (8H, m, -C*H*$_2$OOCNH-), 4.08 (6H, s, -OC*H*$_3$-), 4.03 (6H, s, -OC*H*$_3$-), 3.96-3.91 (4H, m, -NC*H*$_2$CH$_2$OS), 3.83-3.79 (4H, m, -NHCOOCH$_2$C*H*$_2$O-), 3.64-3.62 (m, -C*H*$_2$OCH$_2$-) + 3.57-3.49 (m, -OC*H*$_2$CH-) + 3.41-3.39 (m, -C*H*CH$_3$) + 3.36 (8H, m, -OCNHC*H*$_2$-) ~1000H, 2.89-2.79 (8H, m -C*H*$_2$SSC*H*$_2$-), 2.18-2.16 (4H, m, -NCH$_2$C*H*$_2$CH$_2$O-) 1.15-1.12 (~195H, m, -CHC*H*$_3$);
- **$^{13}$C-NMR** (100 MHz, $CDCl_3$, 25°C): δ = 169.4, 168.9, 166.9, 157.2, 156.5, 154.5, 153.6, 148.6, 146.7, 142.8, 140.5, 132.4, 126.5, 126.1, 125.9, 124.8, 123.5, 121.6, 100.2, 82.3, 81.6, 75.5, 75.5, 75.1, 73.3, 72.9, 72.8, 70.8, 63.6, 61.5, 56.8, 40.8, 39.8, 17.4, 17.3.

Di-BHQ-PEG derivative of F127 **F127-SS-BHQ-PEG** (yield 87 %)

- **$^{1}$H-NMR** (400 MHz, $CDCl_3$, 25°C): δ = 8.38 (4H, d, *J* = 8.9 Hz, ar. C*H*), 8.06 (4H, d, *J* = 8.8 Hz, ar. C*H*), 7.93-7.90 (4H, m, ar. C*H*), 7.70-7.61 (4H, s, -CC*H*-), 7.50 (2H, s, ar. C*H*), 7.45 (2H, s, ar. C*H*), 6.90 (4H, d, *J* = 8.7 Hz, ar. C*H*), 4.81-4.79 (4H, s, -

NC$H_2$C-), 4.54-4.48 (8H, m, -NNNC$H_2$-), 4.46-4.31 (12H, m, -C$H_2$OOCNH-), 4.10 (6H, s, -OC$H_3$-), 4.04 (6H, s, -OC$H_3$-), 3.98-3.94 (4H, m, -NC$H_2$C$H_2$O-), 3.88-3.81 (4H, m, -OOCNHC$H_2$C-) + (4H, m, -NHCOOC$H_2$C$H_2$O-), 3.65-3.54 (30H, m, -OC$H_2$C$H_2$O-), 3.64-3.62 (m, -C$H_2$OC$H_2$-) + 3.57-3.49 (m, -OC$H_2$CH-) + 3.41-3.39 (m, -C*H*C$H_3$) + 3.36 (8H, m, -OCNHC$H_2$-) ~1000H, 3.04-2.97 (8H, m -C$H_2$SSC$H_2$-), 2.29-2.28 (4H, m, -NC$H_2$C$H_2$C$H_2$O-), 1.16-1.13 (~195H, m, -CHC$H_3$);

- **$^{13}$C-NMR** (100 MHz, $CDCl_3$, 25°C): δ = 169.9, 156.1, 153.3, 150.9, 150.8, 150.7, 148.2, 146.2, 144.9, 142.1, 125.8, 124.5, 123.6, 123.0, 122.9, 112.0, 104.9, 101.1, 100.8, 100.0, 75.3, 75.2, 74.9, 73.1, 2.8, 72.4, 71.7, 70.3, 61.4, 58.8, 56.6, 50.1, 29.5, 17.2, 17.1.

### 8.8.2 F127-D-BHQ-PEG


**Figure 8.15** *Schematization of the synthesis of F127-D-BHQ-PEG*

Di-BHQ-Pegylated DEVD derivative of F127 ***F127-D-BHQ-PEG*** (yield 52 %). Synthetic procedure and purification identical to the previous case, with DMF in place of Dioxane/Water.

## 8.9 Nanoparticles synthesis

The preparation of core-shell silica-PEG dye doped nanoparticles was obtained adapting existing procedures.[29,30] For the preparation, 200 mg of Pluronic F127 and the desired amount of alkoxysilane dye(s) (or drug) were solubilized with a small amount (~1.0 mL) of dichloromethane in a 20 mL glass scintillation vial. The solvent was then evaporated from the homogeneous solution under vacuum at room temperature. NaCl (137 mg) was added to the solid residue and the mixture was solubilized at 25°C under magnetic stirring with 1560 µL of acetic acid 1.0 M. TEOS (360 µL, 1.6 mmol) was then added to the resulting aqueous homogeneous solution followed by TMSCl (20 µL, 0.16 mmol) after 180 min. The mixture was kept under stirring for 48 hours at 25°C before dialysis treatments. The dialysis purification steps were carried out versus water on a precise amount of nanoparticles solution (3000 µL) finally diluted to a total volume of 10.0 mL with water (For the purification of nanoparticles for drug delivery, see Section 8.1.

## 8.10 Notes and references


(1) Soper, S. A.; Mattingly, Q. L. *Journal of the American Chemical Society* **1994**, *116*, 3744.
(2) Montalti, M.; Credi, A.; Prodi, L.; Gandolfi, M. T. *Handbook of Photochemistry*; 3rd Ed. ed.; CRC Taylor & Francis: Boca Raton 2006.
(3) Voltan, R.; di Iasio, M. G.; Bosco, R.; Valeri, N.; Pekarski, Y.; Tiribelli, M.; Secchiero, P.; Zauli, G. *Clinical Cancer Research* **2011**, *17*, 5649.
(4) Secchiero, P.; Corallini, F.; di Iasio, M. G.; Gonelli, A.; Barbarotto, E.; Zauli, G. *Blood* **2005**, *105*, 3413.
(5) Secchiero, P.; Melloni, E.; Corallini, F.; Beltrami, A. P.; Alviano, F.; Milani, D.; D'Aurizio, F.; di Iasio, M. G.; Cesselli, D.; Bagnara, G. P.; Zauli, G. *Stem Cells* **2008**, *26*, 2955.
(6) Secchiero, P.; Melloni, E.; Voltan, R.; Norcio, A.; Celeghini, C.; Zauli, G. *British Journal of Haematology* **2012**, *157*, 510.
(7) Voltan, R.; Castaldello, A.; Brocca-Cofano, E.; Altavilla, G.; Caputo, A.; Laus, M.; Sparnacci, K.; Ensoli, B.; Spaccasassi, S.; Ballestri, M.; Tondelli, L. *Pharmaceutical Research* **2007**, *24*, 1870.
(8) Secchiero, P.; Voltan, R.; di Iasio, M. G.; Melloni, E.; Tiribelli, M.; Zauli, G. *Clinical Cancer Research* **2010**, *16*, 1824.
(9) Zauli, G.; Voltan, R.; Bosco, R.; Melloni, E.; Marmiroli, S.; Rigolin, G. M.; Cuneo, A.; Secchiero, P. *Clinical Cancer Research* **2011**, *17*, 762.
(10) Zauli, G.; Voltan, R.; di Iasio, M. G.; Bosco, R.; Melloni, E.; Sana, M. E.; Secchiero, P. *Clinical Cancer Research* **2011**, *17*, 2712.
(11) Tisato, V.; Zauli, G.; Voltan, R.; Gianesini, S.; di Iasio, M. G.; Volpi, I.; Fiorentini, G.; Zamboni, P.; Secchiero, P. *PLoS ONE* **2012**, *7*, e39543.
(12) Zauli, G.; Celeghini, C.; Melloni, E.; Voltan, R.; Ongari, M.; Tiribelli, M.; di Iasio, M. G.; Lanza, F.; Secchiero, P. *Haematologica* **2012**, *97*, 1722.
(13) Candido, R.; Toffoli, B.; Corallini, F.; Bernardi, S.; Zella, D.; Voltan, R.; Grill, V.; Celeghini, C.; Fabris, B. *Journal of Vascular Research* **2010**, *47*, 252.
(14) Vercauteren, D.; Vandenbroucke, R. E.; Jones, A. T.; Rejman, J.; Demeester, J.; De Smedt, S. C.; Sanders, N. N.; Braeckmans, K. *Molecular Theraphy* **2010**, *18*, 561.
(15) Secchiero, P.; Rimondi, E.; di Iasio, M. G.; Voltan, R.; Gonelli, A.; Zauli, G. *Journal of Cellular Physiology* **2012**, *227*, 1829.
(16) Biffi, S.; Dal Monego, S.; Dullin, C.; Garrovo, C.; Bosnjak, B.; Licha, K.; Welker, P.; Epstein, M. M.; Alves, F. *PLoS One* **2013**, *8*, e57150.
(17) Abulrob, A.; Brunette, E.; Slinn, J.; Baumann, E.; Stanimirovic, D. *Molecular Imaging and Biology* **2007**, *6*, 304.
(18) Bouteiller, C.; Clavé, G.; Bernardin, A.; Chipon, B.; Massonneau, M.; Renard, P.-Y.; Romieu, A. *Bioconjugate Chemistry* **2007**, *18*, 1303.
(19) Hirata, T.; Kogiso, H.; Morimoto, K.; Miyamoto, S.; Taue, H.; Sano, S.; Muguruma, N.; Ito, S.; Nagao, Y. *Bioorganic and Medicinal Chemistry* **1998**, *6*, 2179.
(20) Chipon, B.; Clavé, G.; Bouteiller, C.; Massonneau, M.; Renard, P.-Y.; Romieu, A. *Tetrahedron Letters* **2006**, *47*, 8279.
(21) Rampazzo, E.; Bonacchi, S.; Juris, R.; Montalti, M.; Genovese, D.; Zaccheroni, N.; Prodi, L.; Rambaldi, D. C.; Zattoni, A.; Reschiglian, P. *Journal of Physical Chemistry B* **2010**, *114*, 14605.
(22) Boxer, M. B.; Jiang, J.-k.; Vander Heiden, M. G.; Shen, M.; Skoumbourdis, A. P.; Southall, N.; Veith, H.; Leister, W.; Austin, C. P.; Park, H. W.; Inglese, J.; Cantley, L. C.; Auld, D. S.; Thomas, C. J. *Journal of Medicinal Chemistry* **2010**, *53*, 1048.
(23) *Tetrahedron Letters* **1985**, *26*, 1362.
(24) K. Huang, B. L., P.B. Messersmith *Polymer Preprints* **2001**, *42*, 147.
(25) Soster, M.; Juris, R.; Bonacchi, S.; Genovese, D.; Montalti, M.; Rampazzo, E.; Zaccheroni, N.; Garagnani, P.; Bussolino, F.; Prodi, L.; Marchio, S. *International Journal of Nanomedicine* **2012**, *7*, 4797.
(26) Zhang, J.; Li, C.; Wang, Y.; Zhuo, R.-X.; Zhang, X.-Z. *Chemical Communications* **2011**, *47*, 4457.
(27) Liu, J.; Jiang, X.; Xu, L.; Wang, X.; Hennink, W. E.; Zhuo, R. *Bioconjugate Chemistry* **2010**, *21*, 1827.
(28) Juris, R. *Dottorato di ricerca in Scienze Chimiche* **2012**.
(29) Genovese, D.; Bonacchi, S.; Juris, R.; Montalti, M.; Prodi, L.; Rampazzo, E.; Zaccheroni, N. *Angewandte Chemie International Edition* **2013**, *52*, 5965.
(30) Rampazzo, E.; Bonacchi, S.; Juris, R.; Montalti, M.; Genovese, D.; Zaccheroni, N.; Prodi, L.; Rambaldi, D. C.; Zattoni, A.; Reschiglian, P. *Journal of Physical Chemistry B* **2010**, *114*, 14605.